

PART-THROUGH CRACK FATIGUE LIFE PREDICTION

J. B. Chang, *editor*

 **STP 687**

**AMERICAN SOCIETY FOR
TESTING AND MATERIALS**

PART-THROUGH CRACK FATIGUE LIFE PREDICTION

A symposium
sponsored by ASTM
Committee E-24 on
Fracture Testing
AMERICAN SOCIETY FOR
TESTING AND MATERIALS
San Diego, Calif., 13-14 Oct. 1977

ASTM SPECIAL TECHNICAL PUBLICATION 687
J. B. Chang, Rockwell International,
editor

List price \$26.25
04-687000-30



AMERICAN SOCIETY FOR TESTING AND MATERIALS
1916 Race Street, Philadelphia, Pa. 19103

Copyright © by AMERICAN SOCIETY FOR TESTING AND MATERIALS 1979
Library of Congress Catalog Card Number: 79-53285

NOTE

**The Society is not responsible, as a body,
for the statements and opinions
advanced in this publication.**

Printed in Baltimore, Md.
October 1979

Foreword

This publication on Part-Through Crack Fatigue Life Prediction contains papers presented at a symposium held 13-14 Oct. 1977 at San Diego, Calif. The symposium was sponsored by the American Society for Testing and Materials through its Committee E-24 on Fracture Testing. J. B. Chang, Rockwell International Military Aircraft Division, served as symposium chairman and editor of this publication. Those who served as session chairmen were J. P. Gallagher, University of Dayton Research Institute; G. A. Vroman, Rockwell International/Rocketdyne; and C. M. Hudson, NASA/Langley Research Center.

Related ASTM Publications

Cyclic Stress-Stain and Plastic Deformation Aspects of Fatigue Crack Growth, STP 637 (1977), \$25.00, 04-637000-30

Thermal Fatigue of Materials and Components, STP 612 (1976), \$27.00, 04-612000-30

Fatigue Crack Growth Under Spectrum Loads, STP 595 (1976), \$34.50, 04-595000-30

Handbook of Fatigue Testing, STP 566 (1974), \$17.25, 04-566000-30

A Note of Appreciation to Reviewers

This publication is made possible by the authors and, also, the unheralded efforts of the reviewers. This body of technical experts whose dedication, sacrifice of time and effort, and collective wisdom in reviewing the papers must be acknowledged. The quality level of ASTM publications is a direct function of their respected opinions. On behalf of ASTM we acknowledge with appreciation their contribution.

ASTM Committee on Publications

Editorial Staff

Jane B. Wheeler, *Managing Editor*
Helen M. Hoersch, *Associate Editor*
Ellen J. McGlinchey, *Senior Assistant Editor*
Helen Mahy, *Assistant Editor*

Contents

Introduction	1
Surface Crack Life Prediction: An Overview—T. A. CRUSE, A. E. GEMMA, R. F. LACROIX, AND T. G. MEYER	3
A Review and Assessment of the Stress-Intensity Factors for Surface Cracks—J. C. NEWMAN, JR.	16
Development of Basic Material(s) Data for Evaluating Crack Growth Life—R. J. BUCCI	47
Aspect Ratio Variability in Part-Through Crack Life Analysis— R. M. ENGLE, JR.	74
Life Prediction Analysis of Part-Through Cracks—G. A. VROMAN	89
Part-Through Crack Growth Predictions Using Compact Tension Crack Growth Rate Data—J. L. RUDD	96
NASA-Langley Research Center's Participation in a Round-Robin Comparison Between Some Current Crack-Propagation Prediction Methods—C. M. HUDSON AND P. E. LEWIS	113
Computer-Aided Fracture Mechanics Life Prediction Analysis— D. E. PETERSON AND G. A. VROMAN	129
Prediction of Constant Amplitude Fatigue Crack Propagation in Surface Flaws—W. S. JOHNSON	143
Assessment of the Sensitivity of Crack Growth Rate Constants to Predictive Accuracy of Part-Through Crack Fatigue Life Predictions—J. B. CHANG	156
Part-Through Crack Problems in Aircraft Structures—J. L. RUDD, T. M. HSU, AND H. A. WOOD	168
Surface Crack <i>K</i>-Estimates and Fatigue Life Calculations in Cannon Tubes—J. H. UNDERWOOD AND J. F. THROOP	195
Summary	211
Index	215

Introduction

The practical importance of part-through surface cracks has been recognized for many years. The results of careful fracture failure examinations of hydro-test fractures of Polaris rocket chambers (1958–1962) were clearly illustrative. In most of these, crack propagation started from a surface crack defect. The rocket chambers were welded and the shell material was a hot-die steel with a yield strength in the 200 to 220 ksi range. Most of the initial cracks were located at weld borders or at solidification boundaries related to weld repairs. It seemed clear that surface contour, lack of fusion, and additions of bending to in-plane tension all favored the formation of surface cracks. The importance of part-through surface cracks was discussed in the first report of the ASTM Special Committee which later became ASTM Committee E-24.¹ Footnote 1 described the relationship of part-through surface cracks to the “leak-before-burst” criterion for adequate toughness.

Subsequent applications of fracture mechanics to fatigue and to stress-corrosion cracking added to the probability of service component initial cracks of the part-through surface crack type. Pertinent considerations included surface folds, deep surface scratches, damage at edges of holes, and access of aggressive environments to surface features.

Although the practical importance of part-through surface cracks has been clear, the development of adequate fracture mechanics treatment of these cracks has been handicapped by formidable complexities. The complexities are of two kinds, K -value analysis and resistance to crack extension. With regard to K -value analysis, our first assistance came from a function theory solution for the problem of a flat-elliptical crack with remote normal tension by Green and Sneddon.² Footnote 3 provided equations for K around the elliptical crack front and suggested an initial, approximate method for K -value estimates applicable to part-through surface cracks.

Numerical as well as function theory analyses of three-dimensional crack problems are, of course, much more difficult than analyses of two-dimensional crack problems. The analysis problems become extreme or

¹“Fracture Testing of High Strength Sheet Materials,” *ASTM Bulletin*, Jan. 1960, pp. 34–37.

²Green, A. E. and Sneddon, I. N., *Proceedings*, Cambridge Philosophical Society, 1950, Vol. 46, p. 159.

³Irwin, G. R., *Transactions*, American Society of Mechanical Engineers, 1962, Series E, Vol. 29, p. 651.

unimportant, depending upon viewpoint, as the front of a part-through crack approaches intersection with the plate (or shell) surface. The surface region adjacent to the crack front develops plastic yielding early in the loading cycle. In addition to the corresponding influence of local yielding upon stress distribution and K -value estimates, the effect of the near-by free surface upon resistance to crack extension must be considered.

Given a part-through surface crack of nearly half-elliptical shape, it seems reasonable to assume that the central and deepest half of the crack front would be governed by conditions of local plane-strain and would respond in predictable ways to crack extension forces. Uncertainties would remain with regard to regions of the crack front close to the plate surface intersections. Presumably these uncertainties would be at a minimum in fatigue loading but even then should not be overlooked.

Experience has shown that advances in fracture technology proceed best through mutual interaction between analysis and experimental observations. The technical papers in this ASTM Special Technical Publication provide an appropriate collection of theoretical and experimental investigations which will substantially assist fracture mechanics technology in application especially to part-through surface cracks fatigue life predictions.

G. R. Irwin

Visiting professor of Mechanical Engineering,
University of Maryland, College Park,
Md. 20742.

Surface Crack Life Prediction: An Overview

REFERENCE: Cruse, T. A., Gemma, A. E., Lacroix, R. F., and Meyer, T. G., "Surface Crack Life Prediction: An Overview," *Part-Through Crack Fatigue Life Prediction*, ASTM STP 687, J. B. Chang, Ed., American Society for Testing and Materials, 1979, pp. 3-15.

ABSTRACT: Successful application of fracture mechanics methodology to component fatigue life prediction requires knowledge of flight cycle loading, local stress and material conditions, da/dN characterization for the material, and the stress intensity factor(s) for the appropriate crack geometry(ies). It is generally assumed that all of the aforementioned conditions are well within current state-of-the-art design procedures for through-thickness cracks. It is further assumed that the part-through, surface crack stress intensity factor distribution is now sufficiently easily characterized that accurate fatigue life predictions can be made for this class of crack geometries. Major unresolved issues for surface cracks exist for small surface cracks, which are initiated within surface layers of machining stress and flight cycle-induced plastic zones near structural notches. The issues include definition of the material properties within the surface layer, unknown surface "values" of the stress intensity factor distribution, crack growth through highly varying stress/material property fields at the surface, and the applicability of macrocrack growth models to small cracks. Further experimental and analytical effort is required in order to achieve accurate fatigue life prediction design methodologies for small surface crack problems in real structures.

KEY WORDS: fatigue (materials), gas turbine disk, crack initiation, crack propagation, stress concentration, titanium alloys, stress gradients, structural analysis

Fatigue life prediction for gas turbine engine disks traditionally has involved two distinct problems: initiation (and subsequent growth) of surface cracks at highly stressed notches in inherently defect-free material; and, propagation of cracks from inherent defects in smooth regions of large material volume with moderate stress levels. A recent paper [1]³ has

¹Project engineer, senior assistant project engineer, and senior analytical engineer, respectively, United Technologies Corp., Pratt and Whitney Aircraft Group, Commercial Products Division, East Hartford, Conn. 06108.

²Assistant project engineer, Materials Engineering and Research Laboratory, Middletown, Conn. 06457.

³The italic numbers in brackets refer to the list of references appended to this paper.

presented a study of the initiation problem for titanium fan disks, subjected to complex mission load cycle histories. The critical fatigue location in the selected fan disk problem was the bolt hole, which can be simulated by a bolt-hole specimen (see Fig. 1). The current paper seeks to present an overview of some basic features of surface crack growth prediction technology by fracture mechanics modeling of the bolt-hole fatigue problem discussed in Ref 1.

Surface crack fatigue life prediction for large cracks in elastically loaded plates with and without notches has been shown to be within the state of the art [2]. This earlier work showed that simple hypotheses can be used to reduce the general surface crack geometry to two, coupled crack growth problems for the crack surface length and depth. Correlation of the surface crack growth data showed good agreement between experimental and analytical values of the stress intensity factors and the growing crack size and shape. Finally, this study demonstrated a cost effective means for incorporating local stress gradients due to elastic loading of a bolt-hole type specimen.

The current study seeks to demonstrate some current deficiencies in surface crack growth prediction. The fatigue life of the bolt-hole specimens in Ref 1 consisted primarily of the early initiation and subsequent propagation of very small surface cracks. The local stresses in the bolt-hole specimen consist of elastic-plastic stresses due to the high load amplitude, together with local residual stresses due to machining. One major concern in the current study is the ability to account for these important, inelastic stress fields. A second major concern is the issue of surface length retardation due to inaccurate crack growth models in the surface layer. These inaccuracies do appear to exist, although the question of whether the

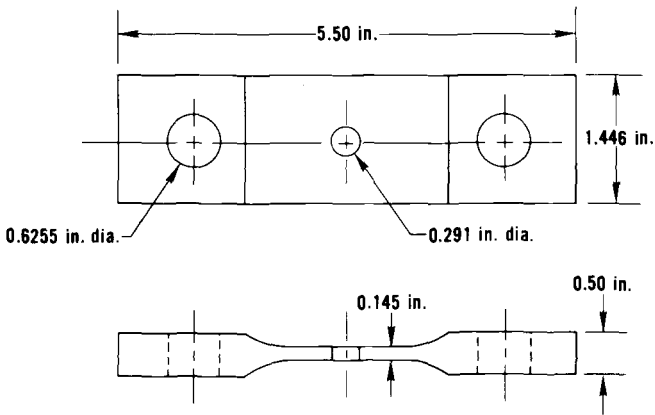


FIG. 1—Bolt-hole specimen (1 in. = 2.54 cm).

problem is the surface stress intensity factor calculation or the growth model is not yet resolved.

Analytical crack growth modeling was performed to predict cyclic crack size and aspect ratio as a function of various stress distributions near the bolt-hole: elastic, elastic-plastic with zero R -ratio (minimum stress/maximum stress), and a full accounting of the local elastoplastic field, including variable R -ratio into the specimen depth. Experimental data have been taken from eight bolt-hole specimens, subjected to identical low cycle fatigue load histories. The data include documentation of the failure sites, crack morphologies, and limited striation spacing.

Experiment

Baseline Materials Data for Ti-6Al-2Sn-4Zr-6Mo

The same heat of material was used in the fabrication of all specimens. The room temperature monotonic and cyclic stress-strain data for Ti-6-2-4-6 have been reported elsewhere [1]. The baseline crack propagation behavior was determined from a series of tests using center-notched sheets and tube specimens machined from a compressor disk forging. The following relationship was found to characterize the test results.

$$\frac{da}{dN} = 1.55 \times 10^{-11} \left(\frac{1.54}{1.64-R} \right)^{4.86} (\Delta K)^{4.86}$$

$$\frac{da}{dN} \geq 7 \times 10^{-7}; -5.0 \leq R \leq 0.5; 20 \text{ cpm}$$

units: ΔK , ksi $\sqrt{\text{in.}}$; da/dN , in./cycle

(1 in. = 0.0254 m; 1 ksi $\sqrt{\text{in.}}$ = 1.099 MN/m^{3/2})

Fatigue Tests of Bolt-Hole Specimens

The primary experimental phase of the study consisted in the testing of eight bolt-hole specimens under constant amplitude fatigue with a net section stress range of 344.75 ± 344.75 MN/m² at a frequency of 15 cpm and room temperature. All specimens were machined from two disk forgings of the same heat code to ensure that each specimen had the same processing history and microstructure. Final machining was controlled carefully so that the surface finish and residual (machining) stresses would be similar for each specimen. The configuration and dimensions of the bolt-hole specimen are given by Fig. 1. At selected intervals during the fatigue testing, visual inspection of the surface of the hole was made using

the wink-zyglo technique, (the surface was coated with a fluorescent dye-penetrant and viewed in black light). An attempt was made to estimate the number of cycles to first indication of a crack permitted by the sensitivity of the inspection method, which is approximately 0.0127 to 0.01778 cm. The results of the fatigue tests can be found in Table 1. The data indicate that the observed surface macrocrack growth accounts for approximately 20 percent of total life; however, unobservable crack growth (from initiation to approximately 0.0127 cm) accounts for a much larger fraction of the total life.

Fractography

Subsequent to failure, each specimen was examined in a scanning electron microscope to determine the shapes and sizes of the fatigue cracks at the onset of final fracture. The fracture surfaces of all specimens were similar in that they contained multiple fatigue origins and extensive regions of shear and tear fracture. The specimens shown in Figs. 2a and 2b are representative of all of the specimens examined. The primary fracture in each case progressed from one origin or from two or three origins located in close proximity to each other. The remainder of the fatigue cracks were isolated from the primary fracture until joined by shearing or tearing in the final stages of fracture. Many (possibly all) of the secondary fatigue cracks may have ceased to grow before the onset of final fracture. This is indicated by the "stretched" zones at the peripheries of these cracks similar to those produced in specimens containing arrested fatigue cracks which are subjected to sudden overloads (such as that occurring in fatigue cracked parts which are broken open by impact). Thus the sizes and shapes of the secondary cracks at the time of final fracture are clearly discernible. In contrast are the primary cracks which eventually led to

Table 1—Specimen data.

Specimen No.	Observed Crack Length (inches) ^a versus Cycles				
	First Observed (0.005 to 0.007)	1/64	1/32	1/16	Failure
1	7000	...	7600 ^b	7700	8380
2	5000	5500	6500 ^b	7000	7347
3	5000	...	5800 ^b	6000	6200
4	...	5000	5300 ^b	5500	5615
5	4500 ^b	...	4757
6	6000	7000	7400 ^b	...	7695
7	5000	5500	6000	...	6207
8	4200	5000	5600 ^b	6000	6830

^a 1-in. = 2.54 cm.

^b Estimated.

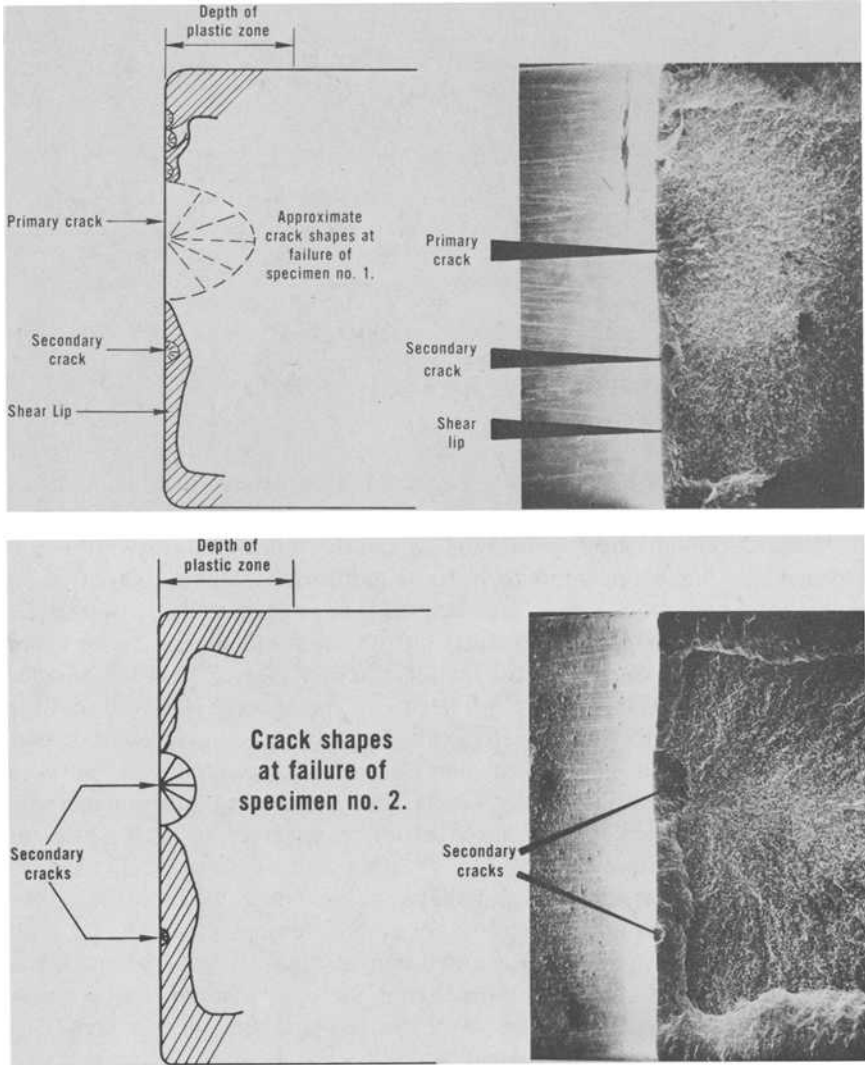


FIG. 2—(a) Fracture surface showing multiple crack origins, and (b) fracture surface showing well-defined secondary crack shapes.

failure of the specimens. They display no stretched zones and the extent of fatigue fracture can be estimated only because the fractographic features associated with rapid fatigue crack growth are identical to those produced by tearing.

Aspect ratios (the ratio of surface crack length to crack depth) were determined for all but a few of the fatigue cracks. In Fig. 3, the aspect

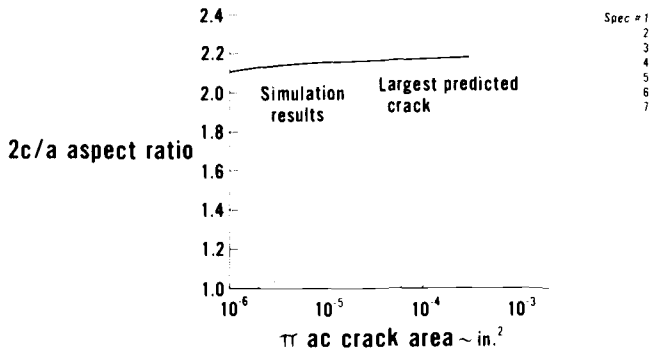


FIG. 3—Comparison of measured and predicted crack aspect ratios (1 in. = 2.54 cm).

ratios of all “isolated” cracks are plotted as a function of crack area. Included in Fig. 3 are measurements of cracks on primary and secondary surfaces. Although there were wide ranges for both the crack size and aspect ratio, there appeared to be no significant systematic variation in aspect ratio with crack size. Crack lengths ranged from 0.00584 to 0.09728 cm, crack depths from 0.00381 to 0.0762 cm, and aspect ratios from 1.17 to 2.33. The average ratio for all cracks was 1.68; for the smaller cracks (lengths 0.0508 cm, depth 0.0254 cm) the average was 1.63 and for the larger cracks it was 1.85. Replicas of the fracture surfaces were prepared and examined in a transmission electron microscope for the purpose of measuring the striation spacings and thereby determining the microscopic crack growth rates. The measured striation spacings as a function of crack depth are shown in Fig. 4. It was hoped that these data could be used to determine crack sizes and shapes at various cyclic intervals. However, this was found to be infeasible for several reasons. There was a high degree of random variation in the striation spacings. The locations of the measured striations with respect to the fatigue origins could not be determined with sufficient accuracy. Well defined and measurable striations were, in some cases, very scarce. Another complicating factor was the observation that the local (microscopic) crack growth directions (indicated by the orientation of the striations) were not always consistent with the dominant (macroscopic) crack growth direction. However, since all cracks were relatively small (~ 0.0762 cm), the deviations observed in this study were not as large as the variation usually found for large cracks. Figure 5 indicates the deviations in crack directions typically observed.

Some difficulty was also encountered in correlating the fractographic observations with the macrocrack data of Table 1. For example, most of the specimens reportedly contained (by wink-zyglo) cracks as long as 0.1588 cm prior to failure, whereas in the fractographic examination none

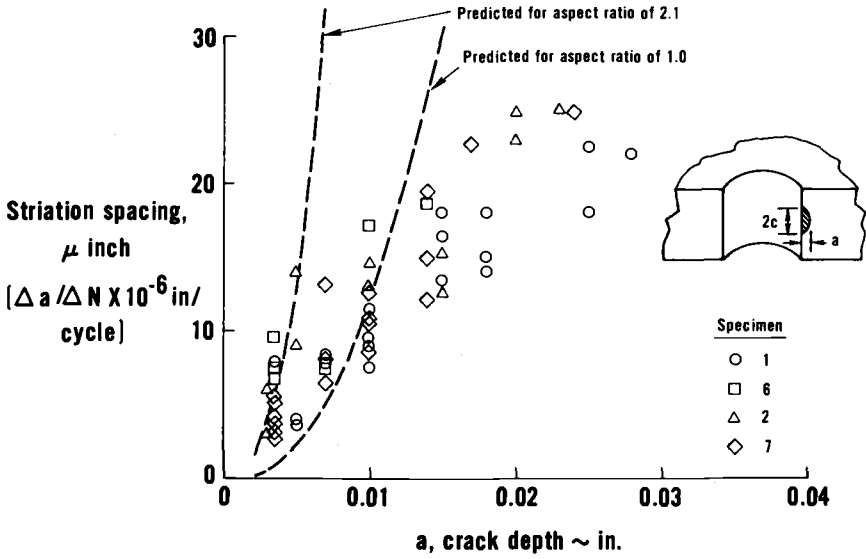


FIG. 4—Actual and predicted striation spacings versus crack depth (1 in. = 2.54 cm).

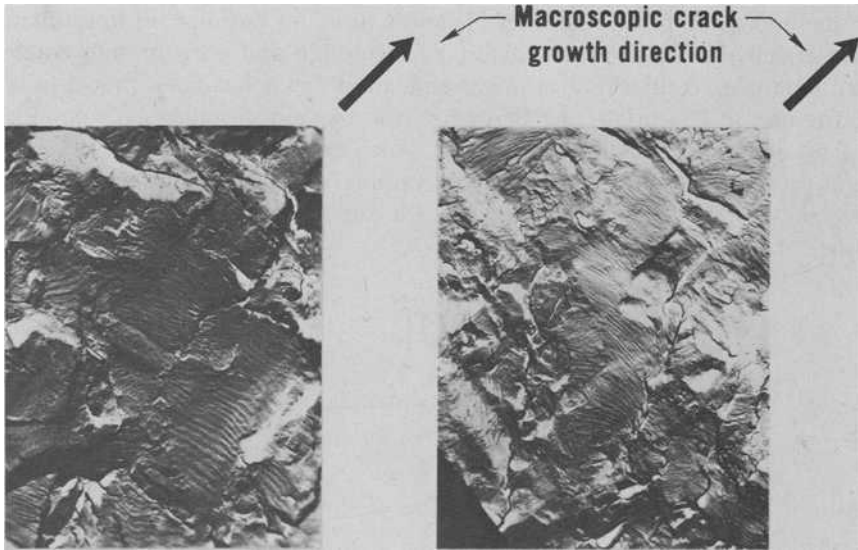


FIG. 5—Macroscopic versus microscopic crack growth direction.

of the specimens was found to contain a fatigue crack of this length. This may imply that the observed cracks (by wink-zyglo) consisted of several smaller cracks which gave the appearance of a single crack.

Analysis

Finite Element Stress Analysis of Bolt-Hole Specimen

The finite element method was used to carry out three stress analyses (plane stress) of the bolt-hole specimen in order to determine the stress distribution at the critical region, $\sigma_y(x, 0)$, following a single load cycle. Each one of the three analyses was based, in turn, upon one of the following assumptions concerning material behavior and loading conditions: (1) purely elastic behavior, (2) elastoplastic behavior without unloading, and (3) elastoplastic behavior with elastic unloading. Only the last analysis yields residual stresses and the corresponding variable R -ratio distribution, and is given by Fig. 6. It is noteworthy that the R -ratio is approximately -0.4 at the surface of the hole and it remains negative for a depth of 0.05334 cm which is deeper than most of the cracks found by fractographic examination.

Crack Modeling and the Effective Stress Intensity Factor

The stress intensity factor, $K(s)$, along the crack front of a part-through surface crack emanating from the hole is a complex 3D problem. However, a method developed by Besuner [3] and Cruse and Besuner [4] to estimate the effective stress intensity factor(s) for through and part-through cracks with complex configurations in variable stress fields has been shown to be quite useful. Essentially the Besuner-Cruse method introduces the concept of an effective stress intensity factor which can be identified as the area rms (root-mean-square) value of the varying stress intensity factor, $K(s)$, where s is the crack-tip boundary, for the corresponding increment of

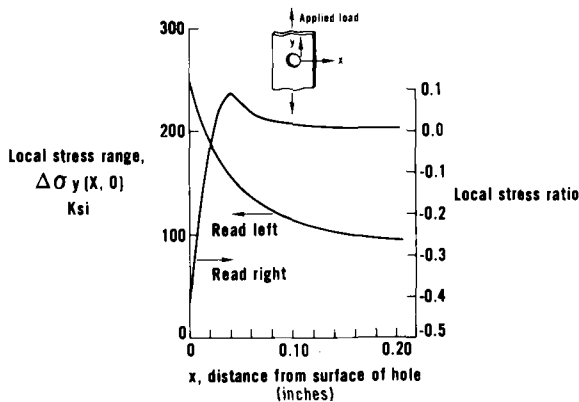


FIG. 6—Stress range and stress ratio near the bolt-hole (1 in. = 2.54 cm; 1 ksi = 0.1450 MN/m²).

surface area. In other words, the effective stress intensity factor is an area-weighted function of the point function, $K(s)$. Furthermore, since K_{ii} , the effective stress intensity factor is related to the energy release rate obtained by the perturbation of its corresponding freedom, a_{ii} , alone, then a two degree-of-freedom (DOF) crack model corresponds to an elliptical crack, which appears to be a particularly appropriate model for a surface crack emanating from a hole.

Life Prediction

The life prediction studies were based on a two DOF crack model using the effective stress intensity approach and the baseline macrocrack growth relationship. The computer program which embodies the life prediction method requires an initial crack configuration, the assumed crack model (for example, two DOF), the stress distribution and the crack law. The initial crack (flaw) was assumed to be a semicircular surface crack with a 0.000762 cm radius. This choice was based on the characteristic size of the α phase, an hcp (hexagonal-close-packed) structure, which is found to develop microcracks in the slip bands that extend across the α phase during fatigue. The secondary β phase has a body-centered-cubic structure and is typically two to four times larger than the α phase and is rarely observed to be the initiation site of fatigue cracks.

Evaluation

The stress analyses used in this paper attempted to model with various degrees of accuracy the actual local condition in the bolt hole region. The fidelity of these analyses ranged from a simple two-dimensional elastic analysis to an analysis which models the first order effects of elastoplastic material behavior.

It is recognized that the plane stress assumptions used here neglect the truly three-dimensional nature of the problem. It is known from elastic three-dimensional stress analysis [6, 7] of thick plates with circular cylindrical holes that the maximum stress concentration factor, SCF, occurs at the midplane and not at the plate surface and is a function of Poisson's ratio and (thickness/hole diameter). For the bolt-hole specimen (Fig. 1) the maximum SCF is estimated to be 7 percent greater than at the surface. In addition, unlike the plate surface which is subject to uniaxial stress, the midplane region of the plate (at the hole surface) is under a biaxial state of stress [8] and Weiss [9] has shown for several titanium alloys that the material ductility is reduced markedly by the degree of biaxiality present (by as much as a factor of five and greater). Although three-dimensional elastoplastic analyses are within the current state of the art, such analyses cannot yet be considered to be practical design tools due to

their complexity and expense. For this reason a three-dimensional elastoplastic analysis was not used in this study. However, three-dimensional analyses may provide valuable information that could be factored into the design procedure.

A comparison of the predicted crack growth behavior is given by Fig. 7. It should be pointed out that any life estimate is strongly dependent upon the assumed initial crack size, so that the only meaningful comparison permitted is the one between the predictions, since an initial crack size can be chosen so that any one of the predictions can be made to coincide with the average test life. It is evident from Fig. 7 that the accuracy with which the actual stress field is modeled has a significant effect on the predicted life. It can be concluded that the residual stress field (R ratio) cannot be neglected without introducing serious error.

Comparison of actual and predicted crack morphologies can be useful in evaluating the accuracy of current fracture mechanics modeling techniques. Such comparisons were made with respect to two parameters: (a) aspect ratio of the elliptical crack versus crack area, Fig. 3, and (b) crack depth versus crack area, Fig. 8. The bolt-hole region stress field used in the prediction model was the elastoplastic analysis with unloading as shown in Fig. 7. Within the limits just discussed, this stress analysis most faithfully models the actual stress fields.

No correlation (see Fig. 3) was found between actual and predicted aspect ratios. A fourth analysis (not shown in Fig. 7) which attempted to model the large compressive surface layer stresses due to machining operations showed a minor effect on the predicted crack aspect ratios. This result suggests that the area-weighted effective stress intensity factor may not be appropriate for very small surface cracks. On the other hand, the multiple crack initiation sites found at the surface of the hole may suggest

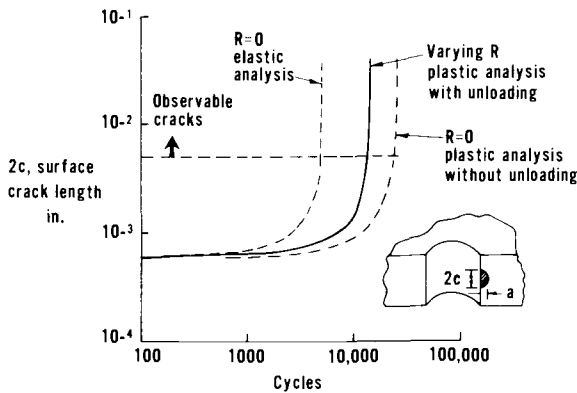


FIG. 7—Comparison of three growth simulations showing sensitivity to stress analyses used ($1 \text{ in.} = 2.54 \text{ cm}$).

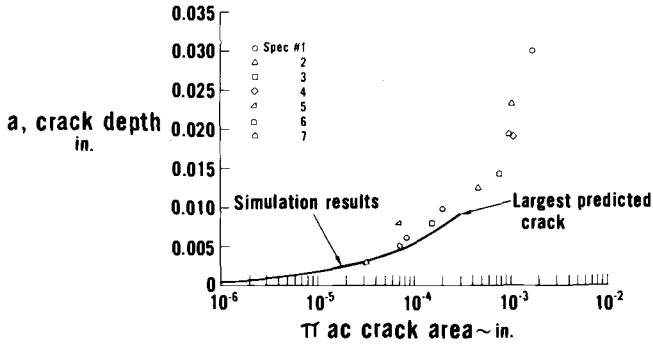


FIG. 8—Comparison of measured and predicted crack depths (1 in. = 2.54 cm).

that the crack modeling is too simplistic, that is, a single dominant crack without interaction of neighboring microcracks.

Koterazawa [5] in a fractographic study of surface and subsurface cracking in aluminum alloys and carbon steels, found that at the surface a crack propagated discontinuously by coalescence of the main crack with a microcrack ahead of it. In other words, the surface crack extended intermittently through the repetition of microcrack initiation. He found that the interior cracks propagated continuously forming a striation in each stress cycle. He suggested that the observed differences in crack growth behavior may be related to the degree of constraint between surface crystals and interior crystals.

Agreement (see Fig. 8) between actual and predicted crack depths was good for small crack depths; however, for cracks deeper than 0.0254 cm, there was a total lack of agreement.

Since the crack aspect ratio, $2c/a$, was found to vary from 1.2 to 2.3 (Fig. 3), the prediction method was used to estimate the crack growth rate for two specific aspect ratios 1.0 and 2.1. These estimates are shown in Fig. 4 and it is readily seen that there is little agreement with the measured striation spacing data. This is additional evidence that the crack model is too simplistic or that the effective stress intensity concept is not appropriate for very small surface part-through cracks.

Since striation spacing is equivalent to local crack growth rate, $(\Delta a/\Delta N)$, and the factor ΔK can be estimated from the two DOF model, a comparison of the local and baseline (macrocrack) growth behavior can be made. The striation spacing measurements, Fig. 4, were used together with the calculated ΔK results for various crack depths to make the comparison shown in Fig. 9. In addition, the predicted da/dN versus ΔK for the varying R -ratio analysis is included in Fig. 9. It is clear that the prediction does not agree with the results based on striation measurements. Furthermore, the striation measurements and baseline data show little agreement.

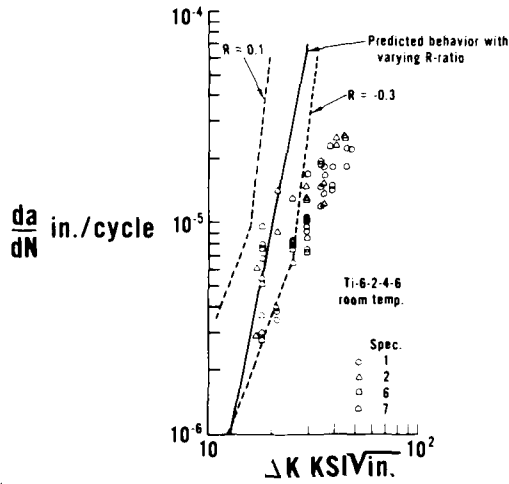


FIG. 9—Comparison of constant amplitude baseline data with striation measurements on bolt-hole specimens (1 in. = 25.4 cm; 1 ksi $\sqrt{\text{in.}}$ = 1.099 MN/m $^{3/2}$).

However, it must be noted that the points indicating striation spacing measurements are based on calculated values of ΔK which in turn have been deduced from the stress analysis and the effective K calculations. Therefore, there are several potential sources of error which make it difficult to draw definite conclusions concerning the lack of correlation. Nevertheless, the use of striation spacing measurements to deduce load or stress levels and fatigue life, does not seem to be applicable for Ti-6-2-4-6.

Conclusions

This study was an attempt to evaluate the current design state of the art for life prediction of components with small surface cracks emanating from highly stressed (plastic) regions. It is clear that many issues require further experimental and analytical work before accurate fatigue life prediction for such situations in real structures is possible. These issues include definition of material properties within the surface layer, the surface “values” of the stress intensity factor distribution, crack growth through highly varying stress/material property fields at the surface, and the applicability of macrocrack growth models to small cracks.

Acknowledgments

The authors gratefully acknowledge the partial support of this effort by the Air Force Aero Propulsion Laboratory, Contract F33615-75-C-2063 under the direction of R. J. Hill/TBP, Project Engineer.

References

- [1] Cruse, T. A. and Meyer, T. G., "A Cumulative Fatigue Damage Model for Gas Turbine Engine Disks Subjected to Complex Mission Loading," ASME Paper 78-WA/GT-14, *Journal of Engineering for Power*, to appear.
- [2] Cruse, T. A., Meyers, G. J., and Wilson, R. B. in *Flow Growth and Fracture, ASTM STP 631*, American Society for Testing and Materials, 1977, pp. 174-189.
- [3] Besuner, P. M. in *Mechanics of Crack Growth, ASTM STP 590*, American Society for Testing and Materials, 1976, pp. 403-419.
- [4] Cruse, T. A. and Besuner, P. M., *Journal of Aircraft*, Vol. 12, No. 4, April 1975, pp. 369-375.
- [5] Koterazawa, R. in *Proceedings, International Conference on Mechanical Behavior of Materials*, Vol. 2, Fatigue of Materials, Kyoto, 15-20 Aug., 1971, pp. 209-217.
- [6] Green, A. E. in *Transactions, Royal Society, Series A*, 1948, 240, pp. 561-597.
- [7] Rubayi, N. A. and Yadava, V., *Journal of Strain Analysis*, Vol. 8, No. 3, 1973, pp. 220-226.
- [8] Quesnel, D. J. and Meshii, M., *Journal of Testing and Evaluation*, Vol. 4, No. 5, Sept. 1976, pp. 319-326.
- [9] Weiss, V. in *Proceedings, International Conference on Mechanical Behavior of Materials*, Vol. 1, 1972, pp. 458-474.

A Review and Assessment of the Stress-Intensity Factors for Surface Cracks

REFERENCE: Newman, J. C., Jr., "A Review and Assessment of the Stress-Intensity Factors for Surface Cracks," *Part-Through Crack Fatigue Life Prediction*. ASTM STP 687, J. B. Chang, Ed., American Society for Testing and Materials, 1979, pp. 16-42.

ABSTRACT: The stress-intensity factor solutions proposed for a surface crack in a finite plate subjected to uniform tension are reviewed. Fourteen different solutions for the stress-intensity factors are compared. These solutions have been obtained over the past 16 years using approximate analytical methods, experimental methods, and engineering estimates.

The present paper assesses the accuracy of the various solutions by correlating fracture data on surface-cracked tension specimens made of a brittle epoxy material. Fracture of the epoxy material was characterized by a constant value of stress-intensity factor at failure. Thus, the correctness of the various solutions are judged by the variations in the stress-intensity factors at failure. The solutions were ranked in order of minimum standard deviation. The highest ranking solutions correlated 95 percent of data analyzed within ± 10 percent, whereas, the lowest ranking solutions correlated 95 percent of data analyzed within ± 20 percent. However, some solutions could be applied to all data considered, whereas, others were limited with respect to crack shapes and crack sizes that could be analyzed.

KEY WORDS: fracture properties, fracturing, mechanical properties, stresses, cracks, fatigue (materials), crack propagation

Nomenclature

- a Depth of surface crack, m
- c Half-length of surface crack, m
- F Boundary-correction factor on stress intensity
- K Mode I elastic stress-intensity factor, $\text{N}/\text{m}^{3/2}$
- K_{cr} Fracture toughness, $\text{N}/\text{m}^{3/2}$

¹ Research engineer, NASA-Langley Research Center, Hampton, Va. 23665.

$M_e, M_k, M_s, M_t, M_1, M_2$	Magnification factors defined in text
n	Number of data analyzed
Q	Elastic shape factor for an elliptical crack
S	Gross-section stress, N/m ²
t	Specimen thickness, m
W	Specimen width, m
σ	Standard deviation
Φ	Complete elliptic integral of second kind
ϕ	Parametric angle of ellipse

Surface cracks [1,2]² are among the most common flaws in many practical structures. Accurate stress-intensity factors for surface cracks are needed for reliable prediction of crack-growth rates and fracture strengths. Exact solutions are not available, but solutions have been obtained by approximate methods. However, due to the difficulties involved, these approximate solutions differ considerably.

In 1973, Merkle [3] and Keays [4] presented reviews of some of the earlier stress-intensity factor solutions for the surface crack. Since these reviews, the number of proposed solutions have nearly doubled. The objective of the present paper was to review the stress-intensity factor solutions proposed for the surface crack in a finite plate subjected to uniform tension and to assess the accuracy of the various solutions by correlating fracture data on a brittle material. Fourteen stress-intensity factor solutions were reviewed. Other solutions, those that had severe limitations on crack shape and crack size, were not considered in the assessment. This review was limited to linear-elastic analyses and to application to brittle materials.

The present assessment of the 14 solutions was based on correlating fracture data. Fracture data from a large number of tests on surface-cracked tension specimens made of a brittle epoxy material were available in the literature [5]. In these data, the crack-depth-to-specimen-thickness ratios ranged from 0.15 to 1 and the crack-depth-to-crack-length ratios ranged from 0.3 to 0.84. Fracture of the epoxy material was characterized in the present paper by a constant value of stress-intensity factor at failure. Thus, the correctness of the various solutions was judged by the variations in the stress-intensity factors at failure, and the solutions were ranked in order of minimum standard deviation. The range of applicability of the various solutions also was considered in assessing their usefulness.

Elastic Stress-Intensity Factors

The stress-intensity factor solutions for cracks in finite plates usually are expressed in terms of a boundary-correction factor that modifies the stress-

²The italic numbers in brackets refer to the list of references appended to this paper.

intensity factor for cracks in infinite bodies. Thus, the elastic solution for an elliptical crack embedded in an infinite solid (Fig. 1) has a major role in the surface-crack solution. In this section, a brief review of the stress-intensity factors for the elliptical crack embedded in an infinite solid and the form of stress-intensity factor for the surface crack in a finite plate are presented.

Infinite Solid

Irwin [1] derived an exact expression for the Mode I stress-intensity factor around an elliptical crack in an infinite elastic solid subjected to uniform tension (Fig. 1) based on an exact stress analysis by Green and Sneddon [6]. The stress-intensity factor along the boundary of the elliptical crack was given by

$$K = \frac{S\sqrt{\pi a}}{\Phi} \left(\frac{a^2}{c^2} \cos^2 \phi + \sin^2 \phi \right)^{1/4} \quad (1)$$

where Φ is the complete elliptic integral of second kind and is given by

$$\Phi = \int_0^{\pi/2} \left(\sin^2 \phi + \frac{a^2}{c^2} \cos^2 \phi \right)^{1/2} d\phi \quad (2)$$

As is customary, the elliptic integral is expressed in terms of the elastic shape factor, Q . The shape factor Q equals Φ^2 .

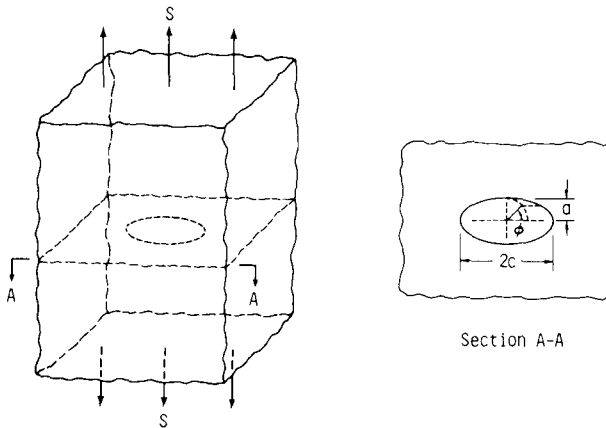


FIG. 1—Embedded elliptical crack in an infinite solid subjected to uniform stress.

Very useful empirical expressions for Q have been developed by Rawe [3]. The expressions are

$$Q = 1 + 1.464 \left(\frac{a}{c}\right)^{1.65} \quad \text{for } \frac{a}{c} \leq 1 \quad (3a)$$

$$Q = 1 + 1.464 \left(\frac{c}{a}\right)^{1.65} \quad \text{for } \frac{a}{c} > 1 \quad (3b)$$

The maximum error in the stress-intensity factor by using these equations for Q was about 0.13 percent for all values of a/c . (Rawe's original equation was written in terms of $a/2c$.)

For $c > a$ the maximum stress-intensity factor is at $\phi = \pi/2$ and is given by

$$K = S \sqrt{\pi \frac{a}{Q}} \quad (4)$$

Finite Plate

The surface crack in a finite plate is shown in Fig. 2. The crack is semi-elliptical with a crack of half-length c and of depth a . The plate is of thickness t and width, W , which is usually large with respect to the crack length. The configuration is subjected to a uniform tensile stress, S , normal to the crack plane. The form of the Mode I stress-intensity factor is given by

$$K = S \sqrt{\pi \frac{a}{Q}} F\left(\frac{a}{t}, \frac{a}{c}, \frac{c}{W}, \phi\right) \quad (5)$$

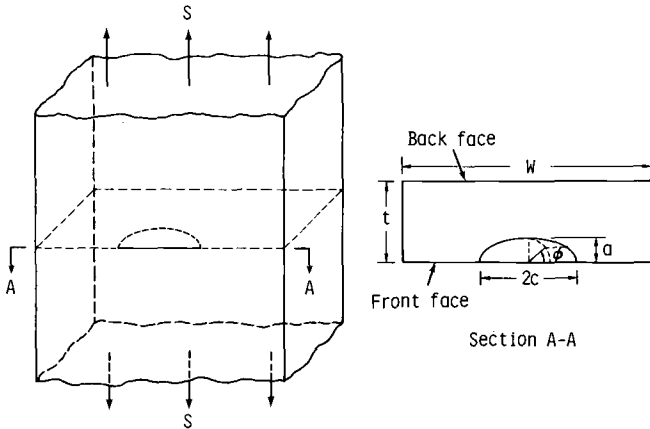


FIG. 2—Surface crack in a finite plate subjected to uniform stress.

The boundary-correction factor, F , accounts for the influence of the front face, back face, and finite width on the stress-intensity factor for a crack in an infinite solid. The parametric angle is defined in the insert on Fig. 2. Many analysts, through approximation techniques, have tried to determine the correct expression for F . Some of the approximate methods used were the alternating method, finite-element method, boundary-integral equations, method of lines, line-spring model, experimental methods, and engineering estimates.

In the Appendix, 14 solutions [1,7-24] for the boundary-correction factor, F , are presented. Table 1 gives the chronological order of development for these solutions, the method used, limitations on a/c , a/t and $2c/W$, and the form of the results. The solutions were given in either graphical or equation form. Most solutions were proposed for analyzing fracture of surface-cracked tension specimens and give the stress-intensity factor at the maximum depth point. A few give the stress-intensity factors at other locations along the crack front for a/c ratios greater than about 0.6. Some solutions also included plasticity corrections for analyzing fracture of ductile materials. However, in the present paper only the elastic solutions are presented and used.

Comparison of Stress-Intensity Correction Factors

Figures 3 to 6 show a comparison among the various stress-intensity correction factors for the surface crack subjected to uniform tension for some common crack shapes (a/c) as a function of a/t . Figure 3 shows the stress intensity correction factor, F , at the maximum depth point ($\phi = \pi/2$) for a crack with an a/c ratio of 0.2. The stress-intensity factor at the maximum depth point was also the maximum stress-intensity value. The solid and dashed curves show correction factors obtained from equations and graphs, respectively. These results show that for a/t ratios less than about 0.2, most solutions were in good agreement (± 5 percent). However, for a/t ratios greater than 0.2, the differences among the various solutions were considerable. The percentage differences were as large as 80 percent for an a/t ratio of 0.6. The upper solid line at $a/t = 1$ ($F = 2.35$) denotes the equivalent correction factor for a through crack of length $2c$ in an infinite plate. This is the approximate limiting value for the surface crack as a/t approaches unity.

Figure 4 shows the correction factor at the maximum-depth point but for a crack with an a/c ratio of 0.6. The stress-intensity factor at $\phi = \pi/2$ was also the maximum stress intensity for most solutions which reported the variation in stress intensity along the crack front [3,18,22]. In Ref 22, for an a/t ratio of 0.8, the maximum stress intensity did not occur at the maximum depth point but occurred near the intersection of the crack with the front face ($\phi = 0$). Figure 4 shows that for a/t ratios less than about

TABLE 1—Stress-intensity factor solutions for surface crack in chronological order.

Investigator(s)	Date	Ref	Method ^a	Limitations			Form of Results
				a/t	a/c	$2c/W$	
Irwin	1962	1	EE	≤ 0.5	0 to 1	b	equation
Paris-Sih	1965	7	EE	≤ 0.75	0 to 1	b	equation
Smith	1966	3,8	AM and EE	$f(a/c)$	0.2 to 1	b	graph
Kobayashi-Moss	1969	10	AM and EE	≤ 0.98	0 to 1	b	graph
Masters-Haese-Finger	1969	11	EM	≤ 0.85	0.1 to 0.8	b	graph
Smith-Alavi	1969	13	AM and EE	≤ 0.8	0.4 to 1	b	graph
Rice-Levy	1970	14	LSM	≤ 0.7	0 to 1	b	graph
Anderson-Holms-Orange	1970	15	EE	≤ 1.0	0 to 1	b	equation
Newman	1972	16	EE	≤ 1.0	0.02 to ∞	< 1	equation
Shah-Kobayashi	1972	17	AM	≤ 0.9	0.1 to 1	b	graph
Smith-Sorensen	1974	19	AM	≤ 0.9	0.1 to 1	b	graph
Kobayashi	1976	20	AM and EE	≤ 0.9	0.2 to 1	b	graph
Raju-Newman	1977	21,22	FEM	≤ 0.8	0.2 to 2	b	graph
Newman-Raju	1978	24	FEM and EE	≤ 1.0	0.03 to ∞	$< .5$	equation

^a Engineering estimate (EE), alternating method (AM), line-spring model (LSM), finite-element method (FEM).

^b Effects of finite width were not considered.

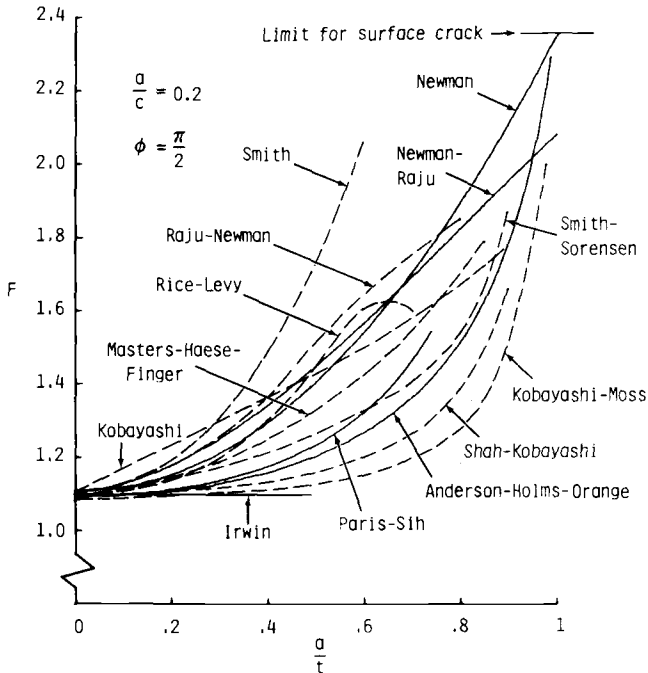


FIG. 3—Stress-intensity correction factor at maximum depth point for semi-elliptical surface crack ($a/c = 0.2$).

0.3, most solutions agree within about 5 percent. For an a/t ratio of 0.6, the percentage difference between the upper and lower bounds was about 20 percent. Again, the upper solid line at $a/t = 1$ ($F = 1.65$) denotes the approximate limiting value for the surface crack as a/t approaches unity.

Figures 5 and 6 show the correction factor at $\phi = \pi/2$ and the maximum value, respectively, for a semi-circular surface crack ($a/c = 1$). The maximum stress-intensity factor occurred at or near the intersection of the crack with the front surface, $\phi = 0$. Some of the 14 solutions reviewed were not included in these figures because they did not consider the semi-circular crack or because their results should not be applied to these particular values of ϕ . Figure 5 shows that all solutions, except the estimate from Irwin [1], agree within about 5 percent for a/t ratios less than 0.4. For larger a/t ratios, the percentage difference was as large as 35 percent. The results from Hellen and Blackburn [27] (not included in the 14 solutions reviewed) have also been included in Fig. 5 for comparison. Hellen and Blackburn analyzed only the semicircular surface crack using a three-dimensional finite-element analysis.

Figure 6 shows the maximum stress-intensity factors for semi-circular

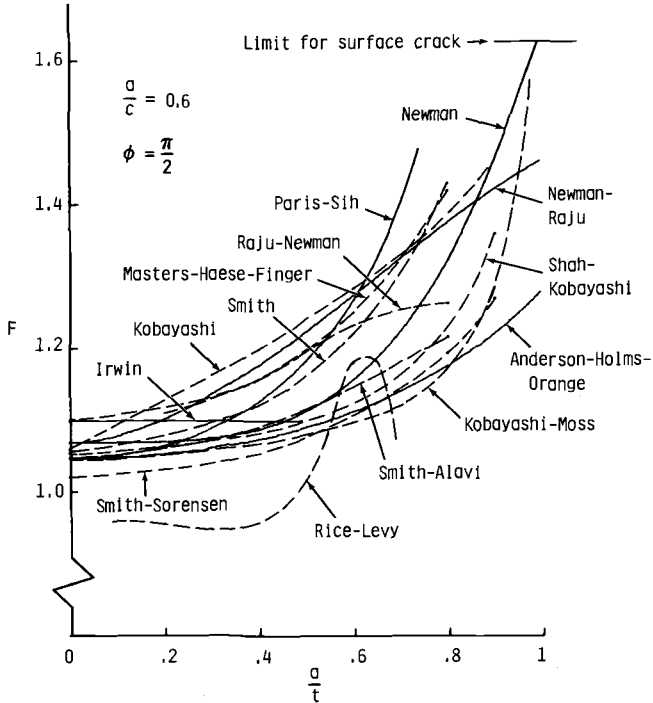


FIG. 4—Stress-intensity correction factor at maximum depth point for semi-elliptical surface crack ($a/c = 0.6$).

surface cracks as calculated by four investigators. The maximum stress-intensity values reported in the literature [3,21,27], occurred at or near the intersection of the crack with the front face. Again, the finite-element results from Hellen and Blackburn [27] and unpublished results from Kobayashi also have been included for comparison. The results from Kobayashi were obtained using the analysis described in Ref 20. For a/t ratios less than 0.3, the solutions were in good agreement. However, for larger a/t ratios, the solutions generally disagree (as much as 30 percent). The results from Kobayashi and Raju and Newman [21] were in good agreement (within 5 percent).

Some of the differences shown in Figs. 3 to 6 may be attributed to improper boundary conditions imposed on the surface-crack configuration. Some of the earlier stress-intensity factor solutions [10,17] did not analyze the surface-crack configuration, but analyzed approximate configurations for which solutions could be readily obtained, such as an elliptical crack approaching a free boundary in a semi-infinite solid [18] or two elliptical cracks approaching each other in an infinite solid. Kobayashi [20] also has demonstrated that his earlier applications of the alternating method inad-

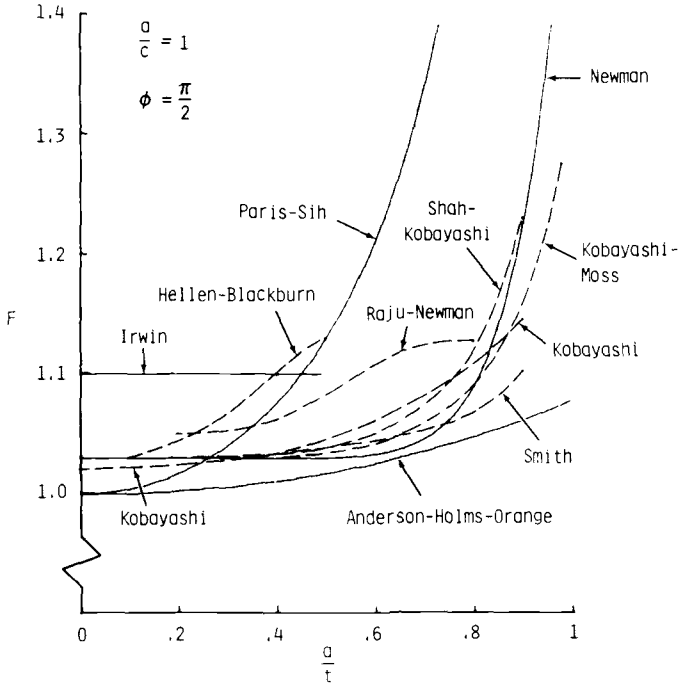


FIG. 5—Stress-intensity correction factor at maximum depth point for semi-circular surface crack ($a/c = 1$).

vertently induced improper bending restraint by limiting the areas of front and back faces that are free of residual surface tractions. The more recent analyses of the surface crack [21,26,27] have used the finite-element method and any inaccuracies in these analyses would be associated with modeling the surface crack and with how well the governing equations in the interior were satisfied.

Analysis of Fracture Data

The accuracy of the stress-intensity factor solutions, previously reviewed, were verified independently herein by analyzing fracture data from the literature on brittle epoxy materials. These data had a wide range in crack shape (a/c) and crack size (a/t). Solutions which gave the best correlation of data and which applied over the widest range of a/c and a/t were regarded as the most useful.

Smith [5] conducted fracture tests on a large number of surface-crack tension specimens made of a brittle epoxy material (ultimate tensile strength of about 60 MPa). All his specimens were 25 mm wide and had

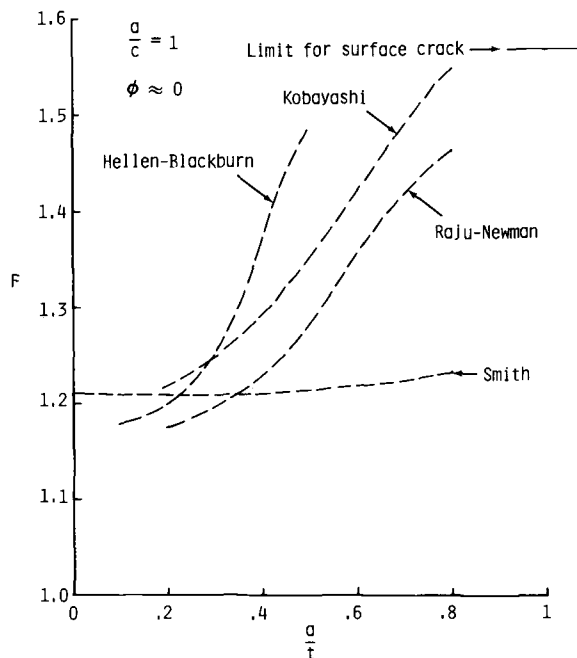


FIG. 6—Maximum stress-intensity correction factor for semi-circular surface crack ($a/c = 1$).

thicknesses ranging from 2.5 to 9.5 mm. He conducted 150 fracture tests on specimens with a/t ratios that ranged from 0.15 to 1 and a/c ratios that ranged from 0.3 to 0.84. The specimens were arranged into five different groups. Each group of specimens was manufactured at a different time (denoted with a “plate date”) and each group had the same specimen thickness. The estimated plane-strain plastic-zone size using the largest value of fracture toughness (computed) was about 0.015 mm. This estimated plastic-zone size was orders of magnitude smaller than the minimum specimen thickness. The extremely small plastic zone indicates that linear-elastic analyses are adequate.

The 14 stress-intensity factor solutions presented in the Appendix were used herein to analyze Smith’s fracture data on epoxy specimens. Fracture was characterized herein by a constant value of stress-intensity factor at failure (denoted as K_{cr}). The fracture toughness, K_{cr} , for each group of specimens was calculated for each solution by averaging the stress-intensity factors at failure for data where the a/t ratios were less than 0.5 and was given by

$$K_{cr} = \frac{1}{n} \sum_{i=1}^n K_i \quad (6)$$

where n is the number of data analyzed for each group of specimens. This particular limit on a/t was chosen because, as previously mentioned, for low a/t ratios most solutions were in fair agreement. Thus, the calculated fracture toughness values would also be in fair agreement. The fracture toughness values computed from the various solutions for each group of specimens are given in Table 2. As expected, the maximum and minimum K_{cr} values from the various solutions for each "plate date" material were in fair agreement (within ± 10 percent of their average value).

Assessment of the Solutions

To assess the accuracy of the various stress-intensity factor solutions, comparisons are made between the calculated stress-intensity factors at failure and the fracture toughness, K_{cr} , for all fracture data considered ($0.15 \leq a/t \leq 1$; $0.3 \leq a/c \leq 0.84$). Thus, for a/t ratios greater than 0.5, these comparisons show how well the various solutions predict failure of the epoxy specimens. Fracture data which exceeded the limitations on a/t or a/c for each solution (see Table 1) were not included in the analysis using that particular solution.

Figures 7 through 20 show the ratio of the stress-intensity factor at failure normalized by the fracture toughness, K_{cr} , plotted against the a/t ratio for each solution. The fracture toughness values used for each group of specimens are given in Table 2. The solid line at unity denotes perfect agreement and the dashed lines denote ± 10 percent scatter. Stress-intensity factor ratios (K/K_{cr}) that deviate substantially from unity indicate

TABLE 2—Fracture toughness, $K_{cr}(kN/m^{3/2})$ for brittle epoxy material calculated from various stress-intensity factor solutions.

Investigator(s)	Plate Date				
	8-7-69	10-6-70	12-5-70	4-11-71	6-10-71
Irwin	686	634	678	664	681
Paris-Sih	653	648	692	672	684
Smith	697	670	699	697	710
Kobayashi-Moss	654	609	658	652	670
Masters-Haese-Finger	699	663	712	696	704
Smith-Alavi	659	619	671	664	680
Rice-Levy	597	565	599	613	640
Anderson-Holms-Orange	646	608	660	674	693
Newman	658	616	670	674	693
Shah-Kobayashi	653	610	659	653	671
Smith-Sorensen	638	604	652	652	670
Kobayashi	676	661	733	729	741
Raju-Newman	708	697	724	716	729
Newman-Raju	677	682	731	713	723

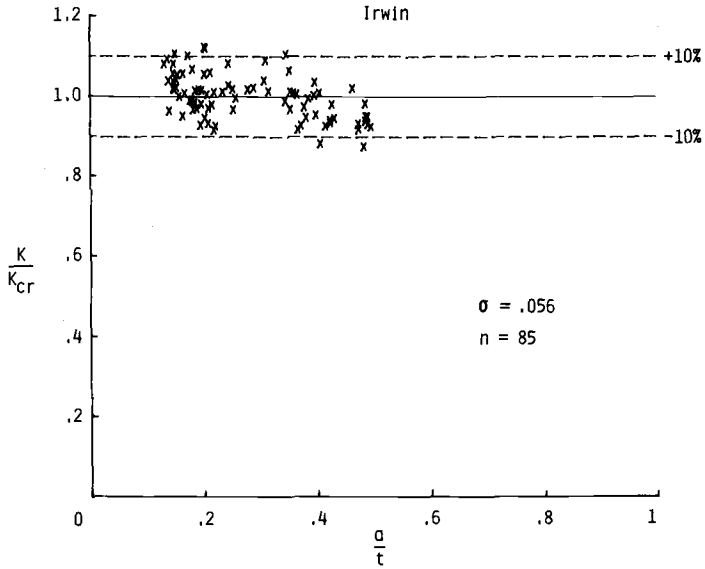


FIG. 7—Correlation of brittle-epoxy fracture data using the Irwin [1] solution.

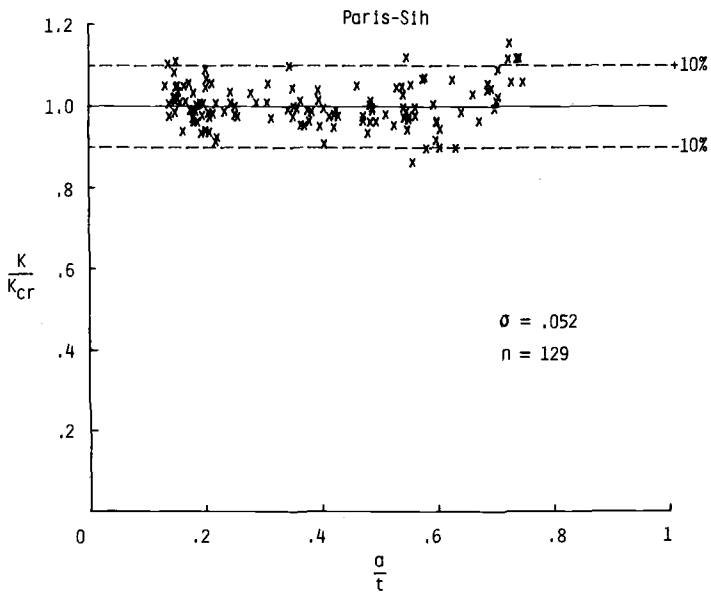


FIG. 8—Correlation of brittle-epoxy fracture data using the Paris-Sih [7] solution.

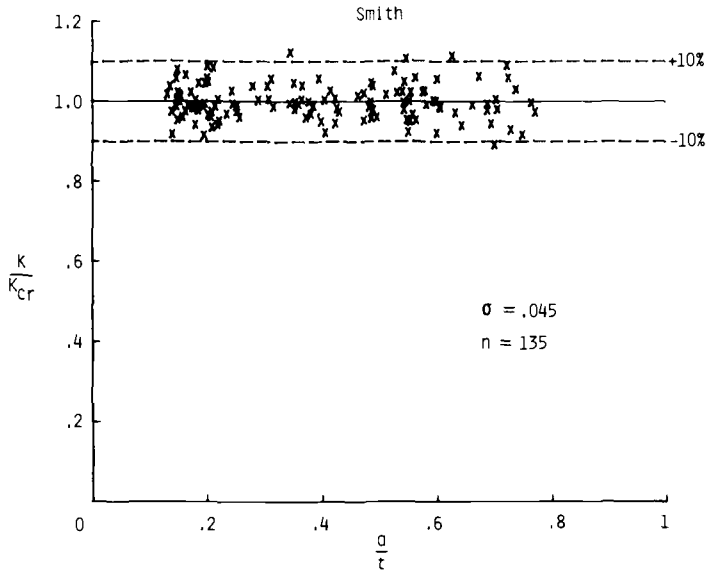


FIG. 9—Correlation of brittle-epoxy fracture data using the Smith [3,8] solution.

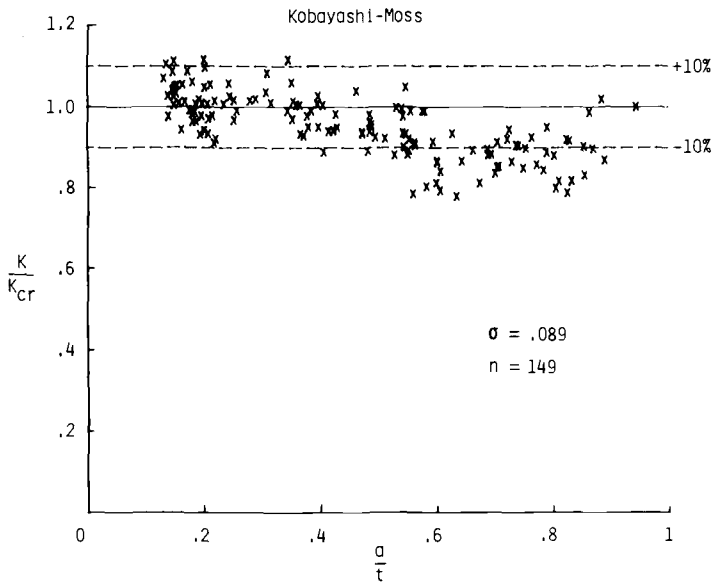


FIG. 10—Correlation of brittle-epoxy fracture data using the Kobayashi-Moss [10] solution.

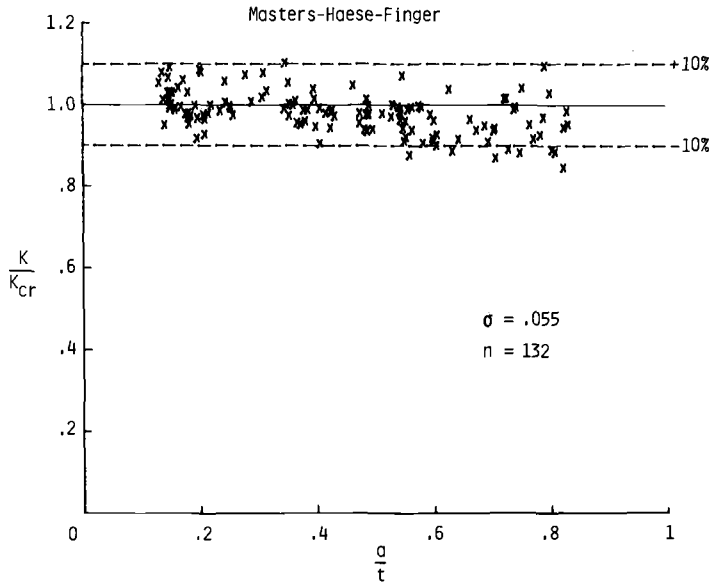


FIG. 11—Correlation of brittle-epoxy fracture data using the Masters-Haese-Finger [11] solution.

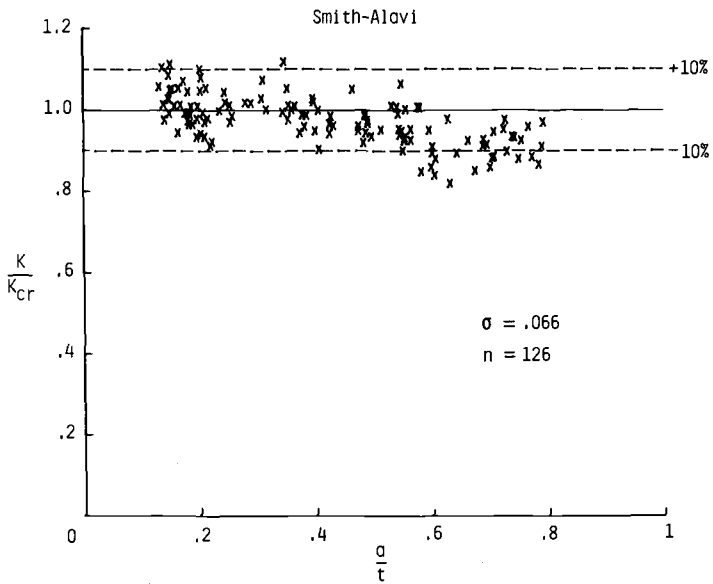


FIG. 12—Correlation of brittle-epoxy fracture data using the Smith-Alavi [13] solution.

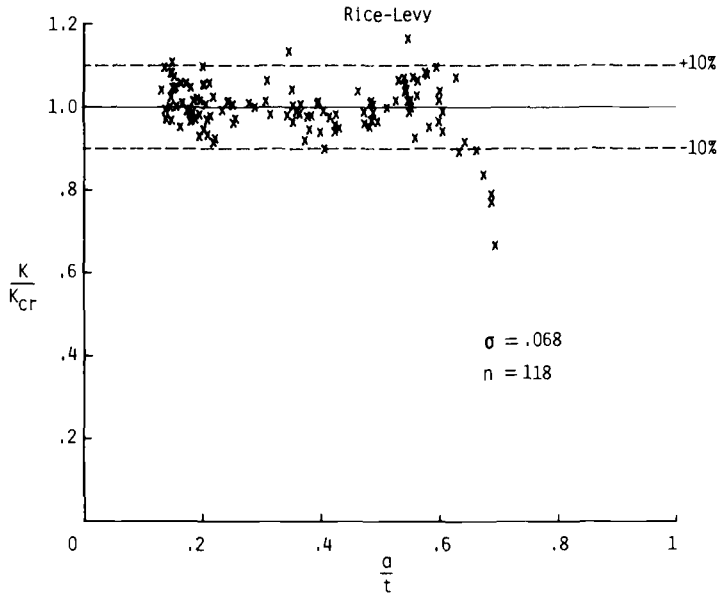


FIG. 13—Correlation of brittle-epoxy fracture data using the Rice-Levy [14] solution.

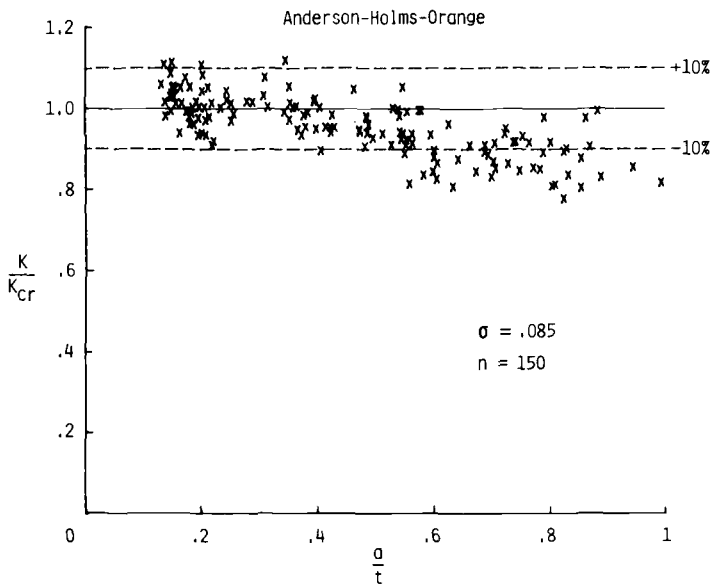


FIG. 14—Correlation of brittle-epoxy fracture data using the Anderson-Holms-Orange [15] solution.

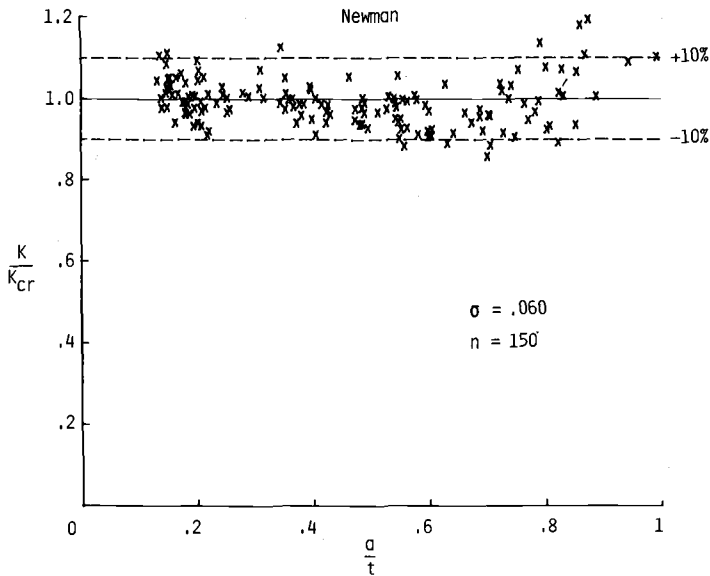


FIG. 15—Correlation of brittle-epoxy fracture data using the Newman [16] solution.

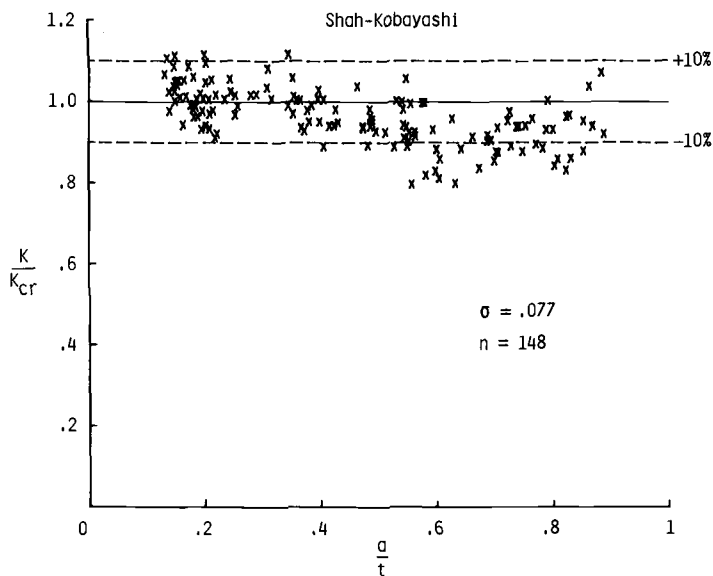


FIG. 16—Correlation of brittle-epoxy fracture data using the Shah-Kobayashi [17] solution.

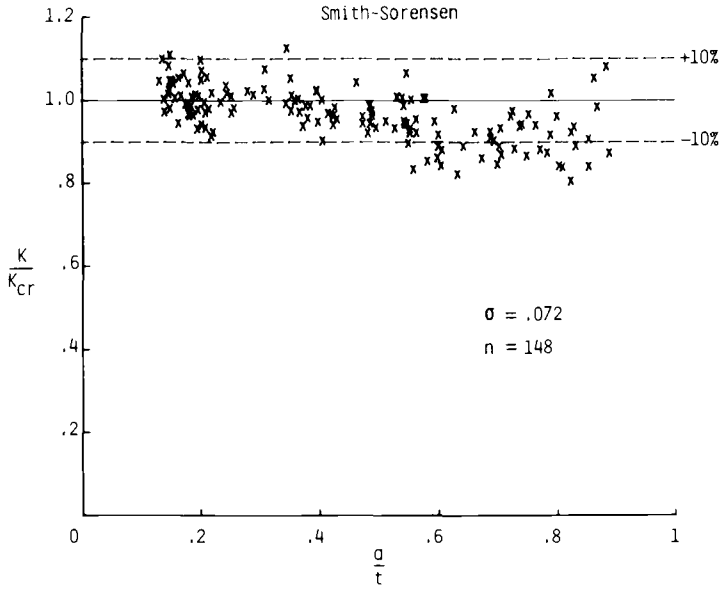


FIG. 17—Correlation of brittle-epoxy fracture data using the Smith-Sorensen [19] solution.

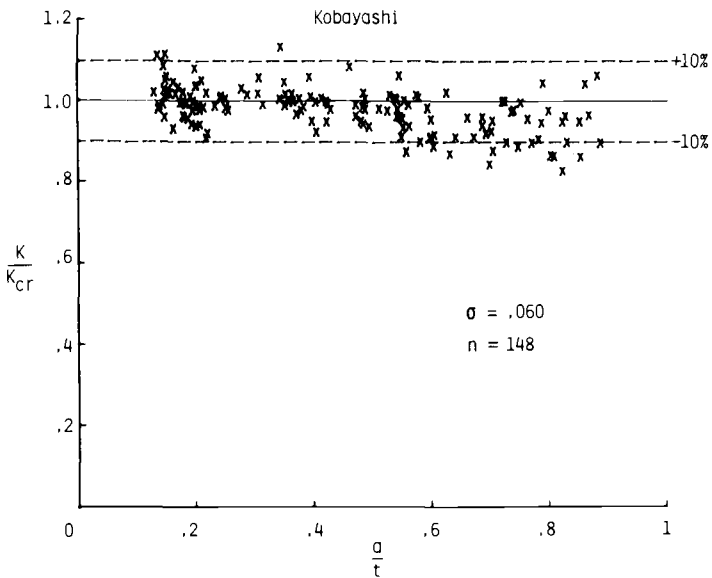


FIG. 18—Correlation of brittle-epoxy fracture data using the Kobayashi [20] solution.

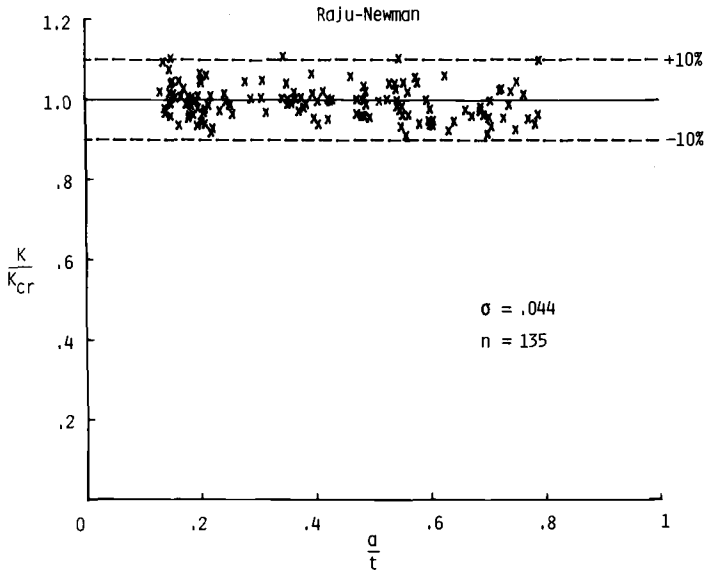


FIG. 19—Correlation of brittle-epoxy fracture data using the Raju-Newman [21,22] solution.

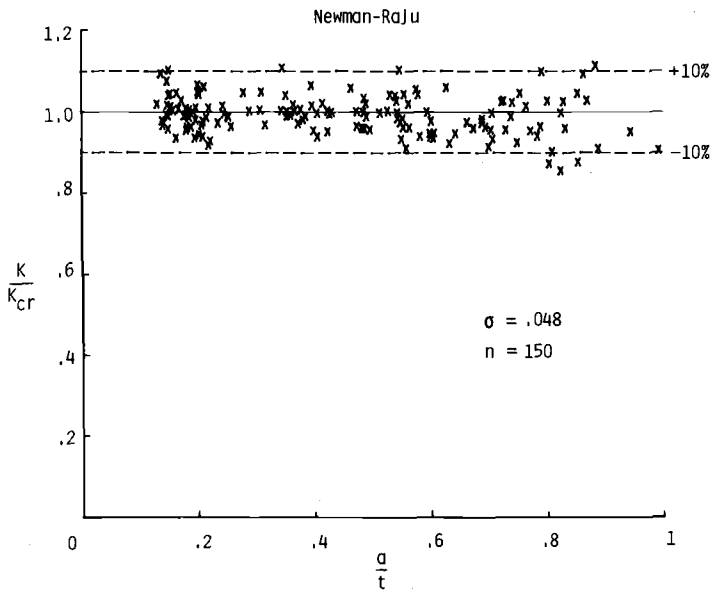


FIG. 20—Correlation of brittle-epoxy fracture data using the Newman-Raju [24] solution.

substantial deficiencies in that particular solution. (The ratio of K/K_{cr} is equivalent also to the ratio of experimental failure stress to predicted failure stress.) The standard deviation (σ) and the number of tests analyzed (n) are also shown on each figure.

To rank the various solutions, the standard deviation was calculated from the results for each stress-intensity factor solution. The standard deviation was given by

$$\sigma = \sqrt{\frac{\sum_{i=1}^n e_i^2}{n-1}} \quad (7)$$

where n is the number of data points analyzed and

$$e_i = \frac{K_i}{K_{cr}} - 1 \quad (8)$$

K_i is the stress-intensity factor at failure for each data point considered and K_{cr} is the fracture toughness for that particular group of specimens.

The ranking of the various solutions in order of minimum standard deviation is shown in Table 3. This table shows the investigator(s), date of publication, limitation on a/t , percent of data analyzed, standard deviation, and the form of the results for each solution. The standard deviations ranged from 0.044 to 0.089 for the 14 solutions considered. Assuming a normal distribution, two standard deviations ($\pm 2\sigma$) about the mean ($K/K_{cr} = 1$) form bounds in which 95 percent of the data should fall. The highest ranking solutions correlated 95 percent of the data analyzed within ± 10 percent, whereas the lowest ranking solutions correlated 95 percent of the data analyzed within ± 20 percent. However, the percent of data analyzed ranged from 57 to 100 percent. Of the lowest ranking solutions, most underestimated the stress-intensity factors for a/t ratios greater than 0.5 (K/K_{cr} less than unity); and one solution (Newman, Fig. 15) overestimated the stress-intensity factors for a/t greater than about 0.8.

The stress-intensity factor solutions which gave low values of standard deviation tended to give large values for the correction factors shown in Figs. 3 to 5. Those solutions which used stress-intensity factors at locations other than the maximum-depth point for the near semicircular cracks (Figs. 9, 19, and 20), generally, gave low values of standard deviation. Only three solutions (Figs. 15, 19 and 20) used a finite-width correction on the stress-intensity factor for the surface crack. Analyses made with a finite-width correction gave slightly lower values of standard deviation than did the same analyses made without a width correction (see Table 3, Raju and Newman, 1977).

TABLE 3—Ranking of stress-intensity factor solutions for surface crack in order of minimum standard deviation.

Investigator(s)	Date	Ref	Limitation <i>a/t</i>	Percent of Data Analyzed	Standard Deviation	Form of Results
Raju-Newman	1977	21,22	0.8	90	0.044 ^a	graph
Smith	1966	3,8	$f(a/c)$	90	0.045	graph
Newman-Raju	1978	24	1.0	100	0.048	equation
Paris-Sih	1965	7	0.75	86	0.052	equation
Masters-Haese-Finger	1969	11	0.85	88	0.055	graph
Irwin	1962	1	0.5	57	0.056	equation
Newman	1972	16	1.0	100	0.060	equation
Kobayashi	1976	20	0.9	98	0.060	graph
Smith-Alavi	1969	13	0.8	84	0.066	graph
Rice-Levy	1970	14	0.7	79	0.068	graph
Smith-Sorensen	1974	19	0.9	98	0.072	graph
Shah-Kobayashi	1972	17	0.9	98	0.077	graph
Anderson-Holms-Orange	1970	15	1.0	100	0.085	equation
Kobayashi-Moss	1969	10	0.98	99	0.089	graph

^a Standard deviation without finite-width correction, f_w , was 0.048.

Concluding Remarks

The stress-intensity factor solutions proposed for a surface crack in a finite plate subjected to uniform tension were reviewed. These solutions have been developed over the past 16 years using approximate analytical methods, experimental methods, and engineering estimates. Comparison of the various solutions at the maximum depth point showed good agreement (± 5 percent) for crack-depth-to-specimen-thickness ratios less than about 0.3. However, for larger crack-depth-to-specimen-thickness ratios (0.3 to 1) the solutions were in considerable disagreement (20 to 80 percent), especially, for cracks with small crack-depth-to-crack-length ratios (0.2 to 0.6). Some of the discrepancies among the various solutions were attributed to improper boundary conditions imposed on the surface-crack configuration.

To assess the accuracy of the various solutions, fracture data on surface-crack tension specimens made of a brittle epoxy material were analyzed. The various solutions were ranked on the variation in the stress-intensity factors at failure. Standard deviations ranged from 0.044 to 0.089 for the 14 stress-intensity factor solutions considered. The solutions, ranked in order of minimum standard deviation, were Raju-Newman, Smith, Newman-Raju, Paris-Sih, Masters-Haese-Finger, Irwin, Newman, Kobayashi, Smith-Alavi, Rice-Levy, Smith-Sorensen, Shah-Kobayashi, Anderson-Holms-Orange, and Kobayashi-Moss. The highest ranking solutions correlated 95 percent of the data analyzed within ± 10 percent, whereas the lowest ranking solutions correlated 95 percent of data analyzed within ± 20 percent. However, some solutions were applied to all of the data considered, whereas others were limited on crack shapes and crack sizes that could be analyzed.

APPENDIX

Boundary-Correction Factors for Surface Cracks in Finite Plates

The 14 expressions for the boundary-correction factor, F , used in the text are briefly reviewed herein. The stress-intensity factor is given by Eq 5.

Irwin (1962) [1]—He estimated the boundary-correction factor for a shallow semi-elliptical surface crack in a finite-thickness plate at $\phi = \pi/2$ as

$$F = \sqrt{1.2} \approx 1.1 \quad (9)$$

The coefficient 1.1 accounted for the combined influence of both the front- and back-face effects in the range $0 \leq a/t \leq 0.5$ and $0 \leq a/c \leq 1$.

Paris and Sih (1965) [7]—They estimated the correction factor at $\phi = \pi/2$, which included a front- and back-face correction, as

$$F = \left[1 + 0.12 \left(1 - \frac{a}{c} \right) \right] \sqrt{\frac{2t}{\pi a} \tan \left(\frac{\pi a}{2t} \right)} \quad (10)$$

for $a/t \leq 0.75$ and $a/c \leq 1$. The "tangent" term was obtained from an analysis of an infinite plate (two dimensional) containing an infinite periodic array of cracks.

Smith (1966) [3,8]—He proposed a modification of the semi-circular surface crack solution [8] to obtain an estimate for a semi-elliptical surface crack in a finite-thickness plate under tension (Boeing Airplane Co., Structural Development Research Memorandum No. 17, August 1966 [3]). The solution presented in Ref 8, using the alternating method, was the first analysis to consider the variation of stress intensity around the crack front for a semi-circular surface crack in a semi-infinite solid.

For fracture, he proposed to use the maximum stress-intensity factor for which the correction factor was given by

$$F = M_1 M_2 f(\theta) \quad (11)$$

where M_1 and M_2 are the front- and back-face magnification factors, respectively, and $f(\theta)$ is an angular function [8] ($\theta = \pi/2 - \phi$). The maximum value of the product M_1 times $f(\theta)$ for various a/c ratios is

a/c	$M_1 f(\theta)$
0.2	1.09
0.4	1.075
0.6	1.06
0.8	1.07
1.0	1.21

The back-face magnification factor, M_2 , for $a/c = 1$ was obtained by Smith using the alternating method [3]. Using M_2 for $a/c = 1$ and the single edge-crack solution for $a/c = 0$ [9], curves of M_2 for other a/c ratios were estimated by graphical interpolation. The curves for M_2 have been reproduced in Ref 3 on page 25. These curves had various limitations on the maximum a/t ratio. For $a/c = 0.2$, the maximum a/t ratio was less than 0.6 and for $a/c = 1$, the maximum a/t ratio was less than about 0.9.

Kobayashi and Moss (1969) [10]—They estimated the correction factor as

$$F = M_1 M_2 \quad (12)$$

where M_1 , the front-face magnification factor, was given by

$$M_1 = 1 + 0.12 \left(1 - \frac{a}{c} \right)^2 \quad (13)$$

The back-face magnification factor, M_2 , was obtained from an existing solution for a pair of coplanar elliptical cracks under uniform tension, with a plane of symmetry (simulated back face) located midway between the two cracks [10]. Assuming no interaction between the front- and back-faces, boundary-correction factors were estimated for ratios of a/c ranging from 0 to 1 and ratios of a/t ranging from 0 to

0.98. The curves for the correction factors (product of M_1 and M_2) are given in Ref 10 (page 42).

Masters, Haese, and Finger (1969) [11]—They used an experimental method to obtain the correction factors. The experimental method involved fracture tests of surface-crack tension specimens (with various a/c and a/t ratios) made of 2219-T87 aluminum alloy material ($t = 16$ mm) at room and cryogenic temperature. The correction factors then were obtained by requiring that the calculated stress-intensity factor be equal to the plane-strain fracture toughness, K_{Ic} , at the same test temperature. The correction factors were given as

$$F = 1.1 M_K \quad (14)$$

for $a/t < 0.85$ and $0.1 \leq a/c \leq 0.8$. The curves for M_K are given in Ref 11 (page 67, Fig. 58). These same correction factors also have been used to correlate fracture data on aluminum and titanium alloys in Ref 12.

Smith and Alavi (1969) [13]—They were the first to analyze the part-circular surface crack in a semi-infinite solid using the alternating method. The crack was a segment of a circle where the crack depth, a , was less than the crack length, c . The boundary-correction factor for the part-circular surface crack in a finite-thickness plate was given by

$$F = M_s M_t \quad (15)$$

for $a/t \leq 0.8$ and $0.4 \leq a/c \leq 1$. M_s was the front-face magnification and M_t was the back-face magnification. M_s was the same as the product of M_1 times $f(\theta)$ in Eq 11. The back-face magnification was estimated from the solution for an embedded circular crack near a free boundary in a semi-infinite solid. Curves of M_t for various a/c ratios are given in Ref 3 (page 33).

Rice and Levy (1970) [14]—They determined the stress-intensity factors at $\phi = \pi/2$ using a line spring model. The line spring model reduces the three-dimensional crack problem to a two-dimensional analogy (single-edge-cracked plate) where the crack is represented as a line of reduced stiffness. The results of their analysis were presented graphically in terms of the ratio of the stress-intensity factor at the deepest point of a semi-elliptical surface crack (K_1) to the stress-intensity factor for a single-edge-cracked specimen (K_∞) with a crack of the same depth. The correction factor, rewritten in terms of Eq 5, was given by

$$F = \left(\frac{K_1}{K_\infty} \right) \sqrt{Q} f \quad (16)$$

where K_1/K_∞ was obtained from Ref 14 for uniform tension and f , the correction factor for a single-edge-cracked plate [9], was given by

$$f = 1.12 - 0.23 \left(\frac{a}{t} \right) + 10.55 \left(\frac{a}{t} \right)^2 - 21.71 \left(\frac{a}{t} \right)^3 + 30.38 \left(\frac{a}{t} \right)^4 \quad (17)$$

They calculated the ratio of K_1/K_∞ for $0.1 \leq a/t \leq 0.7$ and $0 \leq a/c \leq 1$.

Anderson, Holms, and Orange (1970) [15]—They modified the boundary correction factor equation of Paris and Sih [7] and estimated the correction factor as

$$F = \left[1 + 0.12 \left(1 - \frac{a}{c} \right) \right] \sqrt{\frac{2tQ}{\pi a} \tan \left(\frac{\pi a}{2tQ} \right)} \quad (18)$$

for $a/t \leq 1$ and $a/c \leq 1$ where Q is the elastic shape factor.

Newman (1972) [16]—He used the analytical results from Smith and Alavi [12], Rice and Levy [13], and Gross and Srawley [9] for particular ranges of a/c to obtain an expression for the correction factor. The results from Smith and Alavi for a near semi-circular crack ($a/c = 0.4$ and 1), Rice and Levy for shallow cracks ($a/c = 0.1$ and 0.2), and Gross and Srawley for a single-edge crack ($a/c = 0$) were used. An equation was chosen to fit these particular results. The equation for the correction factor was given by

$$F = M_e = \left[M_1 + \left(\sqrt{Q \frac{c}{a}} - M_1 \right) \left(\frac{a}{t} \right)^p \right] \sqrt{\secant \left[\frac{\pi c}{W} \frac{a}{t} \right]} \quad (19)$$

where

$$p = 2 + 8 \left(\frac{a}{c} \right)^3 \quad (20)$$

The expression for Q was approximated by

$$Q = 1 + 1.47 \left(\frac{a}{c} \right)^{1.64} \quad \text{for } \frac{a}{c} \leq 1 \quad (21a)$$

$$Q = 1 + 1.47 \left(\frac{c}{a} \right)^{1.64} \quad \text{for } \frac{a}{c} > 1 \quad (21b)$$

The maximum error in the stress-intensity factor by using three equations for Q was about 0.25 percent. The front-face correction, M_1 , was given by

$$M_1 = 1.13 - 0.1 \left(\frac{a}{c} \right) \quad \text{for } 0.02 \leq \frac{a}{c} \leq 1 \quad (22a)$$

$$M_1 = \sqrt{\frac{c}{a}} \left(1 + 0.03 \frac{c}{a} \right) \quad \text{for } \frac{a}{c} > 1 \quad (22b)$$

For $a/c < 0.02$, the stress-intensity factor for the single-edge cracked plate ($a/c = 0$) subjected to uniform tension [9] was assumed to apply and F was given by Eq 17.

As a/t approaches unity for any value of a/c (except zero), Eq 5 with F given by Eq 19 reduces to the stress-intensity factor for a through crack of length $2c$ in a finite-width plate. The secant term in Eq 19 is the finite-width correction.

Shah and Kobayashi (1972) [17]—They estimated the correction factors from an empirical front-face magnification (M_1) and from an analytical back-face magnification (M_2) obtained from the solution for an embedded elliptical crack approaching the free surface of a semi-infinite solid [18]. The front-face magnification was given by Eq 13. The correction factor, due to both the front and back faces, was obtained by multiplying the back-face magnification, M_2 , by Eq 13. The correction factor was given by

$$F = M_K = M_1 M_2 \quad (23)$$

for $a/t \leq 0.9$ and $0.1 \leq a/c \leq 1$. The curves for M_K are given in Ref 17 (page 114).

Smith and Sorensen (1974) [19]—They used the alternating method to calculate the variation of the stress-intensity factor along semi-elliptical surface cracks in finite-thickness plates. They made calculations for a/c ratios ranging from 0.1 to

0.6. The results for a/c ratios of 0.8 and 1 used by Smith and Sorensen were obtained from Shah and Kobayashi [17]. The boundary-correction factors are presented in Ref 19 (page 88).

Kobayashi (1976) [20]—He used the alternating method with improved boundary conditions to obtain the correction factors. In previous analyses by Kobayashi using the alternating method, some inappropriate boundary conditions (bending restraints) were induced inadvertently by limiting the areas of front- and back-face surfaces that are free of residual surface tractions. To estimate the effect of this bending restraint, a two-dimensional finite-element model of a single-edge-cracked tension plate was analyzed with side constraints. The side constraints induced a similar bending moment. The change in stress intensity caused by this bending moment was calculated and used to modify the stress intensity for the surface crack. The stress-intensity factors at the maximum depth point were calculated for $a/c = 0.2$ and 0.98. The stress-intensity factor for other a/c ratios (0.4, 0.6 and 0.8) were obtained by interpolation between the results from $a/c = 0.2$ and 0.98. The correction factors were given by $F = M_K$ for $a/t \leq 0.9$ and $0.2 \leq a/c \leq 0.98$. The curves for M_K are given in Ref 20 (Fig. 12).

Raju and Newman (1977) [21,22]—They used a three-dimensional finite-element analysis with singularity elements to obtain the correction factors. To verify the accuracy of the finite-element method, elliptical cracks ($a/c = 0.2$ to 1) embedded in a large solid body were analyzed [21] and the stress-intensity factors agreed generally within 1 percent of the exact solutions [6]. To verify the finite-element models employed, convergence was studied by varying the number of degrees of freedom from 1500 to 6900. The correction factors were calculated for semi-elliptical surface cracks ($a/c = 0.2$ to 2) in finite-thickness plates with a/t ranging from 0.2 to 0.8 for $W \geq 10c$. The correction factors are tabulated in Refs 21 and 22.

For fracture, they proposed to use the maximum stress-intensity factor for $a/c < 0.6$. For a/c ratios between 0.6 and 1, an "average" stress-intensity factor (average between the values at $\phi = 0$ and $\phi = \pi/2$) was used. These results were calculated for a surface crack in a wide plate. To compensate for the influence of finite width, the results were multiplied by f_w , the finite-width correction [23] given by

$$f_w = \sqrt{\secant \left[\frac{\pi c}{W} \sqrt{\frac{a}{t}} \right]} \quad (24)$$

Newman and Raju (1978) [24]—They used the results from Raju and Newman [21,22] for the semi-elliptical surface crack and from Gross and Srawley [9] for a single-edge crack to obtain an equation for the correction factors. The form of the equation was similar to that used in Ref 16. The equation was given by

$$F = M_e = \left[M_1 + \left(\sqrt{Q \frac{c}{a}} - M_1 \right) \left(\frac{a}{t} \right)^p + \sqrt{Q \frac{c}{a}} (M_2 - 1) \left(\frac{a}{t} \right)^{2p} \right] f_w \quad (25)$$

where $p = \sqrt{\pi}$ and Q is given by Eqs 3a and b. The front-face correction, M_1 , was given by

$$M_1 = 1.13 - 0.1 \left(\frac{a}{c} \right) \quad \text{for } 0.03 \leq \frac{a}{c} \leq 1 \quad (26a)$$

$$M_1 = \sqrt{\frac{c}{a}} \left(1 + 0.03 \frac{c}{a} \right) \quad \text{for } \frac{a}{c} > 1 \quad (26b)$$

and M_2 was given by

$$M_2 = \sqrt{\frac{\pi}{4}} \quad \text{for } \frac{a}{c} \leq 1 \quad (27a)$$

$$M_2 = 1 + \frac{c}{a} \left(\sqrt{\frac{\pi}{4}} - 1 \right) \quad \text{for } \frac{a}{c} > 1 \quad (27b)$$

The finite-width correction, f_w , was given by Eq 24. For $a/c < 0.03$, the stress-intensity factor for the single-edge crack plate, $a/c = 0$, subjected to uniform tension [9] was assumed to apply and F was given by Eq 17.

Other Analyses of the Surface Crack—A large number of reports consider the surface-crack configuration. Some of these reports analyze [25–28] or experimentally determine [29] the stress-intensity factors for only a few select configurations. The results from these reports were too limited in values of a/c and a/t to use in the “Analysis of Fracture Data” section. Many other reports (see, for example, Refs 30 and 31) use stress-intensity factor solutions previously reviewed. One report [32] analyzes the surface-crack configuration from a nonfracture mechanics approach.

References

- [1] Irwin, G. R., *Journal of Applied Mechanics*, American Society of Mechanical Engineers, Vol. 29, No. 4, 1962, pp. 651–654.
- [2] *The Surface Crack: Physical Problems and Computational Solutions*. American Society of Mechanical Engineers, J. L. Swedlow, Ed., 1972.
- [3] Merkle, J. G., “A Review of Some of the Existing Stress Intensity Factor Solutions for Part-Through Surface Crack,” ORNL-TM-3983, Oak Ridge National Laboratory, Jan. 1973.
- [4] Keys, R. H., “A Review of Stress Intensity Factors for Surface and Internal Cracks,” Report ARL/SM 343, Australia Aeronautics Research Laboratory, April 1973.
- [5] Smith, F. W. in *The Surface Crack: Physical Problems and Computational Solutions*, J. L. Swedlow, Ed., 1972, pp. 125–152.
- [6] Green, A. E. and Sneddon, I. N. in *Proceedings*, Cambridge Philosophical Society, Vol. 46, 1950, pp. 159–164.
- [7] Paris, P. C. and Sih, G. C. in *Fracture Toughness Testing and Its Application*, ASTM STP 381, American Society for Testing and Materials, 1965, pp. 30–83.
- [8] Smith, F. W., Emery, A. F., and Kobayashi, A. S., *Journal of Applied Mechanics*, Vol. 34, No. 4; *Transactions*, American Society of Mechanical Engineers, Vol. 89, Series E, Dec. 1967, pp. 953–959.
- [9] Gross, B. and Srawley, J. E., “Stress-Intensity Factors for Single-Edge Notch Specimens in Bending or Combined Bending and Tension by Boundary Collocation of a Stress Function,” NASA TN D-2603, National Aeronautics and Space Administration, 1965.
- [10] Kobayashi, A. S. and Moss, W. L. in *Fracture*, Chapman and Hall, New York and London, 1969, pp. 31–45.
- [11] Masters, J. N., Haese, W. P., and Finger, R. W., “Investigation of Deep Flaws in Thin Walled Tanks,” NASA CR-72606, National Aeronautics and Space Administration, Dec. 1969.
- [12] Masters, J. N., Bixler, W. D., and Finger, R. W., “Fracture Characteristics of Structural Aerospace Alloys Containing Deep Surface Flaws,” NASA CR-13487, National Aeronautics and Space Administration, Dec. 1973.
- [13] Smith, F. W. and Alavi, M. J. in *Proceedings*, 1st International Conference on Pressure Vessel Technology, Delft, The Netherlands, American Society of Mechanical Engineers, 1969, pp. 783–800.
- [14] Rice, J. R. and Levy, N., “The Part-Through Surface Crack in an Elastic Plate,” Technical Report NASA NGL 40-002-080/3, Division of Engineering, Brown University,

- Transactions, American Society of Mechanical Engineers, Journal of Applied Mechanics*, Paper No. 71-APM-20 (1970).
- [15] Anderson, R. B., Holms, A. G., and Orange, T. W., "Stress Intensity Magnification for Deep Surface Cracks in Sheets and Plates." NASA TN D-6054, National Aeronautics and Space Administration, Oct. 1970.
 - [16] Newman, J. C., Jr., "Fracture Analysis of Surface- and Through-Cracked Sheets and Plates," Symposium on Fatigue and Fracture, George Washington University, 1972, (also, *Engineering Fracture Mechanics*, Vol. 5, 1973, pp. 667-689).
 - [17] Shah, R. C. and Kobayashi, A. S. in *The Surface Crack: Physical Problems and Computational Solutions*, J. L. Swedlow, Ed., 1972, pp. 79-124.
 - [18] Shah, R. C. and Kobayashi, A. S., *International Journal of Fracture*. Vol. 9, No. 2, June 1973.
 - [19] Smith, F. W. and Sorensen, D. R., "Mixed Mode Stress Intensity Factors for Semi-elliptical Surface Cracks," NASA CR-134684, National Aeronautics and Space Administration, 1974.
 - [20] Kobayashi, A. S. in *Proceedings, 2nd International Conference on Mechanical Behavior of Materials*, American Society of Mechanical Engineers, 1976, p. 1073.
 - [21] Raju, I. S. and Newman, J. C., Jr., "Improved Stress-Intensity Factors, for Semi-Elliptical Surface Cracks in Finite-Thickness Plates." NASA TMX-72825, National Aeronautics and Space Administration, Aug. 1977.
 - [22] Raju, I. S. and Newman, J. C., Jr., "Stress-Intensity Factors for a Wide Range of Semi-Elliptical Surface Cracks in Finite-Thickness Plates," *Engineering Fracture Mechanics Journal*, Vol. 11, No. 4, 1979, pp. 817-829.
 - [23] Newman, J. C., Jr., "Predicting Fracture of Specimens With Either Surface Cracks or Corner Cracks at Holes," NASA TN D-8244, National Aeronautics and Space Administration, June 1976.
 - [24] Newman, J. C., Jr. and Raju, I. S., "Analyses of Surface Cracks in Finite Plates Under Tension or Bending Loads," NASA TP (in preparation), National Aeronautics and Space Administration, 1978.
 - [25] Miyamoto, H. and Miyoshi, T., "Analysis of Stress Intensity Factor for Surface Flawed Tension Plate," *Proceedings, Symposium on High Speed Computing of Elastic Structures*, IUTAM, Liege, Aug. 1970.
 - [26] Atluri, S. and Kathiresan, A., "An Assumed Displacement Hybrid Finite Element Model for Three-Dimensional Linear Fracture Mechanics Analysis," *Proceedings, 12th Annual Meeting of the Society of Engineering Science*, University of Texas, Austin, Tex., Oct. 1975.
 - [27] Hellen, T. K. and Blackburn, W. S. in *Computational Fracture Mechanics*. American Society of Mechanical Engineers, 1975, p. 103.
 - [28] Gyekenyesi, J. P. and Mendelson, A., "Stress Analysis and Stress Intensity Factors for Finite Geometry Solids Containing Rectangular Surface Cracks," NASA TMX-71964, National Aeronautics and Space Administration, 1977.
 - [29] Harms, A. E. and Smith, C. W., "Stress Intensity Factors for Long, Deep Surface Flaws in Plates Under Extensional Fields," NASA CR-132015, National Aeronautics and Space Administration, Feb. 1973.
 - [30] Orange, T. W., "A Semiempirical Fracture Analysis for Small Surface Cracks," NASA TN D-5340, National Aeronautics and Space Administration, July 1969.
 - [31] Broek, D., Nederveen, A., and Meulman, A., "Applicability of Fracture Toughness Data to Surface Flaws and to Corner Cracks at Holes," NRL TR 71033U, National Aerospace Laboratory, Jan. 1971.
 - [32] Kuhn, P., "Residual Tensile Strength in the Presence of Through Cracks or Surface Cracks," NASA TN D-5432, National Aeronautics and Space Administration, March 1970.

DISCUSSION

*H. Tada and P. Paris*¹ (written discussion)—It is noted that a factor $(\sin^2 \phi + b^2/a^2 \cos^2 \phi)^{1/4}$ repeatedly appears in K -formulas for an embedded elliptical crack under various loading conditions (Fig. 21).²

The following observation of this factor is interesting and worth some attention. That is $b(\sin^2 \phi + b^2/a^2 \cos^2 \phi)^{1/2}$ is the length of the normal of the ellipse which is represented by the length l in Fig. 21. This observation considerably simplifies the K -expressions for an elliptical crack. For example, when the crack is subjected to an internal pressure, p , the K -expression is now written in a simple form

$$K_{at A} = \frac{p\sqrt{\pi l}}{E(k)} \quad (28)$$

This is a very compact form and convenient to memorize.

It also should be noted that a circular crack, a parabolic crack, and a 2-D tunnel crack are simply special cases of an elliptical crack. Therefore, this length-of-normal concept is applied directly to these special cases. For example, corresponding to Eq 28

$$K = \frac{2}{\pi} p\sqrt{\pi a} \quad (29)$$

$$K = p\sqrt{\pi l} \quad (\text{Fig. 22a}) \quad (30)$$

and

$$K = p\sqrt{\pi b} \quad (\text{Fig. 22b}) \quad (31)$$

are derived readily without difficulty for a circular crack, a parabolic crack, and a 2-D tunnel crack, respectively, under internal pressure p (Fig. 22).

In addition, it is known that K -formulas for a crack consisting of two straight edges (Fig. 23a) also contains l as the major length factor. Thus, it seems reasonable to assume the length-of-normal concept to have some

¹School of Engineering and Applied Science, Dept. of Engineering, Washington University, St. Louis, Mo. 63130.

²Tada, H., Paris, P., and Irwin, G., *The Stress Analysis of Cracks Handbook*, Del Research Corporation, St. Louis, Mo., 1973.

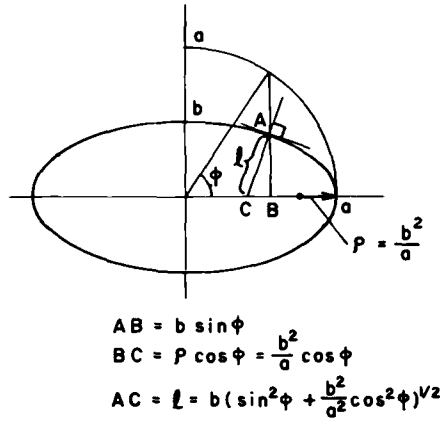


FIG. 21—Elliptical crack in an infinite solid.

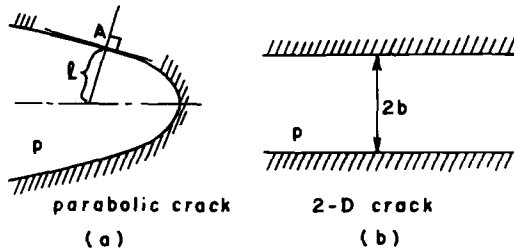


FIG. 22—Parabolic and two-dimensional tunnel crack in an infinite solid.

generality for estimation purposes. That is, when an embedded flat crack which has an axis of symmetry (Fig. 23b) is subjected to an internal pressure, p , K is assumed to be in the form

$$K = p\sqrt{\pi l} \cdot f \tag{32}$$

where f is a factor dependent on crack shape (and, in general, loading conditions).

The objective of this discussion is to show the possibilities of engineering estimates of K -value for surface and corner cracks. As best illustrated by Irwin and Paris empirical formulae for part-through cracks,^{3,4} an engineering estimate based on sound judgment can provide the K -value with a

³Paris, P. and Sih, G., "Stress Analysis of Cracks," *ASTM STP 381*. American Society for Testing and Materials, 1965.

⁴Newman, J. C., Jr., this publication, pp. 16-42.

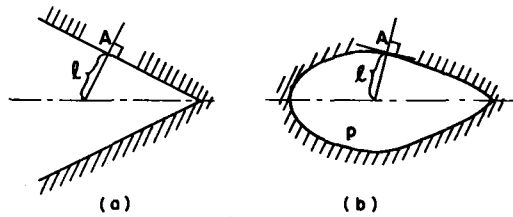


FIG. 23—Arbitrarily-shaped cracks in an infinite solid.

sufficient accuracy for practical purposes. A few very simple examples are given as follows.

The surface or corner flaws do not necessarily have semi or quarter elliptical shapes (Fig. 24).

For a surface crack shown in Fig. 24a subjected to a uniform tension, σ , the following expression provides a conservative estimate of K

$$K = \frac{\sigma\sqrt{\pi l}}{E(k)} \times 1.15 \quad (33)$$

where l is the measured value for the crack and $E(k)$ is calculated for the ellipse shown by a dotted line in the figure. For a corner crack which has approximately parabolic shape (Fig. 24b), the following expression is conservative

$$K = \sigma\sqrt{\pi l} \times 1.15 \quad (34)$$

where l is the measured value. Equations 6 and 7 should not be applied to the points in the immediate neighborhood of the intersections of crack edge and free surfaces. For some discussions on the engineering estimate of this type see footnote 5.

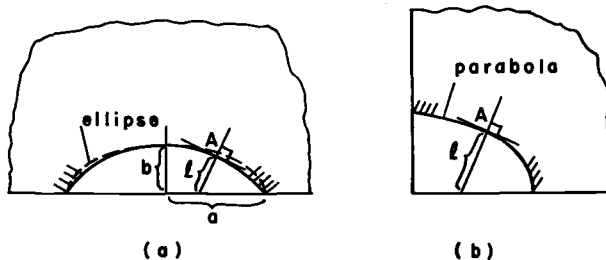


FIG. 24—Surface crack and corner crack in a semi-infinite solid.

⁵Tada, H. and Irwin, G., "K-Value Analysis for Cracks in Bridge Structures," Fritz Engineering Laboratory Report, Lehigh University, Bethlehem, Pa., June 1975.

If a rigorous numerical analysis, for example FEM, is used for spot checks of the estimation or to provide some additional information to assist refinement of the estimation, the computational efforts may be reduced substantially.

J. C. Newman, Jr. (author's closure)—The observation made by Tada and Paris provides a very useful estimation procedure for stress-intensity factors for arbitrarily shaped cracks in infinite bodies. However, the influence of various shaped boundaries on stress-intensity factors, such as free surfaces and holes, must still be obtained from rigorous numerical analyses. Most numerical analyses have only considered circular- or elliptical-shaped cracks in finite bodies. The proposed estimation procedure could be useful in modifying elliptical-crack solutions in finite bodies to obtain estimates for arbitrarily shaped cracks in the same finite bodies. This would reduce greatly the computational efforts required for obtaining stress-intensity factors for arbitrarily shaped cracks in the neighborhood of boundaries.

Development of Basic Material(s) Data for Evaluating Crack Growth Life

REFERENCE: Bucci, R. J., "Development of Basic Material(s) Data for Evaluating Crack Growth Life," *Part-Through Crack Fatigue Life Prediction, ASTM STP 687*, J. B. Chang, Ed., American Society for Testing and Materials, 1979, pp. 47-73.

ABSTRACT: Fracture toughness, fatigue crack growth rate, and sustained load crack growth data comprise a basic package of materials property information used in predicting growth of cracks by fracture mechanics methods. Accurate analysis requires carefully developed laboratory results using various simple specimen configurations to describe these properties. A contributing factor to variability in life prediction is the lack of consistent procedures for obtaining and reporting this information for use in design. Though a standard does exist for direct fracture toughness determinations (ASTM Method E 399), standards for subcritical crack growth measurement are in various stages of development. Accuracy of life prediction is further confounded by judgment required of the analyst in selecting the most appropriate test and interpreting material property data for use in the computational methodology.

This paper reviews the status on standardization of test practices for characterizing basic material properties used in crack growth analysis. Emphasis is given to aspects of fatigue crack growth because of the relative importance of its characterization to life prediction by damage integration techniques. Other criteria are outlined to provide helpful guidelines to the design engineer seeking to recognize problems and minimize variability in life prediction.

KEY WORDS: fatigue crack growth, stress corrosion cracking, fracture toughness, crack growth rate, fracture mechanics, test methods, life prediction, fatigue (materials), crack propagation

Technological demands for higher performance and more efficient engineering structures, availability of increased strength materials, and improved analytical methods have produced a trend toward higher operating stresses in engineering components. However, these same factors enhance the prospect of failure by rapid fracture emanating from preexisting crack-like defects in a structural part. Historically, a high percentage of failures en-

¹Staff engineer, Engineering Properties and Design Division, Alcoa Laboratories, Alcoa Center, Pa. 15069.

countered for fracture critical parts have developed through propagation of a part-through crack (PTC). This crack-like defect may originate early in the life at areas of high stress concentration, such as corners, holes, attachments, and corrosion pits, or they may develop from manufacturing defects present in the initial structure such as tool marks, weld discontinuities, forging laps, inclusions, and the like.

Evaluation of PTC behavior has been based on experimental simulation. However, new requirements in which designs must guarantee safe crack growth life have established the need for analytical evaluation of the PTC. Perhaps the most notable of these is the Air Force structural integrity requirement [1].² Compliance with such requirements involves the evaluation of large numbers of candidate materials and structural details where testing of each option may not be economically feasible. Analytical life prediction uses a material(s) data base that can be input into a crack growth model which is based on principles of fracture mechanics. The basic material(s) data package consists of tensile properties, fracture toughness, fatigue crack growth rate, and sustained load cracking (SLC) information. The fracture properties usually are established from various precracked laboratory fracture mechanics specimens that are considerably more efficient to test than the PTC specimen. Ability to predict PTC behavior is verified by the degree of success that basic laboratory material(s) data, combined with stress analysis and descriptive equations of the crack growth model, are able to predict actual PTC test results. Once confidence in PTC life prediction is established, a number of steps in the design process can be performed by analysis, thereby permitting reduction in testing costs and relaxation to binding conservatism of a more empirical approach.

Objective

This paper reviews the status on standardization of test practices for characterizing basic material properties for input in crack growth analyses. Though the scope of this symposium addresses the PTC, much of the discussion herewith can be applied more generally toward establishment of baseline data for use in analysis of "flawed" engineering components, including those containing the PTC. Guidelines are given to help the design engineer recognize potential problems and minimize variability in the basic material(s) data package. As other areas of PTC analysis such as stress intensity solutions, crack geometry effects, transitioning from PTC to through-thickness cracks, stress/strain history effects, continue to develop, greater accuracy in crack growth prediction will result. Progress in these areas is described in other papers included in this symposium volume.

²The italic numbers in brackets refer to the list of references appended to this paper.

Crack Growth Integration Model

An obstacle to an analytical approach to crack growth prediction is the requirement for a model which combines physical significance with feasible computational procedures. To facilitate use, physical requirements are often compromised to streamline computations. Presently, there does not exist a universal model which can predict consistently all forms of interaction between material, load, environment, and component configuration variables encountered in service. Therefore, it is not intended that analytical life prediction replace the need for service simulation tests in verification of design. The crack growth integration model described herewith provides a cost effective computational process which establishes a basic link between material(s) property data and actual behavior. The basic material(s) testings, which serve as input to the model, are essential to understanding crack growth mechanisms and evaluating behavior under more complex conditions.

The crack growth integration model is generally written as

$$a = a_o + \sum_i \Delta a_i \quad (1)$$

where a_o is the initial flaw size, and Δa_i is the growth increment associated with the i^{th} applied load event. The purpose of Eq 1 is to calculate by numerical integration the growth increment, Δa_i , for each incrementally applied load event. The integration process continues until a terminal flaw size is reached.

Fatigue

If fatigue is the subcritical crack growth mechanism, the load event may represent an increment of one or more fatigue cycles, ΔN , at fixed maximum and minimum loads. Over ΔN cycles, the crack growth increment, Δa_i , could then be computed as

$$\Delta a_i = (da/dN)_i \cdot \Delta N_i \quad (2)$$

where the fatigue crack growth rate characteristic of the material, da/dN , is described as a function of stress intensity factor range, ΔK , the environment, and usually the stress ratio, R ($R = K_{\min}/K_{\max}$), for the i^{th} load event. That is

$$(da/dN)_i = f_1(\Delta K_i, R_i, \text{environment}) \quad (3)$$

The functional relationship of Eq 3 is developed from constant amplitude fatigue crack growth rate data established from precracked fracture

mechanics specimens. Fracture mechanics assumes that fatigue crack growth in an engineering structure occurs at the same da/dN as that of the precracked specimen of the same material when the range and mean stress intensities for both configurations are the same. Assuming crack growth increment, Δa_i , in Eq 1 to be small, the stress intensity factor of the i^{th} load event is given as

$$\Delta K_i = f_2(\Delta\sigma_i, a_{i-1}, Y(a_{i-1})) \quad (4)$$

where $\Delta\sigma_i$ is the stress range of the i^{th} event, a_{i-1} is the terminal crack size of the previous $(i-1)^{\text{th}}$ load event, and factor Y interrelates crack geometry to the configuration of the part. The functional form of Eq 4 is developed from linear elasticity. Solutions for many common engineering configurations are tabulated in handbooks [2-4]. Therefore, component crack propagation life may be estimated by numerical integration of crack growth rates established from the laboratory specimen.

The validity of Eqs 1 and 2 assume that Δa_i is independent of prior history, that is, load interaction effects are ignored. Several fatigue crack growth retardation models have been advanced to account for high to low load interaction effects (that is, phenomena whereby growth of a crack is slowed by application of a high load in the fatigue spectrum). For aircraft load spectra, treatment of retardation effects generally leads to less conservative life prediction than models which ignore these interactions (that is, linear damage models) [5-7]. Retardation models exist in numerous forms, but a basic mechanism, common to most, is that localized plastic deformation left by a high load excursion causes residual forces that effectively reduce the stress intensity factor during subsequent cycles of lower stress magnitude. The mathematical formulation of the stress intensity factor reduction is beyond the scope of this paper, but it is founded generally on semi-empirical relationships derived from experiment, and included as part of the retardation model. Material(s) parameters, such as yield strength, may be included in the model. To account for load interaction effects in crack growth prediction, most retardation models modify ΔK_i and R_i in Eq 3, and establish a new $(da/dN)_i$ according to the functional crack growth rate relationship established from basic material(s) data.

Time Dependent Sustained Load Cracking (SLC)

A model analogous to that for fatigue may be considered when the subcritical crack growth process is time dependent (for example, stress corrosion cracking or elevated temperature creep crack growth, or both), when reliable laboratory data relating crack growth velocity, da/dt , to stress intensity factor exists, the crack growth integration model may be used. In this case, the

i th applied load event of Eq 1 would correspond to a sustained load held over time increment, Δt_i . Equations 2, 3, and 4 would be written analogously as

$$\Delta a_i = (da/dt)_i \cdot \Delta t_i \quad (2')$$

$$(da/dt)_i = f_3(K_i) \quad (3')$$

$$K_i = f_2(\sigma_i, a_{i-1}, Y(a_{i-1})) \quad (4')$$

where $(da/dt)_i$ is the characteristic crack growth rate at sustained stress intensity, K_i , determined from laboratory data.

Terminal Crack Size

Repetitive application of Eqs 1 through 4 accomplishes the integration steps to predict crack length as a function of load history. This computational process continues until a terminal value of crack size is reached. Terminal flaw size is usually based on residual strength requirements set by design. Often the terminal flaw size is established as the critical size where rapid fracture is likely to occur, that is, when K approaches the critical toughness (K_{Ic} or K_c), or where K exceeds the stress corrosion threshold (K_{Isc} or K_{Isc}) and failure is imminent if aggressive environment persists. For the PTC terminal flaw size may also be the "leak-before-break" condition at breakthrough, or it may be dictated by limitations of inspection or economic restraints of repair and rework.

Basic Material(s) Data Package

The basic material(s) data package for crack growth life prediction consists of: (a) subcritical crack growth rate information (namely, fatigue or SLC, or both) for establishment of the functional relationships given by Eqs 3 and 3', and (b) fracture toughness for determination of the terminal flaw size. The terminal flaw size is set generally by the failure criteria of design. In addition, basic tensile properties, fatigue and SLC "thresholds," and fracture toughness are sometimes incorporated as material parameters in crack growth prediction models.

A contributing factor to variability in life prediction is the lack of consistent procedures for measurement and interpreting basic material(s) fracture data for use in the prediction model. Though ASTM Test for Plane-Strain Fracture Toughness of Metallic Materials (E 399-78) does exist for direct fracture toughness determination, standards for subcritical crack growth measurement are in various stages of development. Accurate prediction of life requires judgment in selecting the most appropriate test and in interpreting material property data for computational use.

Fracture Toughness

Values of fracture toughness used for life prediction should represent conservative values preferably obtained from the specific material and product form involved. The values should be justified on the basis of current technology and should take into account material variability, testing techniques, and other factors which might alter toughness values.

Partially or fully embedded flaws are usually subjected to plane-strain deformations in the vicinity of the flaw periphery. Under plane-strain constraint, the onset of unstable fracture is abrupt, occurring with little warning or gross deformation preceding fracture. In the plane-strain state of stress the material is at its lowest point of resistance to unstable fracture. The basic material property defining this characteristic is K_{Ic} , the plane-strain fracture toughness. Procedures for direct measurement of K_{Ic} are well established and have been standardized by ASTM Method E 399. Basic steps and validity requirements of this standard are summarized in Tables 1 and 2, respectively. The requirements of this standard that generally cause the greatest concern are items 2, 3A, and 9 of Table 2. Comparatively, other requirements cause relatively few problems and generally can be avoided. Size requirements, items 2 and 3, of Table 2 represent the first major judgment in performing the test. Since specimen size is established by the level of fracture toughness, this requirement cannot be satisfied until the final test result is known. The size requirement stipulates that specimen thickness, crack size, and remaining uncracked ligament are approximately 50 times the plane-strain plastic zone size estimated at $(1/6\pi) \cdot (K_{Ic}/\sigma_{ys})^2$ [8]. Nonlinearity in the load-displacement test record may be attributed to crack growth and plasticity. The limiting P_{max}/P_Q ratio, item 9 of Table 2, attempts to discriminate and restrict the amount of plastically induced nonlinearity in a valid test record. This is to ensure that P_Q , the critical load point determined by the 5 percent secant offset, represents a true measure of toughness and is not superficially suppressed because of gross plasticity.

The size requirement of ASTM Method E 399 imposes a rather severe restriction for relatively tough materials, since relatively large specimens are needed to ensure validity. The validity requirements of ASTM Method E 399 have been the subject of continuing review. The generation of data that pro-

TABLE 1—Steps in K_{Ic} testing.

Select specimen size
Machine specimen
Precrack specimen by fatigue loading
Obtain autographic recording of load versus crack opening deflection while loading to fracture by monotonic loading
Analyze test record; select critical load
Calculate critical stress intensity factor
Ascertain validity of results

TABLE 2—Principal requirements for valid K_{Ic} measurement (paragraph and nomenclature in accordance with ASTM Method E 399)

-
1. Specimen proportions:
 - $B = 0.25W$ to $1.0W$ (bend specimen) 7.3.1
 - $B = 0.25W$ to $0.50W$ (compact specimen) 7.3.2
 - $B = 0.5W$ most commonly employed, 7.3
 2. Specimen thickness:
 - $B > 2.5 (K_{Ic}/ys)^2$, 7.1.1
 3. Crack length:
 - A. $a > 2.5 (K_{Ic}/ys)^2$, 7.1.1
 - B. $0.45W < a < 0.55W$, 7.3.3
 4. Fatigue precracking:
 - A. $[(K_f) \max/E] \leq 0.002$ (in.)^{1/2}, 7.4.2
 - B. $(K_f) \max \leq 0.60 K_{Ic}$, 7.4.2
 - C. $K \geq 0.9 (K_f) \max$, 7.4.3
 5. Fatigue crack length:
 - $\geq 0.05a$ or ≥ 0.050 in., whichever is greater, 7.2.3, 7.4
 6. Crack front curvature:
 - A. in mid-thickness, difference between any two a measurements (center and midway) $\leq (0.05 \times \text{average } a)$, 8.2.3
 - B. a at surface $\geq (0.9 \times \text{average } a)$, 8.2.3
 7. Crack plane parallel to width-thickness plane to within ± 10 deg, 8.2.4
 8. Loading rate range:
 - 30 to 150 ksi $\sqrt{\text{in.}}$ /min., 8.3, 8.4
 9. $P_{\max}/P_Q \leq 1.10$, 9.1.2
-

vide information on effects of specimen geometry and testing procedure which are not confounded by other test variables is slow. Kaufman [9] has provided a summary of more recent data. Discussion of these data is beyond the scope of this presentation. However, such data will eventually lead to some relaxations or modification to validity requirements of ASTM Method E 399 which will reduce costs and simplify workability with K_{Ic} test results.

For high toughness materials or thin sheet sections, or both, where insufficient material is available for valid K_{Ic} determination, alternate approaches for characterizing the material toughness may be used. Several test methods have already been developed by ASTM Subcommittee E24.01 on Fracture Mechanics Test Methods, notably ASTM Method for Sharp-Notch Tension Testing of High-Strength Sheet Materials (E 338-68 (1973)), ASTM Tentative Recommended Practice for R-Curve Determination (E 561-76T), and ASTM Tentative Test for Sharp-Notch Tension Testing with Cylindrical Specimens (E 602-76T). A number of others are in progress. Recent developments on standardization of fracture toughness test methods within ASTM Subcommittee E24.01 are summarized in Ref 10, and a comprehensive survey of inexpensive test methods to determine fracture toughness is available in Ref 11. Further discussion on fracture toughness test methods, therefore, is not warranted here.

An important part of accurate life prediction is the selection and use of basic material(s) data in the analysis which matches the processed material

form used in the engineering component to be analyzed. For example, general trends observed in most engineering materials indicate that strength increase generally is accompanied by toughness decrease and vice versa. Therefore, factors known to affect a material's strength are likely to influence toughness [12,13]. Actually, the integrity of a material is controlled by its microstructure. As such, toughness is dependent on a number of factors such as alloy composition, homogeneity, and mechanical and thermal processing. The control of these factors may have significant impact on the magnitude and variability of product toughness independent of the general level of strength. For example, Fig. 1 shows controlled high toughness of 2124 and 7475 aluminum alloys are achieved by special processing and tightening impurity limits of iron and silicon over those of their 2024 and 7075 alloy counterparts of comparable high strength [13]. A large quantity of fracture toughness information established over many production lots of commercial 2124-T851 aluminum alloy plate is summarized in Table 3. Product thicknesses greater than 102 mm (4 in.) show a lower average K_{Ic} value, indicating sensitivity to processing variables [14]. Similar observations have been made in other alloy systems [15].

Fracture properties also are known to vary with orientation of principal stress direction with respect to grain flow. This is shown in Table 3 by variations in fracture toughness values of specimens removed from the three principal orientations (L-T, T-L, and S-L) in aluminum plate. In thin sections or cutaways machined from thick plate, or in forged or extruded shapes, the direction of grain flow may not always be predictable from the external configuration of the machined part, as shown in Fig. 2. Therefore, it is important to consider direction of stress relative to the grain flow of the part when selecting baseline data for analytical life prediction. A complexity of PTC

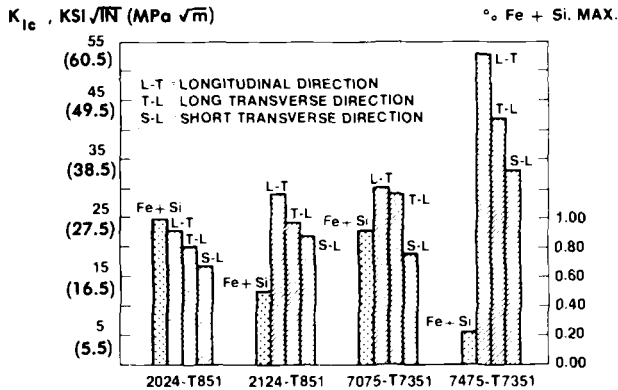


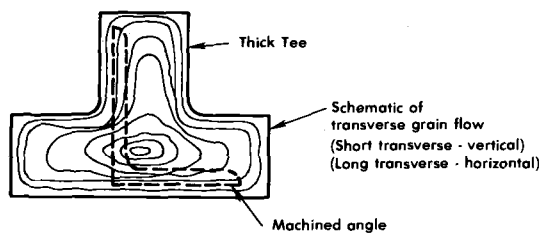
FIG. 1—Aluminum alloy 2124 and 7475 are tougher versions of alloys 2024 and 7075. High purity metal (low iron and silicon contents) and special processing techniques are needed to optimize toughness in these materials.

TABLE 3— K_{Ic} distributions for 2124-T851 plate versus product thickness.

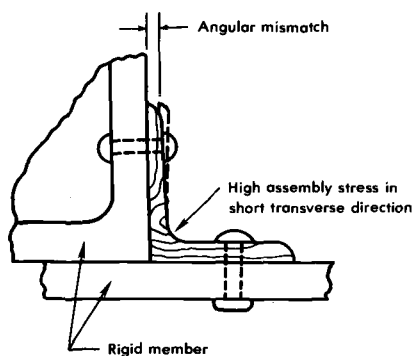
	Product Thickness ≤ 102 mm (≤ 4.0 in.)	Product Thickness > 102 mm (> 4.0 in.)
<i>L-T Orientation</i>		
No. of tests ^a	78	40
Average K_{Ic} (ksi $\sqrt{\text{in.}}$) ^b	29.9	27.2
Standard deviation	2.7	1.4
Skewness coefficient	...	+0.7
<i>T-L Orientation</i>		
No. of tests ^a	55	25
Average K_{Ic} (ksi $\sqrt{\text{in.}}$)	25.2	22.2
Standard deviation	2.2	1.2
Skewness coefficient	+0.6	+0.4
<i>S-L Orientation</i>		
No. of tests ^a	35	9
Average K_{Ic} (ksi $\sqrt{\text{in.}}$)	22.2	21.8
Standard deviation	2.0	...
Skewness coefficient	-0.1	...

^aOnly data representing valid K_{Ic} tests in accordance with ASTM Method E 399 and only one test per lot of material is used in this tabulation.

^b1 ksi $\sqrt{\text{in.}}$ = 1.1 MPa $\sqrt{\text{m}}$.



(a) LOCATION OF MACHINED ANGLE WITH RESPECT TO TRANSVERSE GRAIN FLOW IN THICK TEE



(b) LOCKED IN ASSEMBLY STRESSES FROM MISMATCH

FIG. 2—How grain structure can be adversely oriented with respect to locked-in assembly stresses when a thin part is machined from a thicker one.

analysis is that the grain flow orientation varies along the periphery of the crack.

The sensitivity of toughness input to residual life calculation is generally low for long life structure. For example, a 10 percent shift in K_{Ic} or K_c has negligible effect on calculated cyclic lives greater than 10^5 . However, several mathematical cyclic crack growth rate descriptions used in life prediction incorporate a toughness parameter to serve as an asymptote for fast fracture at high stress intensity [16]. Variability in toughness input to these models may affect the prediction of growth rate behavior at K levels below the critical value. This potential source of variability should be considered in the computation process.

Fatigue Crack Propagation

Constant Amplitude Fatigue Crack Growth Rate Relationship

Resistance to stable crack extension under constant amplitude cyclic loading may be described by fatigue crack growth rate, da/dN , expressed as a function of crack-tip stress intensity factor range, ΔK , using fracture mechanics concepts. Characterizing fatigue crack propagation in this manner provides results which are independent of specimen planar geometry, thus enabling exchange and comparison of data obtained from a variety of test configurations and loading conditions. When data are plotted as $\log da/dN$ versus $\log \Delta K$, generally three regions of crack growth rate may be identified. They are shown schematically in Fig. 3a. The first region occurs at low ΔK where crack growth rate is strongly dependent upon stress intensity and $\log da/dN$ decreases rapidly with small decreases in $\log \Delta K$. Reported da/dN values in this regime may correspond to increments of crack extension per cycle which are less than one atomic spacing. In this case, crack growth is discontinuous along the flaw periphery, and da/dN values represent an increment of crack growth averaged through the specimen thickness. For many engineering structures a major component of fatigue life is spent in Region 1. Growth rates in this regime are of interest to the designer since they often correspond to early stages of crack formation and growth where remedial action can be instituted. Region 2 crack growth rates occur at intermediate stress intensities. Behavior in this region is often represented by a linear relationship between $\log da/dN$ and $\log \Delta K$, particularly in nonhostile environments. Region 2 crack growth rates are of great practical interest since their associated stress intensity factors generally correspond to damage tolerant flaw sizes for in-service inspection. Region 3 behavior occurs as the maximum stress intensity factor of the fatigue cycle approaches the material fracture toughness. Region 3 crack growth rates are highly dependent on stress ratio, R , fracture toughness and specimen thickness (if not plane strain). For analysis of the

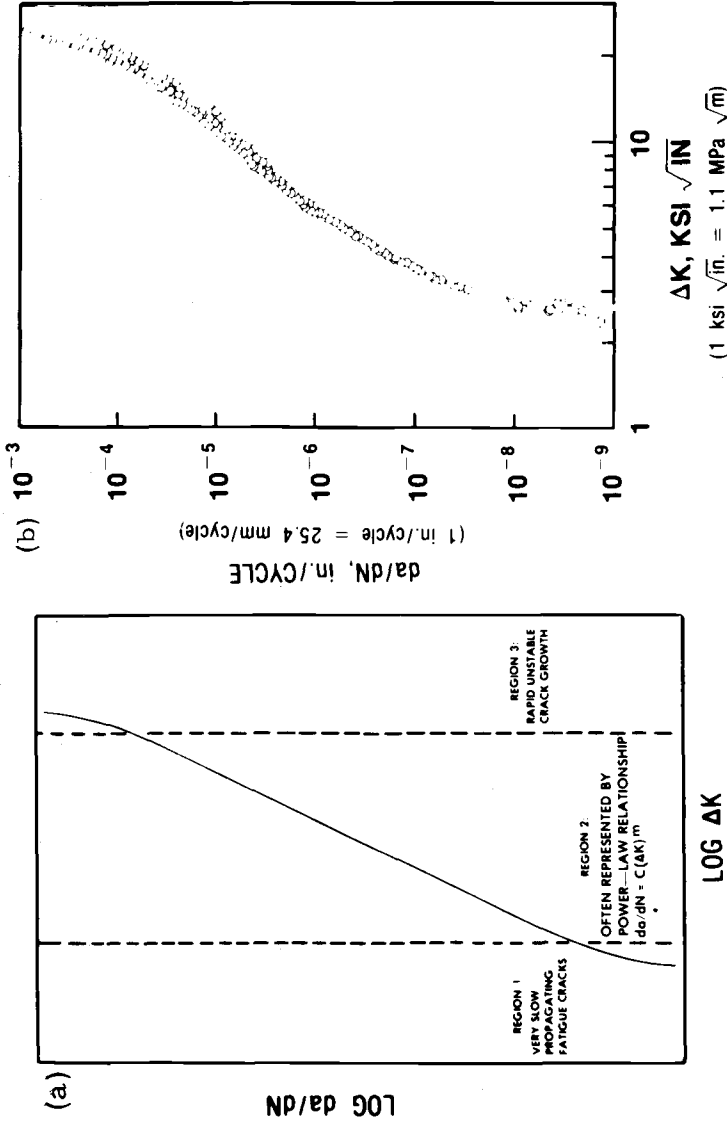


FIG. 3—Fatigue crack growth rate, da/dN, versus cyclic stress intensity range, ΔK, (a) schematic representation of fatigue crack propagation data in a nonhostile environment, and (b) wide range of fatigue crack propagation rates for aluminum alloy 2219-T851, R = 0.1, ambient air.

PTC configuration, which is predominantly one of plane strain, care should be exercised in selecting and using Region 3 crack growth rates generated from thin nonplane-strain specimens. Crack growth information established over the three regions described is shown for aluminum alloy 2219-T851 in Fig. 3*b*.

A value of ΔK in Region 1 above which fatigue crack growth has been observed, but below which crack growth has not been observed has been termed a fatigue crack growth threshold, ΔK_{th} , for the opening Mode I. The task of defining a "true" threshold is difficult and obviously a function of measurement sensitivity, length of observation, and technique. For certain material-environment combinations or applications, or both, the concept of a "true" arrest threshold has been accepted provisionally until better methods to quantify low da/dN fatigue crack growth are needed and available. However, it should be recognized that for some material-environment combinations the slope of Region 1 crack growth has been found to be finite, at least down to low growth rates on the order of 10^{-10} m/cycle, for example, Fig. 4. An operational definition of the fatigue crack growth threshold has been suggested as that ΔK corresponding to a fatigue crack growth rate of 10^{-10} m/cycle [17]. Though the operational definition may be useful for quantifying materials' resistance to crack growth, caution should be exercised when using the latter concept in design.

For design use, ΔK is usually taken as the independent variable and da/dN as the dependent variable with the data considered to be parametric on stress ratio, R . Fitting data in this format permits the use of analytical expressions of the form described by Eq 3. Expressing crack growth rate in this manner permits the da/dN versus ΔK relationship to be described at any R which is useful for predicting crack growth under more realistic load spectra. Moreover, this analytical relationship permits a range of R ratio effects to be established from a limited number of baseline constant amplitude tests. Several mathematical descriptions of the relationship of ΔK and R on da/dN have been proposed and shown to work reasonably well for a wide variety of materials [16].

The quality of component life prediction obviously is influenced by the accuracy to which the fatigue crack growth relationship represents conditions likely to be encountered in service. Care should be exercised to account properly for the full range in ΔK and R experienced by the actual part. For example, small errors at low ΔK may affect life prediction significantly, especially when stress intensity factor reductions in Eq 3 are warranted to account for crack growth retardation and delay. Moreover, data established over one or two decades of crack growth rate may be insufficient to characterize certain trends observed over many decades of crack growth, for example Figs. 4 and 5.

The accuracy of the fatigue crack growth relationship can likewise be affected by variability in test data used to establish the relationship. Over the

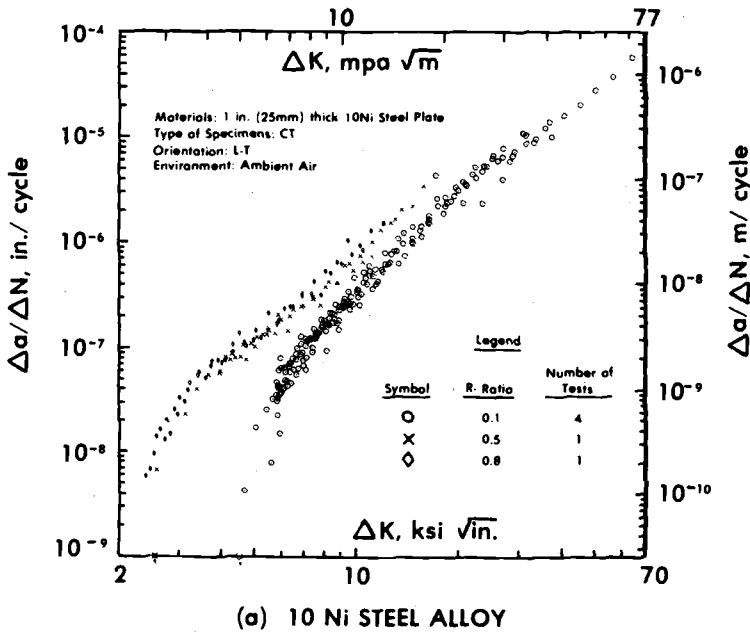
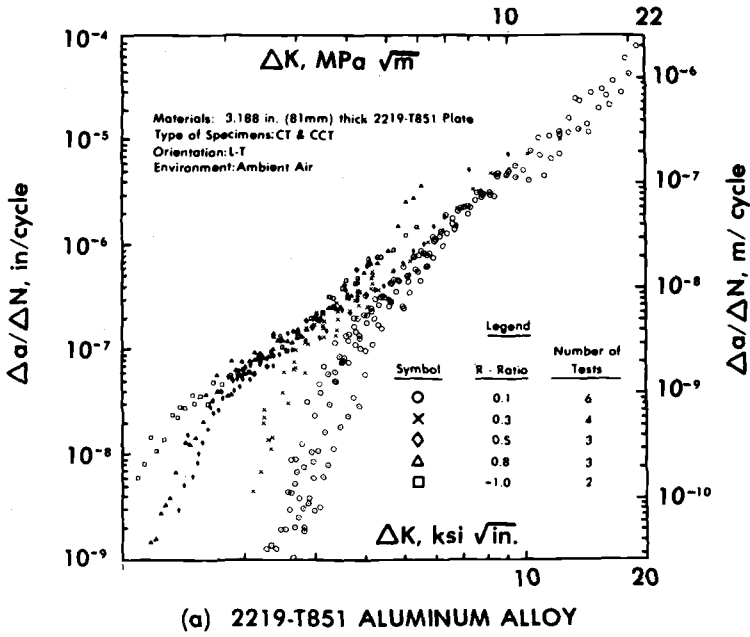


FIG. 4—Effect of stress ratio, R, on low fatigue crack propagation rates of 2219-T851 aluminum and 10Ni steel alloys [19].

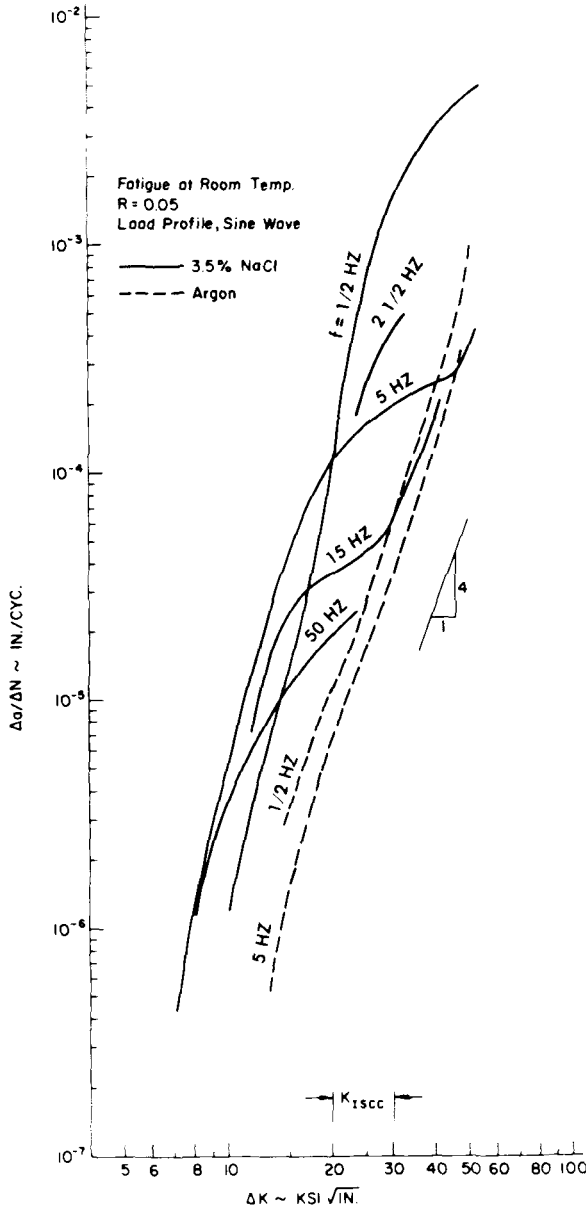


FIG. 5—Frequency effects of mill annealed Ti-8Al-1Mo-1V plate (T-L orientation fatigued in 3.5 sodium chloride solution and argon).

past 15 years extensive crack growth rate information has been determined in the fracture mechanics format and reported by various sources. Discrepancies in typical crack growth relationships reported in the literature are not uncommon. Much of the variability has been categorized as normal scatter. As a result, relatively little is known about fatigue crack growth rate response of materials in use today. Use of statistics to define significance of particular data trends has been minimal. The material, environment, and loading variables noted in Table 4 should be recognized as important factors affecting fatigue crack growth rates [18, 19]. To successfully use the fatigue crack growth relationship in life prediction requires identification of application parameters and their control in the fatigue crack growth test. However, additional and often neglected aspects of the relationship concern variables of the test and analysis methods to establish the basic growth rate data. These factors include specimen design, precrack procedures, precision of load application and crack length measurement, generation of crack length versus elapsed cycles (a versus N) data, processing methods for conversion of a versus N to da/dN versus ΔK , and interpretation and presentation of results. Often these testing variables influence crack growth rate more than the factors cited in Table 4. For example, Fig. 6 [20] illustrates anomalous data which do not fit the general pattern developed from a number of identically shaped specimens tested at various fixed load range, ΔP . In this case, the anomalous behavior was recognized as transient crack growth rate characteristics developed from data established at crack lengths very close to the machined starter notch. This and other supporting data [19] suggested the need for a minimum precrack length requirement that will generally

TABLE 4—Factors that can influence fatigue crack growth rates.

Material Variables

- Composition
- Microstructure
 - Purity, homogeneity
 - Size, type, distribution of second phase particles
- Processing
 - Thermal, mechanical
- Product form
- Mechanical properties

Environmental Variables

- Environmental chemistry and electrochemistry
- Temperature
- Pressure

Loading Variables

- Load history
 - Load range, stress ratio, frequency, waveform, overloads, underloads
 - Stress State
 - Thickness, constraint
 - Type of loading, uniaxial or multiaxial
 - Principal stress direction with respect to grain flow
-

derived from specific experiments constructed to establish guidelines for fatigue crack growth rate testing. Presently, there exists ASTM Tentative Test for Constant-Load-Amplitude Fatigue Crack Growth Rates Above 10^{-8} m/cycle (E 647-78 T). Standardization of low crack growth rate measurement (that is, $da/dN < 10^{-8}$ m/cycle) has progressed on a separate timetable because of the added complexity and more limited experience of data acquisition within this regime. Low crack growth rate test methodology has advanced to the state that a proposed standard practice exists. At this writing, proposed recommended procedures for high and low crack growth rate measurement have been consolidated into one concise document [17]. The remainder of this section is intended to highlight basic steps to be followed for establishing fatigue crack growth rate data according to this document.

Establishment of Test Conditions

The importance of selecting test conditions that are representative of the particular application already has been presented. Material should be tested in the processed form in which it is to be used. Specimen orientation, with respect to grain flow, environment, and mechanical loading variables should be selected likewise. The range of crack growth rates or ΔK traversed, or both, should be commensurate with those expected of the actual part. Sensitivity of fatigue crack growth rates to test parameters, such as those listed in Table 4, should be recognized and controlled in the test to minimize potential sources of variability and enhance understanding of mechanisms. Dependent upon the application, it is often practical to select test parameters typical of the "worst case" to ensure conservative life prediction.

Specimen Type, Size, and K Calibration

Choice of specimen type obviously will be narrowed by conditions of the test. This selection should be confined only to those configurations for which a well established stress intensity factor calibration exists. The compact specimen (CT) and the center crack tension (CCT) specimen have been identified as preferred testing configurations in the ASTM tentative guidelines (ASTM Method E 647). The CT specimen is recommended for tension-tension loading and is the most ideal configuration for measurement of very low rates of crack growth [19]. The CCT specimen is best suited for testing of thin sections and is recommended for tests at negative R values. Recommended proportions and tolerances for the CT and CCT configurations, and their stress intensity calibration³ basically follow those guidelines developed

³Wide range elastic stress intensity solutions valid for dimensionless crack length, $a/W \geq 0.2$ for the CT specimen and $a/W \leq 0.95$ for the CCT specimen are now available (ASTM Method E 647).

for fracture toughness testing. However, an allowable thickness range for the CT specimen is given by the limits, $W/20 \leq B \leq W/2$, where B is the specimen thickness, and W the effective specimen width measured from the centerline of load application. The lower thickness limit provides assurance that buckling will not occur in relatively thin specimens. The upper limit on thickness allows the standard fracture toughness specimen to be used for fatigue crack growth rate testing. However, crack front straightness and curvature can be controlled better and their effects minimized by use of specimens that are thin relative to their planar size. Therefore, a preferred upper limit on CT specimen thickness $B \leq W/4$, is stated in the recommended practice (Ref 17 and ASTM Method E 647). The latter limit is better suited to satisfy validity requirements on crack front straightness and minimize the need for curvature correction on crack length. More discussion on aspects of crack front straightness and curvature is deferred to later sections of this paper. The same rationale is used to set preferred and allowable thickness limits for the CCT specimen as $B \leq W/8$ and $B \leq W/4$, respectively. No lower limit on B for the CCT specimen is given since this limit is sensitive to gage length, method of gripping, and R ratio (positive or negative). Bending strains should be kept to within 5 percent of the nominal strain, and use of antibuckling constraints may be necessary to maintain this strain level.

An additional specimen size requirement is necessary to maintain predominantly elastic conditions in the specimen. This condition is met when the remaining uncracked ligament ($W - a$) of the CT and CCT specimen configurations satisfy

$$(W - a) \geq \frac{4}{\pi} \left(\frac{K_{\max}}{\sigma_{ys}} \right)^2, \quad \text{for the CT specimen}$$

or

$$(W - 2a) \geq \frac{P_{\max}}{B\sigma_{ys}}, \quad \text{for the CCT specimen}$$

where P_{\max} and K_{\max} are the respective maximum cyclic load and stress intensity factor and σ_{ys} the monotonic yield strength (0.2 percent offset).

For high strength, low monotonic strain hardening materials the aforementioned size requirement for the CT specimen has been shown to correspond to the onset of measurable plastic deformation which is accompanied by acceleration in growth rate [19]. The size requirement on this class of materials is therefore justified as being appropriate and necessary. On the other hand, the CT specimen size requirement appears to be overly restrictive for low strength materials which exhibit significant monotonic strain hardening, and several alternatives for relaxation of the aforementioned requirement have been proposed [19, 21].

Load Arrangements and Test Equipment

Specimen gripping fixtures should be designed to conform with boundary conditions assumed in deriving the stress intensity factor of the specimen. Careful attention should be given to achieving as good an alignment as possible. General gripping for the pin loaded CT specimen should be designed to allow free rotation as the specimen is loaded. The type of grip for the CCT specimen depends on the specimen width and loading condition (that is, tension-tension or tension-compression). Single pin, multiple bolts, and mechanical or hydraulic clamping devices, or both, are all suitable fixturing for the CCT specimen. The recommended minimum CCT gage length varies with the type of fixturing and is specified so that a uniform stress develops in the test section. Accordingly, shorter specimen gage lengths are permissible with gripping devices that distribute loads more uniformly. Clamping devices, which are necessary for tension-compression loading, permit the shortest possible CCT gage length, and hence minimize buckling problems. Recommended grip arrangements are described in (Ref 17 and ASTM Method E 647).

Optimum choice of test equipment also depends on the type of test. However, the equipment should be capable of maintaining load accuracies within ± 2 percent of the maximum and range of applied load (that is, P_{\max} and ΔP). An accurate cycle counting device is also needed.

Precracking

The importance of precracking is to provide a sharp, straight (also symmetrical for the CCT specimen) crack of adequate size which assures (1) the effect of the machined starter notch is removed from the specimen K calibration, and (2) elimination of any permanent or transient fatigue crack growth characteristics caused by changing crack front shape or precrack load history. The need for a requirement on minimum precrack length was cited earlier by example. The precracking equipment should ensure symmetry of load distribution with respect to the notch and the maximum stress intensity factor should be controlled carefully during the final stages of precracking. It is preferred that final K_{\max} of the precrack not exceed the initial K_{\max} for which test data are to be obtained. However, in the event that the precrack process is expedited by stepping down loads to initial test values, the magnitude of load steps and crack growth increment per step shall be within prescribed limits given by the recommended practice (Ref 17 and ASTM Method E 647). These precautions are necessary to ensure that crack growth delay effects are eliminated upon commencement of the actual test. Changing R value may introduce transient crack growth effects, particularly at low ΔK , as indicated by Fig. 4. Therefore, it is preferred that R , for the last step of precracking be equivalent to that at the start of the test, especially when targeted initial growth rates are about 10^{-8} m/cycle or less.

Establishment of Crack Length versus Cycles (a versus N) Data

It has been previously recorded that the primary source of variability in fatigue crack growth rates is scatter encountered in establishing nontransient test (*a* versus *N*) data [18]. Of major concern in establishing such data for analysis are potential problems that arise from several forms of transient crack growth phenomena when conditions of the test are changed. For example, crack growth rates are known to become transient with changes in P_{\max} , P_{\min} , or R , or with frequency and waveform, especially when environmental effects are present [22]. Changes in environmental chemistry or electrochemistry also are known to promote transient behavior [23-25]. Sufficient crack extension should be allowed following changes in load or environmental variables, or both, to enable growth rate to attain a steady state value. The amount of crack growth required depends on the magnitude of load change, the material, and the environment. Additional guidance for dealing with changes in loading variables is given in Ref 17 and ASTM Method E 647.

Testing at constant load range, ΔP and fixed loading variables is well suited for establishment of high and intermediate rates of crack growth. However, this may not always be practical, for example, when a wide range in ΔK is sought from a single specimen. Whenever loads are changed, it is preferred that maximum load increase rather than decrease. This is to preclude overload induced delay phenomena; retardation being more pronounced than accelerated crack growth associated with incremental increase in P_{\max} .

A special K -decreasing procedure has been developed for measurement of intermediate and low crack growth rates (less than 10^{-7} m/cycle). Under this approach, reasonable loads are used to precrack the specimen to predetermined crack lengths, whereupon a procedure of progressive shedding of load with increasing crack extension commences. The rate of load shedding is controlled such that K nominally decreases with increasing crack length, and *a* versus *N* information obtained during the shedding process can be converted to da/dN versus ΔK . Load shedding continues until the lowest ΔK or growth rate of interest is achieved. For the establishment of very low da/dN data this approach has considerable merit since significant time spent precracking at low stress intensities is eliminated. Programmed shedding of load may be conducted either as a series of step decreases in load at selected crack length intervals, or in a continuous manner by an automated technique that makes use of an analog or digital computer [26], or both. The load shedding (K -decreasing) test may be halted at any crack length, then continued at constant ΔP to obtain comparison data under K -increasing conditions. This approach, whereby a K -decreasing and K -increasing experiment are conducted on a single test, provides a viable means for detection and elimination of anomalous data. This procedure is recommended when obtaining low crack growth rate data from a limited number of specimens.

Additional guidelines were formulated to ensure validity of low ΔK data established under K -decreasing conditions. The specific requirements and supporting data are too detailed to elaborate on here, but their basis is described in Ref 19 and ASTM Method E 647. Primarily, these additional requirements control the magnitude and rate of load-shed with increasing crack extension to be gradual enough to (1) preclude anomalous data resulting from reductions in stress intensity factor and concomitant growth rates, and (2) allow establishment of about five (da/dN , ΔK) data points of approximate equal spacing per decade of crack growth rate. At very low ΔK it is also preferred that R be fixed because of the significant influence of this variable on low crack growth rates, for example, as shown in Fig. 4.

Measurement of crack length is an integral part of the test data collection process. Measurement procedures should be employed which are capable of resolving crack extensions to recommended accuracies [19] (0.10 mm or 0.002 W , whichever is greater). Maximum limits on the crack growth measurement interval, Δa , are dependent on specimen type, size, and crack resolution capability. The minimum Δa should be 0.25 mm or ten times the measurement precision, whichever is greater. Crack length versus cycles data are considered invalid where the average through the thickness crack departs more than ± 5 degrees from the plane of horizontal symmetry, or where any two surface (front and back side) crack measurements differ by more than 0.025 W or by more than 0.25 B , whichever is less. Upon termination of the test, fracture surfaces shall be examined for excessive crack front curvature. At any visible crack front contour (for example, precrack or terminal crack size) an average through the thickness crack length is to be determined in accordance with ASTM Method E 399. The difference between the average through-thickness crack length and the corresponding crack length measured during the test (for example, surface crack length if visual methods are employed) represents a crack curvature correction. If the crack curvature correction results in a greater than 5 percent difference in calibrated stress intensity, then a correction procedure (Ref 17 and ASTM Method E 647) should be employed when analyzing the data.

Calculation of Crack Growth Rate and Stress Intensity Factor Range Relationship

The rate of fatigue crack growth is to be determined from crack length versus cycles data. The preferred techniques for this calculation are either the secant (point to point) or incremental polynomial method (Ref 17 and ASTM Method E 647). The maximum value and range of applied stress intensity factor, K_{\max} and ΔK , respectively, shall be calculated by substituting measured values of load and crack length into the specimen stress intensity factor relationship. The loading variables K_{\max} , ΔK , and R are related such that specifying two uniquely defines the third according to the relationship $\Delta K = (1 - R) \cdot K_{\max}$ for $R > 0$, and $\Delta K = K_{\max}$ for $R \leq 0$.

Reporting

The test report should include loading and environmental conditions, specimen dimensions, and a complete description of the material, including location and orientation of the specimen with respect to the parent product. Crack growth data which violate validity requirements should be separated from valid data.

Crack growth rate data are generally plotted as da/dN as a function of ΔK on log-log coordinates. For optimum data comparison the size of one log- ΔK decade should be two to four times larger than the size of one log- da/dN decade. A mathematical representation of the crack growth rate curve is useful for subsequent integration; however, at this writing no consensus relationship exists. Additional work is needed in this important area. More specific reporting requirements are prescribed in Ref 17 and ASTM Method E 647.

Sustained Load Cracking (SLC)

Subcritical size cracks may also grow under sustained loading in the presence of a corrosive or elevated temperature environment, or both. Growth does not always begin immediately, but generally occurs after an incubation period, the length of which depends on the alloy-environment system involved. For damage-tolerant analysis it is conservative to assume the incubation time as negligible and life of the part to be that spent in propagating the crack to critical size. Fracture mechanics concepts can be used to develop relationships between applied stress, flaw size, and SLC growth. Baseline data, expressing da/dt in terms of K , are therefore useful for appraising SLC and establishing inspection intervals and limits for damage-tolerant design [27-30].

The relationship between da/dt and K , as well as experimental procedures for its measurement, are very similar for both stress corrosion and creep crack growth. Remaining discussion is restricted to stress corrosion cracking (SCC) where the greatest SLC experience exists. A parallel for creep cracking may be drawn by substituting elevated temperature environment for aggressive environment in the following remarks.

Stress Corrosion Crack (SCC) Growth Relationship

The kinetics of SCC growth encountered in many engineering materials is described by the three regions illustrated schematically in Fig. 7. Regions 1 and 3 of Fig. 7 are analogous to those previously described for cyclic growth, for example, Fig. 3. Within Region 2, SCC growth rates are influenced by environment, and da/dt becomes relatively insensitive to K . Some investigators have found the "plateau" of Region 2 to be a useful index for screening

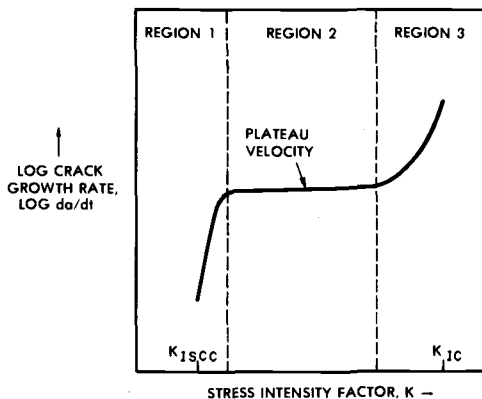


FIG. 7—Schematic representation of stress corrosion crack growth rate data.

resistance to SCC for particular material-environment combinations [31]. For some material-environment combinations, Region 3 and sometimes Region 2 may not exist when toughness is so low that fracture occurs prior to the onset of Region 3. On the other hand, wedging by corrosion products can interfere with the observation of Region 1.

Like fatigue, the concept of a threshold value, $K_{I,SCC}$, below which SCC growth has not been observed has been accepted provisionally in some materials (for example, titanium and most steels in natural aqueous environments). However, some materials, for example, certain high strength aluminum alloys tested in the short transverse orientation, show a continuous finite rate of da/dt decrease with decreasing K down to velocities as low as 10^{-8} to 10^{-9} cm/s. In this case, defining the SCC threshold as some arbitrary low velocity provides a practical means of characterizing a material's resistance to SCC. There are indications that at K levels close to the $K_{I,SCC}$ the incubation period may become very long and sensitive to prior history. Thus, crack growth behavior at low stress intensity factors may not always be consistent and failure times difficult to predict from growth rate data. Therefore, caution is needed when using the concept of $K_{I,SCC}$ for design purposes.

Variations from the typical SCC relationship of Fig. 7 have been reported by many investigators. Metallurgical factors, such as alloy type and processing variations, also chemical environment, stress state, direction of stress with respect to grain flow, and residual stresses are all known to have strong influence on SCC velocities. To emphasize what has been said previously, the selection of test conditions for establishing baseline data has significant bearing on the success of the intended evaluation.

SCC Testing with Precracked Specimens

Since test methods for measurement of SCC growth are widely varied, many factors that contribute to the establishment of uniform test methodology remain to be evaluated. The multiplicity of approaches reflects, in part, varied needs of individual users of these data. Moreover, the wide difference in magnitude of effects in different material-environment combinations makes formulation of standard test practices difficult. Nevertheless, the need for standardization has been recognized, and ASTM Committees E-24 on Fracture Testing of Materials and G-1 on Corrosion of Metals are working jointly to develop recommended practices for precracked SCC specimens. Because mechanisms of the SCC process are complex and not fully understood, standardization will be an evolutionary process. At present, general agreement is needed on one or two standard specimen designs and the necessary operational controls for conducting of the tests. Many of the factors pertinent to standardization of fracture toughness and fatigue crack growth test methods (for example, specimen preparation, fixturing, crack measurement, recording of data, . . .) can be used in formulation of SCC testing guidelines.

Comprehensive surveys of precrack specimen SCC test methods, specimen types and relative merits of each have been presented elsewhere [29,32], and will not be repeated here. Remaining discussion will simply highlight some of the basic differences and pertinent considerations of SCC test methodology in use today. The intent here is to present options available for establishing optimum material(s) data for SCC growth life prediction. The selection of specimen type and means of stress application influences the extent of K versus da/dt information that may be obtained by a given procedure. The selection of a particular test procedure must take into account the desired objective, related experience, and other economic and time constraints.

Depending on the method of load application and specimen configuration, K can be made to increase, decrease, or remain constant as the crack extends. Generally, specimens are provided with fatigue precracks. In some cases the cracks are introduced through mechanical wedging to produce a "pop-in" crack emanating from a sharply machined starter notch. The latter has the advantage of eliminating expensive precrack time. Relatively little information exists concerning the influence of precrack method on SCC growth. Available test results have shown that high precrack stresses or mechanical pop-in on subsequent SCC performance may, or may not, have an effect depending on the material-environment combination involved [29]. Moreover, other test results have shown that fatigue precracks introduced in air could lead to different results in subsequent SCC tests than those in which fatigue precracks were introduced in the corrosive environment [29]. Again, the latter observation depends on the material-environment combination involved.

Specimens in which K increases with crack length are most commonly stressed under conditions of fixed or slowly increasing loads usually achieved by dead weight, mechanical, or hydraulic devices. Fixturing requirements are essentially consistent with those of fatigue, namely good alignment should be maintained and errors that arise from friction in specimen connections should be eliminated. SCC test results can be affected severely by external sources of vibration, therefore the testing arrangement should be constructed to minimize vibration induced stressing. An advantage of the K increasing technique is that once crack growth is initiated, crack length may be monitored over long distances in relatively short periods of time prior to rapid fracture. Generally, behavior in Regions 2 and 3 are characterized effectively by this technique. Region 1 rates and K_{1sc} can be determined by this approach, but a major item of testing hardware is tied up for long periods of time to make these measurements.

Specimens in which K decreases with crack extension generally are stressed under constant deflection usually applied by a bolt, wedge, or other device. Under this form of loading, load and K diminish as the crack extends. The K decreasing specimen is highly attractive because of its portability, and the relative ease with which it is tested. The accuracy of load measurement depends upon the accuracy of the specimen compliance calibration and the exactness of deflection measurement. External vibrations are not expected to be a problem with this approach. The most commonly employed constant deflection technique is that of the bolt-loaded specimen. Specimen shape and proportions are most often selected similar to those of the standard compact specimen, while others have used the long double-cantilever-beam (DCB) specimen to remove the effect of the remaining ligament ($W-a$). Loading generally is applied through a bolt which is drilled and tapped into the top arm of the specimen which contacts with a loading pin or other bolt in the bottom arm of the specimen. The bolt and loading pin generally are machined from high strength steels to prevent plastic flow during test. After precracking the specimen, the bolt(s) is torqued to a predetermined displacement measured by a clip-on displacement gage attached to the specimen mouth. The specimen is placed in the environment and removed when crack arrest occurs. Subsequent reloading in a tensile machine to the arrest deflection corresponding to crack arrest, is used to measure the corresponding final load and an arrest K value. Alternatively, the load may be calibrated by instrumentation of the bolt. Mechanical wedges are employed sometimes in place of bolts in specimens that are too thin to accommodate bolts. In the latter test, care is required not to deform the specimen as the wedge is inserted.

Experience has shown that there are a number of problems that must be recognized and dealt with in order to achieve meaningful interpretation SCC data. For some material-environment combinations, particularly those characterized by SCC branching, cessation of Region 2 crack growth may be

relatively abrupt as K decreases with crack length and, hence, the estimated threshold K value would be nonconservative. In other cases, the crack may depart from a single plane. Side grooves are used sometimes to prevent deviations from the intended fracture path, but this places an unnatural constraint on crack growth. The buildup of corrosion products at the crack tip can cause stresses at the crack tip. In extreme cases, corrosion product wedging action can be so severe as to lift the loading bolts free of contact with the entire stress being supplied by the corrosion product. When corrosion product buildup is expected to be a problem, K -increasing tests generally will provide more accurate descriptions of the da/dt versus K relationship. It should also be appreciated that few laboratory SCC characterization tests are of durations comparable to service conditions, and added conservatism is often warranted converting basic SCC data to service performance.

In summary, basic material characterization of SCC growth behavior requires discretion in selecting the most appropriate test method and interpretation of the data. There is obvious need for further development of standardized test practices for this purpose.

Summary

Fracture toughness, fatigue crack growth, and stress corrosion crack growth data comprise a basic package of material(s) information for use in crack growth life prediction. Progress toward standardization of testing practices to establish this information is reviewed. Useful guidelines are provided to the engineer seeking to recognize problems and minimize variability of crack growth analysis through proper development of baseline material(s) data.

References

- [1] Airplane Requirements, MIL-STD 1530. Aircraft Structural Integrity Program, United States Air Force, 1 Sept. 1972.
- [2] Tada, H., Paris, P. C., and Irwin, G. R., *The Stress Analysis of Cracks Handbook*, Del Research Corporation, Hellertown, Pa., 1973.
- [3] Sih, G. C., *Handbook of Stress Intensity Factors for Researchers and Engineers*. Institute of Fracture and Solid Mechanics, Lehigh University, Bethlehem, Pa., 1973.
- [4] Rooke, D. P. and Cartwright, D. J., *Compendium of Stress Intensity Factors*, Executive Ministry of Defense Her Majesty's Stationery Office, London, 1976.
- [5] Wheeler, O. E., "Spectrum Loading and Crack Growth," *Journal of Basic Engineering: Transactions*, American Society of Mechanical Engineers, Series D, Vol. 94, March 1972, p. 181.
- [6] Willenborg, J., Engle, R. M., and Wood, H. A., "A Crack Growth Retardation Model Using an Effective Stress Intensity Concept," Technical Report AFFDL-TM-71-1-FBR, Air Force Flight Dynamics Laboratory, Jan. 1971.
- [7] Wood, H. A., Gallagher, J. P., Engle, R. M., and Potter, J. M., "Current Practice on Estimating Crack Growth Damage Accumulation with Specific Application to Structural Safety, Durability, and Reliability," Technical Report AFFDL-TR-75-32, Air Force Flight Dynamics Laboratory, Jan. 1976.

- [8] Brown, W. F., Jr., and Srawley, J. E., *Plane Strain Crack Toughness Testing of High Strength Metallic Materials*, ASTM STP 410, American Society for Testing and Materials, 1966.
- [9] Kaufman, J. G. in *Developments in Fracture Mechanics Test Methods Standardization*, ASTM STP 632, American Society for Testing and Materials, 1977, p. 3.
- [10] *Developments in Fracture Mechanics Test Methods Standardization*, ASTM STP 632, W. F. Brown, Jr. and J. G. Kaufman, Eds., American Society for Testing and Materials, 1977.
- [11] *Rapid Inexpensive Tests for Determining Fracture Toughness*, National Materials Advisory Board, National Research Council, 1976.
- [12] Kaufman, J. G. and Hold, M., "Fracture Characteristics of Aluminum Alloys," Technical Paper No. 18, Alcoa Research Laboratories, 1965.
- [13] Bucci, R. J., "Selecting Aluminum Alloys to Resist Failure by Fracture Mechanisms," ASME Design Engineering Conference, Chicago, May 1977; Alcoa Report No. 57-77-24, Sept. 1977.
- [14] Bucci, R. J., Collis, S. F., Kohm, R. F., and Kaufman, J. G., "Sharply Notched Cylindrical Tension Specimen for Screening Plane-Strain Fracture Toughness, Part 2, Applications in Aluminum Alloy Quality Assurance of Fracture Toughness," *Developments in Fracture Mechanics Test Methods Standardization*, ASTM STP 632, American Society for Testing and Materials, 1977.
- [15] Feddersen, C. E., "Toughness Criteria at the Structural/Materials Interface," *Fracture Prevention and Control*, American Society of Metals, 1974.
- [16] Gallagher, J. P., "Fatigue Crack Growth Rate Laws Accounting for Stress Ratio Effects," ASTM Task Force E24.04.04 of Subcommittee E24.04 on Subcritical Crack Growth, Report No. 1, 1974.
- [17] "Proposed Method of Test for Steady-State Fatigue Crack Growth Rates," Appendix 1, Technical Report AFML-TR-78-40, Air Force Materials Laboratory, May 1978.
- [18] Clark, W. G., Jr., and Hudak, S. J., Jr., *Journal of Testing and Evaluation*, Vol. 3, No. 6, 1975, p. 454.
- [19] Hudak, S. J., Bucci, R. J., Saxena, A., and Malcolm, R. C., "Development of Standard Methods of Testing and Analyzing Fatigue Crack Growth Rate Data," Technical Report AFML-TR-78-40, Air Force Materials Laboratory, May 1978.
- [20] Sullivan, A. M. and Crooker, T. W., "Evaluation of Fatigue Crack-Growth Rate Determination Using a Crack-Opening-Displacement Technique for Crack-Length Measurement, NRL Report 7912, Naval Research Laboratory, Sept. 1975.
- [21] James, L. A., "Some Observations Regarding Specimen Size Criteria for Fatigue Crack Growth Rate Testing," Report HEDL-TME 77-87, Hanford Engineering Development Laboratory, Aug. 1977.
- [22] Hertzberg, R. W., *Deformation and Fracture Mechanics of Engineering Materials*, Wiley, New York, 1976.
- [23] Wei, R. P., *Engineering Fracture Mechanics*, Vol. 1, No. 4, 1970, p. 633.
- [24] Hudson, C. M. and Seward, S. K., *Engineering Fracture Mechanics*, Vol. 8, No. 2, 1976, p. 315.
- [25] Crooker, T. W., *ASTM Standardization News*, May 1975, p. 17.
- [26] Saxena, A., Hudak, S. J., Donald, J. K., and Schmidt, D. W., "Computer Controlled K-Decreasing Test Technique for Low Rate Fatigue Crack Growth Testing," Scientific Paper 77-1E7-FANWL-P1, Westinghouse Research Laboratories, March 1977.
- [27] Brown, B. F., *Metallurgical Reviews*, Vol. 13, 1968, p. 171.
- [28] Wei, R. P. in *Proceedings*, International Conference on Fundamental Aspects of Stress Corrosion Cracking, National Association of Corrosion Engineers, Houston, Tex., 1969, p. 104.
- [29] *Stress Corrosion Cracking in High Strength Steels and in Titanium and Aluminum Alloys*, B. F. Brown, Ed., Naval Research Laboratory, Washington, D.C., 1972.
- [30] Kaufman, J. G., Bogardus, K. O., Mauney, D. A., and Malcolm, R. C. in *Mechanics of Crack Growth*, ASTM STP 590, American Society for Testing and Materials, 1976, p. 149.
- [31] Sprowls, D. O., Coursen, J. W., and Walsh, J. D. in *Stress Corrosion—New Approaches*, ASTM STP 610, American Society for Testing and Materials, 1976, p. 143.
- [32] *Stress Corrosion—New Approaches*, ASTM STP 610, H. L. Craig, Ed., American Society for Testing and Materials, 1976.

R. M. Engle, Jr.¹

Aspect Ratio Variability in Part-Through Crack Life Analysis

REFERENCE: Engle, R. M., Jr., "Aspect Ratio Variability in Part-Through Crack Life Analysis," *Part-Through Crack Fatigue Life Prediction, ASTM STP 687*, J. B. Chang, Ed., American Society for Testing and Materials, 1979, pp. 74-88.

ABSTRACT: A survey of various analytical solutions currently used in part-through crack life prediction is presented. Solutions are included which account for shape change effects as well as constant shape solutions. Comparisons of these solutions with constant amplitude experimental data are examined. Results are presented for three different materials: 2219-T851 aluminum, 6Al-4V (β annealed) titanium and 9Ni-4Co-0.20C steel.

KEY WORDS: part-through cracks, life analysis, stress-intensity factors, crack growth analysis, crack propagation, fatigue (materials)

Nomenclature

a	Crack depth
c	Surface half crack length
C_a	Crack growth rate constant-depth
C_c	Crack growth rate constant-surface
da/dN	Crack growth rate-depth
dc/dN	Crack growth rate-surface
F	Front surface correction factor
K	Stress intensity factor
ΔK	Stress intensity factor range, ($K_{\max} - K_{\min}$)
K_{th}	Threshold stress intensity factor
m	Threshold crack growth rate exponent
M_k	Back surface correction factor
n_a	Crack growth rate exponent-depth

¹Aerospace engineer, Air Force Flight Dynamics Laboratory, Wright-Patterson AFB, Ohio 45433.

- n_c : Crack growth rate exponent-surface
- N : Cycles
- Q : Part-through crack shape parameter
- t : Plate thickness
- β : Parametric angle for elliptical crack
- Φ : Complete elliptical integral of the second kind
- σ : Applied stress
- σ_y : Material yield strength

Many common crack geometries occurring in aircraft structures can be characterized in terms of a single crack length parameter. For example, the edge-through crack, the center-through crack and the radial-through crack emanating from a hole can all be described by a stress-intensity factor (SIF) which depends only upon the variation of the single-dimensioned surface crack length. The SIF for these geometries remains constant through the thickness along the crack front. Many crack propagation computer programs for life prediction have adopted this approach of using a single "characteristic" crack length in the analysis, which will be subsequently referred to as a one-dimensional analysis [1,2].²

The curved crack front presented by the part-through crack (PTC) leads to a variation of the SIF around the periphery of the crack front. Since the SIF does vary, the crack growth rates also will vary around the periphery of the crack front. This implies that crack shape may vary during the crack growth process, making it usually impossible to characterize the PTC in terms of a single crack length parameter. The most popular expression for the SIF for a part-through crack is due to Irwin [3]. This solution contains two parameters, the aspect ratio of the ellipse, a/c , and an angle, β , which characterizes the location on the crack front (see Fig. 1).

Stress-Intensity Factor Formulation

The SIF formulation, based upon Irwin's solution with correction factors for both the front surface [4] and back surface [5] is given by

$$K = \sigma \sqrt{\pi a/Q} [(a/c)^2 \cos^2 \beta + \sin^2 \beta]^{1/4} \cdot F \cdot M_k \quad (1)$$

where

$$Q = \Phi^2 - 0.212 (\sigma/\sigma_y)^2$$

²The italic numbers in brackets refer to the list of references appended to this paper.

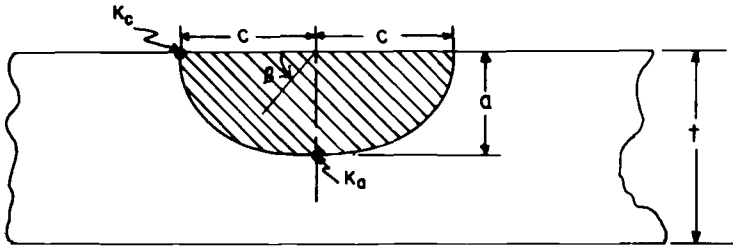


FIG. 1—Geometry for part-through crack.

$$\Phi = \int_0^{\pi/2} \left[1 - \left(\frac{c^2 - a^2}{c^2} \right) \sin^2\theta \right]^{1/2} d\theta$$

and

$$F = 1 + 0.12 (1 - a/2c)^2$$

The back surface correction factor, M_k , is given in Table 1 as a function of $a/2c$ and a/t .

Evaluating Eq 1 at the major and minor axes of the elliptical crack leads to the following expressions for K_a , the SIF at point a , and K_c , the SIF at point c .

$$K_a = \sigma \sqrt{\pi a/Q} [1 + 0.12(1 - a/2c)^2] \cdot M_k \tag{2}$$

$$K_c = 1.12\sigma \sqrt{\pi c/Q} (a/c) \tag{3}$$

TABLE 1—Back surface correction factor.

		$a/2c$					
		0.05	0.10	0.20	0.30	0.40	0.50
		M_K					
a/t	0.0	1.00	1.00	1.00	1.00	1.00	1.00
	0.1	1.01	1.01	1.01	1.01	1.01	1.00
	0.2	1.03	1.03	1.02	1.02	1.01	1.00
	0.3	1.06	1.06	1.04	1.03	1.02	1.00
	0.4	1.12	1.12	1.08	1.05	1.02	1.00
	0.5	1.22	1.18	1.14	1.08	1.03	1.01
	0.6	1.34	1.30	1.22	1.13	1.06	1.01
	0.7	1.48	1.42	1.31	1.20	1.08	1.02
	0.8	1.64	1.57	1.41	1.26	1.13	1.04
	0.9	1.77	1.68	1.50	1.32	1.18	1.08
1.0	1.84	1.75	1.59	1.38	1.22	1.10	

Analytical Assumptions

Most existing aircraft life prediction programs perform one dimensional analyses based on a single crack length parameter. From Eq 1 it is evident that this restriction implies that the parametric angle, β , must be fixed or eliminated. Further, the shape parameter, Q , does not change. Thus, the analyst must decide upon a value for β and a constant shape which will best represent the crack growth pattern for the given initial conditions.

Equation 1 shows that the stress-intensity factor actually varies around the periphery of the crack front. Existing two-dimensional analyses perform independent crack growth analyses in both the depth and surface directions using Eqs 2 and 3. These independent analyses then are coupled through the shape parameter, Q . Hall et al [6] presented an analysis based upon this approach which assumed that the crack growth rate was the same in both directions. Forman et al [7] presented a similar analysis in which the crack growth rate was assumed to be dependent upon the direction of propagation. Forman assumed the crack growth rate along the surface to be twice the crack growth rate in the depth direction.

The obvious questions arise concerning which techniques should be chosen to perform a life prediction for a part-through crack and the impact of the choices made upon the accuracy of the life prediction. The next section of the paper addresses these questions. Six types of analytical assumptions for part-through crack growth are examined. These assumptions are listed in Table 2.

The crack growth rate versus stress-intensity factor range relationship used in this analysis was developed by Hall [6] under a USAF sponsored research program in 1973. The experimental data taken during this program form the basis for the evaluation of the two-dimensional approaches. Hall's crack growth rate relationship may be written

$$da/dN = C_a (K_{\max,a} - K_{th})^m (\Delta K_a)^{n_a} \quad (4)$$

$$dc/dN = C_c (K_{\max,c} - K_{th})^m (\Delta K_c)^{n_c} \quad (5)$$

The study conducted by Hall et al examined three materials: 2219-T851 aluminum, 9Ni-4Co-0.20C Steel and 6Al-4V beta annealed titanium. Table 3 presents all the material properties developed in Ref 6 for the three materials.

Crack Growth Accumulation Algorithm

For the two-dimensional analyses the crack growth accumulation algorithm performs two independent crack growth analyses using Eqs 2 and 4 to

TABLE 2—Basic crack growth assumptions for the types of analysis considered.

Analysis Type	Assumptions
Two-dimensional type assumptions:	
1	The crack growth rate depends on crack growth direction.
2	The crack growth rate is independent of crack growth direction.
One-dimensional type assumptions:	
3	Φ, Q do not change The crack grows so that the initial shape is held constant.
4	The initial crack is replaced with a semi-circular crack which has the same depth as the initial crack. The crack grows maintaining the semi-circular shape.
5	The initial crack is replaced with a semi-circular crack which has the same SIF (at the depth position) as the initial crack. The crack grows maintaining the semi-circular shape.
6	The initial crack is replaced with a semi-circular crack which has the same area within its perimeter. The crack grows maintaining the semi-circular shape.

TABLE 3—Material properties.

Material	σ_y (ksi) ^a	K_c (ksi√in)	K_{th} (ksi√in)	c	m	n
2219-T851 aluminum	52.6	40	1.5	0.34×10^{-8}	0.84	2.40
9Ni-4Co-0.20C steel	186.6	130	10	0.40×10^{-8}	0.57	1.76
6Al-4V(β A) titanium	128	141	5	0.33×10^{-10}	1.02	3.00

^aOriginal measurements in U.S. customary units. Conversion factors are: 1 in. = 25.4 mm; 1 ksi = 0.145 MPa; 1 ksi√in. = 0.9099 MPa√m.

grow the crack in the depth direction and Eqs 3 and 5 to grow the crack in the surface direction. These two crack growth analyses are coupled through the shape factor Q in the following manner: (a) given an initial flaw having a_i and c_i , calculate Q_i , (b) using a_i , c_i and Q_i , calculate $K_{\max,a}$, $K_{\max,c}$, ΔK_a , ΔK_c using Eqs 2 and 3, (c) using $K_{\max,a}$, $K_{\max,c}$, ΔK_a and ΔK_c , calculate da/dN and dc/dN using Eqs 4 and 5, (d) using da/dN , dc/dN , a_i and c_i , calculate a_{i+1} and c_{i+1} , (e) using a_{i+1} and c_{i+1} , calculate Q_{i+1} , (f) repeat steps b through e until failure or breakthrough. The one-dimensional analyses were performed using the current version of the CRACKS computer code [1]. These analyses are performed in the following manner (a) given an initial flaw having a_i and c_i as defined by one of the one-dimensional assumptions in Table 2, calculate $Q_i = Q$, (b) using a_i and Q , calculate $K_{\max,a}$ and ΔK_a using Eq 2, (c) using $K_{\max,a}$ and ΔK_a , calculate da/dN using Eq 4, (d) using a_i and da/dN ,

calculate a_{i+1} , (e) repeat step b through step d until failure or breakthrough.

Experimental Data Base

The constant amplitude tests reported in Ref 6 form the data base for the evaluation and comparison of the two types of two-dimensional algorithms with typical one-dimensional algorithms using various constant shape assumptions. The tests were conducted under uniform tension loading at stress ratios of 0.1 and 0.5. Each specimen contained three parallel surface flaws located a minimum of 75 mm (3 in.)³ apart. Surface crack lengths were measured optically and final flaw shapes were determined fractographically. For each material, the geometrical parameters were varied over the following ranges

$$0.14 < a/2c < 0.50$$

$$0.25 < a/t < 0.85$$

The individual variations are presented in Table 4 for each material.

Evaluation of Analyses

All six analytical assumptions listed in Table 2 were evaluated against the experimental data for each of the 2219-T851 aluminum specimens. Figure 2 presents a comparison of the six analyses by plotting the mean value of the life prediction ratio, N_p/N_i , plus or minus the coefficient of variation. From Fig. 2 it can be seen that both two-dimensional analyses generate smaller coefficients of variation than any of the one-dimensional analyses. The implication is that the variable shape assumption of the two-dimensional analyses leads to more accurate growth patterns and, hence, less scatter. Based upon the results shown in Fig. 2 it would appear that, if the analyst is forced to use a one-dimensional analysis, the Type 3 analysis is superior. In other words, the best constant shape analysis assumption is that the flaw will grow in the shape defined by the initial crack depth and surface length.

Both two-dimensional analyses described in Table 2 were applied to all of the specimens listed in Table 4. Predictions were made for each flaw in each specimen. The predictions for both final flaw shape and cycles to breakthrough are presented in Table 4 along with the test results. The superimposed histograms of final flaw shapes in Fig. 3 give an indication of the overall capability of the analyses to predict flaw shape change. Figure 4

³Original measurements were made in U.S. customary units.

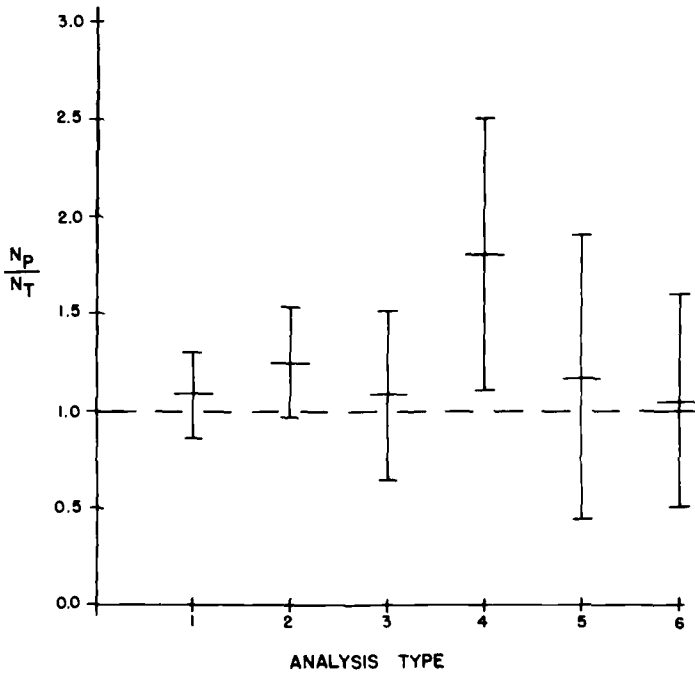


FIG. 2—Comparison of analysis types, 2219-T851 aluminum.

presents a similar evaluation of the capability to predict cycles to break-through. Both analyses are seen to present a significant improvement over all of the one-dimensional analyses (Type 3-Type 6). The improvement of the life prediction capability of Type 1 over Type 2 described previously is not so great; the most significant improvement of the Type 1 analysis over the Type 2 analysis is in the capability of handling the flaw shape change. This is illustrated graphically in Figs. 5 through 7 which compare the two techniques for each of the three materials. Examination of the predicted final flaw aspect ratios in Table 4 shows that the Type 1 analysis matched the test aspect ratios to within plus or minus 15 percent. A similar comparison using the Type 2 analysis was only capable of predicting the final flaw aspect ratio within 30 percent. Figures 5 through 7 graphically illustrate that this difference in aspect ratio leads to a considerable difference in final flaw shape.

Summary

Six different methods for handling the aspect ratio variability in part-through crack life analysis have been evaluated against an experimental data base of surface flaw specimens under constant amplitude cyclic ten-

TABLE 4—Comparison of two-dimensional analyses with test data from Ref 6 (1 in. = 25.4 mm, 1 ksi = 0.145 MPa).

Specimen No.	Thick, in.	Stress Ratio	Peak Cyclic Stress, ksi	Initial Flaw Dimensions		Final $a/2c$		Loading Cycles		
				$(a/2c)_i$	$(a/t)_i$	Actual	Predicted ^a	Actual	Predicted ^a	Predicted ^b
SUTA1-1	0.448	0.1	18	0.191	0.286	0.347	0.388	19 500	23 900	24 200
				0.294	0.317	0.400	0.405	18 800	27 400	25 900
SUTA1-2	0.449	0.1	10	0.428	0.483	0.385	0.420	16 000	17 400	23 200
				0.163	0.548	0.264	0.276	26 500	35 700	36 800
SUTA5-1	0.449	0.5	30	0.293	0.662	0.339	0.368	32 400	35 700	38 900
				0.422	0.813	0.419	0.438	19 000	21 600	24 100
SUTA5-2	0.447	0.5	18	0.171	0.254	0.318	0.384	15 600	18 800	16 500
				0.305	0.330	0.361	0.405	16 200	18 800	15 900
				0.437	0.468	0.359	0.418	14 100	13 500	14 000
				0.142	0.476	0.251	0.273	28 200	26 600	27 300
				0.280	0.635	0.327	0.365	30 200	22 200	24 200
				0.442	0.805	0.394	0.449	18 400	13 900	14 400

^aType 1 Analysis

^bType 2 Analysis

^cExtrapolated

TABLE 4—Continued.
 9Ni-4Co-0.2C Steel Alloy

Specimen No.	Thick, in.	Stress Ratio	Peak Cyclic Stress, ksi	Initial Flaw Dimensions		Final $a/2c$		Loading Cycles		
				($a/2c$) _i	(a/t) _i	Actual	Predicted ^a	Actual	Predicted ^a	Actual
SUTS1-1	0.306	0.10	44	0.163	0.173	0.406	0.381	57 000	52 200	60 900
				0.322	0.245	0.440	0.391	57 000	49 200	63 400
				0.447	0.343	0.427	0.397	43 500	38 800	51 700
SUTS1-2	0.305	0.10	30	0.149	0.484	0.268	0.276	29 200	30 200	31 300
				0.294	0.642	0.373	0.364	27 300	24 700	26 900
				0.441	0.802	0.438	0.440	21 900	15 400	17 100
SUTS1-3	0.300	0.10	60	0.165	0.183	0.396	0.373	22 800	21 200	25 800
				0.318	0.257	0.418	0.388	22 300	20 000	25 900
				0.440	0.370	0.426	0.396	16 400	15 300	20 500
SUTS5-2	0.291	0.50	45	0.149	0.512	0.261	0.261	23 700	25 900	26 800
				0.294	0.670	0.340	0.355	22 500	20 600	22 300
				0.428	0.835	0.402	0.433	15 500	11 300	12 100

6Al-4V β A Titanium Alloy

Specimen No.	Thick, in.	Stress Ratio	Peak Cyclic Stress, ksi	Initial Flaw Dimensions		Final $a/2c$		Loading Cycles		
				($a/2c$) _i	(a/t) _i	Actual	Predicted ^a	Actual	Predicted ^a	Actual
SUTTI-1	0.376	0.10	45	0.145	0.191	0.418	0.415	17 900	19 100	23 000
				0.285	0.268	0.448	0.425	19 700	18 800	25 200
				0.451	0.404	0.443	0.433	13 300	12 800	18 800
SUTTI-2	0.370	0.10	27	0.138	0.470	0.261	0.281	13 800	21 500	22 700
				0.427	0.810	0.416	0.454	9 900	10 800	12 400
			
SUTTS-1	0.372	0.50	70	0.145	0.194	0.385	0.414	15 600	16 300	17 000
				0.297	0.285	0.429	0.425	15 500	15 400	18 400
				0.439	0.398	0.435	0.432	11 700	11 500	16 300
SUTTS-2	0.382	0.50	42	0.157	0.519	0.265	0.287	12 800	15 400	16 100
				0.441	0.810	0.429	0.459	8 182	10 000	11 500
			

^a Type 1 analysis.

^b Type 2 analysis.

^c Extrapolated.

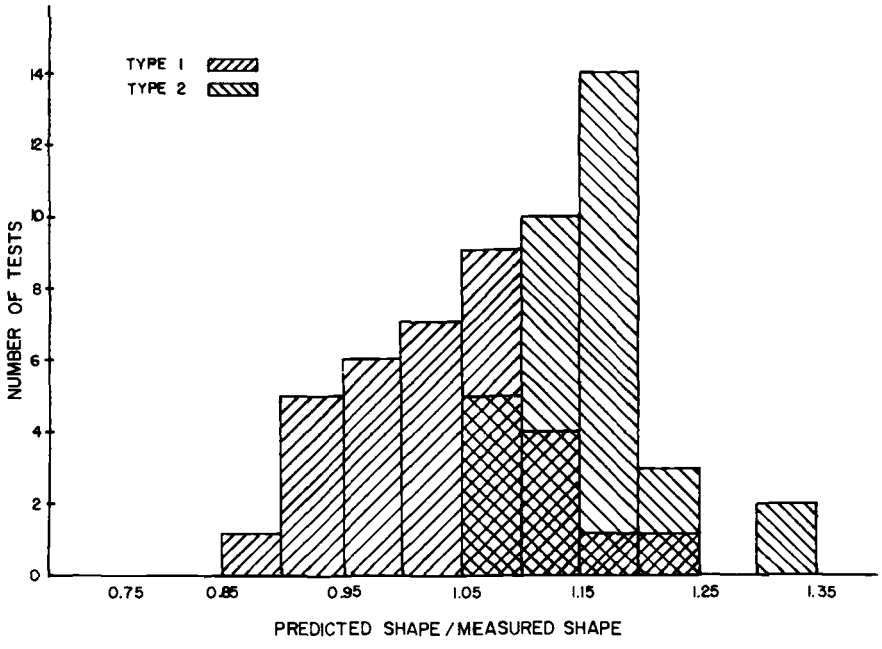


FIG. 3—Final flaw shape predictions, two-dimensional analysis.

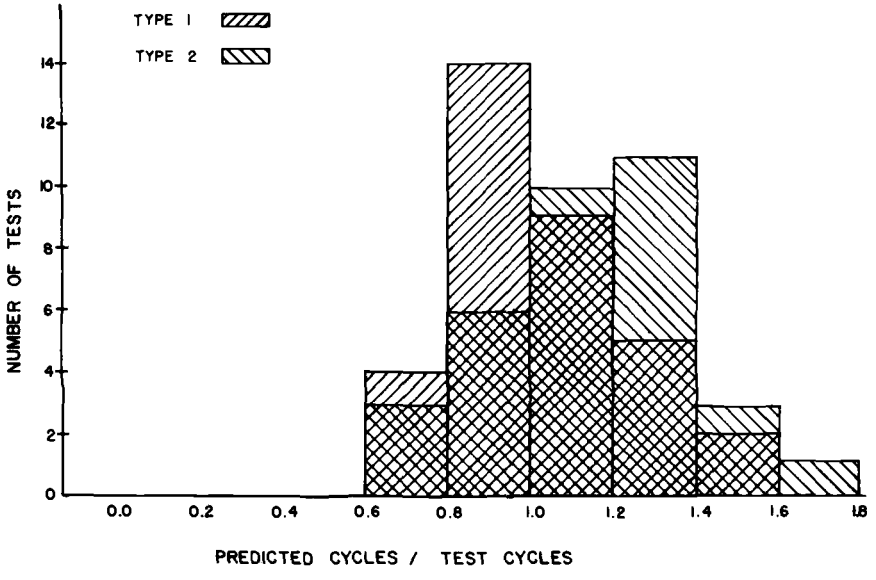


FIG. 4—Cycles to breakthrough, two-dimensional analysis.

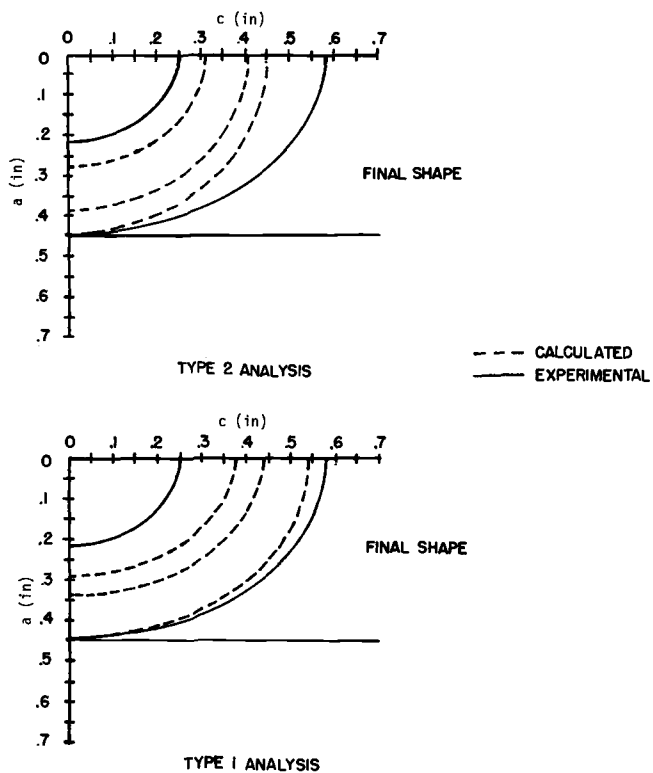


FIG. 5—Flaw shape change predictions, 2219-T851 aluminum (1 in. = 25.4 mm) SUTAI-1 (3).

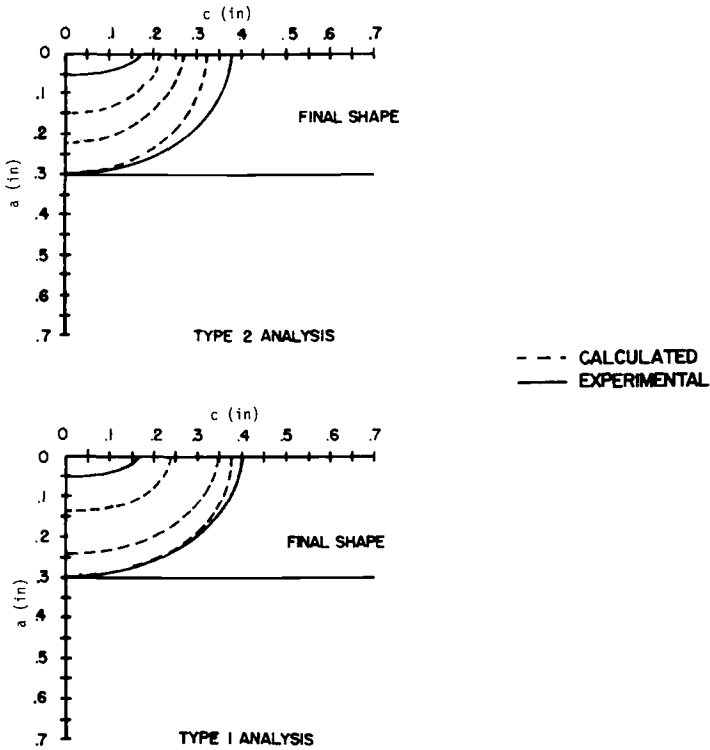


FIG. 6—Flaw shape change predictions, 9Ni-4Co-0.2C steel (1 in. = 25.4 mm) SUTSi-3 (1).

sion-tension loading. Four constant shape (one-dimensional) solutions were evaluated. Two variables shape (two-dimensional) solutions also were evaluated. Both two-dimensional solutions were shown to be superior to all of the one-dimensional solutions. The solution proposed by Forman, which assumes that the growth variation can be modeled by assuming different growth rate properties in the depth and surface directions, gave better results for final flaw shapes than the Hall solution which assumes identical growth rate properties in both directions. Results for cycles to breakthrough for both two-dimensional analyses were excellent and presented significant improvements over all the one-dimensional analyses examined.

Conclusions

Since the stress-intensity factor varies around the crack front and the state of stress also varies, flaw shape change (aspect ratio variability) should be considered in any part-through crack life analysis. Both Hall [6] and Forman [7] selected an existing stress-intensity factor formulation,

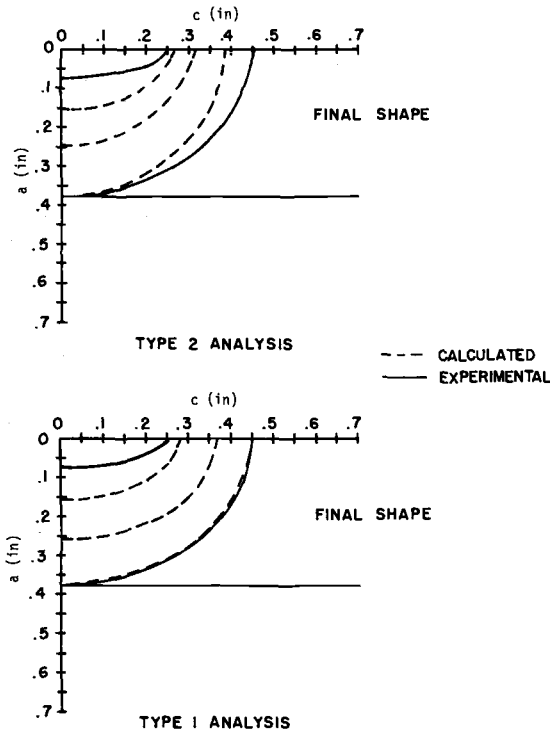


FIG. 7—Flaw shape change predictions, 6Al-4V titanium (1 in. = 25.4 mm) SUTTi-1 (1).

Eq 1, performed two-dimensional analyses using this SIF to account for the variation in growth at the depth and along the surface. In addition, Forman made an attempt to account for the varying state of stress around the crack front by modifying the apparent crack growth rate in the surface direction. Stress-intensity factor formulations are being developed and presented in the literature to eliminate the need for this artifice by providing better descriptions of the variation of stress intensity around the crack periphery.

References

[1] Engle, R. M., Jr., "CRACKS, a FORTRAN IV Digital Computer Program for Crack Propagation Analysis," AFFDL-TR-70-107, Air Force Flight Dynamics Laboratory, Oct. 1970.
 [2] Engle, R. M., Jr., "CRACKS II, a User's Manual," AFFDL-TM-74-173, Air Force Flight Dynamics Laboratory, July 1974.
 [3] Irwin, G. R. in *Journal of Applied Mechanics*, Vol. 29; *Transactions*, American Society of Mechanical Engineers, Series E, Dec. 1962, pp. 651-654.
 [4] Kobayashi, A. S. and Moss, W. L. in *Proceedings*, 2nd International Conference on Fracture, Brighton, England, 1969, pp. 31-45.

- [5] Masters, J. N., Haese, W. P., and Finger, R. W., "Investigation of Deep Flaws in Thin Walled Tanks," NASA CR-72606, National Aeronautics and Space Administration, Dec. 1969.
- [6] Hall, L. R., Shah, R. C., and Engstrom, W. L., "Fracture and Fatigue Crack Growth Behavior of Surface Flaws and Flaws Originating at Fastener Holes," AFFDL-TR-74-47, Vol. 1, Air Force Flight Dynamics Laboratory, May 1974.
- [7] Forman, R. G., Kavanaugh, H. C., and Stuckey, B., "Computer Analysis of Two-Dimensional Fatigue Flaw-Growth Problems," NASA TM X-58086, National Aeronautics and Space Administration, Feb. 1972.

G. A. Vroman¹

Life Prediction Analysis of Part-Through Cracks

REFERENCE: Vroman, G. A., "Life Prediction Analysis of Part-Through Cracks," *Part-Through Crack Fatigue Life Prediction, ASTM STP 687*, J. B. Chang, Ed., American Society for Testing and Materials, 1979, pp. 89-95.

ABSTRACT: The ability to predict part-through crack behavior analytically based on compact specimen crack growth rate data is quantified by comparing analytical predictions of cyclic life under constant amplitude loading with laboratory test results. In three analytical exercises performed by ASTM Task Group E24.06.01, a total of 24 specimens included 2219-T851 aluminum, 6Al-4V-Ti, and 9Ni-4Co-0.20C steel.

KEY WORDS: crack life, part-through cracks, life prediction accuracy, fatigue (materials), crack propagation

During recent years there has been a widespread recognition that the service life of structures often is determined by crack-like flaws undetected during fabrication. This recognition along with advances in fracture mechanics technology has resulted in the adoption of fracture control principles in structural design, thereby reducing the possibility of crack induced failures. The design procedure is to perform a life prediction analysis of the largest crack-like defect that can escape detection during the manufacturing inspection. The life prediction analysis brings together the elements which largely determine the success or failure of the structure in service; the inspection capability, the service imposed stresses, and the material fracture properties.

From a practical standpoint the only material fracture properties available to support design analysis are generated by laboratory testing of compact type specimens. However the usual type of problem in design analysis is to predict the life of initial part-through cracks (surface flaws), so the stress-intensity concept of fracture mechanics analysis is used to predict part-through crack behavior from compact specimen data. This is

¹Project engineer, Rocketdyne Division of Rockwell International, Canoga Park, Calif. 91304.

not simple to do and therefore some doubt is justified regarding the accuracy of life prediction analyses.

At the October 1975 American Society for Testing Materials (ASTM) Committee Week meeting of Subcommittee E24.06 on Applications a spirited discussion of problems associated with design analysis ended with the formation of Task Group E24.06.01 on Part Through Crack Life Prediction Analysis. From the outset there was considerable interest in this activity by other members of ASTM Committee E-24 on Fracture Testing of Materials, not only from those engaged in performing life prediction analyses but also from those interested in developing the technology. Some of this interest diminished as it became known that the principal task of E24.06.01 is to assess the design analysis applicability of material fracture properties data generated in accordance with ASTM sanctioned procedures, and to make recommendations for additional testing if the need became apparent. Any developments in analytical techniques that result from the task group activities are incidental to the principal objective. In other words, the analytical technique used to perform life prediction analyses is not important if an accurate life prediction can be made on the basis of ASTM approved data. In the task group activities chronicled in this paper, there was no intent to standardize the analytical procedures of the different investigators. In fact, diversity was encouraged.

Organizing Task Group Activities

The first meeting of our task group resulted in a general agreement regarding the scope of our activities. In order to minimize the influence of analysis unknowns, we agreed to limit the initial investigations to the simplest crack geometry (the semi-elliptical surface crack), under the simplest loading (constant amplitude sinusoidal wave shape and approximately $R = 0$). It was recognized that other types of surface cracks and other types of loading would be of more general interest, but it was believed that a simple approach would be most likely to establish a correlation between compact specimen data and part-through crack behavior. Certainly the more complicated analytical procedures associated with other problems would introduce a greater variability in the life predictions and therefore a larger disparity between analytical predictions and test results.

Because of a paradox in the chronology of fracture mechanics testing development, it was difficult to obtain test data directly applicable to the simple problem of a semi-elliptic surface crack under constant amplitude loading. Judging from the available literature, it appears that the capability to perform a large number of laboratory tests under cyclic loading was developed coincidentally with a new-found interest in spectrum loading and crack geometries such as corner cracks, cracks emanating from bolt holes, etc. Before this time the relatively few documented tests under cyclic

loading usually did not include comprehensive records of crack size measured versus the number of applied loading cycles.

Our analytical exercises were initiated after J. B. Chang of Rockwell International-Los Angeles Division provided us with two groups of test data: semi-elliptic surface crack size versus number of constant amplitude loading cycles, and compact specimen crack growth rates for the same materials. Each member of the task group was provided with the test specimen description (including initial crack size), the material crack growth rate data, but not the test results. The analytical exercise was to predict the number of loading cycles (life) before breakthrough or rupture. We believed that the objectivity used in performing the analysis was enhanced by not knowing the test results beforehand.

In all of our analytical exercises we tried to discourage the competitive urge to identify one analyst as being better than another. In keeping with our objective, we wanted to establish the predictive accuracy of the average analysis rather than the better analysis. From a practical applications viewpoint, we wanted to know the predictive accuracy of the average part through crack life prediction analysis based on compact specimen data. Therefore, the most important statistical parameter that could be expected from the analytical exercises was the average predictive ability of those participating, including some measure of the variability about the mean.

Summary of Analytical Exercises

Three analytical exercises were performed by participating members of the task group, approximating one per year during 1976 through 1978. The more important results of these exercises are summarized in Tables 1, 2, and 3. In the following paragraphs, the results are discussed relative to our objective of correlating part-through crack behavior with compact specimen data. In all of the tables and in the discussion below, the calcu-

TABLE 1—*First analytical exercise results.*

Specimen Number	Specimen Parameters ^a	Test Parameters ^d	Prediction Ratio ^e
23-18	<i>b</i>	221 (32), LHA	0.754 ± 0.196
23-17	<i>b</i>	97 (14), STW	1.444 ± 0.193
40-8	<i>c</i>	579 (84), LHA	0.670 ± 0.247
40-2	<i>c</i>	248 (36), LHA	1.095 ± 0.527

^a All specimens 12.70 mm (0.50 in.) thick, initial crack size 1.52 mm (0.060 in.) deep by 3.05 mm (0.120 in.) surface length ($a/2c = 1/2$).

^b Material is 2219-T851 aluminum.

^c Material is 6Al-4V-Ti titanium.

^d Stress in MPa (ksi), LHA = low humidity air, STW = sump tank water. All specimens cycled at 0.05 stress range ratio and 60 cpm frequency.

^e Mean and standard deviation from four analysts.

TABLE 2—Second analytical exercise results.

Specimen Number	Specimen Parameters ^a	Test Parameters ^d	Prediction Ratio ^f
23-18	typical	221 (32), LHA	0.692 ± 0.148
37-3	^b	221 (32), LHA	0.988 ± 0.288
32-2	^{b,c}	221 (32), LHA	0.454 ± 0.099
23-16	typical	97 (14), DW	1.388 ± 0.295
23-12	typical	221 (32), DW	0.747 ± 0.127
23-13	typical	221 (32), DW ^e	0.880 ± 0.158
23-17	typical	97 (14), STW	2.186 ± 1.390
27-76	typical	97 (14), STW ^e	1.982 ± 1.027
23-14	typical	221 (32), STW	0.841 ± 0.149
23-10	typical	221 (32), STW ^e	0.900 ± 0.177

^a All material 2219-T851 aluminum.

^b Thickness is 25.40 mm (1.00 in.), all others 12.70 mm (0.50 in.).

^c Initial crack is 2.29 mm (0.090 in.) deep ($a/2c = 1/3$), all others 1.52 mm (0.060 in.) deep ($a/2c = 1/2$).

^d Constant amplitude stress in MPa (ksi), LHA = low humidity air, DW = distilled water, STW = sump tank water, stress range ratio = +0.05 for all specimens.

^e Cyclic loading frequency = 6 cpm, all others 60 cpm.

^f Mean and standard deviation from six analysts.

TABLE 3—Third analytical exercise results.

Specimen Number	Specimen Parameters ^a	Test Parameters ^e	Prediction Ratio ^f
188	typical	32, LHA	0.548 ± 0.286
184	typical	54, LHA	0.798 ± 0.271
583	^b	54, LHA	0.796 ± 0.245
189	typical	54, LHA ^f	0.828 ± 0.342
190	^c	54, LHA ^g	0.690 ± 0.337
186	^d	54, LHA	0.775 ± 0.233
482	typical	54, STW ^h	1.085 ± 0.371
484	typical	54, STW	0.887 ± 0.304
185	typical	126, LHA	0.829 ± 0.212
191	^d	126, LHA	0.642 ± 0.251
483	typical	126, STW ^h	1.068 ± 0.272
486	typical	126, STW	0.877 ± 0.224

^a All material 9Ni-4Co-0.20C steel.

^b Thickness is 25.40 mm (1.00 in.), all others 12.70 mm (0.50 in.).

^c Initial crack is 1.78 mm (0.070 in.) deep, all others 1.52 mm (0.060 in.).

^d Initial crack aspect ratio ($a/2c$) is $1/3$, all others $1/2$.

^e Constant amplitude stress in MPa (ksi), LHA = low humidity air, STW = sump tank water.

^f Stress range ratio = +0.3.

^g Stress range ratio = +0.5, all others stress range ratio = 0.

^h Cyclic loading frequency = 6 cpm, all others 60 cpm.

ⁱ Mean and standard deviation from five analysts.

lated ratio of analysis versus test (predicted cycles to failure divided by actual test cycles to failure) is referred to as the prediction ratio. Any prediction ratio greater than 1.000 is unconservative in the sense that the analysis predicts more life than the specimen demonstrated by test. Additional data relative to the tabulated values are provided and discussed in the text.

In reviewing the results, it is important to remember that the prediction ratio is affected by three statistically independent variables; the variability of the compact specimen crack growth rate data, the accuracy of the analytical procedures used to predict part-through crack behavior and the natural inconsistency of part-through crack test results due to both material variability and test loading misalignments. At this time, there are not sufficient data available to quantify the relative importance of these variables. It is likely that some of the extreme variations from specimen to specimen in the listed prediction ratio averages are due principally to testing variability. On the other hand, the variability (standard deviation) of the prediction ratio for each specimen is due solely to the analytical procedures.

The results from the first analytical exercise are listed in Table 1. With perseverance, the associated specimen and test parameters also can be read from the notes. The results take on a greater importance when viewed with an appreciation of the many variations in the affecting parameters. Therefore, it was very reassuring to find that the average prediction ratio was 0.991, slightly conservative but very close to the perfect value of 1.000. Also, it was encouraging to find that the average standard deviation in the prediction ratio was 0.291, suggesting that the different analytical procedures of the four analysts did not greatly influence the results. On further investigation, the background data showed a tendency for the analytical predictions to be unconservative for high cycle fatigue and conservative for low cycle fatigue. The 1.444 mean prediction ratio of specimen 23-17 resulted from a test life of 192 000 cycles, the 1.095 ratio of 40-2 from 172 200 cycles, and down to the 0.670 ratio of 40-8 from 6784 cycles. This apparent correlation caused the life prediction analysts to re-examine their calculation procedures.

The second analytical exercise results are listed in Table 2. Within the total of twelve specimens, two were repeated from the first analytical exercise (23-17 and 23-18) giving some advantage to the observant analyst who knew the test results. The average prediction ratio for each of these two specimens do not indicate that the replication influenced the analytical results because both specimens had worse average predictions in the second exercise. Another factor that probably influenced the predictions was the crack growth rate data. Whereas in the first exercise a single crack growth rate curve was provided for the two specimens, in the second exercise a large number of curves (all that could be found) were provided, and the

analyst was required to choose between the data. Several of the analysts objected to this variation in the exercise, but the choice between apparently conflicting data is a common occurrence and certainly a factor influencing the accuracy of the life prediction procedure.

In general, the results of the first two analytical exercises were very similar. However, in the second exercise, two specimens showed significantly larger unconservatisms in their prediction ratio; specimens 23-17 and 27-76 (Table 2). A closer examination of the results shows that for specimen 23-17, three of the six analysts had a prediction ratio between 0.974 and 1.401. Similarly for specimen 27-76, the better three prediction ratios ranged between 1.113 and 1.601, as compared to the overall average of 1.982 and the extreme value of 3.738. It seems most likely that such a statistical characteristic would be caused by differences in analysis methodology rather than problems associated with the input compact specimen data. Further support for this opinion was gained in the third analytical exercise.

Table 3 lists the results of the third analytical exercise. It can be seen from the listed prediction ratios that the cyclic life of all twelve specimens were reasonably well predicted. In fact, the overall average prediction ratio of 0.819 (± 0.279 average standard deviation) is close to optimum, slightly conservative but not too conservative. As in the other analytical exercises, a layering effect of stress level appears in the results but the variation is not large at the two higher stress levels. The average prediction ratio for all 869 MPa (54-ksi) stress specimens is 0.837, which is close to the 0.854 average for all 372 MPa (126-ksi) specimens.

An overall summary of the three analytical exercises is shown in Table 4. Also listed are some of the parameters associated with these results. This summary demonstrates that our task group has investigated a wide variety of material and testing parameters, consistently achieving satisfactory predictions of part-through crack behavior from compact specimen crack growth rate data.

TABLE 4—Summary of analytical exercise results.

Year Completed	Material	Stress, MPa (ksi)	Thickness, mm (in.)	Average Ratio Analysis/Test
1976	aluminum	221 (32)	12.70 (0.50)	0.991 (4 analysts) (4 specimens)
	2219-T851	97 (14)	12.70 (0.50)	
	titanium	579 (84)	12.70 (0.50)	
	Ti-6Al-4V	248 (36)	12.70 (0.50)	
1977	aluminum	221 (32)	12.70 (0.50)	1.007 (6 analysts) (10 specimens)
	2219-T851	221 (32)	25.40 (1.00)	
		97 (14)	12.70 (0.50)	
1978	steel	221 (32)	12.70 (0.50)	0.819 (5 analysts) (12 specimens)
	HP-9-4-20	372 (54)	12.70 (0.50)	
		372 (54)	25.40 (1.00)	
		869 (126)	12.70 (0.50)	

Conclusion

The aforementioned analytical exercises demonstrate that the behavior of part-through cracks under constant amplitude loading can be predicted with sufficient accuracy on the basis of crack growth rate data obtained from compact specimens.

Acknowledgments

All of the members of ASTM Task Group E24.06.01 participated in the discussions concerning part through crack life predictions and the significance of the analytical exercise results, thereby influencing the work presented here. The following contributed considerable time and effort by participating in the analytical exercises.

J. B. Chang, Los Angeles Division, Rockwell International

R. G. Forman, Johnston Space Center, National Aeronautics and Space Administration

G. Hales and W. S. Johnson, Fort Worth Division, General Dynamics

C. M. Hudson, Langley Research Center, National Aeronautics and Space Administration

D. E. Peterson, Rocketdyne Division, Rockwell International

L. P. Pook, Department of Trade and Industry, Glasgow, United Kingdom

J. L. Rudd, Air Force Flight Dynamics Laboratory, Wright Patterson Air Force Base

The task group is under the guidance of the Subcommittee, E24.06 on Applications, presently chaired by C. M. Hudson (listed above). E. K. Walker, Lockheed-California, was subcommittee chairman during the initial activities of the task group.

Part-Through Crack Growth Predictions Using Compact Tension Crack Growth Rate Data

REFERENCE: Rudd, J. L., "Part-Through Crack Growth Predictions Using Compact Tension Crack Growth Rate Data," *Part-Through Crack Fatigue Life Prediction, ASTM STP 687*, J. B. Chang, Ed., American Society for Testing and Materials, 1979, pp. 96-112.

ABSTRACT: The validity of using compact tension fatigue crack growth rate data to predict constant amplitude fatigue crack growth of part-through crack specimens was assessed. The assessment reported herein is one of six such assessments made by various members of the ASTM Task Group E24.06.01 on Application of Fracture Data in Life Prediction. Each of six members of this task group predicted the crack growth behavior for ten part-through crack specimens using compact tension crack growth rate data, with only one member having prior knowledge of the part-through crack test results. This author's assessment is presented in detail together with a comparison of the ratio of the analytical/experimental cycles to "breakthrough" and "failure" as determined by each of the six members of the task group.

KEY WORDS: compact tension, part-through crack, round robin, fatigue (materials), crack propagation

While a relatively large amount of subcritical crack growth rate data exists for compact tension specimens, a much smaller amount of such data exists for part-through crack specimens. This is due to the fact that it is easier to make crack length measurements on compact tension specimens and it is easier to characterize the stress intensity solutions for these specimens. Because of the different geometries, crack shapes, etc., involved for the two types of specimens, a question that is often raised is whether it is proper to use compact tension fatigue crack growth rate data to predict the crack growth behavior of part-through crack specimens.

Approach

In order to assess the validity of using compact tension crack growth rate

¹Aerospace engineer, Air Force Flight Dynamics Laboratory (AFFDL/FBE), Wright-Patterson AFB, Ohio 45433.

data to predict the crack growth behavior of part-through crack specimens, an analytical round-robin exercise was performed by members of the ASTM Task Group E24.06.01 on Application of Fracture Data in Life Prediction. Each member predicted the crack growth behavior for ten part-through crack specimens (using compact tension data) for a number of different environments, constant amplitude cyclic loading rates, thicknesses, stress levels, initial crack sizes, and initial aspect ratios. After the analytical predictions were performed, experimental test data for the part-through crack specimens were provided by J. B. Chang. Analytical predictions then were correlated with these experimental test results in order to perform the desired assessment.

Compact Tension Crack Growth Rate Data

Each member of the ASTM Task Group E24.06.01 was furnished with crack growth rate curves, representing compact tension crack growth rate data, by J. B. Chang to be used to predict the crack growth behavior of the ten part-through crack specimens. These computer-generated curves represent a mean fit to the test data generated from compact tension specimens, such as the specimen illustrated in Fig. 1. The material involved was 2219-T851 aluminum. The data were generated for dry air, distilled water, and sump tank water environments at a cyclic loading rate of one cycle per second and a stress ratio of $R = 0.08$. The thicknesses of the specimens were $B = 44.45$ mm (1.75 in.) and 50.8 mm (2.0 in.).² The specimen depth W

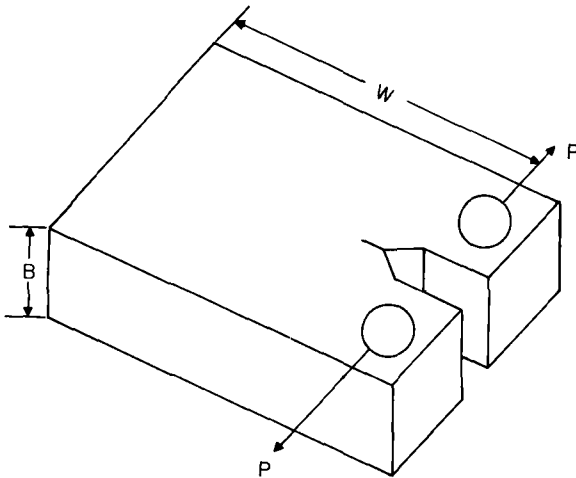


FIG. 1—Compact tension specimen.

²The original measurements were in U.S. customary units.

and the maximum stress level S_{\max} for which the crack growth rate data were generated were unspecified. The crack growth rate curves used in the part-through crack growth predictions will be presented later in this report.

Part-Through Crack Tests

Part-through crack tests for 2219-T851 Al were conducted using specimens of the type illustrated in Fig. 2. The tests were conducted in dry air, distilled water, and sump tank water environments at cyclic loading rates of 0.1 cps and 1 cps. The specimen thicknesses were $B = 12.7$ mm (0.5 in.) and 25.4 mm (1.0 in.) and the specimen width was $W = 101.6$ mm (4.0 in.). The specimens were subjected to maximum stress levels of $S_{\max} = 96.53$ MPa (14 ksi) and 220.64 MPa (32 ksi) at a stress ratio $R = 0.05$. Two initial crack depths, $a_i = 1.52$ mm (0.06 in.) and 2.29 mm (0.09 in.), and two initial aspect ratios, $(a/2c)_i = 0.40$ and 0.50, were considered. It should be noted that while the compact tension crack growth rate data provided were generated for a loading rate of 1 cps, part-through crack growth predictions were also required for a loading rate of 0.1 cps. Also, while the compact tension crack growth rate data provided were generated for thicknesses of $B = 44.45$ mm (1.75 in.) and 50.8 mm (2.0 in.), part-through crack growth predictions were required for thicknesses of $B = 12.7$ mm (0.5 in.) and 25.4 mm (1.0 in.). These differences in the geometric and loading conditions for the compact tension and part-through crack specimens could have contributed to the differences between the analytical predictions and experimental test results.

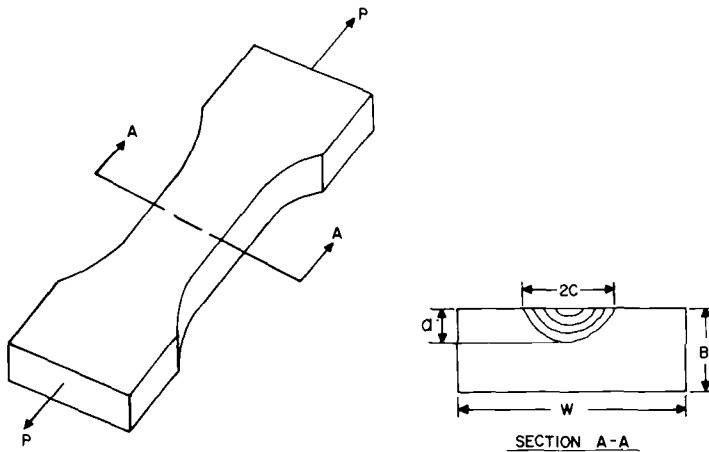


FIG. 2—Part-through crack specimen.

Part-Through Crack Analyses

This member's predictions of the crack growth behavior of the part-through crack specimens were performed using the CRACKS computer program [1].³ The following one-dimensional (that is, the crack was assumed to grow at a constant aspect ratio) stress intensity solution for a surface crack was used in the analyses

$$K = 1.1\sigma \sqrt{\frac{\pi a}{Q}} M_k \tag{1}$$

where

- 1.1 = front surface correction factor,
- σ = far field stress,
- a = crack depth,
- Q = flaw shape parameter, and
- M_k = back surface correction factor.

The flaw shape parameter Q can be expressed as follows [2]

$$Q = \Phi^2 - 0.212 \left[\frac{\sigma}{\sigma_y} \right]^2 \tag{2}$$

where σ_y is the yield strength and Φ is the elliptic integral

$$\Phi = \int_0^{\pi/2} \left[1 - \left[\frac{b^2 - a^2}{b^2} \right] \sin^2 \theta \right]^{1/2} d\theta \tag{3}$$

in which a is the semi-minor axis of the ellipse, b is the semi-major axis, and θ is an angular coordinate. The back surface correction factor M_k [3], currently contained in the CRACKS computer program in tabular form, is presented in Table 1. It can be seen that the back surface correction factor is a function of the ratio of the crack depth to the thickness, a/B , as well as the aspect ratio $a/2c$.

The criterion used in the analyses to represent the transition from a surface crack to a through-the-thickness crack is illustrated in Fig. 3. The surface crack is grown at a constant shape until the crack depth a is equal to the thickness B . At this time, a through-the-thickness crack is assumed to exist, having a crack length $2c$, equal to the surface crack length at the time of transition.

³The italic numbers in brackets refer to the list of references appended to this paper.

TABLE 1—Back surface correction factor.

		<i>a/2c</i>					
		0.05	0.10	0.20	0.30	0.40	0.50
<i>a/B</i>		<i>M_k</i>					
		0.0	1.00	1.00	1.00	1.00	1.00
0.1	1.01	1.01	1.01	1.01	1.01	1.01	1.00
0.2	1.03	1.03	1.02	1.02	1.01	1.01	1.00
0.3	1.06	1.06	1.04	1.03	1.02	1.02	1.00
0.4	1.12	1.12	1.08	1.05	1.02	1.02	1.00
0.5	1.22	1.18	1.14	1.08	1.03	1.03	1.01
0.6	1.34	1.30	1.22	1.13	1.06	1.06	1.01
0.7	1.48	1.42	1.31	1.20	1.08	1.08	1.02
0.8	1.64	1.57	1.41	1.26	1.13	1.13	1.04
0.9	1.77	1.68	1.50	1.32	1.18	1.18	1.08
1.0	1.84	1.75	1.59	1.38	1.22	1.22	1.10

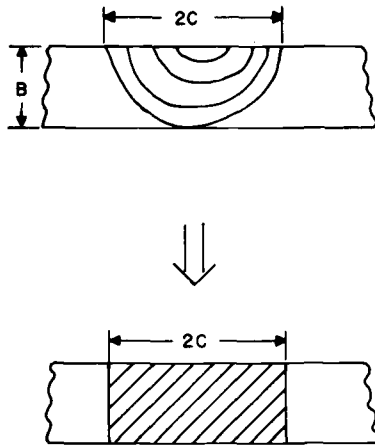


FIG. 3—Transition criterion.

After transition, the following expression was used to represent the stress intensity solution for a through-the-thickness crack

$$K = \sigma\sqrt{\pi a} F(a/w) \tag{4}$$

$F(a/w)$ is the finite width correction factor expressed as [4]

$$F(a/w) = \sqrt{\secant(\pi a/w)} \tag{5}$$

From the data furnished to each member and Ref 5, values selected by this

member for the fracture toughness K_c and the yield strength σ_y were 68.10 MPa \sqrt{m} (62.0 ksi $\sqrt{in.}$) and 330.95 MPa (48 ksi), respectively. Points were selected from the crack growth rate curves furnished to each member and input directly into the CRACKS computer program in tabular form (da/dN versus ΔK). The crack growth for the part-through crack specimens was determined using the Runge-Kutta numerical integration method.

Analytical/Experimental Crack Growth Results

Dry Air Environment

Three part-through crack predictions involved a dry air environment. Crack growth rate curves, representing compact tension crack growth rate data, were furnished to each member for these predictions (Fig. 4). These computer-generated curves represent a mean fit to the test data. The data were generated for a cyclic loading rate of 1 cps and a stress ratio of 0.08. Crack growth rate curves are presented for thicknesses of 44.45 mm (1.75 in.) and 50.8 mm (2.0 in.). The 44.45 mm (1.75 in.) crack growth rate

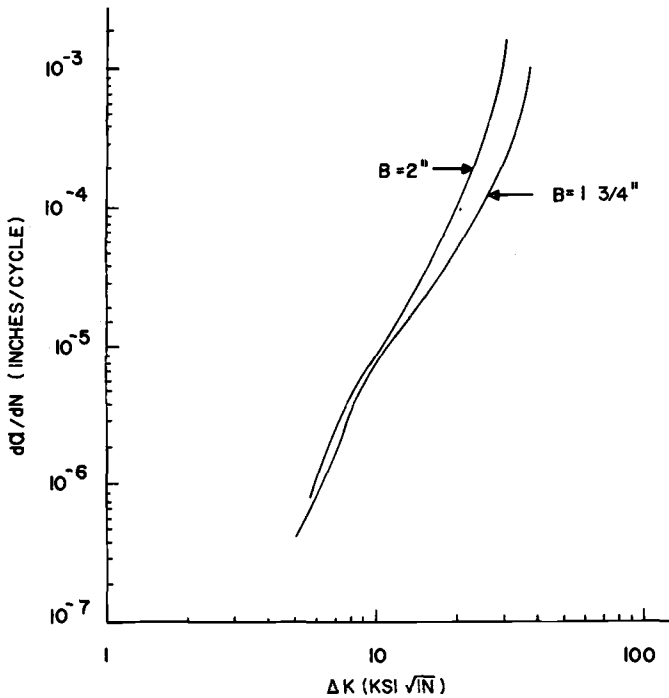


FIG. 4—Crack growth rate data for dry air environment (1 in. = 25.4 mm, 1 ksi = 0.145 MPa).

curve was selected for use in the predictions because this was closer to the 12.7 mm (0.5 in.) and 25.4 mm (1.0 in.) thicknesses of the part-through crack specimens. A straightedge was used to divide the selected crack growth rate curve into 14 linear segments (on the log-log plot). The values of the 15 points for the chosen segments were input directly into the CRACKS computer program in tabular form (da/dN versus ΔK). Desired intermediate values were calculated using a linear interpolation routine contained in CRACKS.

The analytical/experimental correlations for a dry air environment are presented in Figs. 5, 6, and 7. The solid curves represent the analytical predictions and the dashed curves represent the experimental test data. Each figure indicates the loading rate, thickness, maximum stress level, stress ratio, initial crack depth, and initial aspect ratio involved. Conservative lives were predicted for the specimens. It should be mentioned that although the specimen of Fig. 7 was tested with an initial aspect ratio $(a/2c)_i = 0.40$, each member was mistakenly informed that the initial aspect ratio was 0.33. Hence, $(a/2c)_i = 0.33$ was used in the analysis. If the actual initial aspect ratio of 0.40 had been used in the prediction, the predicted life would have been even more conservative.

Distilled Water Environment

Three part-through crack predictions involved a distilled water environ-

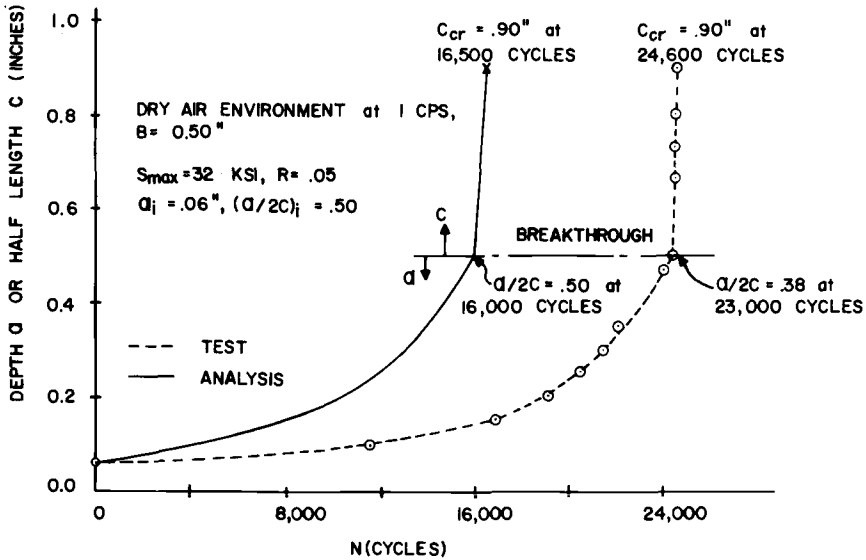


FIG. 5—Crack growth correlation for example No. 1 (1 in. = 25.4 mm, 1 ksi = 0.145 MPa).

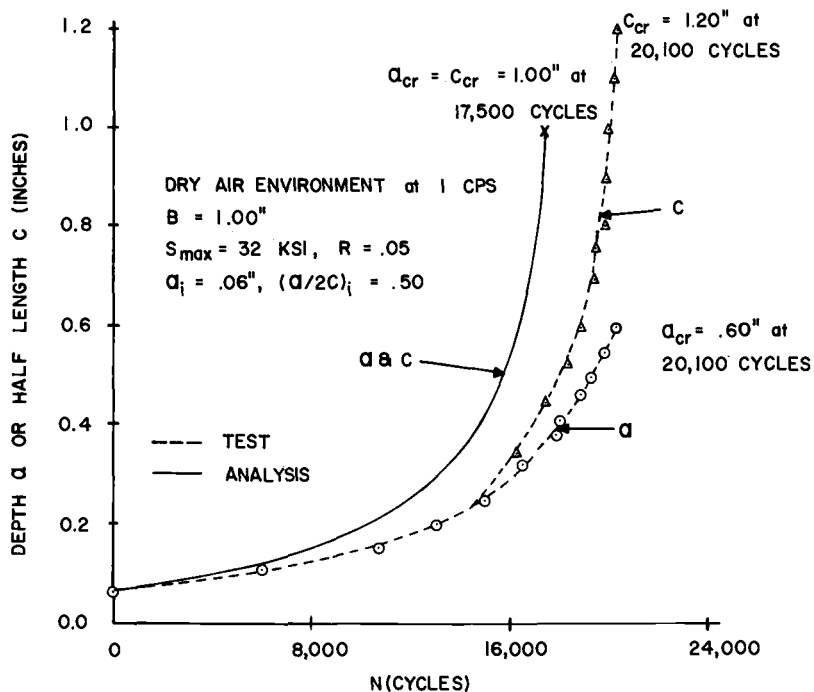


FIG. 6—Crack growth correlation for example No. 2 (1 in. = 25.4 mm, 1 ksi = 0.145 MPa).

ment. A crack growth rate curve, representing compact tension crack growth rate data, was furnished to each member for these predictions (Fig. 8). This computer generated curve represents a mean fit to the test data. The data were generated for a cyclic loading rate of 1 cps, stress ratio of 0.08, and thickness of 50.8 mm (2.0 in.). The furnished crack growth rate curve was divided into 15 linear segments and values for the 16 points defining the linear segments were input into CRACKS in tabular form. Because one of the part-through crack examples for this environment involved stress intensity ranges below those represented by the solid curve, the CRACKS computer program used extrapolated values for this slow growth region. The extrapolated crack growth rate values used in the prediction for this example are represented by the dashed curve in Fig. 8.

The analytical/experimental correlations for a distilled water environment are presented in Figs. 9, 10, and 11. The second example for a distilled water environment (Fig. 10) involved the same basic loading and geometric conditions as the preceding example (Fig. 9) with the exception that the loading rate was 0.1 cps rather than 1 cps. Because crack growth rate data were only furnished for a loading rate of 1 cps, the prediction for the previous example also was used for this example. The example in Fig.

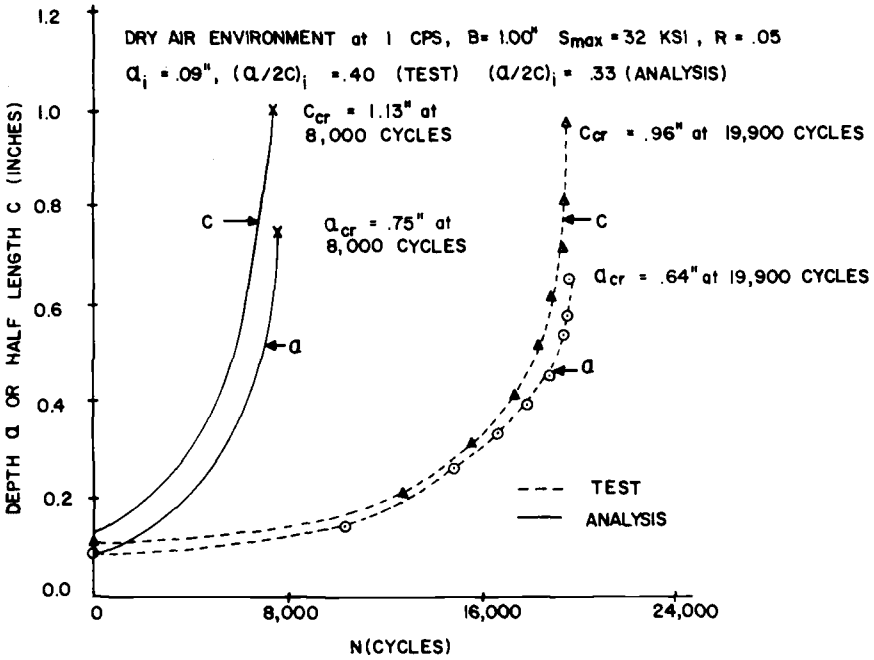


FIG. 7—Crack growth correlation for example No. 3 (1 in. = 25.4 mm, 1 ksi = 0.145 MPa).

11 involved a maximum stress of 96.53 MPa (14 ksi) instead of the 220.64 MPa (32 ksi) stress levels for Figs. 9 and 10. This lower maximum stress level resulted in stress intensity ranges below those of the furnished crack growth rate data. In fact, the majority of the predicted crack growth life involved these low stress intensity ranges for which extrapolated crack growth rates were required. These extrapolated crack growth rates were determined in the CRACKS computer program using the two slowest crack growth rates input into the program. The extrapolated analytical growth rates in this slow growth region were apparently very unconservative, as demonstrated by Fig. 11.

Sump Tank Water Environment

Four part-through crack predictions involved a sump tank water environment. A crack growth rate curve, representing compact tension crack growth rate data, was furnished to each member for these predictions (solid curve in Fig. 12). This computer generated curve represents a mean fit to the test data. The data were generated for a cyclic loading rate of 1 cps, stress ratio of 0.08, and thickness of 44.45 mm (1.75 in.). The furnished

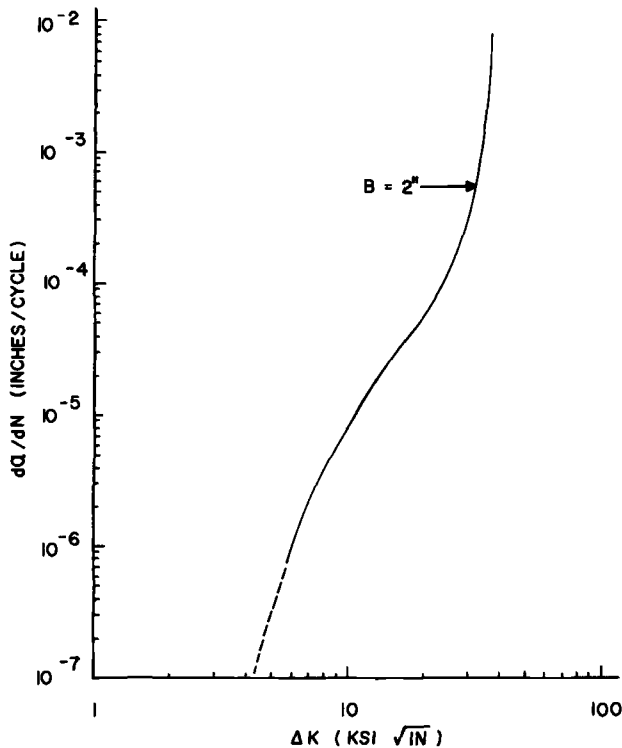


FIG. 8—Crack growth rate data for distilled water environment, (1 in. = 25.4 mm, 1 ksi = 0.145 MPa).

crack growth rate curve was divided into ten linear segments and values for the eleven points defining the linear segments were input into CRACKS in tabular form. Because two of the part-through crack examples for this environment involved stress intensity ranges below those represented by the solid curve, extrapolated values were used for this slow growth region. The extrapolated values used in the predictions for these two examples are represented by the dashed curve in Fig. 12. Also shown in Fig. 12 is a Walker Equation [6] fit to the previous 2219-T851 data (average fit to both dry air and sump tank water environments) which was used in a previous analytical round-robin exercise by the members of the ASTM Task Group E24.06.01. It can be seen that for the slow growth region, the crack growth rates for the Walker Equation are considerably higher (as much as an order of magnitude) than those for the extrapolated curve. Hence, the extrapolated analytical growth rates were apparently very unconservative.

The analytical/experimental correlations for a sump tank water environment are presented in Figs. 13 through 16. The second example for a sump

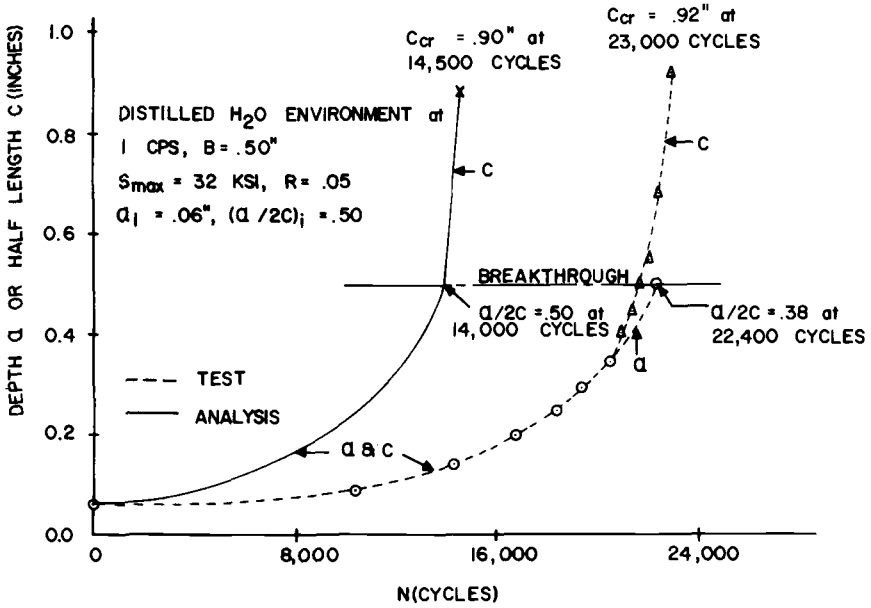


FIG. 9—Crack growth correlation for example No. 4 (1 in. = 25.4 mm, 1 ksi = 0.145 MPa).

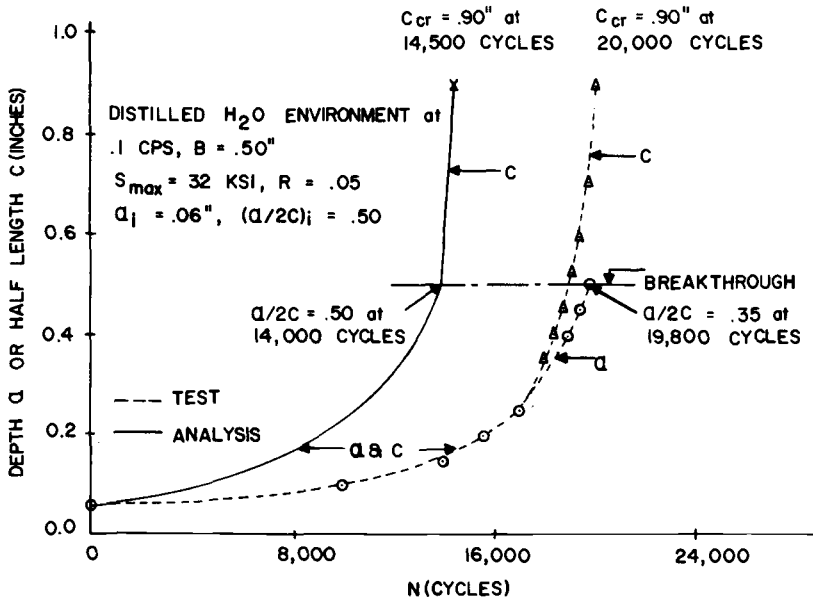


FIG. 10—Crack growth correlation for example No. 5 (1 in. = 25.4 mm, 1 ksi = 0.145 MPa).

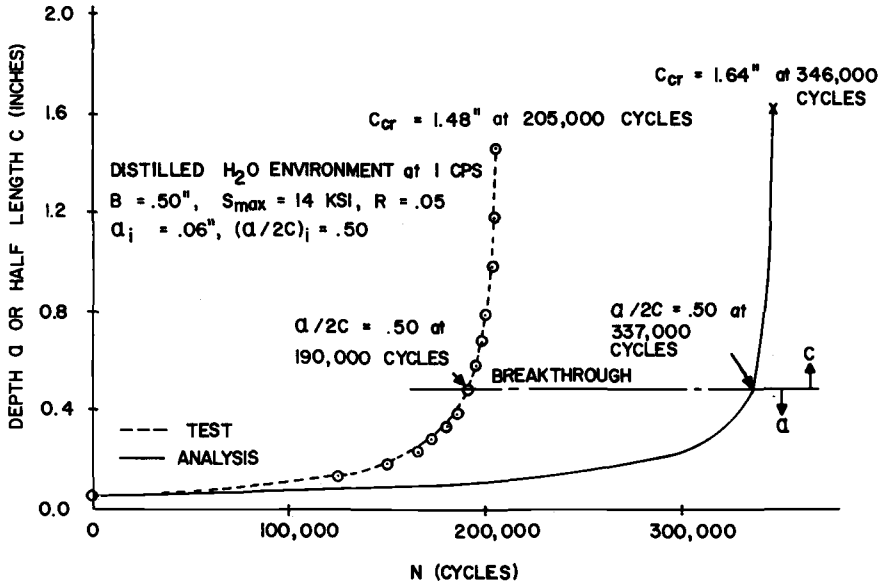


FIG. 11—Crack growth correlation for example No. 6 (1 in. = 25.4 mm, 1 ksi = 0.145 MPa).

tank water environment (Fig. 14) involved the same basic loading and geometric conditions as the preceding example (Fig. 13) with the exception that the loading rate was 0.1 cps rather than 1 cps. Because crack growth rate data were only furnished for a loading rate of 1 cps, the prediction for the previous example also was used for this example. The example in Fig. 15 involved a maximum stress of 96.53 MPa (14 ksi) instead of the 220.64 MPa (32 ksi) stress level for Figs. 13 and 14. This lower maximum stress level resulted in stress intensity ranges below those of the furnished crack growth rate data. In fact, the majority of the predicted crack growth life involved these low stress intensity ranges for which extrapolated crack growth rates were required. As previously discussed, very unconservative crack growth rates in this slow crack growth region were developed in the analytical prediction, as demonstrated by Fig. 15. The example in Fig. 16 involved the same basic loading and geometric conditions as the preceding example (Fig. 15) with the exception that the loading rate was 0.1 cps rather than 1 cps. Again, because crack growth rate data were furnished for only a loading rate of 1 cps, the prediction for the previous example also was used for this example.

Summary of Analytical/Experimental Correlations

Table 2 contains a ratio of this member's predicted life to the experi-

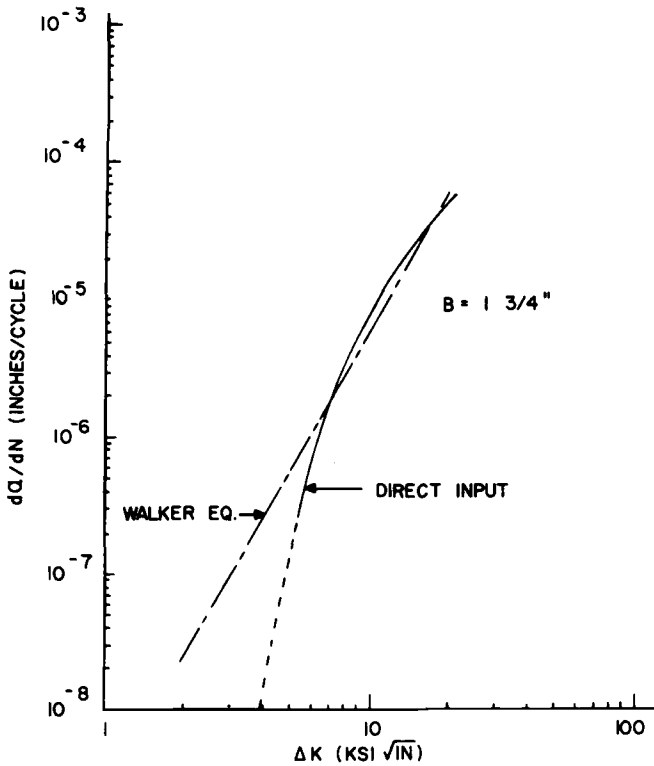


FIG. 12—Crack growth rate data for sump tank water environment (1 in. = 25.4 mm, 1 ksi = 0.145 MPa).

mental test life at breakthrough and failure for each of the ten examples considered in the round-robin exercise. Recalling that examples 1 through 5, 7, 8 involved a maximum stress level of 220.64 MPa (32 ksi), it can be seen that conservative crack growth life predictions were made for these seven examples, for which crack growth rate data were available for the entire stress intensity range of interest. The correlations of the predicted and test lives for these seven examples are within the normal expected scatter of the crack growth rate data. However, unconservative crack growth predictions were made for the three examples involving the lower maximum stress level of 96.53 MPa (14 ksi), for which crack growth rate data were not available for the slow growth region and extrapolated crack growth rate data were used in the predictions. Particularly unconservative is the prediction for Examples 9 and 10 (the same prediction was used for two different loading rates).

Table 3 presents the mean and standard deviation of each member's ratios of predicted lives to experimental lives at breakthrough and failure

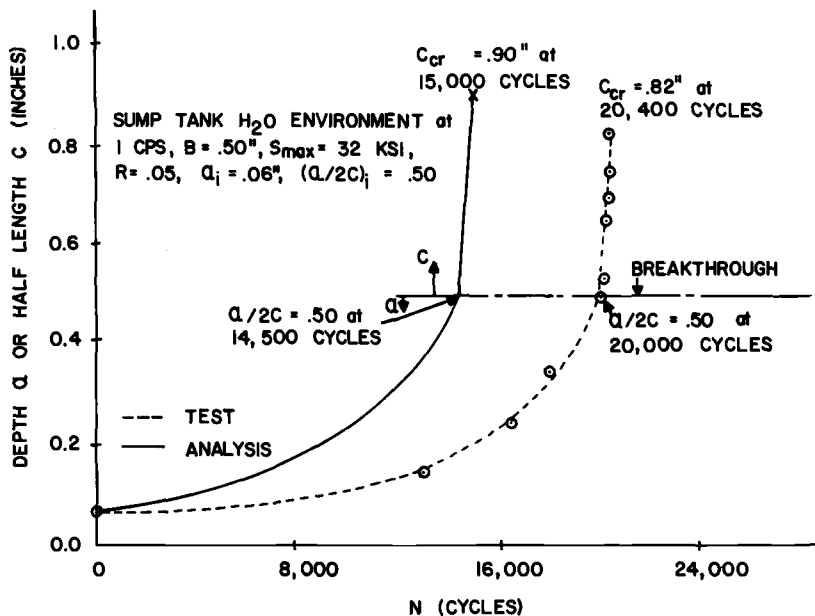


FIG. 13—Crack growth correlation for example No. 7 (1 in. = 25.4 mm, 1 ksi = 0.145 MPa).

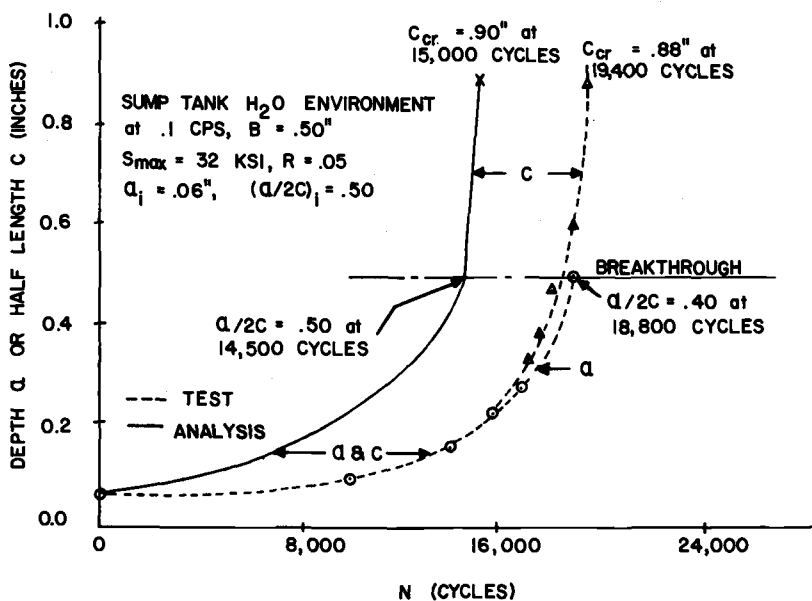


FIG. 14—Crack growth correlation for example No. 8 (1 in. = 25.4 mm, 1 ksi = 0.145 MPa).

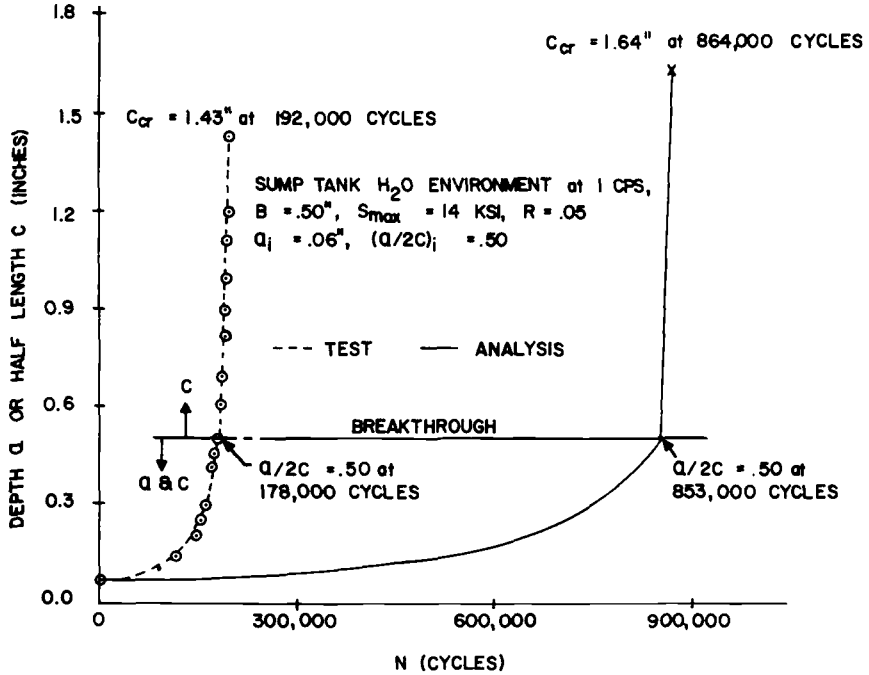


FIG. 15—Crack growth correlation for example No. 9 (1 in. = 25.4 mm, 1 ksi = 0.145 MPa).

for the ten examples considered in the round-robin exercise. It appears that this member's analytical methodology is very unconservative. However, this is due to one very unconservative prediction which was used in two examples (Examples 9 and 10). This is demonstrated by Table 4 which is similar to Table 3 except that it summarizes only the first eight examples (Examples 9 and 10 are not included). Hence, by eliminating one prediction (two examples), this member's analytical methodology now appears to be conservative. It can be seen that summarizing the results in this manner, when only a few examples are involved, can be misleading. This is especially true when one prediction completely dominates the results, such as the case just presented.

Conclusions

The conservative analytical predictions for the seven examples involving crack growth rate data which were available for the entire stress intensity range of interest correlated adequately with the experimental test results (within the expected scatter of the crack growth rate data). The only predictions which were unconservative and which did not correlate adequately

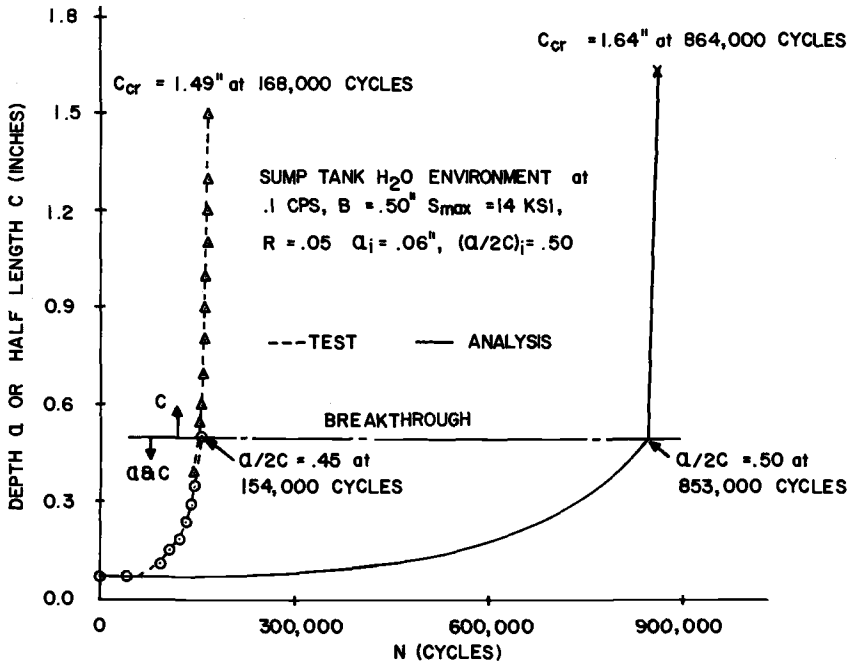


FIG. 16—Crack growth correlation for example No. 10 (1 in. = 25.4 mm, 1 ksi = 0.145 MPa).

TABLE 2—Analytical/experimental correlation.

Example No.	Predicted/Test	
	Breakthrough	Failure
1	0.70	0.67
2	^a	0.87
3	^a	0.40
4	0.63	0.63
5	0.71	0.73
6	1.77	1.69
7	0.73	0.74
8	0.77	0.77
9	4.79	4.50
10	5.54	5.14

^aNo breakthrough.

with the experimental test results were those for the three examples for which there were no crack growth rate data available for the slow growth region, thus requiring the use of extrapolated crack growth rate data in the predictions. It is felt that if slow crack growth rate data had been available and represented adequately, predictions for these three examples probably would have correlated adequately with the experimental test results also.

TABLE 3—Round-robin summary (10 examples).

Analyst	Predicted/Test			
	Breakthrough		Failure	
	Mean	Standard Deviation	Mean	Standard Deviation
A	1.166	0.288	1.075	0.327
B	1.061	0.345	0.712	0.288
C	1.833	0.241	1.169	0.451
D	1.509	1.450	0.942	1.051
E	0.953	0.137	0.787	0.323
RUDD	1.954	2.027	1.858	1.868

TABLE 4—Round-robin summary (8 examples).

Analyst	Predicted/Test			
	Breakthrough		Failure	
	Mean	Standard Deviation	Mean	Standard Deviation
A	1.036	0.172	0.969	0.265
B	0.906	0.215	0.711	0.288
C	1.642	...	1.010	0.332
D	0.761	0.473	0.669	0.406
E	0.894	0.080	0.786	0.323
RUDD	0.883	0.439	0.812	0.379

Therefore, based on the limited number of examples considered in this round-robin exercise, it is concluded that it is possible to use compact tension crack growth rate data to predict the crack growth behavior of part-through crack specimens.

References

- [1] Engle, R. M., "CRACKS II User's Manual," AFFDL-TM-74-173, Air Force Flight Dynamics Laboratory, July 1974.
- [2] Irwin, G. R., *Transactions*, American Society of Mechanical Engineers, Series E; *Journal of Applied Mechanics*, Vol. 29, No. 4, Dec. 1962, pp. 651-654.
- [3] Masters, J. N., Haese, W. P., and Finger, R. W., "Investigation of Deep Flaws in Thin Walled Tanks," NASA CR-72606, National Aeronautics and Space Administration, Dec. 1969.
- [4] Brown, W. F., Jr., and Srawley, J. E. in *Plane Strain Crack Toughness Testing of High Strength Metallic Materials*, ASTM STP 410, American Society for Testing and Materials, 1967, pp. 77-79.
- [5] Ferguson, R. R. and Berryman, R. C., "Fracture Mechanics Evaluation of B-1 Materials," AFML-TR-76-137, Air Force Materials Laboratory, Oct. 1976.
- [6] Walker, K. in *Effects of Environment and Complex Load History on Fatigue Life*, ASTM STP 462, American Society for Testing and Materials, 1970.

NASA-Langley Research Center's Participation in a Round-Robin Comparison Between Some Current Crack-Propagation Prediction Methods

REFERENCE: Hudson, C. M. and Lewis, P. E., "NASA-Langley Research Center's Participation in a Round-Robin Comparison Between Some Current Crack-Propagation Prediction Methods," *Part-Through Crack Fatigue Life Prediction, ASTM STP 687*, J. B. Chang, Ed., American Society for Testing and Materials, 1979, pp. 113-128.

ABSTRACT: A round-robin study was conducted which evaluated and compared different methods currently in practice for predicting crack growth in surface-cracked specimens. This report describes the prediction methods used by the Fracture Mechanics Engineering Section, at NASA-Langley Research Center, and presents a comparison between predicted crack growth and crack growth observed in laboratory experiments.

For tests at higher stress levels, the correlation between predicted and experimentally determined crack growth was generally quite good. For tests at lower stress levels, the predicted number of cycles to reach a given crack length was consistently higher than the experimentally determined number of cycles. This consistent overestimation of the number of cycles could have resulted from a lack of definition of crack-growth data at low values of the stress intensity range.

Generally, the predicted critical flaw sizes were smaller than the experimentally determined critical flaw sizes. This underestimation probably resulted from using plane-strain fracture toughness values to predict failure rather than the more appropriate values based on maximum load.

KEY WORDS: crack propagation, fracture toughness, stress intensity factors, aluminum alloy, fatigue-crack-propagation equations, fatigue (materials)

ASTM Task Group E24.06.01 on Application of Fracture Data in Life Prediction initiated a round-robin study to evaluate and compare different methods currently in practice for predicting crack growth in surface-cracked

¹Head and Aerospace Technologist, FMES, MDB, RFED, respectively, NASA-Langley Research Center, Hampton, Va. 23665.

specimens. Participating organizations were given fracture toughness and fatigue-crack-propagation data from tests on compact specimens. In addition, they were given the initial test conditions for ten surface-cracked specimens. All specimens were made of 2219-T851 aluminum alloy. Using the data and initial conditions provided, each organization was asked to predict the growth of the cracks in the ten specimens by using the organization's in-house prediction methods. The results of the actual tests on these ten specimens were provided subsequently to the participating organizations for comparison with the predicted results. This report describes the prediction methods used by the Fracture Mechanics Engineering Section (FMES) at Langley Research Center, and presents a comparison of the predicted and experimental results.

Nomenclature

Except for the figures, this paper presents physical quantities in both the International System of Units (SI) and the U.S. customary units. For clarity, the figures show only SI units. All measurements and calculations were made in U.S. customary units.

a	Half-length of a through crack or depth of a surface crack
a_0	Initial half-length of a through crack or initial depth of a surface crack.
C	Coefficient of Forman's equation $[1]^2$
c	Half-length of a surface crack
c_0	Initial half-length of a surface crack
da/dN	Rate of fatigue-crack propagation
e	Elongation
K	Stress intensity factor
K_c	Fracture toughness based on maximum load
K_{1c}	Plain-strain fracture toughness
K_{1e}	Experimental elastic fracture toughness
K_{max}	Stress intensity factor at maximum stress
K_{min}	Stress intensity factor at minimum stress
ΔK	Stress intensity range
L	Longitudinal
M_e	Elastic magnification factor on stress intensity
M_1	Front-face magnification factor on stress intensity
N	Number of cycles
n	Exponent on Forman's equation $[1]$
p	Exponent on equation for the elastic magnification factor
Q	Elastic shape factor for an elliptical crack

²The italic numbers in brackets refer to the list of references appended to this paper.

R	Ratio of minimum stress to maximum stress
RA	Reduction in area
RW	Crack normal to rolling direction
S	Stress
S_{\max}	Maximum stress in cycle
S_{\min}	Minimum stress in cycle
ST	Short transverse
T	Transverse
TW	Crack normal to thickness direction
t	Component thickness
W	Component width
WR	Crack normal to width direction
σ_y	Yield strength
σ_u	Ultimate tensile strength
Φ	Complete elliptic integral of the second kind
φ	Coordination angle [2]

Method Used to Predict Crack Growth

Fracture Toughness and Fatigue-Crack-Propagation Data Supplied

Table 1 presents the pertinent fracture toughness data which were supplied by Rockwell-International to each participating organization. Figure 1 is typical of the rate- ΔK plots which were supplied. The dashed line in this figure shows Forman's [1] equation fitted to the extremes of the 1-Hz curve. (The FMES method numerically integrates Forman's equation from an initial flaw size to the critical flaw size to predict crack growth). The following general information, based on fatigue-crack-propagation tests on the compact specimens, also was supplied.

1. Stress ratio, R , significantly affected fatigue crack growth. For a given stress intensity range, higher stress ratios generally produced faster fatigue crack growth.

2. For tests in dry air, a cyclic frequency of 1 Hz produced faster crack growth than a cyclic frequency of 6 Hz. However, cyclic frequencies of 1 and 0.1 Hz produced crack growth at approximately the same rates. Also, cyclic frequencies of 6 and 63.3 Hz produced crack growth at approximately the same rates. For tests in sump tank water, a cyclic frequency of 0.1 Hz produced faster crack growth than a cyclic frequency of 1 Hz.

3. A temperature of 403 K produced faster crack growth than ambient temperature.

4. For plate thicknesses up to 50.8 mm (2 in.), grain direction had little effect on fatigue crack growth. For 76.2 mm (3 in.) thick plate, cracks grew slightly faster in the WR direction than in the RW direction.

TABLE 1—Pertinent fracture toughness data on 2219-T851 aluminum alloy, room temperature.

Plate Thickness		Specimen Thickness		Specimen Width		Crack Orientation		K_{Ic}		K_c	
mm	in.	mm	in.	mm	in.	Orientation	MN/m ^{3/2}	ksi·in ^{1/2}	MN/m ^{3/2}	ksi·in ^{1/2}	
44.5	1.75	38.1	1.5	76.2	3.0	RW	44	40	
44.5	1.75	38.1	1.5	76.2	3.0	RW	44	40	
44.5	1.75	38.1	1.5	76.2	
44.5	1.75	38.1	1.5	76.2	3.0	WR	37	34	
44.5	1.75	38.1	1.5	76.2	3.0	WR	37	34	
44.5	1.75	38.1	1.5	127.0	5.0	RW	49	45	
44.5	1.75	38.1	1.5	127.0	5.0	RW	49	45	
44.5	1.75	38.1	1.5	127.0	5.0	RW	49	45	
44.5	1.75	38.1	1.5	127.0	5.0	RW	51	46	
44.5	1.75	38.1	1.5	127.0	5.0	WR	43	39	
44.5	1.75	38.1	1.5	127.0	5.0	WR	41	37	
44.5	1.75	38.1	1.5	127.0	5.0	WR	41	37	
44.5	1.75	38.1	1.5	152.4	6.0	RW	51	46	
44.5	1.75	38.1	1.5	152.4	6.0	RW	49	45	
44.5	1.75	38.1	1.5	152.4	6.0	WR	43	39	
44.5	1.75	38.1	1.5	152.4	6.0	WR	43	39	
44.5	1.75	38.1	1.5	152.4	6.0	RW	>71	>65	
44.5	1.75	31.8	1.25	152.4	6.0	RW	79	72	
44.5	1.75	31.8	1.25	152.4	6.0	RW	95	86	
44.5	1.75	22.1	0.87	152.4	6.0	RW	88	80	
44.5	1.75	22.1	0.87	152.4	6.0	RW	77	70	
44.5	1.75	12.7	0.50	152.4	6.0	RW	96	87	
44.5	1.75	12.7	0.50	152.4	6.0	WR	69	63	
44.5	1.75	12.7	0.50	152.4	6.0	WR	67	61	
44.5	1.75	12.7	0.50	152.4	6.0	WR	68	62	
44.5	1.75	12.7	0.50	152.4	6.0	WR	114	104	
44.5	1.75	6.4	0.25	152.4	6.0	RW	104	95	
44.5	1.75	6.4	0.25	152.4	6.0	RW	
50.8	2.00	38.1	1.5	127.0	5.0	RW	44	40	
50.8	2.00	38.1	1.5	127.0	5.0	RW	43	39	

50.8	2.00	38.1	1.5	127.0	5.0	RW	42	38	...
50.8	2.00	38.1	1.5	127.0	5.0	RW	42	38	...
50.8	2.00	38.1	1.5	127.0	5.0	WR	37	34-	...
50.8	2.00	38.1	1.5	127.0	5.0	WR	40	36	...
50.8	2.00	19.1	0.75	38.1	1.5	TW	27	25	...
50.8	2.00	19.1	0.75	38.1	1.5	TW	27	25	...
50.8	2.00	19.1	0.75	38.1	1.5	TW	23	21	...
76.2	3.00	50.8	2.0	203.2	8.0	RW	41	37	...
76.2	3.00	50.8	2.0	203.2	8.0	RW	38	35	...
76.2	3.00	50.8	2.0	203.2	8.0	WR	32	29	...
76.2	3.00	50.8	2.0	203.2	8.0	WR	32	29	...
76.2	3.00	22.1	0.87	50.8	2.0	TW	27	25	...
76.2	3.00	50.8	2.0	127.0	5.0	RW	41	37	...
76.2	3.00	22.1	0.87	50.8	2.0	TW	23	21	...

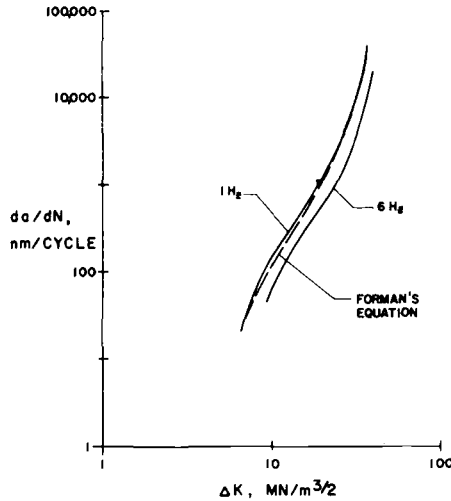


FIG. 1—Solid lines show curves generated using compact specimens. Dashed line shows Forman's equation fit to test curve at 1 Hz (60 cpm). 2219-T851 aluminum alloy. $R = 0.08$. Room temperature. RW grain direction.

5. Specimen thickness had essentially no effect on fatigue crack growth. Specimen thickness ranged from 6.35 to 25.4 mm (0.25 to 1.0 in.).

6. For a given set of test parameters, environment generally had little effect on fatigue crack growth. Test environments included dry air, distilled water, shop cleaning solvent, field cleaning solvent, and sump tank water.

7. Product form had little effect on fatigue crack growth. Product forms included plates, forgings, and extrusions.

8. The material studied was 2219-T851 aluminum alloy.

Test curves supporting this information were also supplied. Table 2 lists the tensile properties of the 2219-T851 aluminum alloy.

Table 3 lists the initial test conditions for the surface-cracked specimens. The tests results for these specimens were not provided until after each group had completed its analysis and forwarded its predictions to the chairman of ASTM Task Force E24:06:01 on Application of Fracture Data in Life Prediction.

Stress Intensity Solutions Used

The Fracture Mechanics Engineering Section (FMES) used Feddersen's [3] semiempirical stress intensity solution for the through cracks. The basic form of this solution is given by

TABLE 2—Nominal tensile properties of 2219-T851 aluminum alloy.

Plate Thickness		Test Direction	σ_u		σ_y		e , percent	RA, percent
mm	in.		MPa	ksi	MPa	ksi		
44.5	1.75	L	455	66	345	50	12	25
44.5	1.75	T	455	66	331	48	10	17
50.8	2.00	L	469	68	345	50	12	28
50.8	2.00	T	469	68	345	50	12	22
50.8	2.00	ST	434	63	345	50	4	8
76.2	3.00	L	476	69	372	54	10	22
76.2	3.00	T	469	68	366	53	10	18
76.2	3.00	ST	455	66	366	53	7	10

$$K = S \sqrt{\pi a \secant \frac{\pi a}{W}} \tag{1}$$

This equation is used widely in the analysis of center-cracked panels subjected to uniform tensile loads [4].

The FMES used Newman’s empirical stress intensity solution [2] for the surface crack. The basic form of this solution is given by

$$K = S \sqrt{\pi \frac{a}{Q}} M_e \tag{2}$$

The elastic shape factor for an elliptical crack, Q , is given by

$$Q = \Phi^2 \tag{3}$$

where

$$\Phi = \int_0^{\pi/2} \left(1 - \left(1 - \left(\frac{a}{c} \right)^2 \right) \sin^2 \varphi \right)^{1/2} d\varphi \tag{4}$$

The expression for Q can be approximated by [2]

$$Q = 1 + 1.47 \left(\frac{a}{c} \right)^{1.64} \quad \text{for } \frac{a}{c} \leq 1.0 \tag{5a}$$

and

$$Q = 1 + 1.47 \left(\frac{c}{a} \right)^{1.64} \quad \text{for } \frac{a}{c} > 1.0 \tag{5b}$$

TABLE 3—Test conditions for the surface cracked specimens. 2219-T8S1 aluminum alloy, room temperature.

Specimen Number	Plate Thickness		Environment	Cyclic Frequency		S _{max}		t		W		a ₀		c ₀	
	mm	in.		Hz	cpm	MPa	ksi	mm	in.	mm	in.	mm	in.	mm	in.
23-18	44.5	1.75	dry air	1	60	221	32	12.7	0.50	101.6	4.0	1.524	0.060	1.524	0.060
37-3	76.2	3.00	dry air	1	60	221	32	25.4	1.00	101.6	4.0	1.524	0.060	1.524	0.060
23-12	44.5	1.75	distilled water	1	60	221	32	12.7	0.50	101.6	4.0	1.524	0.060	1.524	0.060
23-13	44.5	1.75	distilled water	0.1	6	221	32	12.7	0.50	101.6	4.0	1.524	0.060	1.524	0.060
23-14	44.5	1.75	sump tank water	1	60	221	32	12.7	0.50	101.6	4.0	1.524	0.060	1.524	0.060
23-10	44.5	1.75	sump tank water	0.1	6	221	32	12.7	0.50	101.6	4.0	1.524	0.060	1.524	0.060
37-2	44.5	1.75	dry air	1	60	221	32	25.4	1.00	101.6	4.0	2.286	0.090	3.429	0.135
23-16	44.5	1.75	distilled water	1	60	97	14	12.7	0.50	101.6	4.0	1.524	0.060	1.524	0.060
23-17	44.5	1.75	sump tank water	1	60	97	14	12.7	0.50	101.6	4.0	1.524	0.060	1.524	0.060
27-76	44.5	1.75	sump tank water	0.1	6	97	14	12.7	0.50	101.6	4.0	1.524	0.060	1.524	0.060

Newman [2] indicates that the maximum error introduced by using these approximations is nominally 0.25 percent.

The elastic magnification factor, M_e , in Eq 2 is given by

$$M_e = \left[M_1 + \left(\sqrt{\frac{Qc}{a}} - M_1 \right) \left(\frac{a}{t} \right)^p \right] \secant \frac{\pi ca}{Wt} \Big]^{1/2} \quad \text{for } \frac{a}{c} \geq 0.02 \quad (6a)$$

and

$$M_e = 1.12 - 0.23 \left(\frac{a}{t} \right) + 10.55 \left(\frac{a}{t} \right)^2 - 21.71 \left(\frac{a}{t} \right)^3 + 30.38 \left(\frac{a}{t} \right)^4$$

$$\text{for } \frac{a}{c} < 0.02 \quad (6b)$$

The front-face correction, M_1 , in Eq 6a, is given by

$$M_1 = \left(\frac{c}{a} \right)^{1/2} \left(1 + 0.03 \frac{c}{a} \right) \quad \text{for } \frac{a}{c} > 1.0 \quad (7a)$$

and

$$M_1 = 1.13 - 0.1 \left(\frac{a}{c} \right) \quad \text{for } 0.02 \leq \frac{a}{c} \leq 1.0 \quad (7b)$$

The exponent, p , in Eq 6a is given by

$$p = 2 + 8 \left(\frac{a}{c} \right)^3 \quad (8)$$

Newman showed the magnification factors given by Eq 6a agreed quite well with the analytical results of other researchers. A subsequent finite element analysis [5] indicates Newman's solution for the surface crack is accurate within ± 5 percent for a wide range of a/t and a/c values.

Fatigue-Crack-Propagation Program Used

The propagation of fatigue cracks is predicted by numerically integrating the equation of Forman et al [1] from the initial flaw size to the critical flaw size.

Forman's equation has the form

$$da/dN = \frac{C\Delta K^n}{(1 - R)K_{Ic} - \Delta K} \quad (9)$$

The integration of this equation is accomplished in the following steps.

1. Input Data (see Table 4)

K_{Ic}	Experimental elastic fracture toughness
C	Coefficient of Forman's equation
n	Exponent of Forman's equation
t	Component thickness
W	Component width
a_o	Initial depth of crack
c_o	Initial half-length of surface crack
S_{\max}	Maximum stress in cycle
S_{\min}	Minimum stress in cycle

2. Calculate a_o/t

If a_o/t equals one, then the crack is a through crack and stress intensity factors are calculated using Eq 1. Conversely, if a_o/t is less than one, the crack is a surface crack and stress intensity factors are calculated using Eq 2.

3. Calculate Stress Intensities

For through cracks, the maximum stress intensity factor, K_{\max} , and the stress intensity range, ΔK , are given by

$$K_{\max} = S_{\max} \sqrt{\pi a_o \secant \frac{\pi a_o}{W}} \quad (10)$$

and

$$\Delta K = (S_{\max} - S_{\min}) \sqrt{\pi a_o \secant \frac{\pi a_o}{W}} \quad (11)$$

For surface cracks, the maximum stress intensity factor and the stress intensity range are given by

$$K_{\max} = S_{\max} \sqrt{\frac{\pi a_o}{Q}} M_e \quad (12)$$

and

$$\Delta K = (S_{\max} - S_{\min}) \sqrt{\frac{\pi a_o}{Q}} M_e \quad (13)$$

The input data supplies all terms required for these calculations.

If $K_{\max} \geq K_{le}$, the program is terminated. If $K_{\max} < K_{le}$, the program proceeds with the numerical integration of Forman's equation.

4. Integrate Forman's Equation

Forman's equation is set up

$$\Delta N = \frac{(1 - R)K_{le} - \Delta K}{C\Delta K^n} \Delta a \tag{14}$$

where the term Δa is the integration interval. An interval of 0.025 mm (0.001 in.) is used in this program since smaller intervals (a) produce no significant change in the number of cycles calculated for a given amount of crack growth and (b) require more time for calculation. The terms C , n , and K_{le} are input data. The term ΔK is calculated by using Eq 11 or 13, as appropriate. The term R is given by S_{\min}/S_{\max} . Thus all terms on the right side of Eq 14 are defined, and ΔN , the number of cycles required to propagate the crack 0.025 mm (0.001 in.), can be calculated.

For a through crack, the initial crack length then is increased by the integration interval, 0.025 mm (0.001 in.), and the calculation and summing process is repeated. This is continued until $K_{\max} \geq K_{le}$. At that point, the program is terminated.

For a surface crack, the initial crack depth is increased by the integration interval 0.025 mm (0.001 in.). The change in the surface length of the crack is calculated using Forman's equation. This change is given by

$$\Delta c = \frac{C\Delta K^n}{(1 - R)K_{le} - \Delta K} \Delta N \tag{15}$$

where C , n , R , and K_{le} are the same as in Eq 14, and ΔN is the number of cycles required to increase the depth of the crack by 0.025 mm (0.001 in.). The stress intensity range along the boundary of the crack is given by

$$\Delta K = (S_{\max} - S_{\min}) \sqrt{\frac{\pi a_o}{Q}} M_e \left(\sin^2 \varphi + \frac{a^2}{c^2} \cos^2 \varphi \right)^{1/4} \tag{16}$$

At the surface

$$\varphi = 0 \tag{17}$$

thus

$$\Delta K = (S_{\max} - S_{\min}) \sqrt{\frac{\pi a_o}{Q}} M_e \left(\frac{a}{c} \right)^{1/2} \tag{18}$$

TABLE 4—Input data for predicting crack growth in surface cracked specimens, 2219T851 aluminum alloy, room temperature.

Specimen Number	Forman's Coefficient and Exponent (U. S. customary Units)		K_{Ic}		Forman's Coefficient and Exponent (U. S. customary Units)		t, W, a_o, c_o, S_{max}	S_{min}	RS_{max}
	MN/m ^{3/2}	ksi-in ^{1/2}	Rationale	C	n	Rationale			
23-18	44	40	Specimen came from a 44.5 mm thick plate. This value is the nominal average value of K_{Ic} for this plate thickness. A somewhat higher value could have been used, since the specimen thickness is only 12.7 mm.	1.39×10^{-7}	3.02	Obtained by fitting Forman's equation to two points on 1 Hz curve. Fig. 1. Curve selected because cyclic frequencies match. Dry air has little effect.	from Table 3		
37-3	41	37	Specimen came from the 76.2 mm thick plate. Crack orientation was assumed RW (not given).	2.85×10^{-7}	2.56	Same as for Specimen No. 23-18, C and n are slightly different because K_{Ic} is different.	from Table 3		RS_{max}
23-12	44	40	same as Specimen No. 23-18	1.39×10^{-7}	3.02	Same as Specimen No. 23-16	from Table 3		RS_{max}
23-13	44	40	same as Specimen No. 23-18	1.39×10^{-7}	3.02	Obtained by fitting Forman's equation to two points on 1 Hz curve. Fig. 1. Curve selected because, generally, there is no difference in crack growth rates at 60 cpm and 6 cpm. Distilled water has little effect.	from Table 3		RS_{max}
23-14	44	40	same as Specimen No. 23-18	1.39×10^{-7}	3.02	Same as Specimen No. 23-17	from Table 3		RS_{max}
23-10	44	40	same as Specimen No. 23-18	1.39×10^{-7}	3.02	Same as Specimen No. 27-76	from Table 3		RS_{max}
37-2	41	37	same as Specimen No. 37-3	2.85×10^{-7}	2.56	Same as Specimen No. 37-3	from Table 3		RS_{max}
23-16	44	40	same as Specimen No. 23-18	1.39×10^{-7}	3.02	Obtained by fitting Forman's equation to two points on 1 Hz curve. Fig. 1. Curve selected because cyclic frequencies match. Distilled water has little effect.	from Table 3		RS_{max}
23-17	44	40	same as Specimen No. 23-18	1.39×10^{-7}	3.02	Obtained by fitting Forman's equation to two points on 1 Hz curve. Fig. 1. Curve selected because cyclic frequencies match. Sump tank water has little effect at 60 cpm.	from Table 3		RS_{max}

27-76	50	45	<p>Specimen came from a 44.5 mm thick plate. Crack orientation was assumed RW. For this particular plate number and orientation, the average fracture toughness was 50 MN/m^{3/2} (45 ksi·in^{1/2}).</p>	<p>9.00 × 10⁻⁸</p>	3.33	<p>Obtained by fitting Forman's equation to two points on 1 Hz curve, Fig. 1. Points somewhat above curve could have been used since a cyclic frequency of 6 cpm produced faster crack growth than a cyclic frequency of 60 cpm for tests in sump tank water.</p>	<p>from Table 3</p>	<p>RS_{max}</p>
-------	----	----	--	-------------------------------	------	---	---------------------	-------------------------

Thus all terms on the right side of Eq 15 are defined and Δc can be calculated. This change in surface length then is added to the initial surface length.

The calculation and summing process is repeated until either $K_{\max} \geq K_{lc}$, at which point the program is terminated, or $a = t$ at which point the crack breaks through the back surface. If breakthrough occurs, the program then considers the crack to be a through crack of length $2c$ and continues to numerically integrate until $K_{\max} \geq K_{lc}$.

Results and Discussion

Figure 2 shows the predicted and experimental plots of crack length against cycles for the specimens analyzed. The solid curves are test data and the dashed curves are predictions. With the exception of Specimen No. 37-2, the predictions for the tests at 221 MPa (32 ksi) (Specimen Nos. 23-18, 37-3, 23-12, 23-13, 23-14, and 23-10) are quite good. For these six specimens, the ratio of test life to predicted life ranged from 0.70 to 1.27.

For Specimen No. 37-2, the ratio of test life to predicted life was 1.84. Figure 2 indicates the experimental number of cycles to failure for Specimen No. 37-2 is approximately 20 000 cycles. The experimental number of cycles to failure for Specimen Nos. 23-18, 37-3, 23-12, 23-13, 23-14, and 23-14, is nominally 20 000 cycles also. Yet the initial flaw depth for Specimen No. 37-2 is 2.286 mm (0.090 in.) while the initial flaw depth for the six other specimens is only 1.524 mm (0.060 in.). Because of the larger initial flaw size, Specimen No. 37-2 would be expected to have a shorter fatigue life than the other six specimens (as the analysis predicted). The fact that the fatigue lives of all seven specimens were nominally the same is probably attributable to normal scatter in the test results.

The predicted fatigue lives for tests at 97 MPa (14 ksi), Specimen Nos. 23-16, 23-17, and 27-76, were consistently high. For these three specimens, the ratio of test life to predicted life ranged from 0.51 to 0.65. This consistent overestimation of fatigue lives could result from lack of definition of the rate — ΔK curve at low values of ΔK . The rate — ΔK curves are only defined down to a ΔK value of 6.6 MN/m^{3/2} (6 ksi in.^{1/2}). However, for these three specimens, the initial stress intensity factors were nominally 4.4 MN/m^{3/2} (4 ksi in.^{1/2}). The undefined stress intensity range is admittedly quite small. However, the rate — ΔK curve is very steep in this stress intensity range. Consequently, if the extrapolated curve in the undefined region is only slightly to the right of the test data, the predicted lives will be considerably longer than the experimentally determined lives.

Generally, the predicted critical flaw sizes are smaller than the experimentally determined critical flaw sizes. This underestimation probably resulted from using K_{lc} values to predict failure.

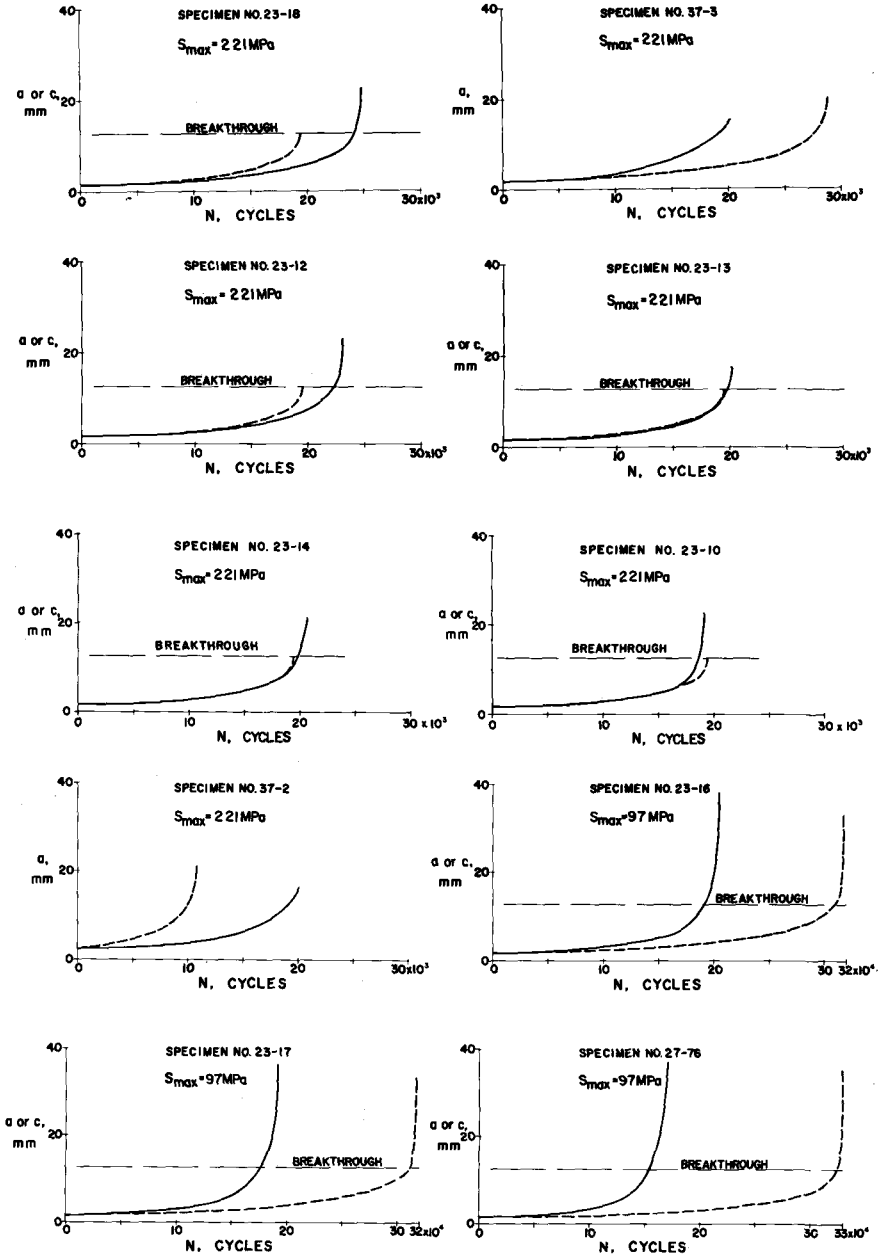


FIG. 2—Variation of crack length with number of cycles for surface-cracked specimens. Solid curves are experimental. Dashed curves are predicted. From the initial flaw size to breakthrough, crack depth, a , is plotted against number of cycles. Past breakthrough, half-surface-crack length, c , is plotted.

The use of the higher K_{Ic} values would probably be more appropriate for specimen thicknesses of 12.7 and 25.4 mm (0.50 and 1.0 in.).

Concluding Remarks

A round-robin study was conducted which evaluated and compared different methods currently in practice for predicting crack growth in surface-cracked specimens. This report describes the prediction methods used by the Fracture Mechanics Engineering Section, at NASA-Langley Research Center, and presents a comparison between predicted crack growth and crack growth observed in laboratory experiments.

For six of seven tests at 221 MPa (32 ksi), the ratio of test life to predicted life ranged from 0.70 to 1.27 which is quite good. For the seventh test at 221 MPa (32 ksi), the ratio of test life to predicted life was 1.84. This high ratio is probably attributable to the normal scatter which occurs in fatigue-crack-propagation tests.

For tests at 97 MPa (14 ksi), the ratio of test life to predicted life ranged from 0.51 to 0.65. This consistent overestimation of fatigue lives could result from lack of definition of the rate — ΔK curve at low values of ΔK .

Generally, the predicted critical flaw sizes are smaller than the experimentally determined flaw sizes. This underestimation probably resulted from using K_{Ic} values to predict failure rather than the more appropriate K_{Ic} values.

References

- [1] Forman, R. G., Kearney, V. E., and Engle, R. M., *Transactions, American Society of Mechanical Engineers, Series D; Journal of Basic Engineering*, Vol. 89, No. 3, Sept. 1967, pp. 459-464.
- [2] Newman, J. C., Jr., *Engineering Fracture Mechanics*, Vol. 5, No. 3, Sept. 1973, pp. 667-689.
- [3] Brown, W. F., Jr., and Srawley, J. E., *Plane Strain Crack Toughness Testing of High Strength Metallic Materials. ASTM STP 410*, American Society for Testing and Materials, 1967.
- [4] Tada, H., Paris, P., and Irwin, G., *The Stress Analysis of Cracks Handbook*, Del Research Corporation Publication, 1973.
- [5] Raju, I. S. and Newman, J. C., Jr., "Improved Stress-Intensity Factors for Semi-Elliptical Surface Cracks in Finite-Thickness Plates," NASA TM X-72825; presented at the 4th International Conference on Structural Mechanics in Reactor Technology, San Francisco, Calif., Aug. 1977.

Computer-Aided Fracture Mechanics Life Prediction Analysis

REFERENCE: Peterson, D. E. and Vroman, G. A., "Computer-Aided Fracture Mechanics Life Prediction Analysis," *Part-Through Crack Fatigue Life Prediction, ASTM STP 687*, J. B. Chang, Ed., American Society for Testing and Materials, 1979, pp. 129-142.

ABSTRACT: The fracture mechanics analysis and computer logic used to perform design life predictions is described. Initial part-through crack defects are analyzed under the conditions of constant-amplitude loading to predict the number of loading cycles applied before breakthrough or failure. A criterion is provided to predict the transition from part-through crack growth characteristics to through crack growth characteristics. A breakthrough criterion is also provided.

KEY WORDS: fatigue crack growth, constant amplitude loading, life predictions, part-through crack, through crack, transitioning, breakthrough, crack propagation, fatigue (materials)

Nomenclature

- a* Crack depth
- b* Crack half-length
- C* Material constant for crack growth in the depth and length directions
- dS* Stress range in a fatigue cycle
- F* Correction factor for the effect of the front surface on the growth of a crack through the thickness
- G* Correction factor for the effect of the front surface on the growth of a crack in the length direction
- K_c, K_{Ic} Critical stress intensity factor for fracture
- M* Correction factor for the effect of the back face on the growth of a crack through the thickness

¹Member of the technical staff and project engineer, respectively, Rocketdyne Division of Rockwell International, Canoga Park, Calif. 91304.

M_b	Magnification factor at the point of maximum crack depth for surface cracks in bending
N	Number of fatigue loading cycles
n	Material constant for crack growth in the depth and length directions
Q	Flaw shape correction factor
S_f	Stress on flawed surface
S_u	Stress on unflawed surface
S_{YS}	Material yield stress
t	Material thickness
Φ	Complete elliptic integral of the second type
ΔK_u	Stress intensity factor range at the point of maximum crack depth
ΔK_b	Stress intensity factor range at the crack front-surface interface

The improvements in fracture mechanics technology occurring in the 1965 to 1970 time period resulted in the use of fracture mechanics life prediction as part of the engineering design procedure. Previously the principal engineering application of fracture mechanics was to assist in material selection by identifying those materials susceptible to brittle fracture (low fracture toughness). Largely as a result of government-sponsored research, an expertise was developed in linear elastic fracture mechanics (mathematical formulas), material fracture characteristics quantifying crack growth rates, and material inspection procedures quantifying the characteristics of material defects. All three of these developments were necessary before fracture mechanics life prediction could be performed, bringing together for the first time the design life requirements, the possible undetected crack-like defects, the design stresses imposed on the cracked region, and the material fracture characteristics. The incorporation of fracture mechanics life prediction into the engineering design process not only provided an assurance of design success but also allowed necessary adjustments to be made in either the design stress or the inspection procedure before the parts were fabricated and before problems were encountered in service.

Fracture mechanics life prediction has served as an engineering design tool in the Space Shuttle Main Engine (SSME) since 1971. Early in the design stage it was recognized that the high stresses necessary for lightweight design and the aggressive environments impinging on the materials would increase the criticality of undetected defects. Therefore, a Fracture Mechanics Plan was developed to incorporate fracture mechanics life prediction into the engineering design procedure for the purpose of preventing service failures caused by undetected crack-like defects. A material fracture properties test program was expanded to obtain data characterizing the critical material-environment combinations, and additional testing was performed to quantify inspection crack detection capability. Parallel with this effort a computer

program was developed to use the supporting data efficiently in performing fracture mechanics life predictions.

The problem-solving requirements for the computer program are relatively simple because of the SSME for which it was developed. The SSME is primarily a welded structure; therefore, bolt holes and their associated defects are not addressed. The design operating requirements are approximated by a zero-to-maximum-pressure-to-zero engine firing cycle so the overload effects of spectrum loading are not included. Also, the range ratio effect is included in the input material properties rather than being accounted for by the computer program. The relatively simple problem solved by the computer program is to calculate the number of constant-amplitude loading cycles before breakthrough or failure of an initial semi-elliptical flaw on the surface of a constant-thickness section.

Analysis Procedure

The computer program requires input information describing the initial flaw, the section thickness, the applied stresses, and the material properties. The initial semi-elliptical flaw is defined by its surface length ($2b$) and depth (a). The constant section thickness of the flawed region is t . The applied stresses are defined by the two surface stresses: the stress on the flawed surface (S_f), and the stress on the unflawed surface (S_u). The input material properties are the yield strength (S_{YS}), the plane strain and the plane stress fracture toughness (K_{Ic} and K_{Ic}), and the fatigue crack growth rate parameters (c and n).

The calculations that will be discussed later lead to the generation of computer output, so they can be better understood by looking ahead to the end product. The computer program produces a complete description of the crack growth as a function of the applied loading cycles. Included in this description are the crack dimensions, the stress intensity at each of the rate-controlling dimensions, the crack growth rate corresponding to each stress intensity, and the associated number of accumulated loading cycles. Significant events in the crack growth history are shown by line statements in the printout identifying transition from part-through crack growth characteristics to through crack growth characteristics, breakthrough (leakage through the thickness), or catastrophic rupture of the total section.

The computational scheme employed in the computer calculations follows a previous program, EFFGRO, originated by G. A. Vroman and in use at several facilities of Rockwell International. In this scheme the numerical integration problems inherent in cycle-by-cycle analysis are avoided. Rather than having the number of loading cycles be an independent variable, the crack size is enlarged by very small increments and the number of loading cycles to cause each growth are calculated. By choosing small increments of growth, the stress intensity variation between the beginning of incremental

growth and the end of incremental growth is negligibly small. This calculation requires little computer run time (relative to Runge-Kutta integration schemes), so the efficient computation program of crack growth was entitled EFFGRO.

Unlike the original EFFGRO computer program, the Rocketdyne-developed program extends the computational scheme to enlarge both the length and depth directions of the crack incrementally. The mathematical formulation developed by Royce Forman [1]² was used as a basis for computer calculations.

$$\Delta K_a = F \cdot (dS) \cdot M \cdot \sqrt{\frac{\pi a}{Q}} \quad (1)$$

applicable when $a \leq b$

$$\Delta K_a = F \cdot (dS) \cdot \left(\frac{b}{a}\right) \cdot \sqrt{\frac{\pi a}{Q}} \quad (2)$$

applicable when $a > b$

$$\Delta K_b = G \cdot (dS) \cdot \left(\frac{a}{b}\right) \cdot \sqrt{\frac{\pi b}{Q}} \quad (3)$$

applicable when $a \leq b$

$$\Delta K_b = G \cdot (dS) \cdot \sqrt{\frac{\pi b}{Q}} \quad (4)$$

applicable when $a > b$

Figure 1 shows the physical relationships of the variables and the points of stress intensity calculation.

In using the above Eqs 1 through 4, the values of F and G were set to 1.12 (commonly used for a free surface correction factor) to save the computer time of reading the more accurate tabular values presented by Forman (varying with aspect ratio). Forman's other tables were programmed into the computer and interpolated to obtain the back-face factor M (varying with both depth-to-thickness ratio and aspect ratio) and the shape factor Φ^2 (varying with aspect ratio). Q was calculated using Eq 5, following Forman's procedure

$$Q = \Phi^2 - 0.212 (S/S_{YS})^2 \quad (5)$$

Because of the interdependence between length and depth dimensions in

²The italic numbers in brackets refer to the list of references appended to this paper.

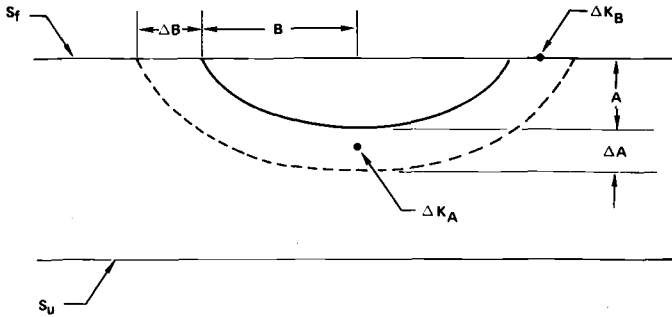


FIG. 1—Part-through crack geometry.

calculating stress intensity (related through aspect ratio), it was necessary to program an iterative loop that would produce compatible values of the incremental growths Δa and Δb . Initially, Δa and Δb are chosen as specific percentages of the crack dimensions a and b . Within the loop, summarized in Fig. 2, Δb is refined until the resulting aspect ratio (a/b) is within 1 percent of that assumed in the stress intensity calculation.

Figure 2 illustrates the calculation procedure used to determine the relationship between the number of loading cycles and the crack size. After each increment of crack growth has satisfied the aspect ratio criterion, the number of loading cycles necessary to cause that growth are calculated by Eq 6.

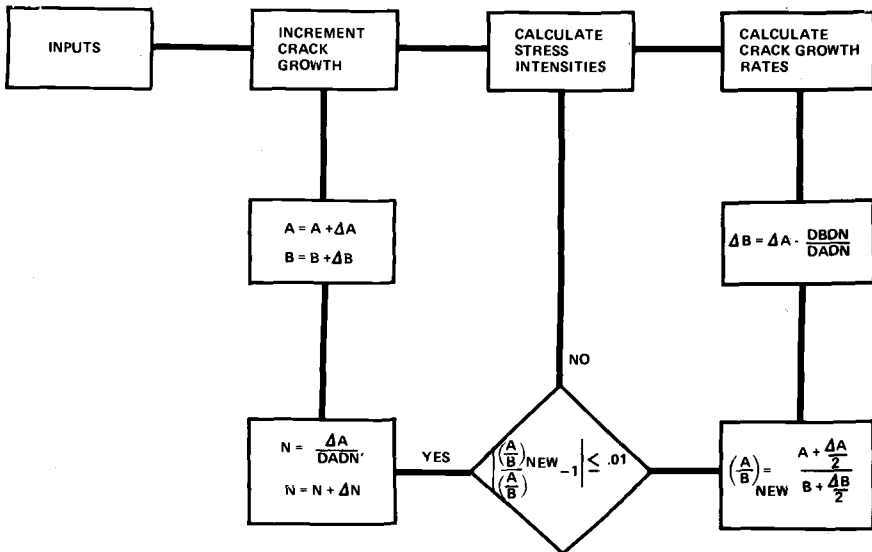


FIG. 2—Crack growth integration technique.

$$\Delta N = \Delta a/da/dN \quad (6)$$

The accumulated loading cycles are obtained by performing a running summation of all the incremental growths, back to the initial crack size.

Combined Tension and Bending

The complex structure of the SSME is rarely subjected to the simple loading of in-plane tension. Therefore, it is necessary to account for both the tension and bending loadings in the life prediction analysis. Although the applied stresses are often nonlinear through the thickness because of the thermal stress distribution, it is usually conservative to assume a linear variation between the two surface stresses. This approximation was used in formulating the computer program, thereby allowing an automated calculation within the program to separate the loading into two components, tension and bending, based on linear superposition.

$$S_{\text{axial}} = \frac{S_j + S_u}{2} \quad (7)$$

$$S_{\text{bend}} = \frac{S_j - S_u}{2} \quad (8)$$

The total stress intensity at the point of maximum crack depth is therefore the sum of the contributions from each component:

$$\Delta K_a = \Delta K_{a_{\text{axial}}} + \Delta K_{a_{\text{bending}}} \quad (9)$$

The contribution in stress intensity due to axial loading component is obtained by substituting the incremental element average dimensions into Eq 1.

$$\Delta K_{a_{\text{axial}}} = F \cdot d S_{\text{axial}} \cdot M \cdot \sqrt{\frac{\pi(a + \Delta a/2)}{Q}} \quad (10)$$

The bending contribution to stress intensity at the maximum crack depth is based on a formulation by Shah and Kobayashi [2]

$$\Delta K_{a_{\text{bending}}} = \frac{M_b \cdot d S_{\text{bending}} \cdot \sqrt{\pi(a + \Delta a/2)}}{\phi} \quad (11)$$

Values of the correction factor M_b are determined by interpolating a computer-stored tabulation, after reading in the quantities of a/b and a/t . Computer predictions using this formulation were within 10 percent of the specimen test data published by Grandt and Sinclair [3]. Other formulations that were tried showed less accuracy.

The total contribution in stress intensity at the crack-front-to-surface intersection (the b dimension) is calculated without the necessity to separate the axial and bending components of the applied loading. By simply using the program input flawed surface stress (S_f) and accepting the conservative approximation of constant stress through the thickness, the simple form of Eq 3 can be used. The combined loading is accounted for because S_f includes both the axial and the bending components.

$$\Delta K_b = G \cdot dS_f \cdot \left(\frac{a}{b}\right) \cdot \sqrt{\frac{\pi(b + \Delta b/2)}{Q}} \quad (12)$$

Characterization of Growth Rate

The crack growth rates are obtained by substituting the calculated stress intensities into the Paris equation, where the material characterization parameters (C and n) are from the initial program input.

$$da/dN = C \cdot (\Delta K)^n \quad (13)$$

The capability of the Paris equation to characterize crack growth rate is enhanced by using multiple values of C and n as a function of the stress intensity value. The equation provides a linear approximation in log-log space so that data plotted on a log-log scale appear as a straight line. In preparing the program inputs the typical double inflection curve is approximated by three straight line segments each having separate values of C and n along with the stress intensity range of applicability. Using this characterization as an input, the computer program chooses the appropriate Paris equation values for the stress intensity and calculates the crack growth rate. Figure 3 shows two examples of the three-segment approximation to the crack growth rate curve.

It is important to recognize that the crack growth rate data used to characterize the material are almost always obtained from compact specimens rather than part-through crack (PTC) specimens. In using these results to perform PTC design life prediction, the influence of crack shape must be considered. Whereas the compact specimen has a nominally straight crack front, the semi-elliptic PTC has a pronounced curvature. Historically, the static fracture toughness data from PTC specimens have been normalized to an equivalent straight front crack by the shape and plasticity factor Q (a/Q = depth of equivalent semi-infinite crack). There is also some precedent to expressing the PTC growth rates by using the Q normalization $(da/Q)/dN$. Forman [1] discusses a normalized crack growth rate theory employed in the Apollo program which was developed by C. F. Tiffany. While that particular theory is not employed here, it suggests that da/dN for a given stress intensity in a compact specimen would equal $(da/Q)/dN$ for

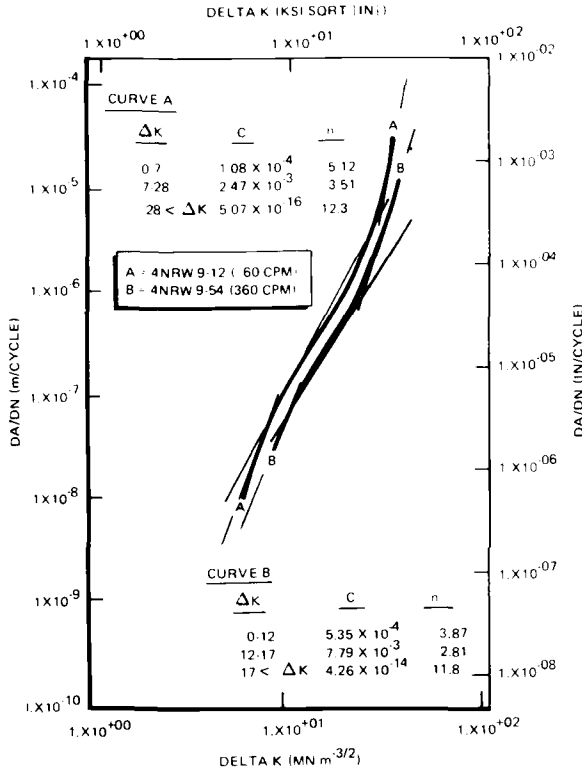


FIG. 3—Example approximation of crack growth rate.

the same calculated stress intensity in a PTC specimen. We investigated this question by comparing PTC life predictions made from compact specimen data against PTC specimen test data. The results suggested that a change in the fracture mechanism occurred at crack growth rates below $0.250 \mu\text{m}/\text{cycle}$ (approximately). It was rationalized that the Q correction was appropriate for higher growth rates associated with low cycle fatigue but not applicable for high cycle fatigue. A branching logic was built into the computer life prediction program that divided the input compact specimen data by Q when the growth rate exceeded $0.250 \mu\text{m}/\text{cycle}$ but made no correction for lower growth rates. Life predictions from the improved program showed excellent correlation with PTC specimen test data.

It is important to note that this normalization of the crack growth rate data is applicable only during the growth period when the crack can be characterized as a PTC. As will be discussed in the next section, a transition point occurs where the crack can better be characterized as a through crack.

The growth of a through crack closely resembles that of a compact specimen and, therefore, does not require a normalization of the crack growth rate data.

Transition to Through Crack

The computer program to perform fracture mechanics life prediction is intended to quantify the growth characteristics of an initial part-through crack. In keeping with this objective, a significant effort was devoted to developing a criterion for characterizing the transition of an initial surface crack to a through crack. Nine years ago it became evident from cyclic crack growth tests that relatively thin or highly stressed part-through crack (PTC) specimens, or both, underwent a change in crack growth rate characteristics when the depth of the flaw was sufficient to induce stresses above yield in the material back face. Predictive analysis based on the "Irwin" surface flaw equation was not adequate to describe the crack front conditions (stress intensity) where the surrounding material was largely inelastic. PTC specimen tests showed fracture face markings consistent with a transition from surface flaw growth characteristics to through crack growth characteristics. It appeared that the surface flaw predictive equations were accurate up to the onset of backface yielding, then the crack effectively transitioned toward the characteristics of a through crack, even before breakthrough occurred. A criterion was developed to control the predictive analysis whereby the crack growth prediction was based initially on surface crack equations, then transferred to through-crack equations when the criterion indicated back-face yielding.

At the Sixth National Fracture Mechanics Symposium (August 1972), the criterion for transitioning was presented for discussion. Considerable interest was generated but very little support. The simplistic approach used to develop the criterion and the lack of supporting data did not instill confidence in the result. However, the lack of supporting data (or conflicting data) was in fact the reason for the simplistic approach. The more sophisticated Kobayashi-Moss solution [4] did not differ radically in the final answers relative to the simplest criterion, so it was decided to stay with a simple approach until test data were available. The simple approach provided a more conservative analytical life prediction than the Kobayashi-Moss results. When additional test data became available in 1974 [5], the question was reopened and after further investigation it was concluded that the Kobayashi-Moss solution was considerably more accurate than the simple criterion. However, the complexities of programming the Kobayashi-Moss solution in explicit form prevented its inclusion in the computer program. In 1976 it was found that a modification of the original yielding criterion (adding one term) provided a good approximation to the Kobayashi-Moss solu-

tion. Using the nomenclature found in the test data, back-face dimpling (yielding) is indicated by the subscript D

$$S_D/S_{YS} = 1 - \frac{\pi a}{4t} + \left(1 - \frac{a}{t}\right) \left(\frac{a}{t}\right) \left(\frac{a}{b}\right) \quad (14)$$

In each increment of crack growth, the computer program checks Eq 14 and goes to the through crack mode of crack growth when back-face yielding is indicated by S_D/S_{YS} equaling or exceeding 1.00.

$$\Delta K_b = dS_{axial} \cdot \sqrt{\pi(b + \Delta b/2)} \quad (15)$$

When transition to the through-crack mode has occurred, the crack surface length (b) continues to grow as controlled by Eq 15. Conversely, crack growth through the thickness is inhibited to such a degree by the plastic state ahead of the crack front that the crack depth remains virtually unchanged until breakthrough occurs. (The prediction criterion for breakthrough is discussed in the next section.) Ideally, the crack growth model should include the effects due to bending in addition to those due to axial loading. Unfortunately, insufficient test data are available in this area to pursue the development of a more sophisticated model. The method described herein results in a conservative estimate of the crack growth when the crack surface length is used in the calculations.

A comparison between the revised transition criterion and the Kobayashi-Moss results are shown in Fig. 4. It can be seen that the percentage difference between the two results is not large. The revised criterion is further supported by the data for two materials shown in Fig. 5 and 6 [6]. The criterion calculation appears to predict the lower edge of the test data. This disparity can be explained by reading the original test report and thereby recognizing the difficulty of measuring the onset of yielding. It could be expected that the detection of yielding (dimpling) during test would often be at stresses higher than the onset of yielding, consistent with the data of Figs. 5 and 6.

Breakthrough

After transition occurs, the crack usually grows for some number of loading cycles before breaking through the back face of the thickness. A criterion for predicting breakthrough was originally developed in 1975, based on very limited test data, and refined in 1976 when the data from Ref 6 was analyzed. The technical approach was crude and largely empirical, based on a speculative relationship of the controlling parameters. At breakthrough

$$\frac{2b}{t} = [0.860 \cdot (a/2b)]^{-0.821} \quad (16)$$

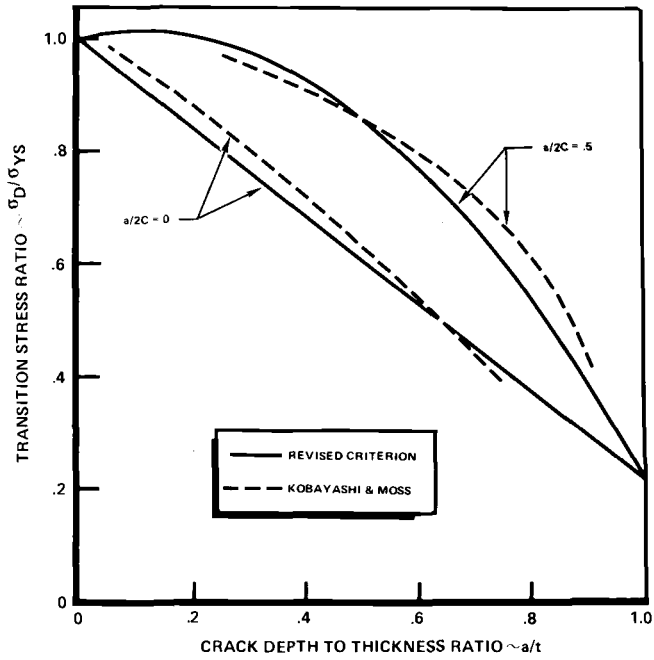


FIG. 4—Comparison of back-face yielding criteria.

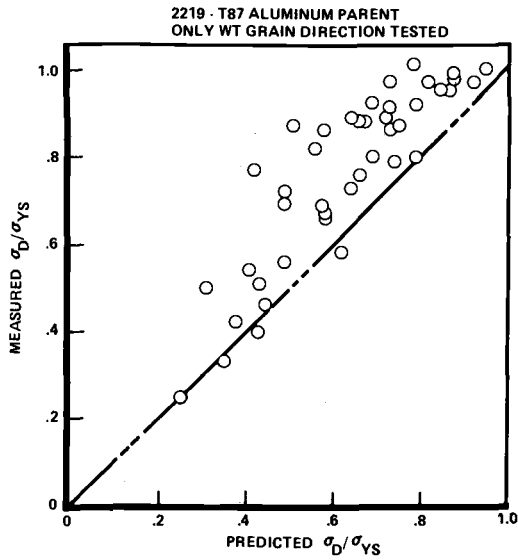


FIG. 5—Test versus prediction of aluminum yielding.

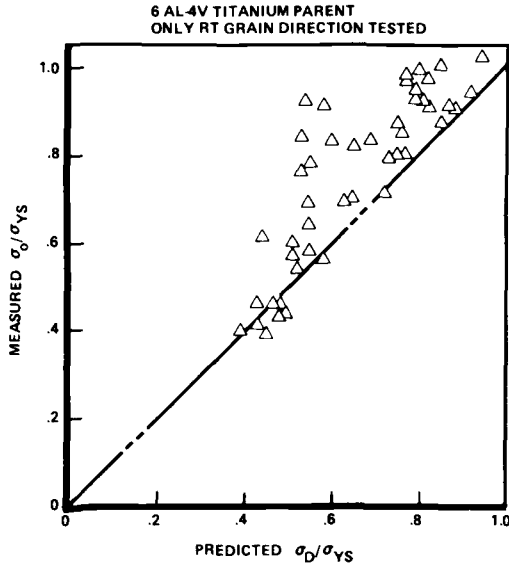


FIG. 6—Test versus prediction of titanium yielding.

In the computer program logic, a test calculation of Eq 16 is made for each increment of crack growth until breakthrough is predicted. The accuracy of this procedure is illustrated in Fig. 7 where the source data are reasonably well fitted by the solid line of the criterion.

Life Prediction Accuracy

In the application of the computer-aided fracture mechanics life prediction program, the individual accuracies of the aforementioned calculation modules are secondary to the overall life prediction accuracy. To assess this accuracy, the computer program was used to predict the number of loading cycles before breakthrough or failure of PTC specimens. (The program is constrained by SSME hardware requirements to assume breakthrough to be failure of the part.) The test data were on hand before the predictions were made, so a skeptic might question the validity of the predictions. However, the point of the exercise was to assess program accuracy rather than to arrive at a given set of answers, so the calculations were performed objectively. A typical set of results is shown in Table 1. All of the specimens in this set were made from 2219-T85 aluminum plate. Variations of the specimen parameters included section thicknesses of 12.7 and 25.4 mm, initial crack aspect ratios ($a/2b$) of $\frac{1}{2}$ and $\frac{1}{3}$, and initial crack depths of 1.5 and 2.3 mm. All specimens were loaded axially with variations in test parameters including test section stress levels of 97 and 221 MPa (14 and 32 ksi), cyclic loading

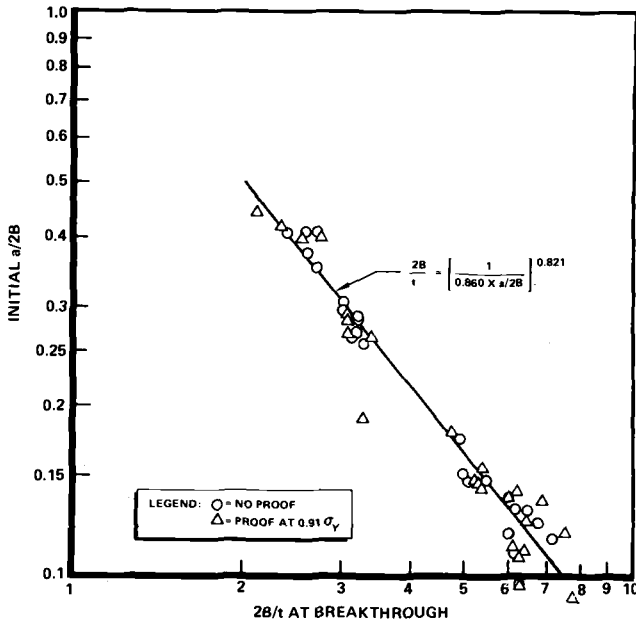


FIG. 7—Effect of aspect ratio on breakthrough.

TABLE 1—Predictions of aluminum PTC specimen data.

Specimen	Test		Analysis		Analysis/Test	
	Breakthrough	Fail	Breakthrough	Fail	Breakthrough	Fail
23-18	23 000	24 600	18 100	...	0.787	...
37-3	...	20 100	...	20 400	...	1.015
32-2	...	19 900	...	11 100	...	0.558
23-16	190 000	205 000	187 000	...	0.984	...
23-12	22 400	23 000	18 100	...	0.808	...
23-13	19 800	20 000	18 100	...	0.914	...
23-17	178 000	192 000	187 000	...	1.051	...
27-76	154 000	168 000	187 000	...	1.214	...
23-14	20 000	20 400	18 100	...	0.905	...
23-10	18 800	19 400	18 100	...	0.963	...

X = 0.953-0.787

S = 0.137-0.323

rates of 6 and 60 cpm, and testing mediums of dry air and both distilled and sump tank water. With all of these variations included in only ten specimens, it is impractical to quantify individual effects. Therefore, this analytic exercise is only a qualitative assessment of computer-aided life prediction accuracy. The ratio of predicted-cycles-to-breakthrough divided by test-cycles-to-breakthrough averaged 0.95, with a statistical standard deviation of 0.14

as shown in Table 1. Similar results were obtained using test data from 6A1-4V-titanium and 9Ni-4Co-0.20C steel specimens. Therefore, it was concluded that the computer-aided fracture mechanics life prediction program provides a good basis for design analysis.

Future Developments

The aforementioned computer program is modularized so that new technology can be incorporated very easily. In general, the IBM 360 computer run times are less than 1 min. This efficiency allows the proposed analytic techniques to be investigated inexpensively before the program is committed to design analysis. At this time several unqualified modules are tentatively in use; one accommodates nonlinear variations of stress through the thickness caused by thermal stress, and another spectrum-type input loading. Further improvements will be incorporated as the fracture mechanics technology becomes available.

Acknowledgments

The fracture mechanics life prediction computer program was developed at the Rocketdyne Division of Rockwell International under NASA Contract NAS8-27980. The cognizant NASA office is Marshall Space Flight Center (MSFC), Huntsville, Ala.

References

- [1] Forman, R. G., Kavanaugh, H. C., and Stuckey, B., "Computer Analysis of Two-Dimensional Fatigue Flaw-Growth Problems," NASA Technical Memorandum TM X-58086, National Aeronautics and Space Administration Manned Spacecraft Center, Houston, Tex. 1972.
- [2] Shah, R. C. and Kobayashi, A. S. in *Proceedings*, 1971 National Symposium on Fracture Mechanics, Part 1; *ASTM STP 513*, American Society for Testing and Materials, 1972, pp. 3-21.
- [3] Grandt, A. F., Jr., and Sinclair, G. M. in *Stress Analysis and Growth of Cracks, Proceedings*, 1971 National Symposium on Fracture Mechanics, Part 1, *ASTM STP 513*, American Society for Testing and Materials, 1972, pp. 37-58.
- [4] Kobayashi, A. S. and Moss, W. L. in *Proceedings*, 2nd International Conference on Fracture, Brighton, England, 1969, pp. 31-45.
- [5] Masters, J. N., Bixler, W. D., and Finger, R. W., "Fracture Characteristics of Structural Alloys Containing Deep Surface Flaws," NASA Report CR-134587, National Aeronautics and Space Administration, Boeing Aerospace Company, Seattle, Wash., Dec. 1973.
- [6] Masters, J. N., Engstrom, W. L., and Bixler, W. E., "Deep Flaws in Weldments of Aluminum and Titanium," NASA Report CR-134649, National Aeronautics and Space Administration, Boeing Aerospace Company, Seattle, Wash., April 1974.

Prediction of Constant Amplitude Fatigue Crack Propagation in Surface Flaws

REFERENCE: Johnson, W. S., "Prediction of Constant Amplitude Fatigue Crack Propagation in Surface Flaws," *Part-Through Crack Fatigue Life Prediction*, ASTM STP 687, J. B. Chang, Ed., American Society for Testing and Materials, 1979, pp. 143-155.

ABSTRACT: A technique used to predict constant amplitude crack growth in a surface flaw is presented. Various aspects of this technique that are discussed include: constant amplitude crack growth data, crack growth models, crack growth accumulation/integration routine, surface flaw stress intensity factors, surface flaw transition to a through crack and the definition of failure/fracture of a specimen. The author's predictions and the results of a round-robin effort are discussed.

KEY WORDS: crack propagation, surface flaw, surface flaw transition, crack growth integration, fatigue (materials)

The objective of this paper is to outline the rationale and methodology used by the author for predicting the constant amplitude crack growth of surface flaws for the round robin sponsored by ASTM Task Group E24.06.01 of ASTM Subcommittee E24.06 on Fracture Mechanics Applications. Details of the round robin effort are presented by Vroman [1].² The purpose of the methodology is to predict analytically (not merely be fitted to) the constant amplitude crack growth behavior.

The author feels that there are at least six separate areas that must be addressed and considered carefully if an accurate prediction technique for constant amplitude crack growth is to be achieved. Constant amplitude is specified because spectrum loading crack growth requires several

¹ Structural engineer, Fatigue and Fracture Analysis Group, General Dynamics, Fort Worth, Tex. 77101. Currently at Duke University, Department of Civil Engineering, Durham, N. C. 27706.

² The italic numbers in brackets refer to the list of references appended to this paper.

additional considerations if the crack growth load interaction is to be modeled properly [2]. Therefore, the following topics will be addressed:

1. Constant amplitude crack growth data
2. Crack growth models
3. Crack growth accumulation/integration routine
4. Surface flaw stress intensity factors
5. Surface flaw transition to a through crack
6. Definition of failure/fracture of specimen.

Constant Amplitude Crack Growth Data

The constant amplitude crack growth data are used to relate the crack tip stress intensity factor, K , to the crack growth rate, da/dN , of a particular material. This relationship is dependent upon material thickness, yield stress, environment, rate of cycling, and stress ratio. The constant amplitude data are evaluated to determine the parameters of a chosen crack growth rate model. Therefore, the selection of the constant amplitude data has a large influence on the accuracy of the predicted crack growth.

Specimens used to generate the candidate data set and specimens that are to be predicted should involve the same (*a*) material (for example 2219-T851 Aluminum) and grain orientation (for example R-T, R-W, etc.), (*b*) approximate thickness, (*c*) chemical environment, and (*d*) approximate values of stress ratio.

Moreover, the candidate data set should be consistent within itself to add validity and confidence to the data. The data set should exhibit increasing crack growth rate (or at least a status quo) with increasingly hostile environment/frequency combinations. Consistency in the shape of the crack growth curve with a minimum of scatter is expected for duplicate tests to give credibility to the experimental procedures and to the data.

Constant amplitude crack growth data were supplied by the task group chairman and were used for the round-robin predictions. However, this supplied data did not meet the validity tests previously described. Therefore, the author selected constant amplitude crack growth from the *Damage Tolerant Design Handbook* [3] for 2219-T851 aluminum. Results obtained using these data will be presented later in the paper. Table 1 presents a description of the constant amplitude data in terms of the parameters n and C of the Paris crack growth equation.

Crack Growth Model

Numerous fatigue crack propagation models have been proposed in the literature to describe the functional relationship between the crack growth

TABLE 1—Paris equation crack growth description parameters for the 2219-T851 aluminum data of Ref 3.

Page Ref 3		Used to Predict Test Number ^a
8.1 to 121 (1/75)	$3^b < \Delta K < 9: n = 4.1900$ $C = 4.20 \times 10^{-10}$	441, 532, 533
	$\Delta K \geq 9: n = 3.0546$ $C = 5.11 \times 10^{-9}$	
8.1 to 115 (1/75)	$\Delta K > 3: n = 3.3866$ $C = 2.7479 \times 10^{-9}$	434, 432
	$\Delta K > 3: n = 3.3866$ $C = 3.00 \times 10^{-9c}$	
8.1 to 120 (1/75)	$3 < \Delta K < 10: n = 4.0589$ $C = 8.7318 \times 10^{-10}$	433, 431
	$\Delta K \geq 10: n = 2.822$ $C = 1.5068 \times 10^{-8}$	
	$3 < \Delta K < 10: n = 4.0589$ $C = 9.0 \times 10^{-10c}$	448, 435
	$\Delta K \geq 10: n = 2.822$ $C = 1.7 \times 10^{-8c}$	

^a Refer to the round-robin introduction article by Vroman [1] for further description of tests.

^b A crack growth threshold value, ΔK_{th} , is assumed to be $3 \text{ MN m}^{-3/2}$.

^c The values of C are increased slightly by judgment to account for lower frequency environmental effects producing higher crack growth rates.

rate, da/dN , and the stress intensity range, ΔK . Many of these relationships consider such parameters as stress ratio, R , and fracture toughness, K_c . Gallagher [4] has summarized a number of these models.

For constant amplitude crack growth predictions, the Paris [5] or Forman [6] model is of adequate complexity. The Paris (Power law) equation was chosen here for simplicity, because the constant amplitude loading is at a constant stress ratio, R

$$\frac{da}{dN} = C(\Delta K)^n \quad (1)$$

The constant amplitude data chosen from Ref 3 was approximately the same stress ratio as the test to be predicted (0.05 versus 0.08), so there exists no need for interpolation such as the Forman model. The da/dN versus ΔK constant amplitude data curve was separated into one or more segments for each data set in order to fit a Paris equation to the crack growth curve over a specific range of stress intensity. Describing individual linear segments (on log-log plot) with separate equations results in an accurate description of the overall shape of the curve. Of course, if the number of segments is too large (greater than three), it may be

advantageous to resort to some type of polynomial or trigonometric curve fitting procedure.

Crack Growth Accumulation/Integration Routine

It is highly advantageous (economical) to perform the crack growth predictions for a rather large number of constant amplitude cycles at a time. This may be accomplished by using closed form integration solutions to the Paris or Forman equations. Express the stress intensity range as

$$\Delta K = (\textit{correct} \Delta\sigma\sqrt{\pi})a^{1/2} \quad (2)$$

where *correct* is the geometric correction factor. For the Paris equation, substitute Eq 2 into Eq 1 and separate variables. The integration of both sides results in an equation for the final crack length, a_f , starting with an initial flaw size, a_i , after N number of cycles at $\Delta\sigma$ stress range.

$$a_f = \left[\frac{2-n}{2} C(\Delta\sigma\sqrt{\pi}\textit{correct})^n N + a_i^{(2-n)/2} \right]^{2/(2-n)} \quad (3)$$

The Appendix presents further details of the solution of the Paris equation and a closed form solution of the Forman equation using a perturbation technique [7]. The Forman equation solution is included since it can be used to describe crack growth rate dependence on stress ratio, R , and fracture toughness, K_c .

There is, of course, a limit to the size of N that can be used, because the *correct* term will vary as the crack grows in many cases. Therefore, Eq 3 was used in blocks of $N = 10$ for the round-robin exercise.

This method of crack growth integration/accumulation is very accurate and economical when it is compared to traditional cycle-by-cycle accumulation or Runge-Kutta numerical integration techniques.

Surface Flaw Stress Intensity Factor

Part-through cracks (surface flaws) are quite common in the aerospace industry. However, the state of the art in the geometric considerations of surface flaws is not as well characterized as that for through-the-thickness cracks due to the three-dimensional nature of the part-through crack. The crack growth of the surface flaw should be calculated in both the depth (a) and surface length ($2c$) directions. The ratio between the depth and surface length ($a/2c$) is referred to commonly as the aspect ratio of the crack.

The stress intensities used for surface flaw crack growth predictions will be described next. They are basically those described by Hall, Shah, and Engstrom [8] with slight alteration. Notice that the backface magnification

factor, M_k , curves are extrapolated to $a/t = 1.0$ in Fig. 4. This enables one to grow the crack depth continuously to the backface, as indicated in Fig. 1. This trend has been observed experimentally at General Dynamics/Forth Worth.

Figure 1 represents the surface flaw geometry during periods of growth. The stress intensity used for the surface crack length (point B, Fig. 2) is

$$K = 1.1\sqrt{\pi a/Q} \sigma\sqrt{a/c} \tag{4}$$

where 1.1 was taken as a best estimate of the effect of the front specimen face on the stress intensity factor at the specimen surface. The Q is the flaw shape parameter as shown in Fig. 3.

The crack growth in the depth direction (point A, Fig. 2) is calculated using the stress intensity equation

$$K = \sigma\sqrt{\pi a/Q} M_k \tag{5}$$

where M_k is the backface magnification factor as shown in Fig. 4 [9].

The crack growth is calculated in both the depth, a , and surface, c , direction simultaneously while accounting for the change in Q as the flaw shape changes.

In many observations of surface flaw crack growth under tension loading, it has been noted by the author that the surface flaw tends to “stabilize” at a ratio of $a/2c$ between 0.38 and 0.50 depending on the material loading. The stress intensities of Eqs 4 and 5 “stabilize” the

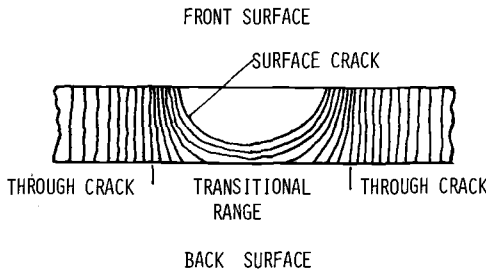


FIG. 1—Typical surface flaw crack growth behavior.

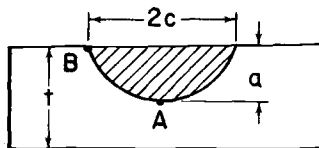


FIG. 2—Surface flaw geometry.

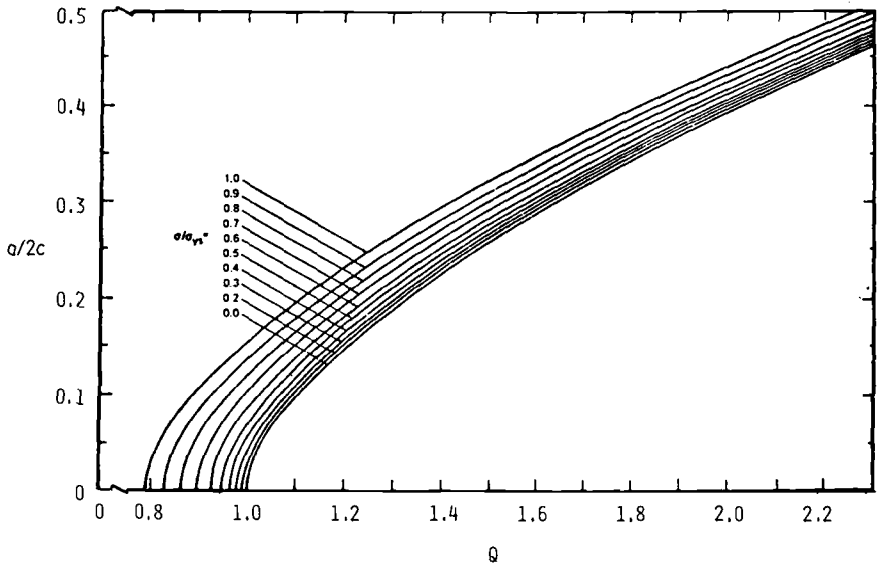


FIG. 3—Flaw shape parameter, Q [8].

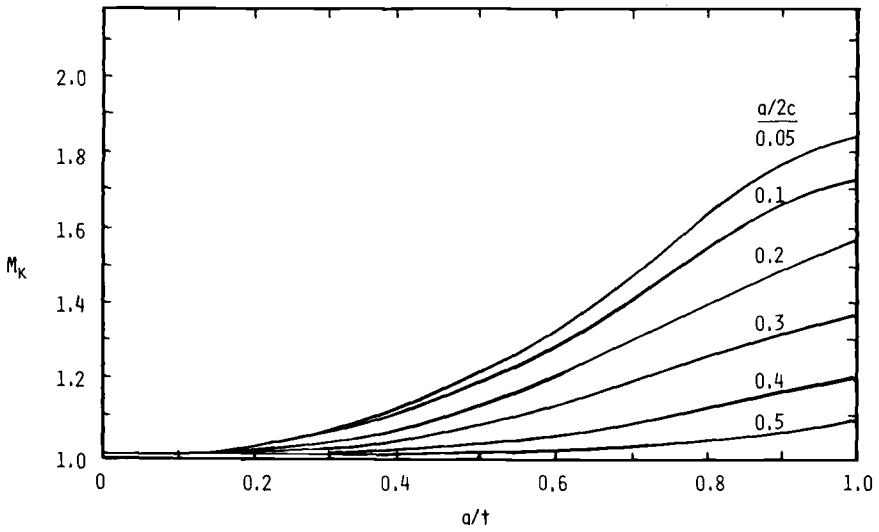


FIG. 4—Back face magnification factor, M_K [9].

aspect ratio at approximately 0.40, which corresponds extremely well with surface flaws of aluminum material tested at General Dynamics. This approximate value of 0.40 is achieved with initial $a/2c$ values above or below 0.40.

Surface Flaw Transition to a Through Crack

A new realistic method for describing a surface flaw transition to a through crack is presented next. Traditionally, the surface flaw would be assumed to grow until the depth equaled the thickness, and then it would be transformed immediately to a through crack. This would create a large increase in the stress intensity value, and it would often cause the crack growth prediction to be overly conservative.

Examination of experimental data reveals that the elliptical surface flaw does not immediately transform to a normal through-the-thickness crack, rather the crack essentially retains its elliptical shape as it grows into a normal through crack as illustrated in Fig. 1.

Therefore, the new model allows the surface flaw to grow with the stress intensity factors cited previously in both the depth and surface length directions. When the crack depth is equal to or greater than the material thickness, t , the crack is assumed to have an elliptical shape that can be described by

$$\frac{c'^2}{c^2} + \frac{t^2}{a'^2} = 1 \quad (6)$$

where

a' = imaginary crack depth if $a > t$, and
 c' = backface surface crack length

as shown in Fig. 5.

As the crack is allowed to grow in the a' and c direction, c' can be calculated using Eq 6. When $c' = 0.9c$, the flaw is assumed to be a through-the-thickness crack, and the appropriate stress intensity factor is used. The only modification to the stress intensity factors during the transitioning period is for the crack depth; Eq 5 becomes

$$K = 1.1\sqrt{\pi a/Q}M_K \quad (7)$$

where the 1.1 accounts for the backface becoming a free surface, and the M_K is fixed at the value when the crack depth reached the backface (that is, $a/t = 1.0$). This transitioning technique is mathematically simple, logical, and agrees well with the actual trends of experimental data observed at General Dynamics.

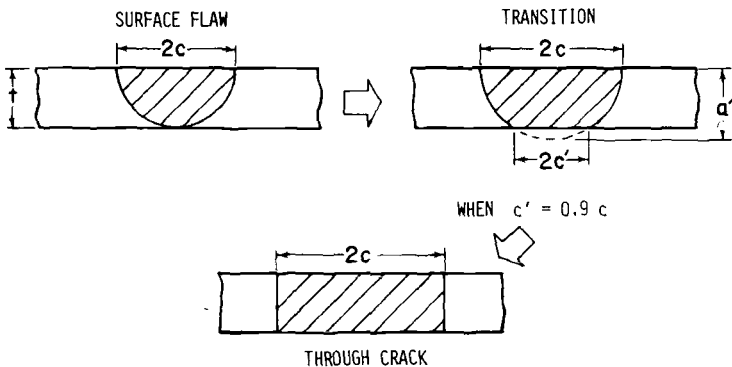


FIG. 5—Surface flaw transition to a through crack.

Definition of Failure/Fracture of Specimen

Essentially, there are two modes of failure in tension-tension crack growth testing. The first is failure due to fracture. This is caused by the stress intensity at some point on the crack front exceeding the critical stress intensity, K_c , for the material and state of stress (function of specimen thickness and loading) being evaluated.

The second common form of failure is static failure. This occurs when the average stress in the specimen cross section containing the crack exceeds the value of ultimate tensile strength for the material being tested.

For the round-robin prediction, the appropriate values of fracture toughness, yield stress, and ultimate stress were selected from the information supplied by the task group chairman. A yield stress of 345 MPa and an ultimate stress of 455 MPa for the 2219-T851 aluminum material were chosen. A fracture toughness of $K_c = 87 \text{ MN m}^{-3/2}$ was selected for the specimens of 1.27 cm thickness and $K_c = 79 \text{ MN m}^{-3/2}$ for the specimens of 2.54 cm thickness.

Predictions and Results

The methodology described in the preceding section are contained within the CGR-GD [9] computerized crack growth rate prediction program. The usual geometric and material parameters are read into the program for each specific problem.

Using the 2219-T851 aluminum crack growth data of Ref 3 resulted in the predictive accuracy presented in Table 2. The values for the predictive accuracy using the supplied data also are presented for comparison. The crack growth data set obtained from Ref 3 yielded more consistent results as indicated by the marked decrease in the standard deviation. However, the mean value of the prediction was not improved, but was about 33 percent conservative.

TABLE 2—Summary of predictive accuracy for the ten predictions of the round robin.

Data	Ratio of Predicted Crack Length to Test Crack Length			
	At Breakthrough		At Failure	
	Mean	Standard Deviation	Mean	Standard Deviation
<i>Damage Tolerant Design Handbook [3]</i>	0.983	0.10	1.086	0.10

Data	Ratio of Predicted Cycles to Test Cycles			
	At Breakthrough		At Failure	
	Mean	Standard Deviation	Mean	Standard Deviation
<i>Damage Tolerant Design Handbook [3]</i>	0.685	0.388	0.697	0.306
Supplied	1.509	1.450	0.942	1.051

Data	Ratio of Predicted Aspect Ratio to Test Aspect Ratio	
	At Breakthrough	
	Mean	Standard Deviation
<i>Damage Tolerant Design Handbook [2]</i>	0.99	0.1

Notice in Table 2 that the predicted aspect ratios ($a/2c$) are in extremely good agreement with the test results. This adds validity to the stress intensity factors variation in the depth and surface directions as described in a previous section.

Conclusion

There are many different aspects to crack growth rate predictions. Each aspect is subject to experimental scatter and theoretical debate. It is a nearly impossible task to evaluate meaningfully the correctness of a particular aspect of the crack growth formulation when there exists considerable uncertainty in the other assumptions. Therefore, it is necessary to continue to explore the various aspects, assumptions, and techniques presently employed, and to advance this state of the art through the interaction of various experts in the field through such organizations as ASTM Committee E-24 on Fracture Testing of Materials.

Acknowledgment

The author would like to acknowledge General Dynamics, Fort Worth Division, for supporting this effort with Internal Research and Development (IRAD) funds.

APPENDIX

Mathematical Formulation of Damage Accumulation Techniques

Solution of Forman Equation

$$\frac{da}{dN} = \frac{C(\Delta K)^n}{(1-R)K_c - \Delta K}$$

Separating terms a and N yields

$$C\Delta N = \int_{a=a_i}^{a=a_f} \frac{(1-R)K_c - \Delta K(a)}{[\Delta K(a)]^n} da \quad (8)$$

Constants C , N , R , K_c , n and a are known. An explicit function of a is available for $\Delta K(a)$, and we wish to find a_f . (Note that n is not necessarily an integer.) For all crack geometries considered

$$\Delta K(a) = (\text{correct } \Delta\sigma\sqrt{\pi})a^{1/2}$$

where *correct* = geometric correction factor

For any crack geometry the integration in Eq 8 may be performed readily. It is

$$C\Delta N = A \frac{2}{2-n} \{a_c^{(2-n)/2} - a_i^{(2-n)/2}\} - B \frac{2}{3-n} \{a_f^{(3-n)/2} - a_i^{(3-n)/2}\} \quad (9)$$

where

$$A = \frac{(1-R)K_c}{(\sqrt{\pi}\Delta\sigma \text{ correct})^n} \quad \text{and} \quad B = (\sqrt{\pi}\Delta\sigma \text{ correct})^{1-n}$$

Since n is generally irrational, Eq 9 is transcendental in a_f thus an exact solution for a_f is not possible. One may also note that if n is near 2 or 3, the appropriate term in Eq 9 is near a logarithmic function of a_f . To circumvent these difficulties attention is redirected to Eq 8. Define

$$\mu = \int_{a=a_i}^{a=a_f} G(a) da \quad (10)$$

where

$$\mu = C\Delta N \quad \text{and} \quad G(a) = \frac{(1-R)K_c - \Delta K(a)}{[\Delta K(a)]^n}$$

By inspecting actual numerical values, μ is generally much smaller than $G(a)$. Hence one might approximate Eq 10 with

$$\mu \approx G(a_i) \int_{a=a_i}^{a=a_f} da = G(a_i)(a_f - a_i) \quad (11)$$

Solution of Eq 11 for a_f may be accomplished quite readily.

Effectually, the procedure described below calculates successive corrections to the

approximate result of Eq 11. In Eq 10 $G(a)$ is expanded in a Taylor series about $a = a_i$, whereupon the resulting series is integrated.

$$\mu = \sum_{m=0,1,2} P_m(\Delta a)^{m+1} \tag{12}$$

where

$$P_m = \frac{a_i^{m+1}}{(m+1)!} \left. \frac{d^m G(a)}{da^m} \right|_{a=a_i}$$

$$\Delta a = \frac{a_f}{a_i} - 1$$

Note that if only the first term is considered, Eq 12 becomes identical to Eq 11. Therefore,

$$\Delta K(a) = (\sqrt{\pi} \Delta \sigma \text{ correct}) a^{1/2}$$

$$G(a) = A a^{-n/2} - B a^{(1-n)/2}$$

where

$$A = \frac{(1-R)K_c}{(\sqrt{\pi} \Delta \sigma \text{ correct})^n}$$

and

$$B = (\sqrt{\pi} \Delta \sigma \text{ correct})^{1-n}$$

as previously stated. Then

$$P_0 = a_i^{(2-n)/2} (A - a_i^{1/2} B)$$

$$P_1 = \left(-\frac{1}{2}\right) \frac{1}{2!} a_i^{(2-n)/2} \{A(n) - a_i^{1/2} B(n-1)\}$$

$$P_2 = \left(-\frac{1}{2}\right)^2 \frac{1}{3!} a_i^{(2-n)/2} \{A(n)(n+2) - a_i^{1/2} B(n-1)(n+1)\}$$

$$P_m = \left(-\frac{1}{2}\right)^m \frac{1}{(m+1)!} a_i^{(2-n)/2} \{A(n)(n+2) \cdots (n+2m-2) - a_i^{1/2} B(n-1)(n+1) \cdots (n+2m-3)\}$$

To calculate Δa , from Eq 12, a power series expansion in the "small parameter" is assumed [10] as

$$\Delta a = \sum_{p=1,2,\dots} \mu^p a_p \tag{13}$$

where each a_p is determined. Upon substituting Eq 13 into Eq 12 and equating to

zero the coefficients of every integral power of μ , one obtains a sequence of equations

$$P_0 a_1 = 1$$

$$P_0 a_2 + P_1 a_1^2 = 0$$

$$P_0 a_3 + P_1 2a_1 a_2 + P_2 a_1^3 = 0$$

Sequential solution of these equations for $a_1, a_2, a_3 \dots$ yields

$$a_1 = 1/P_0$$

$$a_2 = -P_1/P_0^3$$

$$a_3 = (-P_0 P_2 + 2P_1^2)/P_0^5$$

Having determined each successive a_p , Eq 14 and the definition of Δa may be used to calculate a_f

$$a_f = a_i(1 + \Delta a) = a_i \left(1 + \sum_{p=1,2,3,\dots} \mu^p a_p \right) \tag{14}$$

In actual calculations, the series for Δa is carried through $p = 5$ (order μ^5). An estimate of the error involved may be obtained by substituting Eq 13 into Eq 12 and dividing by μm .

Solution of Paris Equation

$$da/dN = C(\Delta K)^n$$

For all crack geometries considered

$$\Delta K = (\text{correct } \Delta\sigma\sqrt{\pi})a^{1/2}$$

Separating terms a and N gives

$$da a^{-n/2} = C(\Delta\sigma\sqrt{\pi} \text{ correct})^n dN$$

By integrating over the range of each load level

$$\int_{a=a_i}^{a=a_f} a^{-n/2} da = \int_{N=0}^{N=N} C(\Delta\sigma\sqrt{\pi} \text{ correct})^n dN$$

or

$$a_f = \left[\frac{2-n}{2} C(\Delta\sigma\sqrt{\pi} \text{ correct})^n N + a_i^{(2-n)/2} \right]^{2/(2-n)} \tag{15}$$

For the special case of $n = 2$,

$$\frac{da}{dN} = C(\Delta K)^2$$

$$\frac{da}{dN} = C(\Delta\sigma\sqrt{\pi a} \text{ correct})^2$$

$$da a^{-1} = C(\Delta\sigma\sqrt{\pi} \text{ correct})^2 dN$$

Integrating over the range of each load level yields:

$$\int_{a=a_i}^{a=a_f} a^{-1} da = \int_{N=0}^{N=N} C(\Delta\sigma\sqrt{\pi} \text{ correct})^2 dN$$

$$\ln a_f - \ln a_i = C(\Delta\sigma\sqrt{\pi} \text{ correct})^2 N$$

$$\ln a_f = C(\Delta\sigma\sqrt{\pi} \text{ correct})^2 N + \ln a_i$$

and finally,

$$a_f = \exp [C(\Delta\sigma\sqrt{\pi} \text{ correct})^2 N + \ln a_i] \quad (16)$$

References

- [1] Vroman, G. A., this publication, pp. 89-95.
- [2] Garver, W. R. and Johnson, W. S., "An Evaluation of the MPYZ Crack Growth Retardation Model for Durability and Damage Tolerance Analysis," General Dynamics Engineering Research Report ERR-FW-1956, Dec. 1978.
- [3] *Damage Tolerant Design Handbook*, MCIC-HB-01, Part 2, pp. 8.1-115, 120, and 121, Jan. 1975.
- [4] Gallagher, J. P., "Fatigue Crack Growth Rate Laws Accounting for Stress Ratio Effects," ASTM Task Force E24.04.04 Report No. 1, 1974.
- [5] Paris, P. C. and Erdogan, F., "A Critical Analysis of Crack Propagation Laws," *Journal of Basic Engineering: Transactions*, American Society of Mechanical Engineers, Series D, Vol. 85, Dec. 1963, pp. 528-534.
- [6] Forman, R. G., Kearney, V. E., and Engle, R. M., *Journal of Basic Engineering: Transactions*, American Society of Mechanical Engineers, Series D, Vol. 89, No. 3, Sept. 1967, pp. 459-464.
- [7] Johnson, W. S., "CGR, An Improved Computerized Model to Predict Fatigue Crack Growth Under Spectrum Loading," Report 4577, Naval Ship Research and Development Center, Jan. 1975.
- [8] Hall, L. R., Shah, R. C., and Engstrom, W. L., "Fracture and Fatigue Crack Growth Behavior of Surface Flaws and Flaws Originating at Fastener Holes," Air Force Flight Dynamics Laboratory, AFFDL-TR-74-47, May 1974.
- [9] Johnson, W. S. and Spamer, T., "A Users Guide to CGR-GD, A Computerized Crack Growth Predicting Program," General Dynamics Report FZS-241, Nov. 1976.
- [10] Nayfeh, Ali Hasan in *Perturbation Methods*, Wiley, New York, 1973, p. 2.

Assessment of the Sensitivity of Crack Growth Rate Constants to Predictive Accuracy of Part-Through Crack Fatigue Life Predictions

REFERENCE: Chang, J. B., "Assessment of the Sensitivity of Crack Growth Rate Constants to Predictive Accuracy of Part-Through Crack Fatigue Life Predictions," *Part-Through Crack Fatigue Life Prediction. ASTM STP 687*, J. B. Chang, Ed., American Society for Testing and Materials, 1979, pp. 156-167.

ABSTRACT: Fatigue crack life predictions were performed for specimens containing part-through cracks subjected to constant-amplitude loading. A computer routine, EFFGRO, was employed in the crack growth predictions. Three rounds of predictions were made by using different crack growth rate constants derived from the compact-type (CT) specimen da/dN versus ΔK data. The predictive accuracies of each round of predictions were assessed. The results show that accurate predictions of part-through crack fatigue lives using CT specimen crack growth rate data can be achieved if there are known part-through crack test data serving as guidelines.

KEY WORDS: fatigue life prediction, part-through crack, constant amplitude, aluminum, stress intensity factor, crack propagation, fatigue (materials)

The emphasis of designing durable and damage-tolerant structures in recent years has initiated many test programs to generate a large quantity of fracture and fatigue crack growth rate data. In most of the test programs, CT specimens have been widely used. Relative low cost is the obvious reason for using CT specimens to generate the baseline data. Yet, the analysts would like to know if the data are directly usable in part-through crack life predictions. A wide range of answers is anticipated, depending on individual experience. Based on this, a round-robin analysis

¹Member of technical staff, Fatigue and Fracture Mechanics, Structures Systems, North American Aircraft Division, Rockwell International, Los Angeles, Calif. 90009.

was initiated by ASTM Task Group E24.06.01. The round-robin participants started with information related to ten test cases which were 2219-T851 aluminum plates containing part-through cracks subjected to constant-amplitude loading. The information furnished consisted of the specimen geometries, initial crack sizes, test loading conditions, and test environments. Table 1 summarizes the detail information of each test case. Crack growth test data for each test case were known by this author at the time of the predictions and were made known to the other participants after they submitted their predictions.

At Rockwell International (Rockwell), North American Aircraft Division (NAAD), each life prediction was performed by employing a crack growth analysis computer routine, EFFGRO [1],² developed in-house at NAAD. This paper describes briefly the crack growth methodology used in EFFGRO and presents the results of the analytical predictions together with test data correlations.

Fatigue Crack Growth Prediction Methodology

EFFGRO is a computer program developed for analyzing crack growth in cyclic-loaded structures based on linear elastic fracture mechanics (LEFM) principles. Based on LEFM concepts, the damage severity at the crack tip can be characterized by a single parameter, the crack-tip stress intensity factor K .

Fatigue Crack Growth Rate Relationship

The fatigue crack growth rate equation chosen for the analysis was the Walker equation [2], which is a modified version of Paris' rate equation [3]. The Walker equation can be written as

$$\frac{da}{dN} = C \left[\frac{\Delta K}{(1-R)^{1-m}} \right]^n$$

where

$\Delta K = K_{\max} - K_{\min}$ = the stress intensity factor range,

R = stress ratio,

C and n = crack growth rate coefficients, and

m = Walker exponent.

Three rounds of life predictions were performed in this round-robin analysis. The first-round predictions were done without comparing the test data, while the second- and third-round predictions were performed after

²The italic numbers in brackets refer to the list of references appended to this paper.

TABLE 1—Summary of part-through crack fatigue testing description issued to ASTM Task Group E24.06.01 life-prediction exercise.

Specimen Number	Specimen Geometry			Crack Dimensions		Loading Condition		Environment	Loading Frequency
	W, mm (in.)	t, mm (in.)	a, mm (in.)	a/2c	σ_{max} MN/m ² (ksi)	R			
23-18	101.6 (4.00)	12.7 (0.5)	1.524 (0.06)	1/2	220.64 (32)	0.05	room temperature lab air	60 cpm	
37-3	101.6 (4.00)	25.4 (1.0)	1.524 (0.06)	1/2	220.64 (32)	0.05	room temperature lab air	60 cpm	
32-2	101.6 (4.00)	25.4 (1.0)	2.286 (0.09)	1/3	220.64 (32)	0.05	room temperature lab air	60 cpm	
23-16	101.6 (4.00)	12.7 (0.5)	1.524 (0.06)	1/2	96.53 (14)	0.05	room temperature distilled water	60 cpm	
23-12	101.6 (4.00)	12.7 (0.5)	1.524 (0.06)	1/2	220.64 (32)	0.05	room temperature distilled water	60 cpm	
23-13	101.6 (4.00)	12.7 (0.5)	1.524 (0.06)	1/2	220.64 (32)	0.05	room temperature distilled water	6 cpm	
23-17	101.6 (4.00)	12.7 (0.5)	1.524 (0.06)	1/2	96.53 (14)	0.05	room temperature sump tank water	60 cpm	
27-76	101.6 (4.00)	12.7 (0.5)	1.524 (0.06)	1/2	96.53 (14)	0.05	room temperature sump tank water	6 cpm	
23-14	101.6 (4.00)	12.7 (0.5)	1.524 (0.06)	1/2	220.64 (32)	0.05	room temperature sump tank water	60 cpm	
23-10	101.6 (4.00)	12.7 (0.5)	1.524 (0.06)	1/2	220.64 (32)	0.05	room temperature sump tank water	6 cpm	

the test data had been compared to the first-set predictions. The fatigue crack growth rate constants used in the first-round analysis were

$$\begin{aligned}
 c_1 &= 9.93 \times 10^{-9} \\
 n_1 &= 2.68 \\
 m_1 &= 0.3 \\
 \Delta K_{th} &= 2.75 \text{ MN/m}^{3/2} \text{ (2.5 ksi } \sqrt{\text{in.}}) \\
 R_{cutoff} &= 0.45
 \end{aligned}$$

The crack growth rate equation coefficients C and n were obtained directly from the first line shown in Fig. 1. This line was drawn through

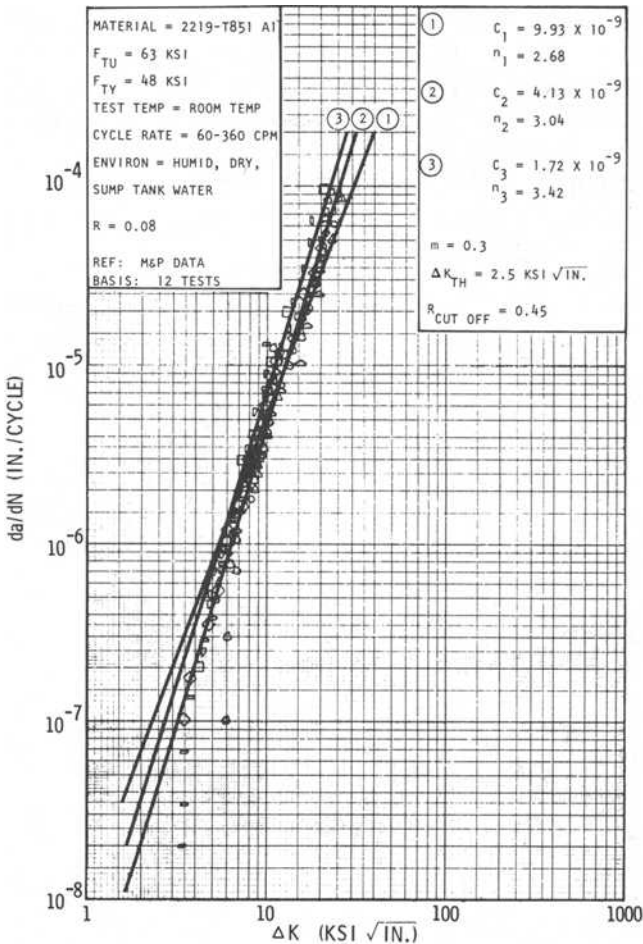


FIG. 1—Baseline fatigue crack growth rate data, 2219-T851 aluminum alloy.

the test points collected from a baseline 2219-T851 aluminum alloy crack growth rate data generation program [4] conducted in-house at Rockwell. The specimens used in this test program were a modification of the ASTM CT specimen configuration as described in ASTM Test for Plane-Strain Fracture Toughness of Metallic Materials (E 399 - 74). The tests were conducted in high- and low-humidity air as well as sump tank water environments. The cyclic loading rates ranged from 60 to 360 cpm. As indicated in Fig. 1, there are no profound distinctions among the growth rate data generated in different environments and cyclic loading rates. Therefore, the same crack growth rate constants were used in the predictions for all ten cases.

In order to study the sensitivity of the crack growth rate coefficients to the predictive accuracy, two additional rounds of predictions were performed by using two other sets of coefficients (c_2, n_2 , and c_3, n_3), which represent the interceptions and the reciprocal of the slopes of the second and third lines shown in Fig. 1. It can be seen that these two lines were tilted toward the direction which provides faster growth rate for higher ΔK values. This is because the results of the first-round predictions showed that the coefficients overwhelmingly overestimated crack lives.

Stress-Intensity Factor Formula

Stress-intensity factors used in the fatigue crack growth behavior predictions were those originally built into EFFGRO. For the part-through crack, the stress-intensity factor for the point on the periphery of the crack at the greatest distance from the front face in EFFGRO is

$$K = M_f \left(\frac{a}{c} \right) M_b \left(\frac{a}{c}, \frac{a}{t} \right) M_w \left(\frac{c}{w} \right) \sigma \sqrt{\frac{\pi a}{Q}}$$

where

σ = remotely applied tensile stress,

a = crack depth,

$2c$ = crack length,

t = thickness,

w = width of the structure, and

M_f and M_b = front and back face correction factors, respectively.

The M_f and M_b for various a/c and a/t values are shown in Tables 2 and 3. They are derived from the results reported by Kobayashi and Moss [5] and Shah and Kobayashi [6]. M_w is the width correction factor. Tada's modified secant function [7] is adopted, which takes the following form

$$M_w = \left[1 - 0.025 \left(\frac{2c}{W} \right)^2 + 0.06 \left(\frac{2c}{W} \right)^4 \right] \sqrt{\secant \frac{\pi c}{W}}$$

TABLE 2—Front face correction factor.

<i>a/c</i>	0	0.1	0.2	0.4	0.6	0.8	1.0
<i>M_f</i>	1.12	1.11	1.1	1.08	1.06	1.04	1.03

TABLE 3—Back face correction factor.

<i>a/c</i>	<i>a/t</i>								
	0.0	0.2	0.3	0.4	0.5	0.5	0.7	0.8	0.9
0.1	1.0	1.02	1.04	1.05	1.08	1.13	1.2	1.36	1.76
0.2	1.0	1.0	1.02	1.03	1.06	1.1	1.16	1.27	1.53
0.4	1.0	1.0	1.02	1.01	1.04	1.07	1.13	1.20	1.37
0.6	1.0	1.0	1.0	1.01	1.02	1.05	1.09	1.16	1.28
0.8	1.0	1.0	1.0	1.01	1.02	1.04	1.07	1.13	1.24
1.0	1.0	1.0	1.0	1.0	1.01	1.02	1.05	1.10	1.19

The quantity *Q* is a combined factor which is expressed in terms of the elliptical shape normalizing factor, ϕ , and the ratio of the applied stress to the material yield strength, σ/σ_{ys} as

$$Q = \phi^2 - 0.212 (\sigma/\sigma_{ys})^2$$

Values of ϕ are the complete elliptical integral of the second kind, which can be expressed as

$$\phi = \int_0^{\pi/2} (\sqrt{1 - (1 - 4\xi^2) \sin^2 \theta}) d\theta, \xi = a/2c$$

Integration Scheme

EFFGRO is essentially a specialized integration routine where an initial crack length is given and da/dN is integrated to yield the relationship between *a* and *N* for a given load spectrum. It is based on the fact that small changes in crack length have a minimal effect on the crack growth rate. This integration scheme was originated by Vroman [1]. The following paragraphs describe the integration procedure.

The load information in the actual integration portion of EFFGRO is given in Table 4.

The integration scheme proceeds by considering a load step (i) and using σ_{max_i} and σ_{min_i} to calculate K_{max} , K_{min} , *R*, and da/dN .

The value of $0.01a/(da/dN)$ is then compared to N_i . If $0.01a/(da/dN)$ is greater than N_i , then the crack growth for that load step is $\Delta a = N_i \times da/dN$. *a* is increased by Δa , and the program proceeds to the next load step.

TABLE 4—Load information in integration portion of EFFGRO.

Step	Max Stress	Min Stress	No. of Cycles/Block (flight)
1	$\sigma_{\max 1}$	$\sigma_{\min 1}$	N_1
2	$\sigma_{\max 2}$	$\sigma_{\min 2}$	N_2
3	$\sigma_{\max 3}$	$\sigma_{\min 3}$	N_3
...
...
i	$\sigma_{\max i}$	$\sigma_{\min i}$	N_i

If $0.01a/(da/dN)$ is less than or equal to N_i , then the number of cycles to grow $0.01a$ is $0.01a/(da/dN)$. This value is subtracted from N_i , the crack size, a , is increased by $0.01a$, and the load step is reconsidered. This process continues with $0.01a/(da/dN)$ being compared to the remaining cycles in the step.

When all load steps in the block (flight) are exhausted, the program proceeds to the first step of the next block (flight). The calculation ends when K_{\lim} computed with the limit load or the maximum spectrum load, whichever is greater, exceeds the defined critical stress intensity factor value.

Breakthrough Criterion

When the boundary of the part-through crack reaches the back face (that is, $a = t$), the part-through crack is said to break through the thickness, and the crack is assumed to be a through crack by EFFGRO. For a through crack, the stress-intensity factor used is

$$K = M_w \left(\frac{c}{w} \right) \sigma \sqrt{\pi c}$$

Crack Growth Termination Criterion

The crack growth termination criterion applied in this fatigue life prediction exercise is based on the critical stress intensity factor values of the material. The life of a cracked structure is said to be ended when the growth of the crack is terminated by the computer program. The program run ends when the calculated K_{\lim} with the maximum cyclic stress exceeds the appropriate critical stress intensity factor value. In the predictions, it was assumed that for the part-through crack, the critical stress intensity factor was $K_{cr} = 49 \text{ MN/m}^{3/2}$ (45 ksi $\sqrt{\text{in.}}$), and for the through crack, $K_{cr} = 83 \text{ MN/m}^{3/2}$ (76 ksi $\sqrt{\text{in.}}$).

Results and Discussion

The crack growth life prediction results were compared to test data. Typical comparisons are shown in Figs. 2 and 3. The broken lines represent the predicted growth behavior of the crack, while the solid lines represent the test result of each case. It can be seen from Fig. 2 that the crack growth life prediction is within 10 percent of the actual life. This is very good for a part-through crack life prediction.

In order to assess the predictive accuracy, the ratios of the predicted life to the test life, R , of the ten correlated cases in the first-round predictions were calculated (Table 5). The mean value of R of the first-round predictions is 1.08. It seems to be an acceptable number; however, as shown in the table, 80 percent of the R values in this round exceed unity, indicating the predictions overwhelmingly overestimated fatigue crack lives. The histogram shown in Fig. 4 illustrates the point.

Two more rounds of predictions were made based on the aforementioned results in order to assess the sensitivity of the crack growth rate constants chosen in the predictions. The crack growth rate coefficients used in the second- and third-round predictions are shown in Fig. 1. Results of the

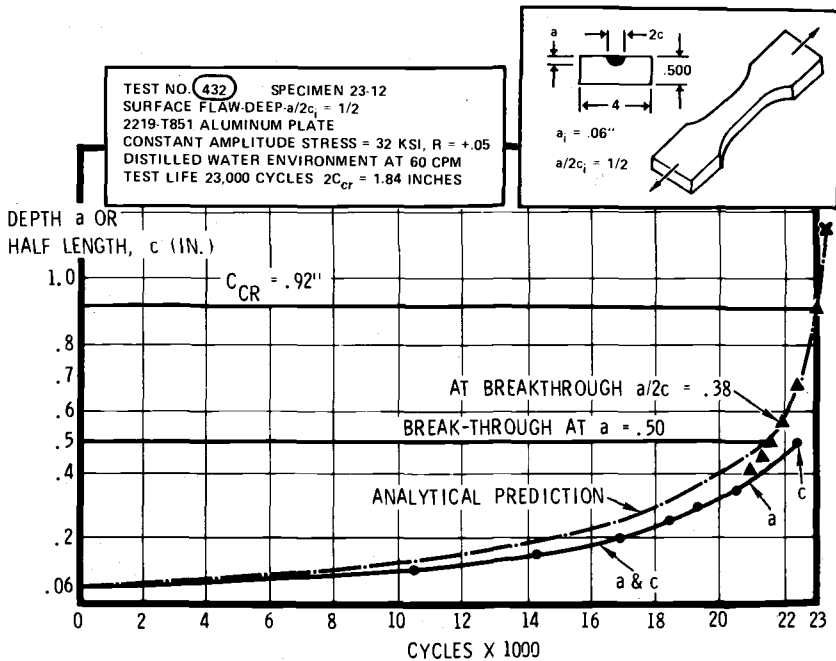


FIG. 2—Crack growth comparison, prediction versus test, Specimen 23-12.

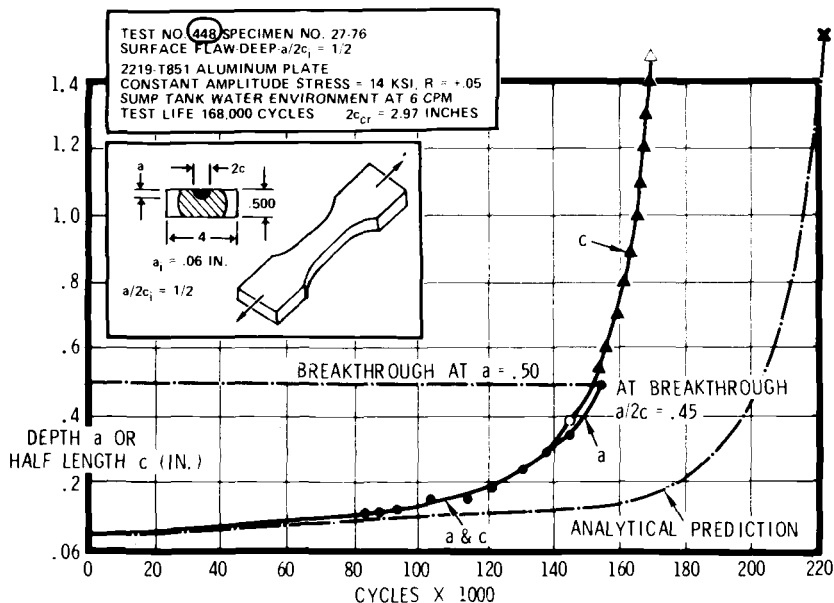


FIG. 3—Crack growth comparison, prediction versus test, Specimen 27-76.

crack life predictions were again compared with the test data. Table 5 summarizes the comparison. Histograms of the ratio of predicted life to tested life (Figs. 5 and 6) were plotted in order to demonstrate the predictive accuracy of each round of predictions. It can be seen that the third-round predictions were the best among the three. Half of the predicted cases were within 20 percent of the actual life, and the percentage of over-estimation dropped to 40.

Conclusions

The results of the present investigation on the sensitivity of the crack growth rate coefficients to the accuracy of the part-through crack fatigue life predictions suggest the following conclusions:

1. To use the crack growth rate coefficients c and n derived from the compact-type specimen da/dN versus ΔK data for part-through crack fatigue life prediction will provide satisfactory answers.
2. Accurate predictions of part-through crack fatigue lives using compact-type specimen crack growth rate data can be achieved if there are known part-through crack test data serving as guidelines.

TABLE 5—Summary of part-through crack specimen data correlation.

Specimen Number	Tested Crack Life Cycles	First-Round Prediction		Second-Round Prediction		Third-Round Prediction	
		N_{PRED} , cycles	R_1	N_{PRED} , cycles	R_2	N_{PRED} , cycles	R_3
23-18	24 600	23 200	0.94	20 900	0.85	18 900	0.77
37-3	20 100	25 300	1.26	22 600	1.12	21 200	1.05
32-2	19 900	10 100	0.51	8 200	0.41	14 000	0.704
23-16	205 000	221 700	1.08	269 000	1.31	256 200	1.25
23-12	23 000	23 200	1.01	20 900	0.91	18 900	0.82
23-13	20 000	23 200	1.16	20 900	1.04	18 900	0.945
23-17	192 000	221 700	1.15	269 000	1.4	256 200	1.33
27-76	168 000	221 700	1.32	269 000	1.6	256 200	1.525
23-14	20 400	23 200	1.14	20 900	1.02	18 900	0.93
23-10	19 400	23 200	1.2	20 900	1.08	18 900	0.974

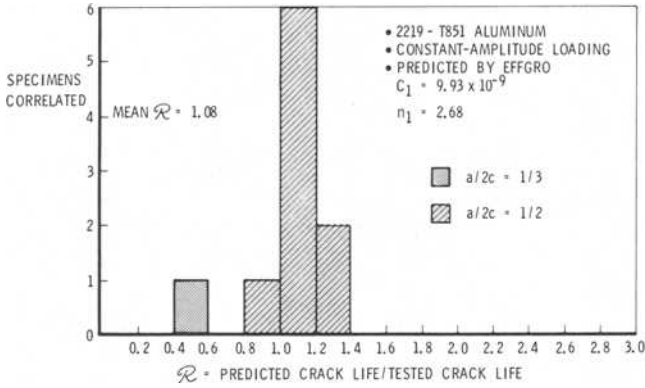


FIG. 4—Histogram, results of first-round correlations.

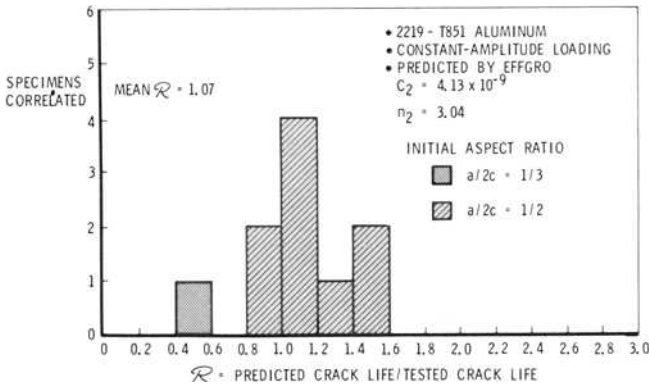


FIG. 5—Histogram, results of second-round correlations.

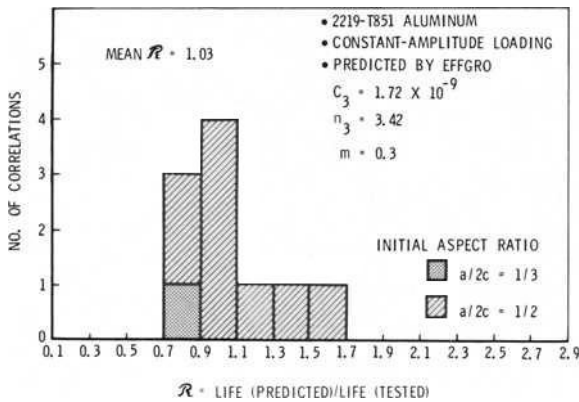


FIG. 6—Histogram, results of final correlation.

Acknowledgments

The authors wish to thank Martha Szamossi for the aid associated with crack growth analyses. The author would also like to thank G. E. Fitch, Jr. for his continued support of this task group activity.

References

- [1] Szamossi, M., "Crack Propagation Analysis by Vroman's Model, Computer Analysis Summary, Program EFFGRO," NA-72-94, Rockwell International, Los Angeles Division, 1972.
- [2] Walker, K. in *Effects of Environment and Complex Load History on Fatigue Life, ASTM STP 462*, American Society for Testing and Materials, 1970.
- [3] Paris, P. C., Gomez, M. P., and Anderson, W. E., "A Rational Analytical Theory of Fatigue," *The Trend in Engineering*, Vol. 13, No. 1, University of Washington, Jan. 1961.
- [4] Ferguson, R. R. and Berryman, R. C., "Fracture Mechanics Evaluation of B-1 Materials," AFML-TR-76-137, Air Force Materials Laboratory, Wright-Patterson Air Force Base, Ohio, 1976.
- [5] Kobayashi, A. S. and Moss, W. L., "Stress Intensity Magnification Factor for Surface-Flawed Tension Plate and Notched Round Tension Bar," *Proceedings*, 2nd International Conference on Fracture, Brighton, England, 1969.
- [6] Shah, R. C. and Kobayashi, A. S., "On the Surface Flaw Problem," *The Surface Crack: Physical Problem and Computational Solutions*, American Society of Mechanical Engineers, New York, 1972.
- [7] Tada, H., *The Stress Analysis of Cracks Handbook*, Del Research Corporation, Hellertown, Pa., 1973.

Part-Through Crack Problems in Aircraft Structures

REFERENCE: Rudd, J. L., Hsu, T. M., and Wood, H. A., "Part-Through Crack Problems in Aircraft Structures," *Part-Through Crack Fatigue Life Prediction, ASTM STP 687*, J. B. Chang, Ed., American Society for Testing and Materials, 1979, pp. 168-194.

ABSTRACT: Flaws occur in aircraft structures due to material and structural manufacturing and processing operations. The most prevalent sources of cracking in aircraft structures are fastener holes, although cracking does occur at locations other than fastener holes (for example, surface cracks). This paper presents a discussion of the most common types of flaws which exist in aircraft structures and the test data and analytical criteria needed to predict their growth. A number of special analytical and structural considerations are discussed such as small flaws, cold-worked holes, plasticity effects, failure criteria, and multiple flaw sites. The analytical crack growth and residual strength requirements which must be met as well as the initial flaw sizes and shapes which must be assumed in the Air Force damage tolerance design requirements (MIL-A-83444) are presented. Recently developed stress intensity factor solutions for quarter elliptical corner cracks emanating from various types of fastener holes are presented. Predictions using these current solutions are correlated with other approximate solutions as well as experimental test data.

KEY WORDS: part-through cracks, aircraft structure, damage tolerance, stress intensity factors, design criteria, fastener holes, crack propagation, fatigue (materials)

It seems most appropriate to begin the discussion of part-through crack problems in aircraft structures by presenting the infamous part-through flaw which generated a tremendous amount of interest by the Air Force in the area of fracture mechanics and has led to the current Air Force damage tolerance design requirements of MIL-A-83444 [1].³ This flaw was introduced during the manufacturing of a F-111 wing forging made of D6AC steel. The flaw was a semi-elliptical surface flaw with a length of 25.4 mm (1 in.) and a depth of 6.35 mm (0.25 in.).⁴ The upper portion of Fig. 1

¹Aerospace engineer and supervisory aerospace engineer, respectively, Air Force Flight Dynamics Laboratory, Wright Patterson AFB, Ohio 45433.

²Aircraft development engineer-specialist, Lockheed-Georgia Co., Marietta, Ga. 30063.

³The italic numbers in brackets refer to the list of references appended to this paper.

⁴The original measurements were in U.S. customary units.

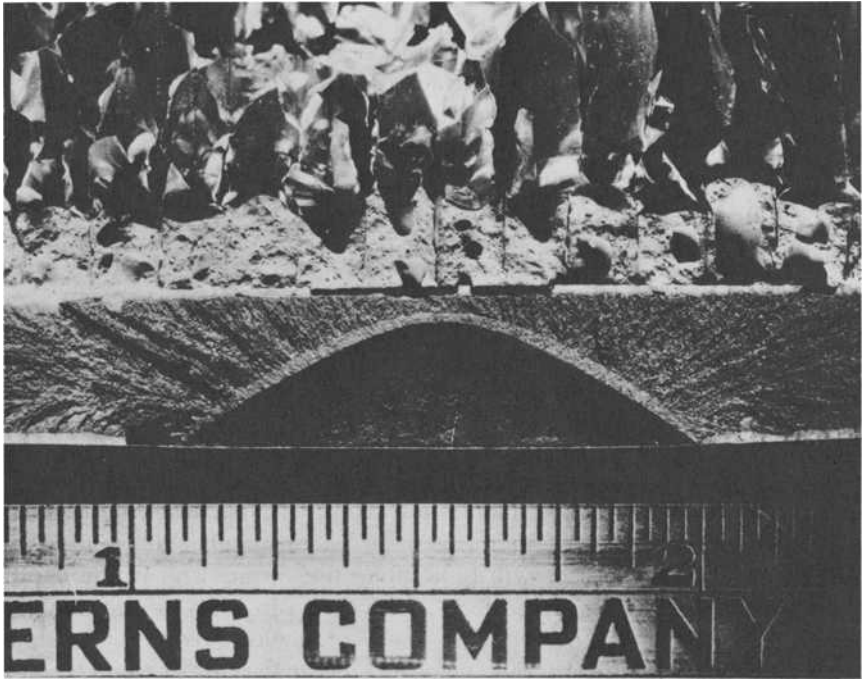


FIG. 1—*F-111 part-through flaw.*

represents a honeycomb fairing. In-service failure of the F-111 aircraft which contained the flawed forging occurred at Nellis Air Force Base, Nevada in 1969 after a relatively small number of flight hours, the growth of the flaw being represented by the narrow band in Fig. 1. This failure had a large impact on the current requirements contained in MIL-A-83444, which include the assumption that flaws exist in aircraft structures due to material and structural manufacturing and processing operations. The emphasis on fracture mechanics in the design, manufacture, and maintenance of military aircraft has increased steadily since that failure.

Common Types of Flaws in Aircraft Structures

Fastener holes are found to be the most prevalent sources of cracking in aircraft structures [2]. This cracking occurs due to a number of different material and structural manufacturing and processing operations as well as due to the large stress concentrations which exist at fastener holes. Some common types of flaws which occur at fastener holes are corner flaws, sur-

face flaws along the bore of a hole, part-through flaws in a countersunk hole, and through-the-thickness flaws.

Flaws also occur in aircraft structures at locations other than fastener holes, such as the part-through surface flaw shown in Fig. 1. Such flaws are most significant in heavy sections such as forgings (for example, landing gear components) and are introduced due to a number of different material and structural manufacturing and processing operations or as a result of pitting or corrosion.

Required Test Data, Analytical Criteria, and Special Analytical and Structural Considerations

Required Test Data and Analytical Criteria

In order to perform crack growth and residual strength analyses for aircraft structures, certain experimental test data and analytical criteria must be available. For example, in the case of part-through cracks, there is interest in predicting the growth both along the surface and in the depth direction. Hence, a two-dimensional analytical capability is required to predict the crack shape change. The prediction requires baseline experimental crack growth rate data for the material. These data are needed for two directions of crack growth, since the material crack growth rate properties may differ in the length and depth directions. These data must be generated at the temperature and in the environment that the structure is expected to be subjected to. Also, for part-through cracks, an analytical criterion is required to predict the transition from a part-through crack to a through-the-thickness crack. Accurate predictions require that the effects of free surfaces and other boundaries must be accounted for. Finally, in order to predict the residual strength and crack growth life of an aircraft structure, a failure criterion must exist, whether it be elastic or elastic-plastic. This also requires the availability of experimental test data, such as fracture toughness versus thickness (K_c versus t) for the particular material involved.

Special Analytical Considerations

A number of special analytical considerations are necessary to predict the flaw growth behavior in aircraft structures. One such consideration involves the applicability of fracture mechanics for very small flaws. For example, the damage tolerance design requirements of Ref 1 specify that a small imperfection equivalent to a 0.127-mm (0.005-in.) corner flaw shall be assumed to exist in each fastener hole of each element in aircraft structure,

with the exception that a larger flaw shall be assumed to exist in the most critical fastener hole of each element. Hence, in order to satisfy the crack growth requirements of this specification, the analytical capability must exist to predict the flaw growth behavior of very small flaws.

Another special analytical consideration involves the capability to predict flaw growth behavior when plasticity is present. Plasticity may be introduced when improved fastener systems are used to increase the structural lives of aircraft components. Two such systems are interference-fit fasteners and cold-worked holes. These systems introduce increased complexities to the analyses due to the large amounts of plasticity involved. Plasticity also is introduced at the crack tip when tensile overloads are present, resulting in retarded crack growth. In order to accurately predict the flaw growth behavior in aircraft structures, these inelastic effects must be accounted for.

Special Structural Considerations

Special structural configurations must be considered when predicting the flaw growth behavior for built-up, complex structure. For example, Ref 1 specifies that multiple flaw sites must be considered when a row of fastener holes is involved. In particular, the specification requires that when the assumed primary initial damage grows into and terminates at a fastener hole, continuing damage shall be assumed to exist in that hole which is equivalent to a 0.127-mm (0.005-in.) corner flaw plus the amount of growth that occurs prior to termination of the primary damage. The continuing damage shall be assumed to exist on the diametrically opposite side of the fastener hole at which the primary damage terminated.

A second structural consideration involves the flaw growth behavior in multilayered structure. Ref 1 specifies that for fastener hole locations in which the assembly drilling of the fastener holes is conducted such that flaws in two or more elements can exist at the same location, the primary initial flaw for each element should be assumed at that location. However, at locations other than fastener holes in which the fabrication and assembly operations are conducted such that flaws in two or more elements are not expected to exist at the same location, the primary initial flaw in each element need not be assumed at the same location.

A third structural consideration involves the load transfer in flawed built-up, complex structure. For example, to predict accurately the flaw growth behavior of skin-stringer structure, the load transferred from the stringer to the skin after failure of the stringer must be accounted for. Similarly, if only one member were flawed, load shedding from the flawed member to the unflawed member also should be accounted for. Structural complexities such as these must be considered in order to obtain accurate flaw growth predictions for aircraft structures.

Damage Tolerance Design Requirements for Aircraft Structures

The Air Force damage tolerance design requirements (MIL-A-83444) [1], applicable to airplane safety of flight structure, are specified as a function of the design concept and the degree of inspectability of the structure. The design concepts include slow crack growth structure and fail-safe (that is, multiple load path and crack arrest) structure while the degrees of inspectability include noninspectable, depot or base-level inspectable, special visual inspectable, walk-around visual inspectable, ground evident inspectable, and in-flight evident inspectable. The design requirements involve both residual strength and crack growth analyses in which flaws are assumed to exist in the most unfavorable location and orientation with respect to the applied stress and material properties. These flaws are assumed to occur due to various material and structural manufacturing and processing operations. The design requirements as well as the sizes and shapes of the assumed flaws are presented in the following.

Slow Crack Growth Structure

The degree of inspectability of slow crack growth structure is either (1) noninspectable or (2) depot or base level inspectable. Ref 1 specifies that for noninspectable, slow crack growth structure, initial primary damage shall be assumed to exist in the most critical location of each element and this damage shall not grow to critical size and cause failure of the structure in two (2) design service lifetimes. In addition to this crack growth requirement, a residual strength requirement must also be met for this time period. The initial primary damage sizes and shapes assumed for noninspectable structure are presented in Fig. 2, with $a_1 = 1.27$ mm (0.05 in.) and $a_2 = 3.175$ mm (0.125 in.). It can be seen that for a fastener hole location, the assumed initial primary damage shall be either a 1.27-mm (0.05 in.) through-the-thickness flaw or a quarter-circular corner flaw at one side of the hole, depending upon the material thickness. For a location other than a fastener hole, the assumed initial primary damage shall be either a through-the-thickness flaw or a semicircular surface flaw, depending upon the material thickness. Other possible surface flaw shapes with an initial stress intensity factor equivalent to that of the specified semicircular surface flaw shall be considered as appropriate (for example, corner flaws at the edges of structural elements, longer and shallower surface flaws in plates subjected to high bending stresses). Smaller initial flaw sizes than those specified above may be assumed subsequent to a demonstration that all flaws larger than the assumed sizes have at least a 90 percent probability of detection with a 95 percent confidence level. Smaller initial flaw sizes may also be assumed if proof test inspection is used, based on the calculated critical size at the proof test stress level.

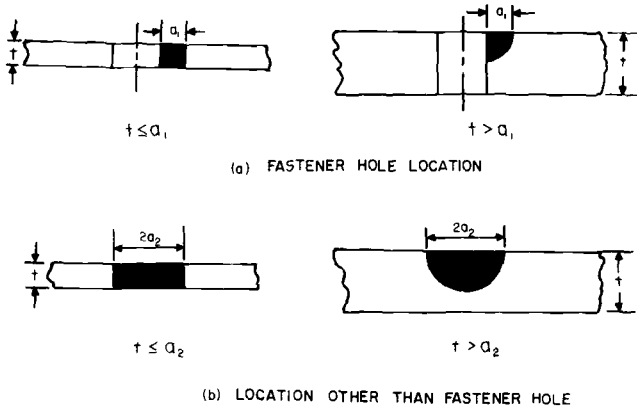


FIG. 2—Initial primary damage assumptions for slow crack growth structure.

For depot or base level inspectable structure, initial primary damage shall be assumed to exist in the most critical location of each element and this damage shall not grow to critical size and cause failure of the structure in one half ($\frac{1}{2}$) the design service lifetime. In addition to this crack growth requirement, a residual strength requirement also must be met for this time period. The assumed initial primary damage sizes and shapes after completion of a depot or base level inspection shall be the same as those previously presented for noninspectable structure (Fig. 2) if the component is to be removed from the aircraft and completely inspected with the same NDI procedures that were used during fabrication. However, when NDI techniques (that is, penetrant, magnetic particle, ultrasonics) are applied without component or fastener removal, the assumed initial primary damage sizes shall be larger. For a fastener hole location, the assumed initial primary damage shall be a through-the-thickness flaw emanating from one side of the hole having a 6.35 mm (0.25 in.) uncovered length (measured from the edge of the fastener head or nut) when the material thickness is equal to or less than 6.35 mm (0.25 in.). For greater material thicknesses, the assumed initial primary damage shall be a quarter-circular corner flaw emanating from one side of the hole having a 6.35-mm (0.25-in.) uncovered length. For a location other than a fastener hole, the assumed initial primary damage shall be as shown in Fig. 2b, with $a_2 = 6.35$ mm (0.25 in.). Other possible surface flaw shapes with an initial stress intensity equivalent to that of the specified semicircular surface flaw shall be considered as appropriate. Where close visual inspection is used, a through-the-thickness flaw having at least 50.8 mm (2 in.) of uncovered length shall be the minimum assumed damage size. When inaccessibility, paint, sealant, or other factors preclude close visual inspection or the use of NDI techniques (that is, penetrant, magnetic particle, ultrasonics), slow

crack growth structure shall be considered to be noninspectable. Smaller initial flaw sizes than those specified previously may be assumed if proof test inspection is used.

In addition to the initial primary damage which must be assumed at the most critical location, initial continuing damage shall be assumed to exist at other locations to represent overall initial quality. For example, continuing damage equivalent to a 0.127-mm (0.005-in.) quarter-circular corner flaw shall be assumed to exist in each fastener hole of each element except the most critical fastener hole containing the primary damage. At locations other than fastener holes, the continuing damage shall be assumed to be a semicircular surface flaw with a length of 0.508 mm (0.02 in.) and a depth of 0.254 mm (0.01 in.). If the contractor has developed initial quality data (for example, fractographic studies which provide a sound basis for determining equivalent initial flaw sizes), these data may be submitted to the procuring activity for review and serve as a basis for negotiating a size different than those specified previously.

Fail-Safe Structure

Fail-safe structure may be classified as either multiple load path or crack arrest structure. The degrees of inspectability of fail-safe structure include depot or base-level inspectable, special visual inspectable, walk-around visual inspectable, ground evident inspectable, and in-flight evident inspectable. Two sets of crack growth and residual strength requirements are specified for multiple load path structure. The first set applies to intact structure (that is, structure prior to load path failure) while the second set applies to the remaining structure subsequent to load path failure. If the intact structure is depot or base-level inspectable, the assumed initial primary damage sizes and shapes after completion of the inspection shall be the same as those previously presented for depot or base-level inspectable slow crack growth structure. The assumed damage shall not grow to critical size and cause failure of the structure in one fourth ($\frac{1}{4}$) the design service lifetime. The structure shall also meet a residual strength requirement for this time period. If the intact structure is not depot or base-level inspectable, the initial primary damage sizes and shapes shall be assumed to be those illustrated in Fig. 2, with $a_1 = 0.508$ mm (0.02 in.) and $a_2 = 1.27$ mm (0.05 in.). The assumed damage shall not grow to critical size and cause failure of the structure in one (1) design service lifetime. The intact structure also shall meet a residual strength requirement for this time period. The remaining structure at the time of load path failure shall meet a separate residual strength requirement which is based on the degree of inspectability of the structure. In addition, subsequent to load path failure, the failed load path plus damage assumed in the remaining adjacent structure shall meet additional crack growth and

residual strength requirements which also are based upon the degree of inspectability of the structure.

Reference 1 also specifies two sets of crack growth and residual strength requirements for crack arrest structure. The first set applies to intact structure (that is, structure prior to unstable crack growth and arrest), while the second set applies to the remaining structure subsequent to encountering unstable crack growth and arrest. The requirements and assumptions which apply to crack arrest structure are basically the same as those which are applicable to multiple load path structure, previously discussed. Hence, no further discussion of the requirements and assumptions for crack arrest structure shall be presented here.

Stress Intensity Factors for Quarter-Elliptical Corner Cracks Emanating from Fastener Holes

As previously mentioned, fastener holes are found to be the most prevalent sources of cracking in aircraft structures, and corner cracks at fastener holes are particularly important in aircraft structures. In order to predict the crack growth behavior for this type of flaw, a stress intensity factor for a quarter-elliptical corner crack emanating from a fastener hole is needed. As no closed form solution exists, this paper presents an approximate stress intensity factor solution recently developed by modifying an existing solution developed by Hsu and Liu [3] for a quarter-elliptical corner crack emanating from an open hole. The development of this solution as well as solutions for quarter-elliptical corner cracks emanating from other types of fastener holes is presented. Also presented are correlations of predictions using the current solution with predictions from other approximate solutions and experimental test data.

Stress Intensity Factor Development

The shape of a corner crack at a fastener hole generally is assumed to be quarter-elliptical with the semi-axes a and c coinciding with the hole wall and the plate surface, respectively. The approximate stress intensity factor solution for a quarter-elliptical crack emanating from the corner of an open hole proposed by Hsu and Liu can be written as

$$K = \left[\sigma_o \sqrt{\pi a} \frac{M\left(\frac{a}{c}, \pi/2 - \beta\right)}{\phi(a/c)} \right] M_1\left(\frac{a}{c}, \beta\right) B\left(\frac{x}{r}\right) \quad \text{for } \frac{a}{c} \leq 1 \quad (1)$$

$$K = \left[\sigma_o \sqrt{\pi a} \sqrt{\frac{c}{a}} \frac{M\left(\frac{c}{a}, \beta\right)}{\phi(c/a)} \right] M_1\left(\frac{c}{a}, \beta\right) B\left(\frac{x}{r}\right) \quad \text{for } \frac{a}{c} > 1 \quad (2)$$

The quantity in square brackets is the exact stress intensity solution for an embedded elliptical crack. M_1 adjusts this expression to account for the front free surface of the plate, and B adjusts for the effect of the hole and hole surface.

To be more explicit, $B(x/r)$ is the Bowie hole correction factor for through-the-thickness cracks [4], evaluated at the normalized distance from the edge of the hole, x/r ; ϕ is the complete elliptical integral of the second kind presented in Fig. 3 as a function of the ratio of the minor and major axes of the ellipse; β is an elliptical angle measured from the hole wall; M is defined as

$$M = \left[\left(\frac{a}{c} \right)^2 \sin^2 \beta + \cos^2 \beta \right]^{1/4}, \quad \text{for } a/c \leq 1 \quad (3)$$

and

$$M = \left[\left(\frac{c}{a} \right)^2 \cos^2 \beta + \sin^2 \beta \right]^{1/4}, \quad \text{for } a/c > 1 \quad (4)$$

and M_1 is the front surface correction factor for a semi-elliptical surface crack in a half space, determined by interpolating between the known solutions for the following three cases: (1) $a/c = 0$, (2) $a/c = 1$, and (3) $a/c =$

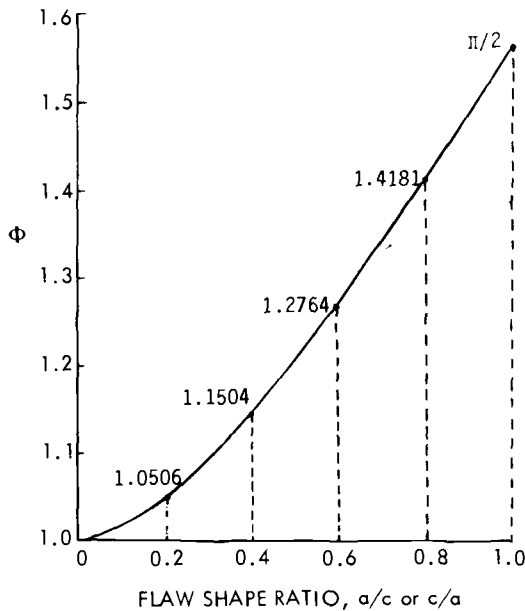


FIG. 3—Elliptical integral Φ .

∞ . For $a/c \cong 0$, the crack geometry is similar to that of an edge crack for which the front surface correction factor is 1.12. For $a/c \cong \infty$, the crack geometry is similar to that of a center crack for which M_1 is equal to 1.0. For $a/c = 1$, M_1 has been obtained numerically and presented as a function of an elliptical angle β by Smith et al [5]. Values of M_1 are presented in Fig. 4 in ten-degree (elliptical angle) increments from the hole wall to the plate surface for all possible a/c ratios.

Combining M and M_1 in Eqs 1 and 2, we obtain

$$K = \sigma_o \sqrt{\pi a} \cdot B\left(\frac{x}{r}\right) \cdot \frac{M_1'}{\phi} \left(\frac{a}{c}, \beta\right) \quad \text{for } a/c \leq 1 \tag{5}$$

and

$$K = \sigma_o \sqrt{\pi a} \sqrt{\frac{c}{a}} \cdot B\left(\frac{x}{r}\right) \cdot \frac{M_1'}{\phi} \left(\frac{c}{a}, \beta\right) \quad \text{for } a/c > 1 \tag{6}$$

The normalized M_1'/ϕ factor is plotted in Fig. 5 as a function of a/c for $a/c \leq 1$ and in Fig. 6 as a function of c/a for $a/c > 1$.

Equations 5 and 6, proposed by Hsu and Liu, are modified in the following manner. For a corner crack with a small c/r ratio, the entire crack surface is located in the region of elevated stress and the unflawed

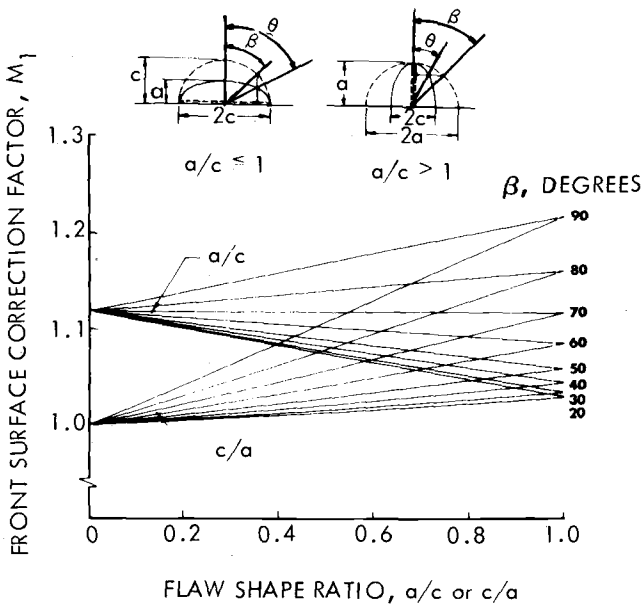


FIG. 4—Front surface correction factor M_1 .

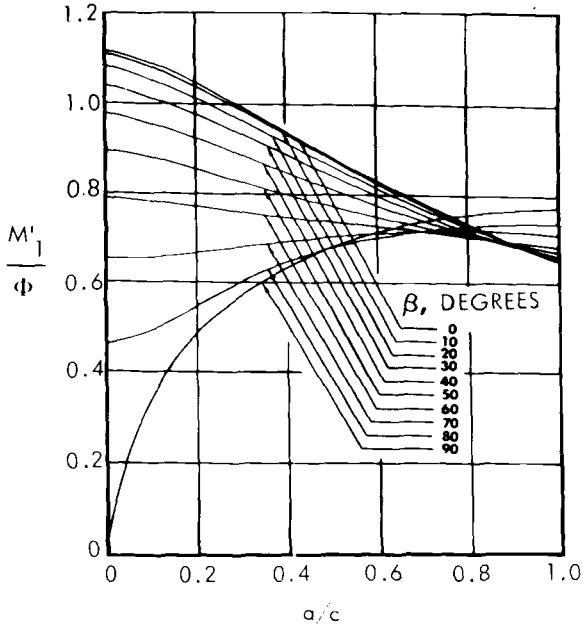


FIG. 5—Normalized factor M_1'/Φ ($a/c \leq 1$).

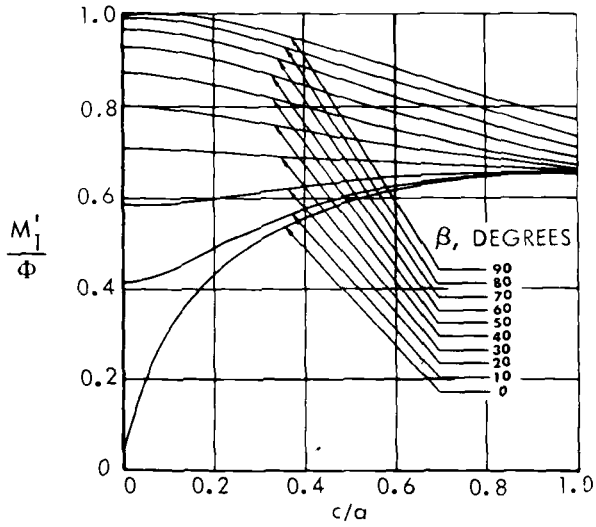


FIG. 6—Normalized factor M_1'/Φ ($a/c > 1$).

stress variation within the crack surface is small. For this case, Eqs 5 and 6 normally result in good estimates of the stress intensity factors. However, when the c/r ratio becomes large, the large crack surface extends into the region of lower stress. Because the stress intensity factors are sensitive to the local stress field in the vicinity of the crack, the actual stress intensity factor at the edge of the hole for this case is expected to be lower than the stress intensity factor computed from Eqs 5 and 6. To account for this effect, Eqs 5 and 6 are modified as follows

$$K = \sigma_o \sqrt{\pi a} \cdot B \left(\frac{x}{r} \right) \cdot \frac{M_1'}{\phi} \left(\frac{a}{c}, \beta \right) \cdot M_c \left(\frac{c}{r}, \frac{x}{c} \right) \quad \text{for } a/c \leq 1 \quad (7)$$

$$K = \sigma_o \sqrt{\pi a} \left(\frac{c}{a} \right)^{1/2} \cdot B \left(\frac{x}{r} \right) \cdot \frac{M_1'}{\phi} \left(\frac{c}{a}, \beta \right) \cdot M_c \left(\frac{c}{r}, \frac{x}{c} \right) \quad \text{for } a/c > 1 \quad (8)$$

where

$$M_c = F + \frac{x}{c} (1 - F) \quad (9)$$

in which the factor F , presented in Fig. 7 as a function of c/r , is obtained from the stress intensity factors estimated by Shah [6] at the edge of the hole and x is the distance from the hole wall to the particular point of interest on the crack periphery.

Equations 7 and 8 represent the stress intensity factor for a quarter-elliptical crack emanating from the corner of an open hole. The stress intensity factor for a quarter-elliptical crack emanating from the corner of a different type of fastener hole can be estimated from the stress intensity factor for a through-the-thickness crack emanating from the same type of

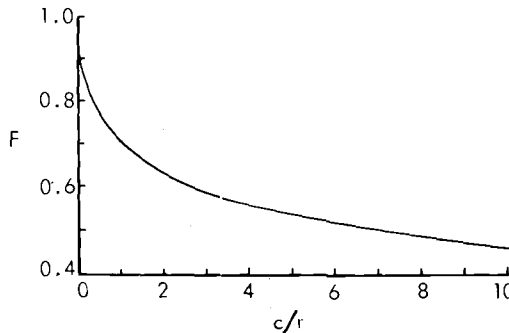


FIG. 7—Nondimensional factor F at the edge of a hole.

fastener hole. This can be accomplished by replacing the Bowie correction factor $B(x/r)$ for an open hole in Eqs 7 and 8 with the corresponding correction factor $B_T(x/r)$ for the type of hole considered. The procedure for calculating $B_T(x/r)$ for a through-the-thickness crack emanating from any type of fastener hole, using the Green's function approach, is presented in Ref 7.

Correlations with Other Approximate Solutions and Experimental Test Data

Normalized stress intensity factors ($K/\sigma\sqrt{\pi a}$) for a double corner crack emanating from an open hole were computed using Eqs 7 and 8 and are presented in Figs. 8 through 11 for a/c ratios of 0.75, 1.0, 1.5, and 2.0, respectively, as a function of the geometric angle θ defined in the sketch in Fig. 4. Solutions also were obtained from Eq 7 for an a/c ratio of 0.5 and are correlated in Fig. 12 with other approximate solutions proposed by Smith [8] and Shah [6]. Similarly, solutions for a single corner crack emanating from an open hole were obtained from Eq 7 for an a/c ratio of 1.0 and are correlated in Fig. 13 with other approximate solutions

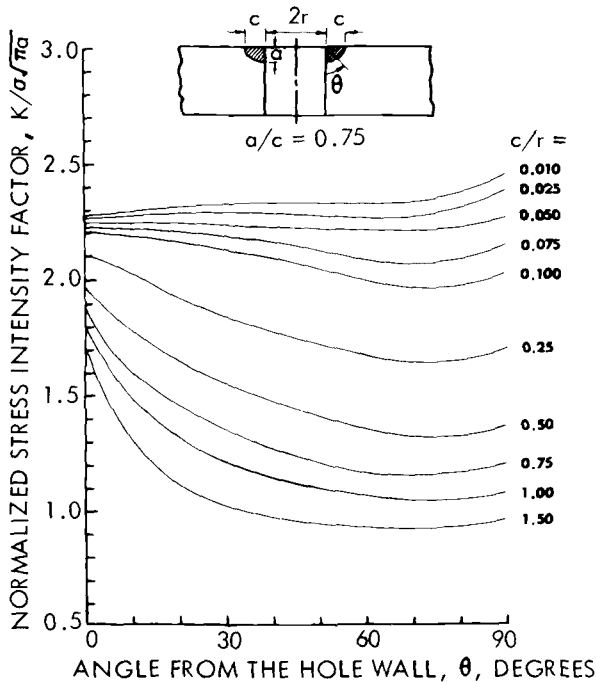


FIG. 8—Normalized stress intensity factors for double corner crack emanating from open hole ($a/c = 0.75$).

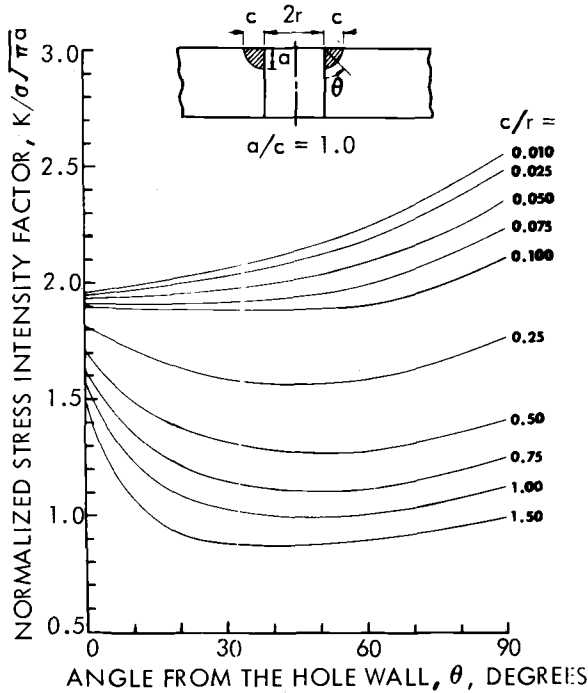


FIG. 9—Normalized stress intensity factors for double corner crack emanating from open hole ($a/c = 1.0$).

proposed by Kobayashi et al [9] and Shah [6]. The magnification factors presented in Fig. 13 were obtained by normalizing the stress intensity factors by dividing by K_{Ie}' (the stress intensity factor for an elliptical crack in an infinite body (see Eqs 1 and 2) subjected to a uniform tensile stress $3\sigma_o$).

Because there is no exact stress intensity factor solution for a quarter-elliptical corner crack emanating from an open hole with which to compare the current solution presented in Eqs 7 and 8, correlations also were made between predictions using the current solution and experimental test data. Two sets of test data were generated under carefully controlled laboratory conditions. The specimens were made of 7050-T73 aluminum plate with a thickness of 6.35 mm (0.25 in.), a width of 76.2 mm (3 in.), and a hole diameter of 6.60 mm (0.26 in.). An electrodischarge machine was used to introduce the initial notch at the corner of the hole (one crack only). Fatigue crack propagation tests then were conducted in 90 to 95 percent relative humidity room temperature air at a loading frequency of 10 cps. The specimens were subjected to constant amplitude loading with a maximum stress of 103.42 MPa (15 ksi) and a stress ratio of 0.1. Crack

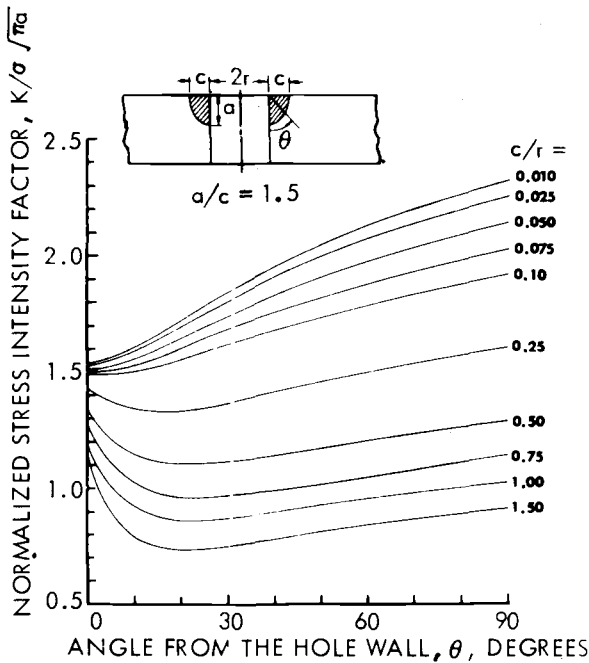


FIG. 10—Normalized stress intensity factors for double corner crack emanating from open hole ($a/c = 1.5$).

lengths (both a and c) were recorded using a macromechanic device. During the test, “marker” loads were applied occasionally to produce bench marks on the fracture surfaces. These bench marks provided a record of the actual shape of the crack during crack propagation and also served to verify the visual crack length measurements made during the test. The maximum stress level for the “marker” load cycles was also 103.42 MPa (15 ksi), but the stress ratio was increased to 0.85. Photographs showing the elox cut and the bench marks resulting from application of the “marker” loads on the crack surface of each specimen are presented in Fig. 14. Figure 15 shows the actual flaw shape on the fracture surface of one of the specimens resulting from the application of the “marker” loads and the result of fitting a quarter-elliptical curve through two readings observed on the surfaces: a and c . The figure indicates the accuracy of assuming that the corner crack is quarter-elliptical in shape.

Correlations of analytical predictions using the current solution and the test data for the two previously mentioned specimens are presented in Figs. 16 and 17. The figures present the number of cycles versus crack length for both the front surface and the hole wall. It was assumed in the predictions that for a given number of applied load cycles, the extension of the

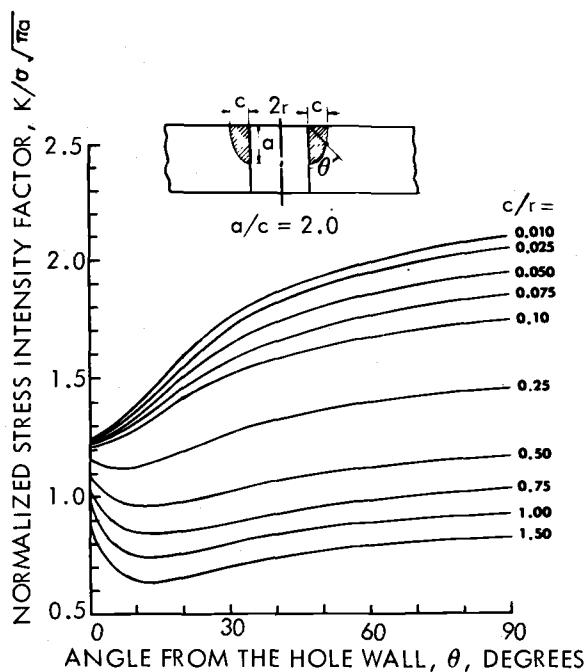


FIG. 11—Normalized stress intensity factors for double corner crack emanating from open hole ($a/c = 2.0$).

quarter-elliptical crack border was controlled by the stress intensity factors at the intersections of the crack periphery and both the hole wall and plate surface (that is, K_A and K_C). In general, the stress intensity factors at these two locations were different, resulting in different crack growth rates. Therefore, the new flaw shape aspect ratio after each crack growth increment differed from the previous one. The new flaw shape aspect ratio was computed using the new crack lengths at both the hole wall and plate surface. The process was repeated until the crack length along the hole wall was equal to the plate thickness. At that time, the crack was assumed to be a through-the-thickness crack with length c . This assumption was made based upon the experimental observation that after the crack penetrates the back surface and the cyclic load application continues, the back surface crack length increases much faster than that of the front surface until the front of the through-the-thickness crack becomes stable. Figures 16 and 17 indicate that good correlations were obtained between the analytical predictions and the experimental test data.

Correlations of analytical predictions using the current solution and experimental test data generated by Snow [10] are presented in Fig. 18. The correlations involve corner cracks emanating from open holes in

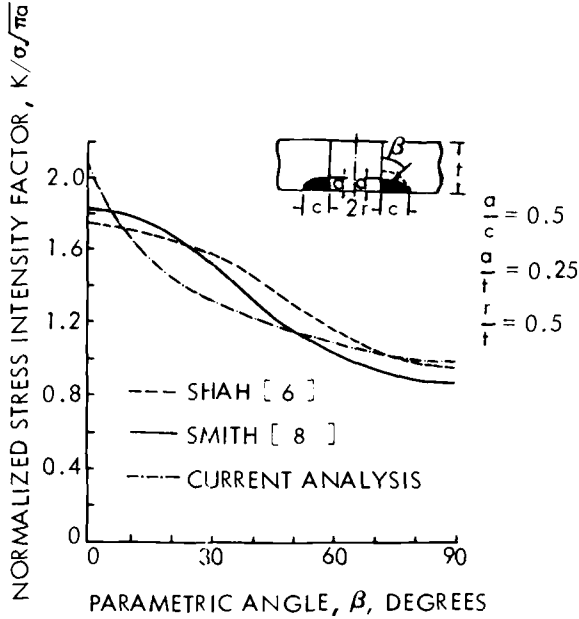


FIG. 12—Correlations of normalized stress intensity factors for double corner crack emanating from open hole ($a/c = 0.5$).

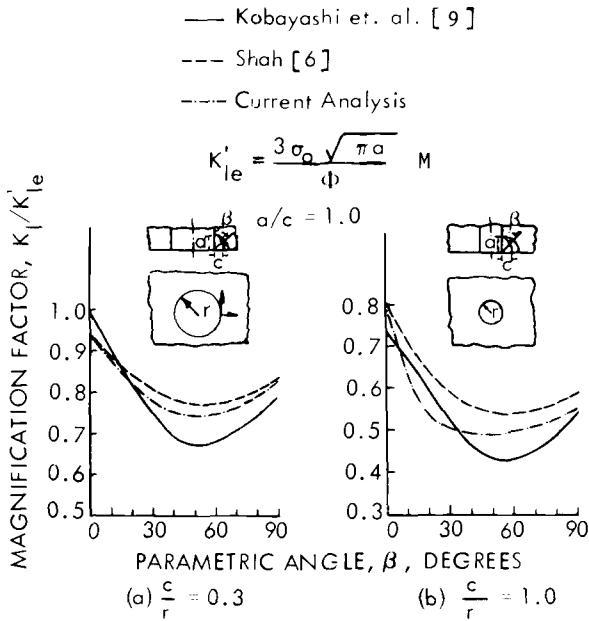
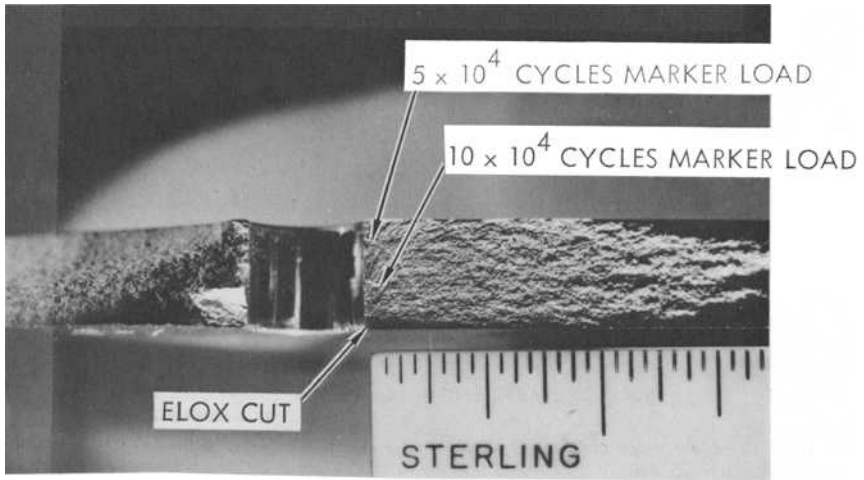
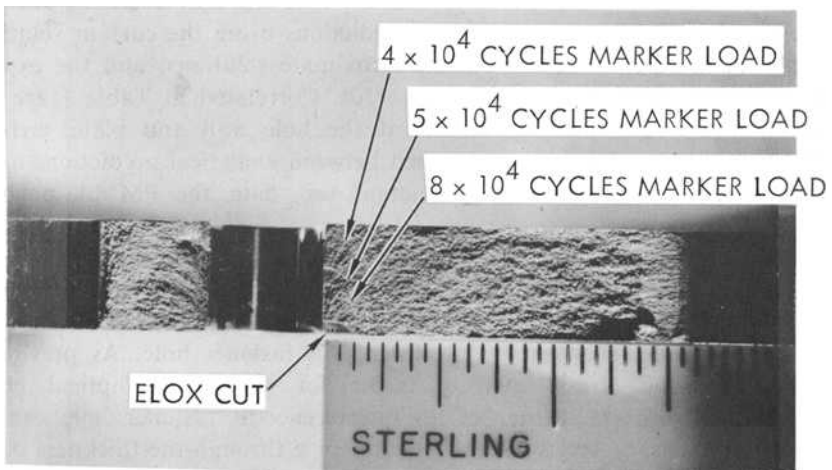


FIG. 13—Correlations of magnification factors for single corner crack emanating from open hole ($a/c = 1.0$).



(a). TEST SPECIMEN NO. 1



(b). TEST SPECIMEN NO. 2

FIG. 14—Fracture surfaces for single corner crack emanating from open hole.

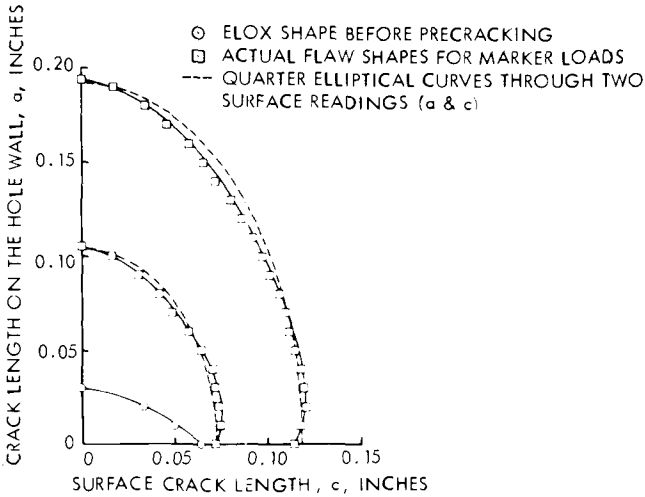


FIG. 15—Flaw shape change for single corner crack emanating from open hole (specimen No. 1) (1 in. = 25.4 mm).

polymethyl methacrylate (PMMA) polymer plates subjected to constant amplitude loading. Figure 18 presents the number of cycles versus crack length for both the front surface and the hole wall. Correlations are also presented in Table 1 for analytical predictions using the current solution, analytical predictions using other approximate solutions, and the experimental test data generated by Snow [10]. Correlated in Table 1 are the normalized stress intensity factors at the hole wall and plate surface. Again, good correlations are obtained between analytical predictions using the current solution and experimental test data for PMMA polymer material.

Correlations have been presented for quarter-elliptical corner cracks emanating from open holes. Let us now consider the stress intensity factor for a quarter-elliptical crack emanating from the corner of a different type of fastener hole, such as an interference-fit fastener hole. As previously mentioned, the stress intensity factor for a quarter-elliptical crack emanating from the corner of an interference-fit fastener hole can be estimated from the stress intensity factor for a through-the-thickness crack emanating from the same type of fastener hole. This can be accomplished by replacing the Bowie correction factor $B(x/r)$ for an open hole in Eqs 7 and 8 with the corresponding correction factor $B_{IF}(x/r)$ for an interference-fit fastener hole. Typical $B_{IF}(x/r)$ factors are presented in Fig. 19 for 2219-T851 aluminum. These factors were obtained from computed stress intensity factors [13] for three different levels of interference: $\delta = 0.0610, 0.0965, 0.1524$ mm ($\delta = 0.0024, 0.0038, 0.0060$ in.). The factors are

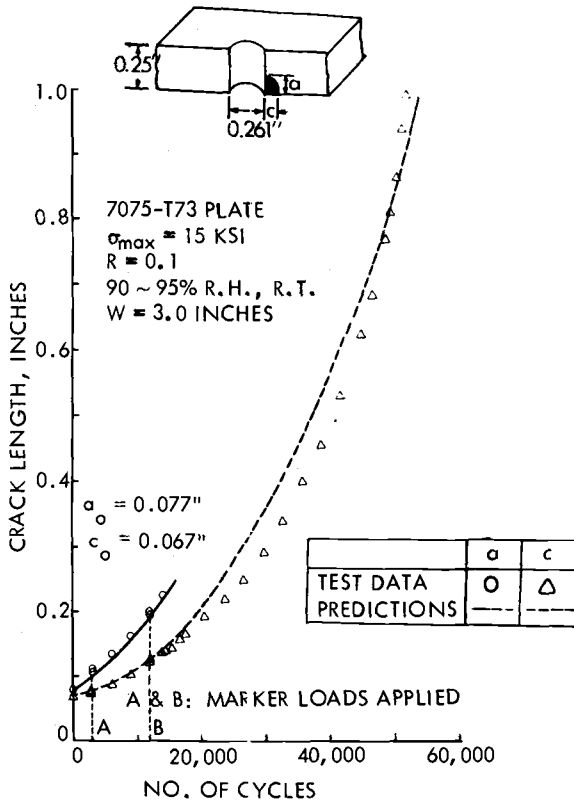


FIG. 16—Correlation for single corner crack emanating from open hole (specimen No. 1) (1 in. = 25.4 mm, 1 ksi = 0.145 MPa).

presented for both loading ($\sigma_o = 124.10 \text{ MPa}$ (18 ksi) far-field loading) and unloading ($\sigma_o = 0 \text{ MPa}$) conditions. The $B_{IF}(x/r)$ factors were substituted for the $B(x/r)$ factors in Eqs 7 and 8 in order to obtain the normalized stress intensity factors at the intersection of the plate surface and the border of a single corner crack presented in Fig. 20 for the three levels of interference and a flaw aspect ratio of 0.75.

Unlike an open hole problem, the stress intensity factor for a crack emanating from an interference-fit fastener hole is not linearly proportional to the far-field applied load. It also depends upon the level of interference, material yield strength, Young's modulus, and Poisson's ratio. For the purpose of verifying the current analytical solution, a crack emanating from an interference-fit fastener hole in a plate subjected to constant amplitude far-field fatigue loading was treated as a crack emanating from a fastener hole having no residual stresses and subjected to variable amplitude loading. The variable amplitude loading was selected to produce

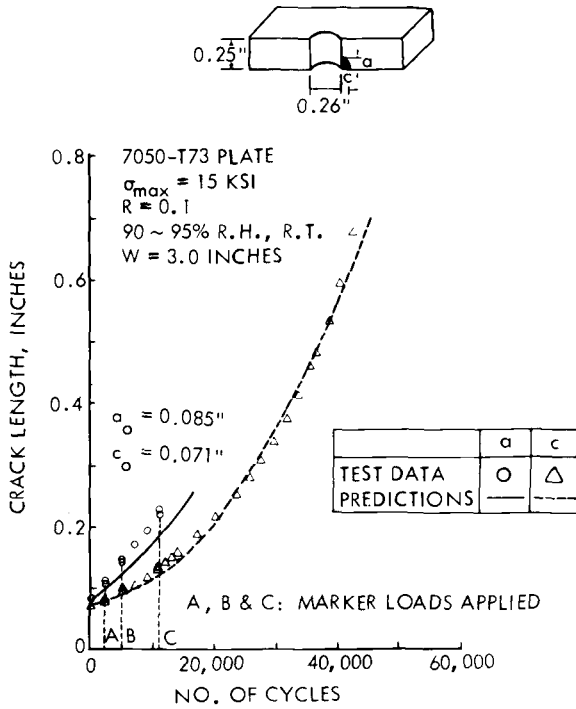


FIG. 17—Correlation for single corner crack emanating from open hole (specimen No. 2) (1 in. = 25.4 mm, 1 ksi = 0.145 MPa).

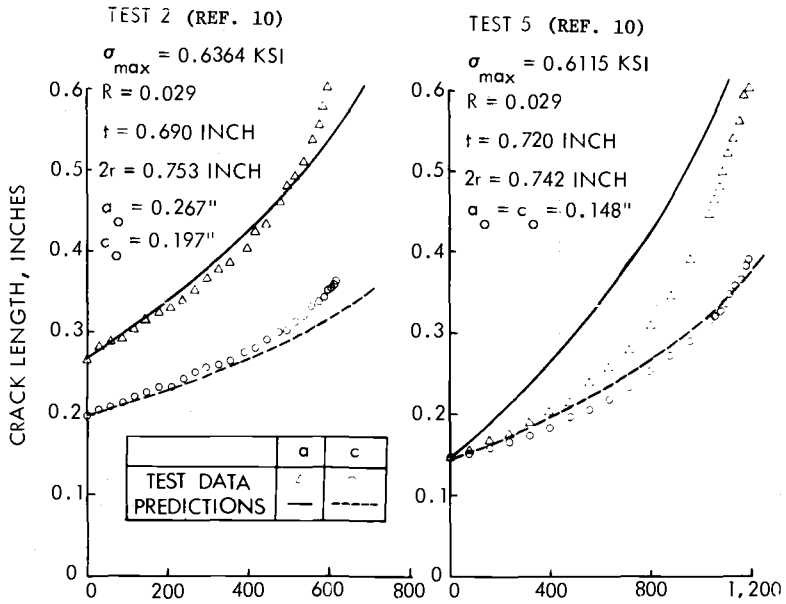


FIG. 18—Correlations for corner cracks emanating from open holes on PMMA polymer plates (1 in. = 25.4 mm, 1 ksi = 0.145 MPa).

TABLE 1—Correlations of normalized stress intensity factors for corner cracks emanating from open holes in PMMA polymer plates.

SIF at Hole Wall, $K_A/\sigma_0\sqrt{\pi a}$									
a/t^a	c/r^b	Snow Data [10]	Gran [2]	Hsu/Liu [3]	Hall/Finger [11]	Shah [6]	Fujimoto [12]	Current	
0.3	0.42	1.39 ^c	2.60	1.79	1.22	1.38	1.65 ^c	1.40	
0.4	0.56	1.31	2.69	1.79	1.17	1.32	1.54	1.36	
0.5	0.69	1.25	2.82	1.79	1.09	1.27	1.40	1.33	
0.6	0.83	1.22	3.01	1.79	1.03	1.25	1.30	1.30	
0.7	0.97	1.19	3.33	1.79	0.98	1.21	1.20	1.26	
0.8	1.11	1.23	3.90	1.79	0.94	1.08	1.15	1.25	
SIF at Plate Surface, $K_C/\sigma_0\sqrt{\pi c}$									
0.3	0.42	1.58	1.34	1.57	1.44	1.52	1.56	1.58	
0.4	0.56	1.46	1.21	1.44	1.38	1.41	1.45	1.45	
0.5	0.69	1.41	1.13	1.32	1.29	1.26	1.38	1.35	
0.6	0.83	1.35	1.06	1.24	1.22	1.18	1.35	1.25	
0.7	0.97	1.36	1.02	1.18	1.16	1.08	1.33	1.19	
0.8	1.11	1.36	0.99	1.14	1.11	1.08	1.33	1.14	

^a $t = 18.29$ (0.72 in.).

^b $r = 9.40$ mm (0.37 in.).

^cFactor $(c/a)^{1/2}$ was omitted in Refs 10 and 12, numbers have been corrected.

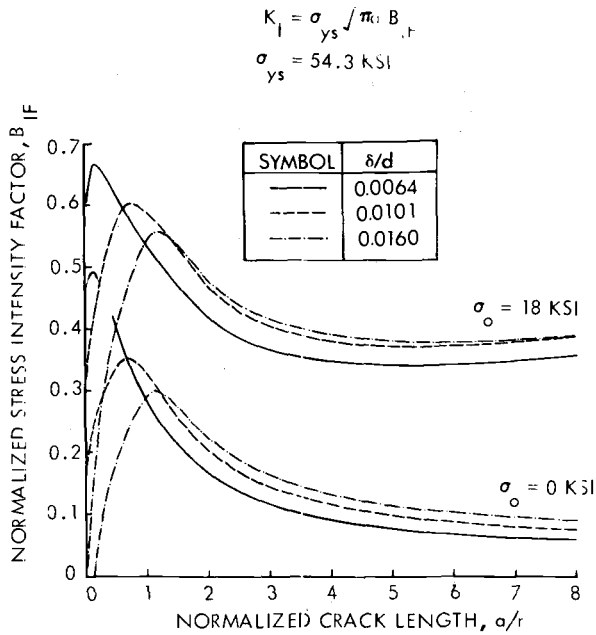


FIG. 19—Normalized stress intensity factors for single through-the-thickness crack emanating from interference-fit fastener hole (loading and unloading) (1 ksi = 0.145 MPa).

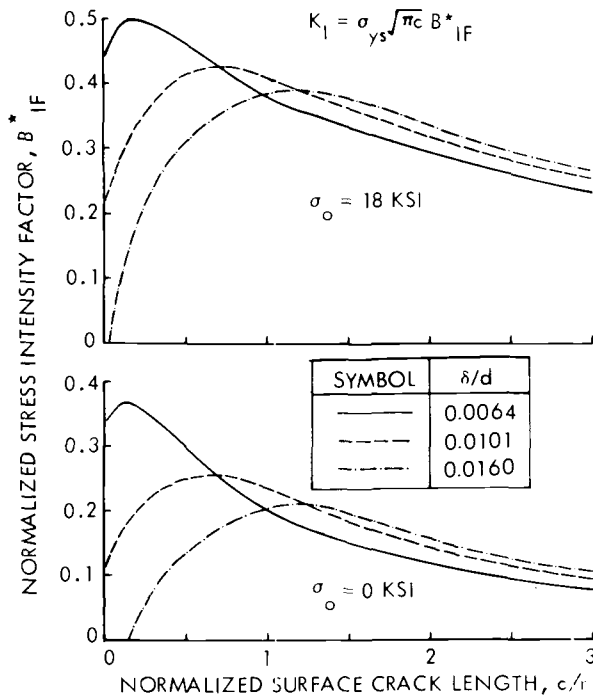


FIG. 20—Normalized stress intensity factors for single corner crack $a/c = 0.75$ emanating from interference-fit fastener hole (loading and unloading) (1 ksi = 0.145 MPa).

the same stress intensity factor ranges and ratios (that is, $K_{max} - K_{min}$ and K_{min}/K_{max}) as those for the constant amplitude loading for the interference-fit fastener hole with residual stresses. Figure 21 presents a correlation of the predicted crack growth history, surface crack length versus number of cycles, and experimental test data for a single corner crack emanating from an interference-fit fastener hole. Three levels of interference were considered (0.0610, 0.0965, and 0.1524 mm) for 2219-T851 aluminum

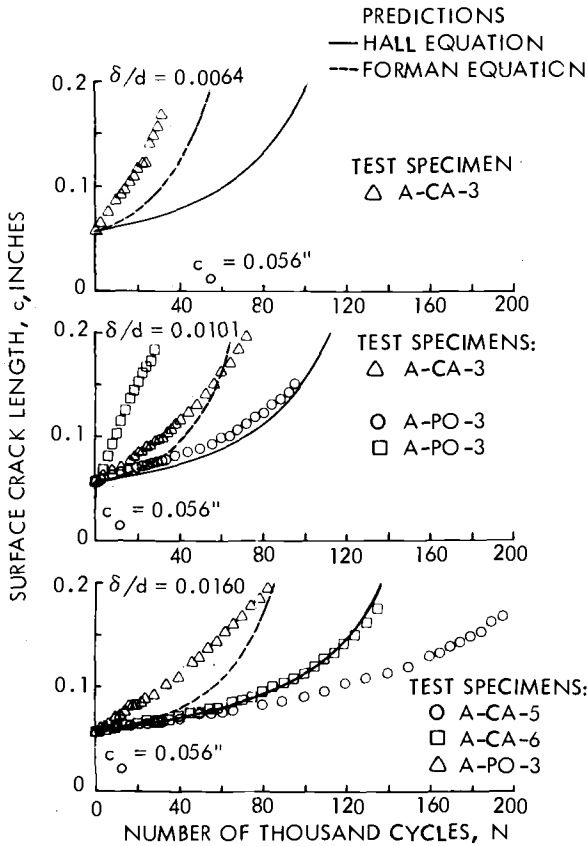


FIG. 21—Correlations for single corner crack emanating from interference-fit fastener holes ($\sigma_0 = 18$ ksi) (1 in. = 25.4 mm, 1 ksi = 0.145 MPa).

plates subjected to a constant amplitude far-field loading of 124.10 MPa and a stress ratio of 0.1. Both Forman's [14] and Hall's [15] crack growth rate equations were used in the predictions. As seen from Fig. 21, the experimental data scatter was up to a factor of four in the tests of cracks emanating from interference-fit fastener holes, and the magnitude of the errors in the predictions is similar.

References

- [1] "Airplane Damage Tolerance Requirements," MIL-A-83444, Air Force Aeronautical Systems Division, July 1974.
- [2] Gran, R. J., Orazio, F. D., Paris, P. C., Irwin, G. R., and Hertzberg, R., "Investigation and Analysis Development of Early Life Aircraft Structural Failures," AFFDL-TR-70-149, Air Force Flight Dynamics Laboratory, March 1971.
- [3] Hsu, T. M. and Liu, A. F., "Stress Intensity Factors for Truncated Elliptical Cracks," presented at the 7th National Symposium on Fracture Mechanics, College Park, Md., 27-29 Aug. 1973.
- [4] Bowie, O. L., *Journal of Mathematics and Physics*. Vol. 35, 1956, pp. 60-71.
- [5] Smith, F. W., Emery, A. F., and Kobayashi, A. S., *Journal of Applied Mechanics*. Dec. 1967, pp. 953-959.
- [6] Shah, R. C. in *Mechanics of Crack Growth, ASTM STP 590*, American Society for Testing and Materials, 1976.
- [7] Hsu, T. M. and Rudd, J. L., *Proceedings*. 4th International Conference on Fracture, Vol. 3, 19-24, June 1977, pp. 139-148.
- [8] Smith, F. W. and Kullgren, T. E., "Theoretical and Experimental Analysis of Surface Cracks Emanating from Fastener Holes," AFFDL-TR-76-104, Air Force Flight Dynamics Laboratory, Feb. 1977.
- [9] Kobayashi, A. S., Polvanich, N., Emery, A. F., and Love, W. J., "Corner Crack at the Bore of a Rotating Disk," Paper No. 75-WA/GT-18, American Society of Mechanical Engineers.
- [10] Snow, J. R., "A Stress Intensity Factor Calibration for Corner Flaws at an Open Hole," AFML-TR-74-282, Air Force Materials Laboratory, May 1975.
- [11] Hall, L. R. and Finger, R. W., "Fracture and Fatigue Growth of Partially Embedded Flaws," *Proceedings*, Air Force Conference on Fatigue and Fracture of Aircraft Structures and Materials, AFFDL-TR-70-144, Sept. 1970.
- [12] Fujimoto, W. T., "Determination of Crack Growth and Fracture Toughness Parameters for Surface Flaws Emanating from Fastener Holes," *Proceedings*, AIAA/ASME/SAE 17th Structures, Structural Dynamics and Materials Conference, King of Prussia, Pa., 5-7 May 1976.
- [13] Rudd, J. L., Hsu, T. M., and Aberson, J. A., "Analysis and Correlation of Crack Growth from Interference-Fit Fastener Holes," presented at the International Conference on Numerical Methods in Fracture Mechanics, Swansea, United Kingdom, 9-13 Jan. 1978.
- [14] Forman, R. G., Kearney, V. E., and Engle, R. M., *Journal of Basic Engineering*, Sept. 1967, pp. 459-464.
- [15] Hall, L. R., Shah, R. C., and Engstrom, W. L., "Fracture and Fatigue Crack Growth Behavior of Surface Flaws and Flaws Originating at Fastener Holes," AFFDL-TR-74-47, Air Force Flight Dynamics Laboratory, May 1974.

Surface Crack K -Estimates and Fatigue Life Calculations in Cannon Tubes

REFERENCE: Underwood, J. H. and Throop, J. F., "Surface Crack K -Estimates and Fatigue Life Calculations in Cannon Tubes," *Part-Through Crack Fatigue Life Prediction, ASTM STP 687*, J. B. Chang, Ed., American Society for Testing and Materials, 1979, pp. 195-210.

ABSTRACT: K solutions for internal surface cracks in pressurized cylinders are compared, including Smith's photoelastic results, Hussain's collocation and compliance results, and Underwood's estimates. Fatigue crack growth observations from cannon tubes are described, particularly in relation to surface crack growth and multiple cracks.

A method is proposed for describing quantitatively the effect of residual stress on K in cylinders with shallow cracks. The combination of compressive residual stress with applied stress reduces ΔK and thus increases fatigue life.

KEY WORDS: fracture mechanics, surface crack, fatigue life, residual stress, pressurized cylinder, crack propagation, fatigue (material)

The growth of cracks in cannon tubes is similar in most respects to crack growth in other pressure vessels. Aside from the initiation of cracks due to high bore-surface temperatures during firing, the growth of cracks in cannon tubes is the classic combination of fatigue propagation followed by fast fracture, both of which can be well described using fracture mechanics. As in most other structural components the fatigue cracks take on the shape of a part-through or surface crack. So this shape must bear the emphasis in any attempt to characterize the crack growth.

The results of fracture tests and analyses related to surface crack growth in cannon tubes will be described here in three sections. First, a description will be given of some predominant types of crack growth which are observed in cannon tube firing and simulation tests. Second, stress inten-

¹Materials engineer and mechanical engineer, respectively, U.S. Army Armament Research and Development Command, Benet Weapons Laboratory, LCWSL, Watervliet, N.Y. 12189.

sity factor, K_I , solutions and estimates which apply to surface cracks in cannon tubes will be described. Using this information, fatigue crack growth and life estimates will be compared with the results from laboratory tests of cannon tube sections containing surface cracks of prescribed starting size and shape. Third, the effect of residual stress on fatigue crack growth will be considered. A method of analysis will be proposed which gives a quantitative description of the effect of residual stress on K_I and in turn on the fatigue crack propagation rate for shallow cracks in specimens under load.

Crack Growth in Cannon

Initiation, Growth, Failure

A macrophotograph of a fracture surface can reveal many of the basic features of fatigue crack growth in a cannon tube. Figure 1 shows the fracture surface of a portion of a tube which has been fired and then subjected to further simulated firing in the laboratory. A few details of the tube material and dimensions are: a 4335 steel forging with yield stress in the range of 1200 MPa; inner radius of 60 mm, outer radius of 130 mm, and hence a diameter ratio of 2.17. The wall thickness shown in the photograph is then 70 mm. This information is useful mainly as background data, because the general features of crack growth in a cannon tube are not very sensi-

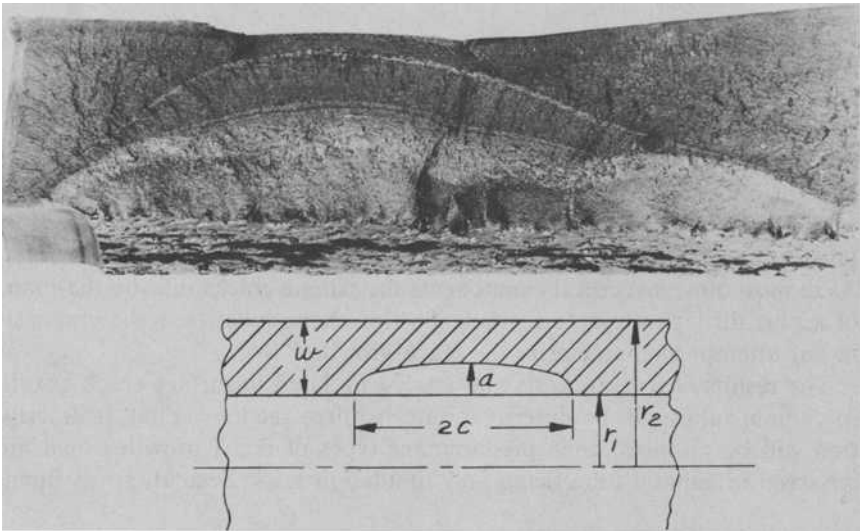


FIG. 1—Fracture surface of cannon tube and sketch of geometry.

tive to the material and dimensions. A sketch is shown in Fig. 1 showing some of the symbols used here.

The section of the tube inner surface, shown at the bottom of the photograph in Fig. 1, shows a severely eroded surface caused by the high surface temperature during firing. Not visible at the magnification of the photo is a network of thermally induced cracks, referred to as heat-checks, which also occurs on the inner surface. Erosion and heat-checking typically combine to produce cracks 0.2 to 1.0 mm deep in cannon tubes in a few tens of firings. So classic fatigue crack initiation is precluded, and a fatigue crack must be assumed present from essentially the first firing cycle. Of course this assumption reduces life estimates, but it simplifies life prediction.

After enough firing cycles to ensure crack initiation, the tube was pressure-cycled in the laboratory using the same pressure as in firing. It is not necessary to simulate the pressure rise-time of firing, about 5 ms, because no loading rate effect is observed for this combination of material and loading rate. The type of fatigue crack growth observed here in Fig. 1 is typical of cannon. The crack starts in the approximate shape of a semi-ellipse with a small aspect ratio, $a/2c$, where a is the depth into the tube wall and is half the minor axis while $2c$ is the length along the tube axis and is the major axis. The $a/2c$ ratio of the crack increases as the crack deepens, as seen by the shadings and marks on the fracture surface caused by interruptions in the test. The crack grows much more rapidly for depths beyond mid-wall, and as the crack approaches the outer surface the crack growth per cycle is often so large that it is later visible on the fracture surface with the unaided eye. Three such crack growth steps can be seen in Fig. 1, the last of which caused the final breakthrough to the outer surface.

The final failure of this example tube is also typical of cannon. The failure is controlled primarily by the fracture toughness, K_{Ic} , of the tube material. The larger the K_{Ic} , then, the deeper is the fatigue crack from which the abrupt breakthrough to the outer surface occurs, and the smaller is the length of the breakthrough. This is the preferred fracture mode, a leak-before-break, in which the final break is small and the tube merely leaks a small amount of the pressurized fluid. A high value of K_{Ic} has the equally important effect of delaying or entirely preventing the rapid, unstable fatigue crack growth as the crack approaches the outer surface. For high enough values of K_{Ic} the relatively slow stable fatigue crack growth, typical of da/dN proportional to ΔK^n relationship, can be observed all the way to the outer radius. This can extend somewhat the fatigue life of a tube. But more important it can eliminate the possibility of an abrupt breakthrough which, in the worst case, can lead to a crack running along the length of the tube.

Multiple Cracks

One of the features of interest in the crack growth behavior of cannon tubes is multiple cracking which can occur in some circumstances. Figure 2 shows an array of cracks in a cross section of a cannon tube. The material, geometry, and test procedure for this tube were similar to that of the tube just discussed. An important difference here, in relation to multiple cracks, is that rifling lands and grooves are present in this tube. Cracks initiate at the corner of the lands, with the driving side preferred. The driving side of the land is that which imparts the force which rotates the projectile as it travels down the tube. The result is a uniformly spaced array of cracks of roughly equal depth, with one major crack for each of the lands. For cracks as in Fig. 2, whose depth is about equal to the spacing between cracks, it seems reasonable to expect that they interfere with each other and cause some sort of load-shedding and a decrease in K_I as compared to that for a single crack. Goldthorpe [1]² has described an approximate K_I analysis for a tube with 40 uniformly spaced uniform depth cracks which shows a significantly lower K_I value than that for a single crack of the same depth. Current work by Pu and Hussain [2] gives finite element calculations of K_I for several different arrays of cracks of uniform spacing and depth. These results also show a decreased K_I for multiple cracks compared to that of a single crack, except for the cases of two and three cracks which result in a higher K_I than that of a single crack. Pu and Hussain's result for 40 cracks with depth of 0.25 of the wall thickness in a cylinder with diameter ratio of 2.0 is a K_I value which is about 37

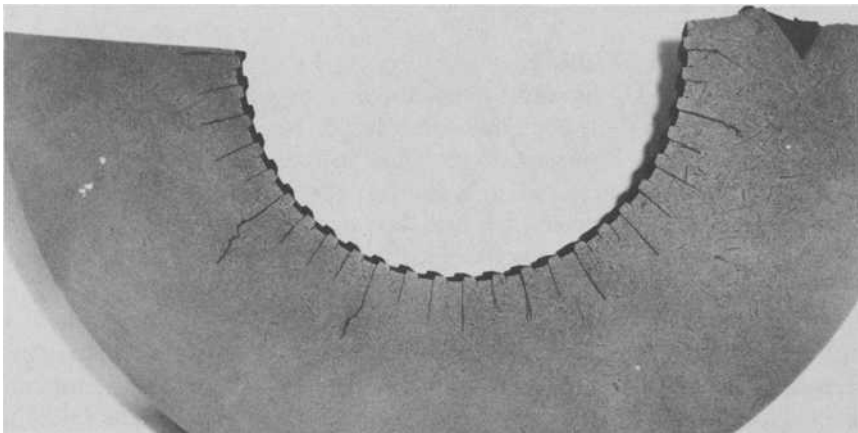


FIG. 2—Cross section of cannon tube showing multiple cracks.

²The italic numbers in brackets refer to the list of references appended to this paper.

percent of the K_I for the single crack, other conditions being the same. For a crack rate, da/dN , proportional to the cube power of ΔK_I this reduced value of K_I produces a da/dN value of only 5 percent of that for a single crack. So it is clear that when multiple cracks do occur in pressurized cylinders, their effect must be included for an accurate description of the fatigue crack growth and life behavior. The multiple-crack K_I solutions currently available are for straight-fronted cracks. These solutions can be applied directly only to relatively shallow cracks in cannon tubes when the $a/2c$ values are small. Fortunately this is the condition in which most of the cyclic life of cannon tubes is expended.

K_I and Life Determinations

The most important geometric factor to be considered in the description of fatigue crack growth and fatigue life of cannon tubes and many other structural components is the semi-elliptical shape which is characteristic of surface cracks. Other effects, such as those due to multiple cracks and the effect of residual stress are certainly important, but obviously only when conditions prevail which produce these effects. Surface cracks, however, nearly always prevail. An important question to be addressed here is: What is a good estimate of K_I for a surface crack in a pressurized thick-wall cylinder?

K_I for Surface Cracks

Underwood [3] made an estimate for K_I at the point of deepest penetration of a surface crack in a pressurized cylinder. The estimate was a combination of the Bowie and Freese [4] solution for a straight-fronted crack in a pressurized cylinder and solutions for straight and surface cracks in a tension loaded plate. More recently Smith et al [5] reported photo-elastic stress freezing evaluations of relatively long and shallow surface cracks in a pressurized cylinder. K_I results have been reported for near semicircular surface cracks by Hussain et al [6] using two quite independent methods, one based on experimental compliance measurements in a cylinder with an $a/2c = 0.50$, the other a three-dimensional collocation method using a simulation of a cylinder geometry with an $a/2c = 0.65$ crack.

The three independent sets of K_I calculations are shown in Fig. 3 along with the estimate of K_I for two values of $a/2c$ and with the Bowie and Freese solution for a straight crack, which corresponds to $a/2c = 0$. In general the Underwood estimate [3] of K_I is a good representation of the calculations of K_I from the three different evaluations. The agreement is the poorest as a/W approaches 0.5, and this is the area in which the accuracy of both the K_I estimate and the three evaluations would be expected

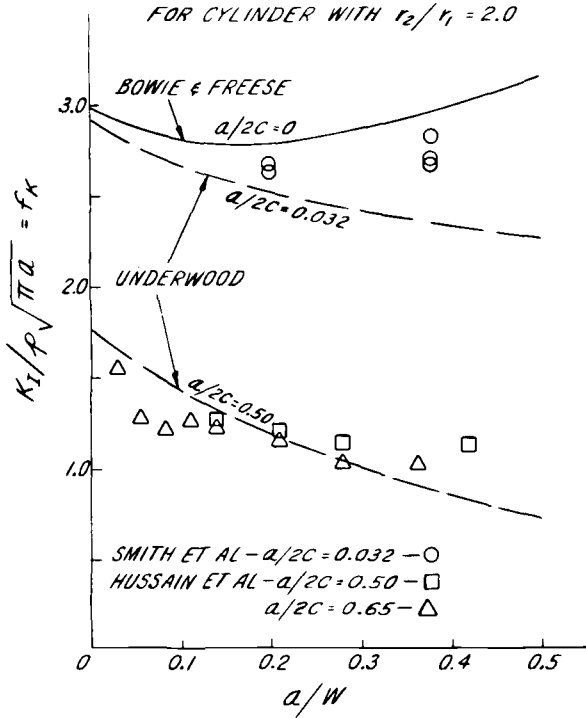


FIG. 3—Calculations and estimate of K_I for surface cracked cylinder.

to be poorest. As mentioned earlier, most of the fatigue life of a cannon tube is expended by the time $a/W = 0.5$, so inaccuracies in K_I at and beyond this point would have little effect on fatigue life calculations.

Another estimate of K_I for a pressurized cylinder with a surface crack has been made by Kobayashi et al [7]. It covers a range of r_2/r_1 up to 1.5, which does not include the applications of primary interest in cannon, (those for r_2/r_1 near 2.0), but does have other application. A comparison of the Kobayashi estimate with that from Ref 3 is shown in Fig. 4. The estimate by Kobayashi and coworkers is higher than that of Underwood, particularly for large a/W . This might indicate that for large a/W the estimate of Kobayashi et al is closer to the true K_I , based on the data shown in Fig. 3. However, it should be noted that the Kobayashi estimate is evidently too high for small a/W . This is indicated by the fact that at $a/W = 0$ it predicts a higher K_I for $a/2c = 0.1$ than does the accurate, upper bound, Bowie and Freese solution for $a/2c = 0$.

Putting aside the accuracy considerations of K_I for surface cracks, all the results discussed here show that crack shape effects can produce a K_I value of less than one half that for straight-fronted cracks. So the fatigue

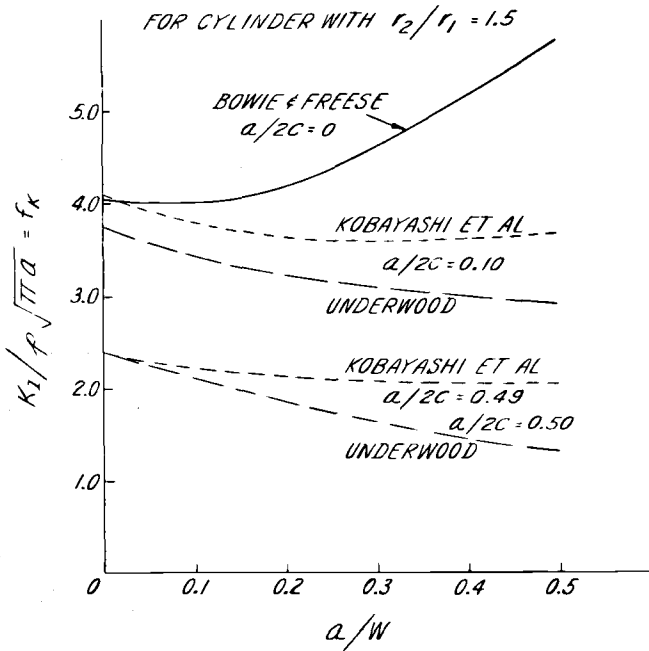


FIG. 4—Two estimates of K_I for surface cracked cylinder.

crack propagation rate for surface cracks can be expected to be in the order of one tenth of that for straight-fronted cracks.

Fatigue Crack Growth Tests

A series of tests is under way at our laboratory to directly measure the growth of surface cracks of known shape in full-size cannon tubes under cyclic loading. One phase of the tests which is completed will be described here. Figure 5 shows the fracture surface of one of the four specimens which make up this phase of the tests. The specimens were 760 mm long sections of cannon tubes with outer radius of 181 mm and inner radius of 90 mm. The material is the same as described earlier in relation to Fig. 1. Notches were electric-discharge-machined into the inner surface of each specimen to a depth of 6.35 mm and with lengths which varied from 12.7 to 510 mm. So the starting values of $a/2c$ are known, as listed in Table 1. The specimens were cycled to failure using a maximum pressure of 330 MPa and a minimum pressure near zero. During the tests measurements of crack depth and length were obtained by use of ultrasonics. They were confirmed by subsequent measurements on the fracture surfaces.

The crack growth measurements plotted in Fig. 6 clearly show the signi-

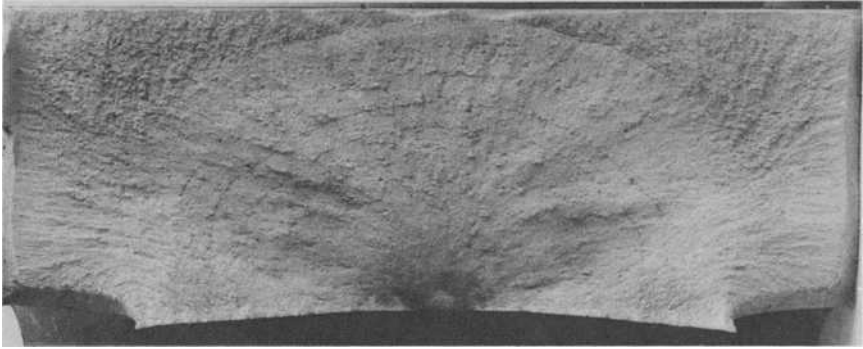


FIG. 5—Fracture surface of cannon tube specimen No. 3A.

ficant effect of crack shape on growth rate and cyclic life. Referring to Table 1, even though $a/2c$ increased considerably for the specimens having low starting $a/2c$ values, there was still a factor of seven difference between the cyclic life of the specimen having $(a/2c)_o = 0.5$ and the average life of the two specimens having $(a/2c)_o = 0.012$. Had $a/2c$ somehow remained fixed at the starting value for all specimens this difference would have been ever larger.

Analytical Description

The significant effect of crack shape on life observed in the tests can be well described by fracture mechanics analysis. By starting with the expression which has been found to be a good representation of the fatigue crack propagation rate in compact and C-shaped specimens of gun steel

$$da/dN = 6.52 \times 10^{-12} \Delta K^3 \quad (1)$$

and integrating, the following general expression for cyclic life is obtained

$$N_f = \frac{2 \left[\frac{1}{\sqrt{a_i}} - \frac{1}{\sqrt{a_f}} \right]}{6.52 \times 10^{-12} [f_K p \sqrt{\pi}]^3} \quad (2)$$

where

$$\begin{aligned} a_i &= \text{initial crack depth,} \\ a_f &= \text{final crack depth,} \\ p &= \text{pressure in the cylinder, and} \\ f_K &= K_I/p\sqrt{\pi a} = \text{dimensionless } K_I \text{ parameter used here.} \end{aligned}$$

Note that the constant in Eqs 1 and 2 is appropriate for da/dN in m/cycle, K in MPa $\sqrt{\text{m}}$ and p in MPa.

TABLE 1—Surface crack test and analysis data; $W = 90.7 \text{ mm}$; $r_2/r_1 = 2.0$.

Specimen Number	Machined Notch	Measured $a/2c$ Ratio		$f_K = K_I/p\sqrt{\pi a}$			Measured Cycles to Failure	Measured a_f , mm
		At $a/W = 0.25$	At Fracture	K-Estimate; for $a/2c$ at $a/W = 0.25$	Selected for Curves in Fig. 6			
1	0.50	0.50	0.48	1.1	1.10	10 600	90.7	
2	0.062	0.22	0.39	1.6	1.60	3 430	90.7	
3A	0.012	0.05	0.08	2.3	1.96	1 500	38.1	
3B	0.012	0.05	0.11	2.3	1.96	1 600	57.2	

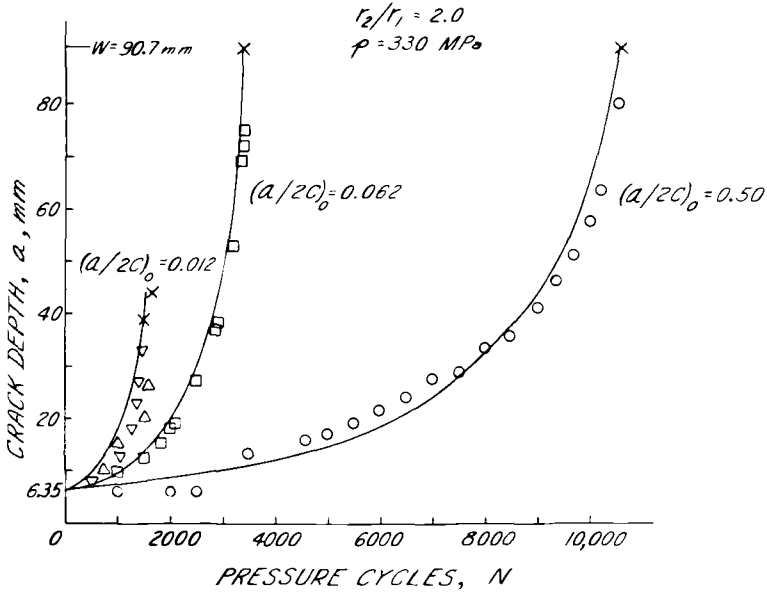


FIG. 6—Crack growth in cannon tube specimens.

Equation 2 was used to calculate the curves in Fig. 6. The values of a_i , a_f , and p were determined from the test conditions. The use of the starting notch depth for a_i in effect requires the assumption that the fatigue crack starts immediately from the notch. This is believed to be a reasonable assumption because the electrical-discharge-machining process produces a relatively sharp notch which in addition has microcracks at its tip. Values of f_K used in Eq 2 were selected so that the curves in Fig. 6 would fit the data. These selected values of f_K are compared in Table 1 with f_K values from the K estimate [3] summarized in Fig. 7. The f_K values from the K estimate are those for the particular $a/2c$ value measured from the fracture surfaces at the point where $a/W = 0.25$. The f_K estimate at $a/W = 0.25$ was chosen to give a representative f_K for the entire crack growth process. Referring to the comparison of f_K values in Table 1, for the specimens having the highest and the intermediate values of $a/2c$ the two values of f_K are the same. This indicates that the use of the constant value of f_K corresponding to the situation at $a/W = 0.25$ gives a good description of the growth of cracks having relatively high values of $a/2c$. For low values of $a/2c$, specimens 3A and 3B in Table 1, this procedure gives too high a value of f_K and would therefore predict too short a fatigue life. The use of a constant value of f_K for low values of $a/2c$ may still be an adequate description of the crack growth portion of life, and the difference between measured and calculated lives may be the result of cycles required to initiate the crack growth from the notch. A few hundred initiation cycles would

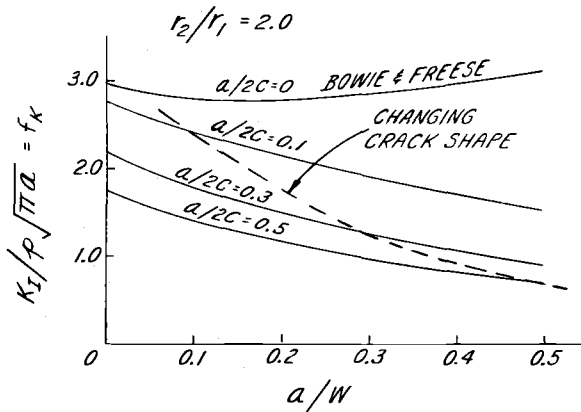


FIG. 7—Estimate of K_I for surface cracked cylinder.

make a noticeable difference in a total life of 1500 cycles but would have less effect on the longer life of specimens having higher starting values of $a/2c$.

The results summarized in Fig. 6 clearly show the large effect of crack shape on life, and the procedure for fatigue life prediction summarized in Eq 2 includes this crack shape effect by way of the parameter f_K . The procedure of using constant f_K is easy to understand and to verify, but it does not directly take into account the changing shape which does occur while the crack grows in a cylinder. As described here in relation to Fig. 1 and Table 1, cracks in cannon tubes start with a low value of $a/2c$ and grow with a steady increase in $a/2c$. Such behavior may be modeled as suggested by the dashed line in Fig. 7. A method for including this changing crack shape in the description of crack growth is to obtain an expression of f_K versus a which fits the observed behavior in the cylinder of interest and which can be integrated to obtain a simple closed-form expression such as Eq 2. This method will have the very significant advantages of ease of application and verification which are often not present in numerical integration schemes.

Residual Stress Effects

The effect of residual stress on fatigue crack growth is of particular concern in cannon tubes. Many large cannons are produced with compressive residual stress present near the bore surface which serves to increase the fatigue life greatly. The residual stress is induced by an overstraining process called autofrettage, which is accomplished either by pressurizing the tube to a level above the yield pressure or more often by forcing an oversized mandrel through the tube. Both methods result in residual stress

distributions of the type shown in Fig. 8, which is a plot of the ratio of circumferential residual stress to uniaxial yield stress versus position through the tube wall. Both partial and complete overstrain are used. A 60 percent overstrain condition, as shown in Fig. 8, is produced by expanding the tube to the point where plastic deformation has proceeded 60 percent of the distance from the inner to the outer surface of the tube. The residual stress distribution which results from a partial overstrain has the advantage of a decrease in the tensile value near the outer surface with a significantly smaller decrease in the compressive value near the inner surface. This is a significant advantage in cases where fatigue cracks can develop at the outer surface as well as at the inner surface of a tube.

These principles of autofrettage design, very briefly sketched here, are being used now in pressure vessels and piping applications as well as in cannon components.

Proposed K Description for Residual Stress

Regardless of the application, a method is required for describing the effect of residual stress on K_1 in a loaded specimen with a notch. The basis for a method which applies to cannon tubes and structural components in general is shown in Figs. 9 and 10. In Fig. 9a is a sketch of a specimen or component with a notch of depth a which is small relative to the size of the piece and with a residual stress distribution which is known over the distance of the notch depth. For these conditions a good estimate of the stress intensity factor due to the residual stress can be obtained by the superposition of two other K_1 solutions as indicated in Figs. 9b and 9c. Figure 9b shows both the residual stress in the specimen and an arbitrary stress

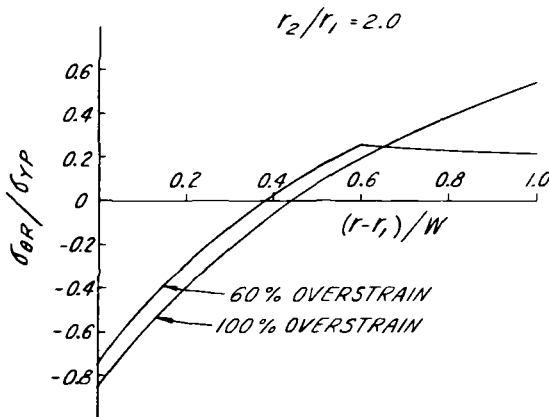


FIG. 8—Residual stress distribution in autofrettaged cylinder.

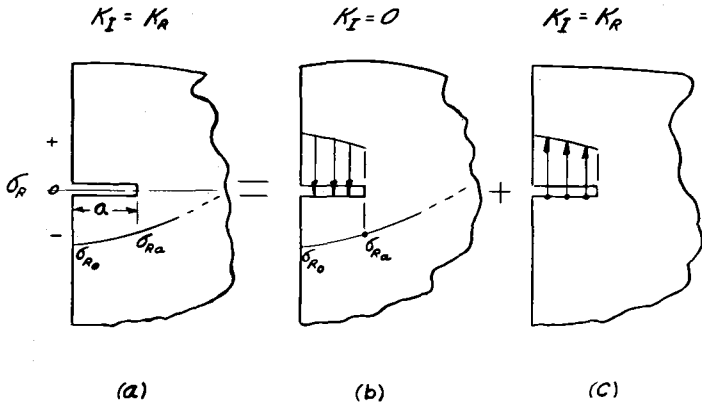
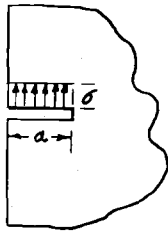


FIG. 9—Superposition to obtain K_I due to residual stress.

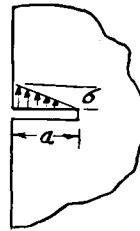
(a) UNIFORM PRESSURE

(b) LINEAR VARYING



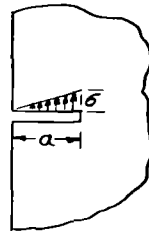
$$K = 1.12 \sigma \sqrt{\pi a}$$

BUECKNER



$$K = 0.439 \sigma \sqrt{\pi a}$$

BENTHEM

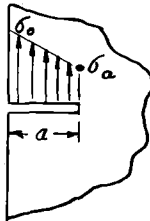


$$K = 0.683 \sigma \sqrt{\pi a}$$

TADA

(c)

GENERAL LINEAR-VARYING CRACK
FACE LOADING



$$K = [1.12 \sigma_0 - 0.68 (\sigma_0 - \sigma_a)] \sqrt{\pi a}$$

FIG. 10—Crack face loading solutions.

applied to the notch with an effect which is equal and opposite to that of the residual stress. In this example of a compressive residual stress, the arbitrary stress applied to the notch faces (shown applied to only one side for clarity) is such that it would open the notch, while the residual stress would close the notch. The net effect of the combined loading in Fig. 9b is that $K_I = 0$. If the situation in Fig. 9c were added to that in Fig. 9b so as

to counteract the arbitrary stress, then the sum would be the problem of interest shown originally in Fig. 9a. The key point is that the K_I for a notched specimen with residual stress present, Fig. 9a, is equivalent to the K_I of the specimen with equivalent stress applied directly to the notch faces, Fig. 9c.

Next, it can be shown in Fig. 10 that a specimen containing a shallow notch with stress applied to the faces can be handled easily. Bueckner [8] described the solution for a shallow notch with uniform pressure applied to the notch faces, see Fig. 10a. Benthem [9] and Tada [10] gave solutions for decreasing and increasing, linear varying pressure applied to the faces of a shallow notch. These three solutions can be combined to describe the K_I for the case of general, linear-varying, crack-face loading as shown in Fig. 10c and repeated here

$$K_I = [1.12 \sigma_o - 0.68(\sigma_o - \sigma_a)] \sqrt{\pi a} \quad (3)$$

Based on the concepts discussed in relation to Figs. 9 and 10, it is proposed that the values from the residual stress distribution which correspond to the surface and to the depth a below the surface (σ_{Ro} and σ_{Ra} respectively in Fig. 9a) can be used in Eq 3 to obtain a measure of the K_I produced by the residual stress. This value, K_R , can then be added to the K_I due to external loads to obtain the total K_I applied to the notch tip. A negative value of K_R , as sketched in Fig. 9a, can be considered but only when a larger positive K_I due to external loads is present so that no closing of the crack can occur. Other limitations of this proposed method for determining K_R are the shallow crack requirement already mentioned and the requirement that the residual stress distribution near the surface must be of a type that can be approximated by a straight line.

Example of Residual Stress Effect on K_I

The proposed method for determining K_R can be used to calculate the effect of residual stress in a hypothetical example. Consider a 60 percent overstrained cylinder with the dimensions shown in Table 2. For a yield stress of 1000 MPa, the values of residual stress at the surface, σ_{Ro} , and at the point in the wall corresponding to the notch tip, σ_{Ra} , are determined from Fig. 8 and listed in Table 2.

Using these values of a , σ_{Ro} , and σ_{Ra} in Eq 3 gives a value of $K_R = -82$

TABLE 2—Example data.

$r_2/r_1 = 2.0$	$\sigma_{yp} = 1000 \text{ MPa}$
$W = 50 \text{ mm}$	$\sigma_{Ro} = -740 \text{ MPa}$
$a = 5 \text{ mm}$	$\sigma_{Ra} = -490 \text{ MPa}$

$\text{MPa}\sqrt{\text{m}}$. If in the example the cyclic loads on the cylinder resulted in a minimum K_I of zero and a maximum K_I of $100 \text{ MPa}\sqrt{\text{m}}$, then the combined effect of external and residual loading would be a ΔK of $18 \text{ MPa}\sqrt{\text{m}}$. This of course would result in a very much slower rate of crack propagation than if the compressive residual stresses were not present.

Equation 3 can be used in the same way to calculate K_R which corresponds to a tensile residual stress. In general, the effect of a combination of positive K_R and positive applied K_I would not cause nearly as large a relative increase in da/dN as the relative decrease expected in the example here. The reason for this is that, although the mean K_I would be increased by a tensile residual stress, ΔK would be unchanged, and it is well known that mean K_I has much less effect on da/dN than does ΔK .

Summary

Three independent calculations of K_I for pressurized cylinders with surface cracks are well represented by Underwood's estimate [3] of K_I . This estimate also gives a good description of the crack growth and fatigue life behavior of nonautofrettaged cannon tube specimens which contain surface flaws of prescribed size and shape.

Multiple cracking in pressurized cylinders can reduce K_I to one half that of a single crack when the spacing between cracks is in the order of the crack depth.

A method is proposed for describing quantitatively the effect of residual stress on K_I in cylinders and other components with shallow cracks. For a compressive residual stress the reduced ΔK due to the combination of residual loading and applied cyclic loading can be calculated and used to predict the rate of fatigue crack propagation and to estimate the number of cycles to failure.

Acknowledgments

We are pleased to acknowledge B. B. Brown and S. L. Pu of our laboratory for their help in the area of cannon tube testing and multiple crack K -analysis respectively and D. J. Cartwright of University of Southampton, United Kingdom, for his discussions and encouragement in the area of residual stress effects.

References

- [1] Goldthorpe, B. D., "Fatigue and Fracture of Thick Walled Cylinders and Gun Barrels," *Case Studies in Fracture Mechanics*, AMMRC MS 77-5, T. P. Rich and D. J. Cartwright, Eds., Army Materials and Mechanics Research Center, Watertown, Mass., June 1977.
- [2] Pu, S. L. and Hussain, M. A., "Stress Intensity Factors for a Circular Ring with Uniform Array of Radial Cracks Using Cubic Isoparametric Singular Elements," *Proceedings, 11th National Symposium on Fracture Mechanics*, June 1978, to be published.
- [3] Underwood, J. H. in *Proceedings, 1971 National Symposium on Fracture Mechanics*,

- Part 1; *Stress Analysis and Growth of Cracks*, ASTM STP 513, American Society for Testing and Materials, 1972, pp. 59-70.
- [4] Bowie, O. L. and Freese, C. E., *Engineering Fracture Mechanics*, Vol. 4, No. 2, June 1972, pp. 315-321.
- [5] Smith, C. W., Jolles, M., and Hu, T., "Stress Intensities for Low Aspect Ratio Surface Flaws in Pressurized Thick Walled Tubes," VPI-E-75-19, Virginia Polytechnic Institute and State University, Blacksburg, Va., Aug. 1975.
- [6] Hussain, M. A., Throop, J. F., Pu, S. L., and Scanlon, R. D., "Stress Intensity Factors for a Pressurized Thick-Wall Cylinder with a Part-Through Circular Surface Flaw—Compliance Calibration and Collocation Method," WVT-TR-76040, Benet Weapons Laboratory, Watervliet, N.Y., Oct. 1976.
- [7] Kobayashi, A. S., Polvanich, M., Emery, A. F., Love, W. J., *Journal of Pressure Vessel Technology*, Vol. 9, Feb. 1977, pp. 83-89.
- [8] Bueckner, H. F., "Some Stress Singularities and Their Computation by Means of Integral Equations," *Boundary Problems in Differential Equations*, R. E. Langer, Ed., University of Wisconsin Press, Madison, Wis., 1960.
- [9] Benthem, J. P. and Koiter, W. T., "Asymptotic Approximations to Crack Problems," *Methods of Analysis of Crack Problems*, G. C. Sih, Ed., Noordhoff International Publishing, Leyden, The Netherlands, 1972.
- [10] Tada, H., Paris, P. C., and Irwin, G. R., *The Stress Analysis of Cracks Handbook*, Del Research Corporation, Hellertown, Pa., 1973.

Summary

The papers in this symposium volume may be divided into three categories: (1) state-of-the-art reviews on part-through crack (PTC) fatigue life prediction methodologies, (2) ASTM Task Group E24.06.01 PTC Life Prediction Round Robin Analysis results, and (3) special PTC problems in industry application.

In the first category, an overview of important features of PTC growth prediction technology was presented in the paper by Cruse et al. Emphasis was placed on the prediction of small surface cracks emanating from highly stressed regions, such as bolt holes. They concluded that many issues require further experimental and analytical work. These issues include the surface value of the stress intensity distribution, crack growth through highly varying stress/material property fields at the surface, and the applicability of macrocrack growth methods to small cracks.

For reliable crack growth life predictions, accurate stress intensity factors solutions are needed. Newman's paper provided a comprehensive review of 14 stress intensity factor solutions proposed for a PTC in a finite plate subjected to uniform tension over the past two decades. Comparison of the stress intensity factor solutions at the maximum depth point showed good agreement for crack depth-to-thickness (a/t) ratios about 0.3 or less. For $0.3 < a/t \leq 1$, the solutions were in considerable disagreement (20 to 80 percent). Newman indicated that some of the discrepancies among the various solutions were attributed to improper boundary conditions imposed on the PTC configuration.

Additional to accurate stress intensity factor solutions, the ability to accurately predict fatigue crack growth behavior relies heavily on the material's crack growth rate data and its fracture properties. The paper by Bucci reviewed the status of the standardization on test practice for characterizing basic material properties for inputting in the crack growth analysis. Bucci provided guidelines to help the design engineer to recognize potential problems and minimize variability in the basic material package which consists of tensile properties, fracture toughness, cyclic crack growth rates, and sustained load cracking information.

It is a well known fact that the shape of a PTC may vary during the crack growing process. The need to account for the shape change effect in the analytical prediction procedure is obvious. The paper by Engle presented six different methods for handling the shape changes in PTC life predictions. Engle reported the results of the evaluation of four constant

shape (one-dimensional growth) solutions and two variable shape (two-dimensional growth) solutions. Although one can argue about whether it is always true that the crack growth rate in the width direction is faster than the crack growth rate in the depth direction, the crack growth accumulation algorithm described in Engle's paper provided a clear picture for the best way of handling the shape change effect for PTC fatigue life predictions.

Papers by Hudson and Lewis, Peterson and Vroman, Johnson, Rudd, as well as Chang, presented in detail the methodology and procedure utilized by each participated organization in the prediction of the fatigue crack growth behaviors for the PTC test cases selected for the round-robin analysis conducted by ASTM E24.06.01 Task Group belonged to the second category. In summary, all predictions were done by using certain computerized damage accumulation package including computer program such as CRACKS and EFFGRO. The fatigue crack growth rate relationships used mostly were the Paris equation or its modified versions, Forman equation, and Walker equation. The PTC stress intensity factor solutions used in the analyses varied slightly from one another. Primarily, the variation was the value of the back face correction factor. Most of the predictions were done by assuming constant shape (one dimensional growth). Since the initial shapes for most of the PTC cases in the round-robin analysis were in the stable shape, that is, $a/2c \approx 0.45$, the constant shape approach taken by most participants is justifiable. Majority of the authors reported that the simple break-through criterion was adopted in their analyses, that is, when the crack depth a reaches to the thickness t , a PTC is said to translate to a through crack (TC).

Correlations of predicted crack growth behaviors to the actual crack growth data were presented in the papers just listed. In general, satisfactory correlations have been shown. Vroman's paper presented a summary of the three round-robin analysis results. The conclusion that was drawn in Vroman's paper is worthwhile to be repeated here. That is, the fatigue crack growth behavior of PTC under constant amplitude loading is able to be predicted with sufficient accuracy on the basis of crack growth rate data obtained from the compact specimens.

Two papers related to the third category, the special PTC problems in industry application, are collected in this symposium volume. The paper by Rudd et al presented a comprehensive summary of the analytical crack growth and residual strength requirements which must be met as well as the initial flaw shapes and sizes which must be assumed in the Air Force Airplane Damage Tolerance Design Requirements (MIL-A-83444). Their paper provided a clear picture as to what are the PTC problems in airframe structural designs. It also presented techniques for predicting the crack growth behavior on various type of cracks emanating from fastener holes.

The paper by Underwood and Throop unveiled the PTC problems in cannon tubes. These include the thermally induced cracks occurring on the severely eroded inner surface caused by high temperature during firing, and the fact that multiple cracks can occur in some circumstances. They described in detail the results of fracture tests and analyses related to PTC growth in cannon tubes. Emphasis was placed on a proposed method for describing quantitatively the effect of residual stresses on the stress intensity factor calculations and crack growth predictions for the cannon tube and other components with shallow surface cracks. The effect of residual stresses on fatigue crack growth which is of particular concern in cannon tubes is due to the fact that, to improve fatigue lives, many large cannons are produced with compressive stress presented near the bore surface by an overstraining process called autofrettage. It seems that their proposed method to account for the residual stress effect can be applied to any structural components containing residual stresses including cold-worked fastener holes, shot-peened parts, etc.

The papers collected in this symposium volume reflect the fact that all the authors did an excellent job in contributing to the symposium and stimulating interest in this important area. It is hoped that the information contained in this publication will be of use to design, analysis, and test engineers, as well as to other technologists who are concerned with this important problem. There is no doubt that further experimental and analytical efforts are needed in order to achieve more accurate PTC crack life predictions. This is particularly true for predicting fatigue crack growth behavior of PTC under spectrum loading. It is wished that ASTM Committees E-9 on Fatigue and E-24 on Fracture Testing will act jointly to coordinate the studies required and that further progress would be reported in future publications.

J. B. Chang

Fatigue and Fracture Mechanics Group,
North American Aircraft Division, Rockwell
International Corporation, Los Angeles,
Calif. 90009; editor.

Index

A

Aircraft structure, 75, 170
 Aluminum, 54, 96, 114, 144, 150,
 157, 193
 Aspect ratio, 5, 74, 99
 ASTM standard for fracture testing
 E 399-78, 51
 E 338-68, 51
 E 647, 51
 Autofrettage, 205

B

Back face correction (magnification)
 factor, 37, 99, 121, 132, 160,
 176
 Body-centered-cubic structure, 11
 Bowie correction factor, 176

C

Cannon tube, 195
 Center crack tension specimen, 63
 Coefficient of variation, 79
 Compact specimen, 63, 91, 97, 156
 Constant amplitude loading, 56, 90,
 144
 Corrosive environment, 68
 C-shaped specimen, 202
 Crack arrest structure, 172
 Crack growth algorithm
 One dimensional, 79
 Two dimensional, 79
 Crack growth rate, 13, 49, 77

Crack growth rate constants (co-
 efficients), 156
 Crack growth retardation, 50

D

Damage tolerance design, 168
 Damage tolerant structure, 156
 Degree of inspectability, 172
 Distilled water, 97
 Double-cantilever-beam specimen,
 71

E

Elastic-plastic stress, 4
 Elevated temperature, 68
 Elliptical crack, 11, 16, 76
 Elliptical integral, 16, 161
 Epoxy, 16

F

Fail-safe structure, 174
 Fastener (bolt) hole, 4, 168
 Fatigue crack, 6
 Finite element, 10, 23, 198
 Finite width correction factor, 34,
 100, 160
 Firing cycle, 197
 Forman's equation, 121, 152
 Fractography, 6
 Fracture mechanics, 3, 130, 157, 168,
 195
 Fracture surface, 8

- Fracture toughness
 Critical, 16, 47, 145
 Plane strain, 16, 131
 Plane stress, 16, 131
- Front face correction (magnification)
 factor, 37, 121, 160, 176
- G**
- Gas turbine engine disk, 3
- H**
- Hexagonal-close-packed structure,
 11
- Histogram, 79, 164
- K**
- K*-decreasing procedure, 66
K-value, 1
- L**
- Leak-before-break, 51
 Life prediction, 3, 48, 89, 96, 130
 Load interaction effect, 50
 Low-cycle fatigue, 5
- M**
- Morphology, 12
 Multiple cracks, 198
- O**
- Overload, 6
- P**
- Parabolic crack, 43
 Paris' equation, 135, 145
 Part-through crack, 10, 48, 75, 89,
 96, 135
 Plastic-zone size, 25
- Poisson's ratio, 11, 187
 Precracked specimen, 50
 Principal stress, 54
- R**
- Radial crack, 75
 Residual strength, 170
 Residual stress, 4, 193, 196
R-ratio, 5, 49, 115
 Runge-kutta method, 101, 132
- S**
- Scanning electron microscope, 6
 Shape factor, 16
 Slow crack growth structure, 172
 Semi-circular crack, 22
 Space shuttle, 130
 Standard deviation, 34
 Striation spacing, 8
 Stress concentration factor, 11
 Stress corrosion cracking, 68
 Stress intensity factor, 10, 16, 75, 119
 Stress intensity factor range, 49, 77
 Stress range, 50
 Structural integrity, 48
 Surface crack (flaw), 3, 16
 Sustained loading, 48
 Sump tank water, 92, 97, 164
- T**
- Taylor series, 153
 Threshold stress intensity factor
 range, 58
 Through crack, 10, 48, 118, 162
 Titanium, 4, 77, 91
 Transition criterion, 138
 Transmission electron microscope, 8
- W**
- Walker's equation, 157
 Wink-zyglo technique, 6